8-2022

Translating particulate hexavalent chromium-induced chromosome instability from human lung cells to experimental animals, human lung tumors and whale cells.

Haiyan Lu
University of Louisville

TRANSLATING PARTICULATE HEXAVALENT CHROMIUM-INDUCED CHROMOSOME INSTABILITY FROM HUMAN LUNG CELLS TO EXPERIMENTAL ANIMALS, HUMAN LUNG TUMORS AND WHALE CELLS

By

Haiyan Lu
M.D., Wenzhou Medical University, 2003
M.S., Wenzhou Medical University, 2008

A Dissertation
Submitted to the Faculty of the
School of Medicine of the University of Louisville
In Partial Fulfillment of the Requirements
for the Degree of

Doctor of Philosophy in Pharmacology and Toxicology

Department of Pharmacology and Toxicology
University of Louisville
Louisville, KY

August 2022

TRANSLATING PARTICULATE HEXAVALENT CHROMIUM-INDUCED CHROMOSOME INSTABILITY FROM HUMAN LUNG CELLS TO EXPERIMENTAL ANIMALS, HUMAN LUNG TUMORS AND WHALE CELLS

By

Haiyan Lu
M.D., Wenzhou Medical University, 2003
M.S., Wenzhou Medical University, 2008

A Dissertation Approved on
July 27, 2022
By the following Dissertation Committee:

_____
John Pierce Wise, Sr., Ph.D.

_____
Lu Cai, M.D., Ph.D.

_____
J. Calvin Kouokam, Ph.D.

_____
Ke Jian Liu, Ph.D.

_____
Sandra S. Wise, Ph.D.

_____
Qunwei Zhang, Ph.D.

DEDICATION

This dissertation is dedicated to my husband, Chunlei Qian. Thank you for your unwavering love and unconditional support. Thank you for cheering me on as I take on a new challenge. Thank you for taking care of the children over the years and allowing me to conduct my scientific research without any worries. Your support makes me successful!

ACKNOWLEDGEMENTS

First, I would like to thank Dr. Wise, my mentor, for all his support, guidance, and encouragement. He not only gave me the opportunity, but also gave me a lot of patient support. His support made my research a success and made it possible for me to become a scientist. His kindness, erudition, and passion for science have guided me through the years. I would also like to thank him for his great encouragement for me to believe in myself. I could not have imagined all the incredible opportunities I have had because of his support and confidence in my ability to succeed. I also thank him for holding pumpkin carvings, thanksgiving dinners, Christmas parties, and Chinese New Year dumpling parties and for fostering a wonderful work environment that always feels like a big, warm family.

I would also like to thank my doctoral committee: Dr. Lu Cai, Dr. Calvin Kouokam, Dr. Ke Jian Liu, Dr. Sandra Wise, and Dr. Qunwei Zhang for all their knowledge, guidance, and suggestions during all these years. Thank you to Dr. Hein for all the guidance and support over the past 6 years as a leader of the Department of Pharmacology and Toxicology, and to everyone in the Department for the opportunity to learn so much more through the research and inspiration over the years.

I also want to thank everyone in the Wise Lab (current and past members). Special thanks to Dr. Sandy Wise, Dr. Rachel Speer and Dr. Cynthia Browning for

their guidance, support, and great training when I first started in the lab. Special thanks to Dr. Tayler Croom-Pérez and Dr. Adam Pérez for their guidance and great training in lab techniques. Thanks to Jennifer Toyoda, Idoia Meaza, and Aggie Williams for their support and friendship. Thanks to Dr. Gary Hoyle and Dr. Jamie Young for their training in animal experiments. Thanks to Dr. John Wise Jr., for training in the confocal technique. Thanks to Dr. Jun Yan for teaching me flow cytometry techniques. Thanks to Dr. Alicia Bolt for assistance in flow cytometry experiments.

Finally, I must thank my family and friends who have always supported me. Thank you for always having confidence in my ability to succeed and for providing so much support. I want to thank my parents and mother-in-law, their love greatly encouraged me, and financial support help me through these years. I also want to thank my husband, Chunlei, for all the support and made me grow so much with his help. Thanks to my son, Leon, for his smile giving me hope while the difficult days. Thanks to my daughter, Daisy, for her company and love. I am so grateful for everything you have ever done for me.

This dissertation would not have been possible without all the financial support provided by many different sources. I received numerous travel awards and research awards from the University of Louisville and the Society of Toxicology which allowed me to present my research at many conferences. This work was supported by the National Institute of Environmental Health Sciences [R01ES016893 and R35ES032876 to JPWSr.] and the University of Louisville School of Medicine Basic Grants Program (SSW).

ABSTRACT

TRANSLATING PARTICULATE HEXAVALENT CHROMIUM-INDUCED CHROMOSOME INSTABILITY FROM HUMAN LUNG CELLS TO EXPERIMENTAL ANIMALS, HUMAN LUNG TUMORS AND WHALE CELLS

Haiyan Lu

July 27, 2022

Lung cancer is a major human health problem. While smoking is the most well-known cause of lung cancer, people who never smoked develop the disease. Understanding how non-tobacco environmental carcinogens cause lung cancer is key to combating this disease. Hexavalent chromium [Cr(VI)] is a well-established human lung carcinogen, but its carcinogenic mechanism is uncertain.

Chromosome instability (CIN) is a hallmark of lung cancer and a major factor in Cr(VI)-induced lung cancer. Studies in human lung cells show Cr(VI) induces DNA double strand breaks and suppresses homologous recombination (HR) repair by targeting RAD51, resulting in CIN.

We translated these outcomes to rats, as this species develops Cr(VI)-induced lung tumors. We exposed 12-week-old Wistar rats to a single dose of zinc chromate for 24 hours or a weekly dose for 90 days via oropharyngeal aspiration. DNA double strand breaks and HR repair increased in a concentration-dependent manner in rat lungs after 24-hour Cr(VI) exposure. After 90-day exposure, DNA double strand breaks increased, but HR repair decreased. These effects were

distinct in bronchioles but muted in alveoli, consistent with Cr(VI)-induced human lung tumors originating in bronchial epithelium.

We translated these outcomes to Cr(VI)-associated human lung tumors. DNA double strand breaks significantly increased but RAD51 expression decreased in lung tumors; demonstrating Cr(VI)-induced DNA double strand breaks and HR inhibition persist in tumors.

Long-lived whales can experience long-term exposure to environmental contaminants but have low cancer rates. We measured the ability of Cr(VI) to induce DNA double strand breaks, HR repair, and chromosome damage in bowhead whale lung cells. Cr(VI) induced DNA strand breaks in whale cells, but the HR repair response remained intact. Thus, whale cells are resistant to Cr(VI)-induced loss of HR repair with no apparent CIN. These results indicate significant differences in the response of human and bowhead whale lung cells to Cr(VI) exposure.

Overall, our studies translate Cr(VI)-induced DNA double strand breaks and HR repair impacts to rat lung tissue, human lung tumors and whale lung cells. Cr(VI) induces DNA double strand breaks and inhibits HR repair *in vivo*, but does not cause HR repair failure and CIN in whale lung cells.

.

TABLE OF CONTENTS

PAGE

LIST OF FIGURES

LIST OF TABLES

PAGE

CHAPTER I

INTRODUCTION

Chromium

Discovery and use history

Chromium (Cr), atomic number 24, is a relatively abundant element present in the Earth's crust. It was discovered in 1797 by the French chemist Louis-Nicholas Vauquelin while examining a material known as crocoite (PbCrO4), a mineral (Kyle and Shampo, 1989). The following year he isolated metallic chromium from the chromium ore, crocoite (IARC, 1990). Its brilliant color inspired Vauquelin to give the metal its current name (from the Greek word "chroma", meaning color). Chromium is a hard, steel-gray metal widely dispersed in natural deposits. It is always combined with other elements, especially oxygen. Chromite (FeCr2O4) is the major ore, and the ores are refined to metal after mining. Iron-containing chromium was first produced in the mid-19th century, and the first use of chromium as an alloying agent in the steel manufacture took place in France in the 1860s.

With the discovery of global chromite deposits, the chromium industry has developed rapidly (Barnhart, 1997). In 2013, the largest producers of chromium ore were South Africa (48%), Kazakhstan (13%), Turkey (11%), and India (10%), and chromium ore production in several other countries accounted for about 18%

of the world production (Papp, 2015). In 2019, the global production of chrome ore increased to 44,000 kilotons. The largest producers were South Africa (38.6%), India (22.7%), and Kazakhstan (15.2%) (Schulte, 2020).

Although only small amounts of chromium are mined in the United States, the latter is a major producer of chromium end products, including chromium chemicals, metals, and stainless steel (ATSDR, 2012). Chromium is a hard metal that requires a high polish and has a high melting point. Due to its hardness and resistance to corrosion, chromium is used in alloys and stainless steel to increase the hardening ability and corrosion resistance (ATSDR, 2012; Barnhart, 1997). Globally, approximately 80% of chromium is used in metallurgical applications, from chrome plating to stainless steel production. Chromium salts show a variety of bright colors, which justify their use in many other applications, including pigment production, leather tanning, and the production of wood preservatives (ATSDR, 2012; Barnhart, 1997).

Physical and chemical properties

Cr exists in many chemical and physical forms that are different in their environmental behaviors and biological activities. While the valence states of Cr range from -2 to +6, Cr(0), Cr(III), and Cr(VI) are the three main oxidative states of Cr that are most commonly present in the workplace and general environment (Pechova et al., 2007). Cr compounds with oxidation states of +1, +2, +4, and +5 are very unstable and rarely occur in the environment. Cr(0) is usually encountered in the form of metal in alloys with other metals such as nickel, iron, and cobalt.

Stainless steel is the product with the largest amount of metal chromium. Although Cr(0) is stable to atmospheric oxygen oxidation under ambient conditions, high-temperature processes (such as welding or exposure to corrosive chemicals) result in the formation of higher oxidation states: Cr(III) and Cr(VI). Cr-based prostheses may also undergo slow oxidation, thereby releasing higher oxidation forms of Cr (Case et al., 1994; Merritt et al., 1995). Cr(III) is easily found in nature, but Cr(VI) rarely occurs and is mainly produced through industrial activities (Kotas et al., 2000).

Chromium compounds are usually classified as soluble or insoluble in water. Common water-soluble compounds include chromium chloride, chromium acetate, sodium chromate, and potassium chromate; water-insoluble chromium compounds include chromium oxide, chromium sulfate, lead chromate, and zinc chromate (IARC, 1990). The mutual transformation between Cr (VI) and Cr (III) can occur naturally in the environment. These chemical reactions depend on many factors such as the availability of oxygen, the capacity of oxidizing or reducing agents, temperature, and pH. Generally, under acidic conditions, Cr (VI) can be reduced to Cr (III), while under alkaline conditions, Cr (III) can be oxidized to Cr (VI) (Kotaś et al., 2000; Richard et al., 1991; Zhitkovich, 2005). Due to the organic matter in biological systems, Cr (VI) is also quickly reduced to Cr (III). However, oxidation from Cr (III) to Cr (VI) does not occur in biological systems (Barceloux et al.,1999; Dayne et al., 2001).

Chromium exposure

Environmental exposure

Cr is naturally present in the environment through the presence of continental dust, which is released due to soil and rock erosion or volcanic eruptions (Kotaś et al., 2000). However, most Cr(VI) is released into the environment through anthropogenic activities (ATSDR, 2012). Due to Cr's widespread use, the anthropogenic sources include fixed points in the metal, textile and cement industries, as well as leather tanneries. According to the Toxics Release Inventory, about 36 million lbs of Cr compounds were released into US waters, soils, and air in 2009 (ATSDR, 2012).

Anthropogenic activities account for 60-70% of all Cr in the atmosphere (Bielicka et al., 2005). Cr is released into the atmosphere by burning of fossil fuels, incineration of electronic waste, production of refractory bricks, cement processing, and production of chromium-containing pigments (Catrambone et al., 2013; Singh et al., 2015). In a survey between 1977 and 1984, typical airborne total chromium concentrations in the US were between 0.01 and 0.03 ug/m^3 (ATSDR, 2000). Industrial disposal of Cr-containing dust can significantly increase non-occupational exposure. Estimates of atmospheric chromium emissions in Los Angeles, California, and Houston, Texas in 1976 and 1980 showed that emissions from combustion of fixed fuels accounted for about 46-47% of the total Cr, and emissions from the metal industry range from 26 to 45% of the total Cr. (ATSDR, 2000). The combustion of coal and oil is estimated to emit 1,723 tons of chromium in the atmosphere each year. However, only 0.2% of this chromium is Cr(VI).

Meanwhile, it is estimated that the chrome-plating source contributes 700 metric tons of chromium annually to air pollution, of which 100% is considered to be Cr(VI) (ATSDR, 2000).

Many Cr(VI) compounds have high water solubility, and at neutral pH, monochromate may be found as a pollutant in groundwater. However, in the presence of low pH and/or organic materials, Cr(VI) tends to be reduced to Cr (III). Although Cr(VI) released into the soil is expected to be reduced to the trivalent state, in case of high concentration in water or low reducing power of the soil (for example in sandy soil), Cr(VI) may not be reduced before it gets to groundwater (Paustenbach et al., 2003). Electroplating, leather tanning and textile industries release relatively large amounts of chromium into surface water. Leaching from topsoil and rocks is the most important natural source of chromium into water bodies. If the solid waste generated by chromate treatment facilities is not properly processed in a landfill, it may become a source of groundwater pollution, and the residence time of chromium may be several years (ATSDR, 2011). According to the Toxics Release Inventory, in 1997, it was estimated that the chromium released into water from 3,391 large-scale processing facilities was 111,384 pounds, accounting for about 0.3% of the total environmental emissions (ATSDR, 2000).

Cr(VI) enters the soil mainly through waste disposal activities. Between 1991 and 1994, about 39 tons and 162 tons of total Cr(VI) as sewage sludge were disposed to landfills and farmland annually, respectively (DoE, 1996). Industrial solid Cr(VI) waste is mostly dumped in restricted landfills nowadays. However, past

industrial activities have caused severe land pollution. The world's largest chrome producer in the 19th century (headquartered in Shawfield, Scotland, operating until 1967) widely used chromite ore processing residues as landfill materials in southeastern Glasgow. According to reports, between 1960 and 1966, 60 to 70 tons of Cr(VI) waste were dumped every day (EHD, 1991a). According to the Toxics Release Inventory, the estimated chromium released into the soil from 3,391 large-scale processing facilities in the United States in 1997 was 30,862,235 pounds, accounting for approximately 94.1% of total environmental emissions (ATSDR, 2000).

Occupational exposure

As Cr is commonly used in metallurgical and chemical industries, workers experience exposure through inhalation of dust, mists, or fumes, and direct dermal contact with chromium-containing materials. More than 80 occupations that may expose chromium have been identified (IARC, 1990). In 1994, Meridian Research, Inc. estimated that there are 808,177 production workers may be exposed to Cr (VI) in U.S. industries (Meridian, 1994). The industries involved in the survey include electroplating, welding, painting, paint and coating manufacturers; chromate producers, chromate pigment manufacturers, CCA manufacturers, printing ink manufacturers, chromium catalyst manufacturers, plastic colorant manufacturers, plating mixture manufacturers, producers of wood preserving materials, ferrochromium producers, iron and steel foundries. More than 98% of the potentially exposed workers were found in six industries: electroplating,

painting, welding, paint and coating production, iron and steel foundries, and iron and steel production. Although occupational exposure in the U.S. has decreased significantly since the 1980s due to improved emissions control, in 2006, the Occupational Safety and Health Administration (OSHA) estimated that 558,000 American workers were exposed to Cr (VI) compounds. Of these, 352,000 were exposed to more than 0.25 micrograms per cubic meter, and 68,000 were above the permissible exposure limit (PEL) of 5 micrograms per cubic meter (OSHA, 2006). Table 1.1 shows the estimated number of workers exposed by the application group (Shaw Environmental, 2006).

Specifically, workers engaged in industrial or chromite production are exposed to higher levels of Cr(VI) compared to the general public (ATSDR, 2012). In particular, the occupations with the highest potential risks are metallurgy, tanning, pigment production, and chromate manufacturing (ATSDR, 2012). In the occupational environment, the content of hexavalent chromium in the air may vary depending on the occupation, with concentrations of 5-600 ug/m^3 (Stern, 1982). Table 1.2 shows the inhalation exposure levels in chromium industries. In 1971, OSHA introduced the PEL of 52 ug/m^3 for Cr(VI). Even when the PEL of Cr (VI) came into effect, stricter regulations came into effect when the PEL was reduced to 5 ug/m^3 in 2006 (OSHA, 2006). However, the occupational exposure limits for insoluble hexavalent chromium compounds in other countries are still high (Table 1.3).

Table 1.1 Estimated number of workers exposed to Cr(VI) by application group

Application Group	Total Number of Exposed Workers
Welding (stainless steel)	127,746
Welding (carbon steel)	141,633
Painting	82,253
Electroplating	66,859
Steel Mills	39,720
Iron and Steel Foundries	30,222
Textile Dyeing	25,341
Wood Working	14,780
Printing	6,600
Paint and Coating Producers	2,569
Producers of Chromates	150
Chromium Dye Producers	104

Adapted from Federal Register 10099, Table VIII-3 (2006)

Table 1.2 Airborne Cr(VI) levels in various industries.

Industry	Total Airborne Cr(VI) Levels (ug/m³)
Chrome plating	5-25
Ferrochrome alloy production	10-140
Stainless-steel industry welding	50-400
Chrome pigment production	60-600
Cr(VI) production	100-500

Adapted from Stern et al. (1982)

Table 1.3 Occupational exposure limits for insoluble Cr(VI) in different countries

Country	Insoluble Cr(VI) TWA (ug/m³)
Australia	50
Ireland	50
Japan	10
Mexico	10
Netherlands	10
Poland	100
Sweden	20
United Kingdom	50

Adapted from ACGIH (2011). *TWA= time weighted average

Health effects of chromium exposure on the respiratory system

Chromium in different valences differs in toxicity and chemical properties. While Cr (III) compounds serve as a nutritional supplement and appear to have pharmacological effects in certain diabetic populations, Cr (VI) compounds generally exert carcinogenic effects in exposed individuals, as well as injuries in cells, including DNA damage, chromosomal aberrations, and microsatellite instability (Zhitkovich, 2005; O'Brien, 2003; Nickens et al., 2010; Wise et al., 2012). Cr(VI) enters the body through inhalation, ingestion, or absorption through the skin. For occupational exposure, the respiratory tract and skin are the main routes of absorption. Various physical, physiological, and anatomical factors determine the fraction and regional deposition of inhaled particles (OSHA, 2006). Due to the airflow pattern in the airway, more particles tend to deposit in certain prone areas in the lung. Therefore, this may cause chromium to accumulate in certain locations of the bronchial tree, resulting in high chromium concentrations in these areas (OSHA, 2006). Large inhaled particles (> 5 um) are effectively removed from the airflow in the extrathoracic area. Particles larger than 2.5 um are usually deposited in the tracheobronchial area, while particles smaller than 2.5 um are usually deposited in the lung area (OSHA, 2006). Yu et al. found the particle size distribution of Cr(VI) ranged from 0.18 to 18 um in the New Jersey Meadowlands District. In the particle size range of 1.0 to 5.6 um, the Cr(VI) concentration was higher than other particle size fractions and Cr(VI) was enriched in particles with diameter less than 2.5 um (Yu et al., 2014). The particles deposited in the extrathoracic and tracheobronchial regions of the lung are predominantly cleared

by the mucociliary escalator. Individuals exposed to high concentrations of Cr(VI) may also have altered respiratory mucosal cilia clearance (OSHA, 2006). The particles that reach the alveoli can be absorbed by the blood or cleared by phagocytosis.

The absorption of inhaled chromium compounds depends on various factors, including the physical and chemical properties of the particles (size, solubility, oxidation state) and the activity of alveolar macrophages. Hexavalent chromate anions enter cells by facilitated diffusion, through non-specific anion channels (similar to phosphate and sulfate anions) (Wiegand et al., 1985), while Cr(III) compounds cannot pass through the cell membrane using this means (Gray and Sterling, 1950). Chromium has been found in the tissues of chromium workers, indicating that chromium can be absorbed from the lungs (Cavalleri and Minoia, 1985; Gylseth et al., 1977; Minoia and Cavalleri, 1988; Randall and Gibson, 1987). Animal studies have also shown blood amounts of chromium increase after inhalation or intratracheal instillation (Bragt and van Dura, 1983; Langård et al., 1978; Wiegand et al., 1987). Unabsorbed chromium in the lungs can be removed by mucociliary clearance and enter the gastrointestinal tract.

The respiratory tract is the main target for the inhalation of chromium compounds. In 2012, an ATSDR review showed many reports and studies published from 1939 to 1991 found workers exposed to Cr(VI) compounds for different durations from 15 to 364 days had the following respiratory effects: nosebleeds, chronic rhinorrhea, itchy and sore nose, nasal mucosa atrophy, perforations, nasal septal ulcers, bronchitis, pneumoconiosis, decreased lung

function and pneumonia (ATSDR, 2012).

Numerous studies have reported nasal septal perforation and other respiratory effects on workers chronically exposed to Cr(VI) compounds. NIOSH reported that 4 of 11 male employees exposed to “hard-chrome” in an Ohio electroplating facility had nasal septum perforation (NIOSH, 1975c). Totally 11 cases of nasal septal perforation were reported in 2,869 shipyard welders in South Korea. The affected workers had welded for 12-25 years. The concentration of Cr(VI) in welding fumes ranged from 0.044 mg/m^3 to 0.34 mg/m^3 in their workshop (Lee et al., 2002).

Two cross-sectional epidemiological studies of chrome plating workers and stainless-steel production workers showed no nasal septal perforation at an average chromic acid concentration < 2 ug/m^3. The workers exposed to Cr(VI) experienced nasal ulcers and/or nasal septal perforation at concentrations from 2 ug/m^3 to 20 ug/m^3. Nasal mucosal ulcers and/or nasal septal perforation appeared in exposed workers at the peak concentrations of 20-46 ug/m^3 (Lindberg and Hedenstierna, 1983; Huvinen et al., 1996; 2002a,b). Cr(VI) is considered a respiratory sensitizer that can trigger immune-mediated narrowing of airways and inflammation of bronchial tubes, causing asthma. Not all exposed workers are sensitive to Cr(VI); Cr(VI)-triggered asthma only occurs in sensitized individuals. The level of occupational exposure to Cr(VI) causing airway sensitization or occupational development of asthma is unclear (OSHA, 2006). Many case studies and reports have shown an association between occupational chromate exposure and asthma (Bright et al., 1997; Budanova, 1980; Burges et al., 1994; Fernandez-

Nieto et al., 2006; Hannu et al., 2005; Leroyer et al., 1998; Moller et al., 1986; Park et al., 1994).

Chromium carcinogenicity

A large number of epidemiological studies of chromate workers have provided conclusive evidence that Cr is a carcinogen. This was supported by the results of subsequent numerous animal and cell culture studies. In 1990, the IARC classified Cr as a Group 1 carcinogen, considered “carcinogenic to humans” (IARC, 1990). Epidemiological studies have shown the main target organ of Cr is the lung. Therefore, the following discussion focuses on the carcinogenicity of Cr to the lung.

Epidemiology studies of Cr(VI) exposed workers

Many studies have examined the ability of Cr(VI) to induce carcinogenic effects, specifically lung cancers. In 1948, Machle and Gregorious reported the first study on Cr(VI)-induced lung cancer in the US. This first comprehensive epidemiological study found that 21.8% of all deaths in the chromate industry were due to cancers of the respiratory system. More importantly, the latter study concluded that it appears the problem in the chromium industry is limited to cancers of the respiratory system, suggesting that chromium targets the lung (Machle and Gregorious, 1948). Since then, a large number of studies have successively reported the incidence of lung cancer among chromium workers (Alderson et al., 1981; Satoh et al., 1981; Korallus et al., 1982; Langard, 1990;

Gibb et al., 2000; Luippold et al., 2003; Luippold et al., 2005; Birk et al., 2006). Epidemiological studies have shown that insoluble, particulate Cr(VI) compounds are more carcinogenic than soluble Cr(VI) compounds (Baetjer, 1950; Hayes et al., 1979; Alderson et al., 1981; NIOSH, 2006). Epidemiological studies targeting specific chromate compounds are difficult due to the confounding nature of occupational exposures. However, an increased incidence of bronchial cancer was found in workers exposed to sodium chromate (raw material for the production of zinc chromate) and zinc chromate in a zinc chromate production factory (Langard and Norseth, 1975). In addition, a factory that exclusively used zinc chromate pigments had high chromate tumor incidence among workers (Langard and Vigander, 1983). Pathological examination showed Cr particles are deposited at the bifurcation of the bronchus, which are the main formation sites of chromium-induced tumors (Ishikawa et al., 1994a). Kondo et al. reported Cr accumulates in the bronchial stroma instead of epithelial cells, and Cr levels are higher in the bronchioles and subpleural areas of the lung (Kondo et al., 2003). There is a strong correlation between cumulative exposure to Cr and lung cancer, with lung cancer mortality increasing with exposure time (Davies et al., 1984; Gibb et al., 2000; Luippold et al., 2003). The main pathological type of Cr-induced lung tumors is squamous cell carcinoma, with a small percentage of small cell carcinoma and adenocarcinoma (Ewis et al., 2001; Ewis et al., 2006; Hirose et al., 2002; Katabami et al., 2000; Kondo et al., 1997).

Evidence from animal studies

Chronic inhalation studies provide evidence that Cr(VI) is carcinogenic in animals. Multiple studies have shown Cr induces tumor formation in the lungs of experimental animals. For example, lung tumors were observed in Wistar rats exposed to sodium dichromate aerosol (0.1 mg Cr/m^3) for 18 months (Glaser et al. 1986). Tumor formation was found in the lungs of Sprague Dawley rats continuously administered 1.25 mg/kg sodium dichromate solution by intratracheal instillation once weekly for 30 months (Steinhoff et al. 1986). Takahashi et al. found 1 squamous cell carcinoma, 7 carcinomas *in situ* or dysplasia, 8 squamous metaplasia, and 5 goblet cell hyperplasia in 15 rats after inserting a pellet of strontium chromate into the bronchus for 9 months. Chromium accumulation increases significantly with the progression of bronchial epithelial malignancy (Takahashi et al. 2005b). Among 20 different Cr compounds tested, strontium chromate induced the highest number of bronchial carcinomas, followed by zinc chromate and lead chromate (Levy et al., 1986). Levy and Venitt reported squamous metaplasia is increased in rats exposed to Cr(VI)-materials but not increased in rats exposed to Cr(III) materials. Of the rats exposed to Cr(VI), only those receiving insoluble materials developed bronchial squamous carcinoma (Levy and Venitt 1986).

Evidence from cell culture studies

The carcinogenicity of chromium has also been demonstrated in many cell culture studies. Cr(VI) compounds have the ability to induce cellular transformation in various cell lines (Patierno et al., 1988; Elias et al., 1989; Xie et al., 2007;

Rodrigues et al., 2009). Recently, multiple studies have shown lung epithelial BEAS-2B cells or BEP2D cells can be transformed by Cr(VI) compounds (Azad et al., 2010; Park et al., 2016; Sun et al., 2011; Xie et al., 2007). Moreover, tumor formation was found when Cr(VI)-transformed cells were injected into nude mice (Rodrigues et al., 2009; Sun et al. 2011, Wang et al. 2011). Cell culture studies further confirmed that particulate Cr(VI) is more carcinogenic than soluble Cr(VI). Elias et al. found chromate pigments containing Zn or Pb with moderate to very low water solubility can induce neoplastic transformation in SHE cells (Elias et al., 1989). Other studies found particulate lead chromate is more cytotoxic and genotoxic to human lung cells than soluble sodium chromate (Wise et al., 2002; Wise et al., 2006a). These studies have shown Cr(VI) has carcinogenic potential and particulate chromium is more carcinogenic, but further mechanistic information is still under investigation.

Characteristics of Cr-induced lung tumors

Pathological examination showed Cr-induced lung tumors were mainly squamous cell carcinoma, and a small part was small cell carcinoma and adenocarcinoma (Ewis et al., 2001; Ewis et al., 2006; Ishikawa Y et al., 1994a; Ishikawa Y et al., 1994b; Kondo et al., 1997). Kondo et al. found precancerous manifestations of atypical hyperplasia and squamous metaplasia in bronchial biopsy specimens of follow-up chromium workers, and with the progression of bronchial epithelial malignancy, the accumulation of chromium in corresponding parts increased significantly (Kondo et al., 2003). Cumulative Cr exposure is

strongly associated with lung cancer, and lung cancer mortality increases with the duration of Cr exposure (Davies et al., 1984; Gibb et al., 2000; Luippold et al., 2003). Pathological examination revealed Cr particles deposited at the bronchial bifurcations, which are the main sites of Cr-induced tumor formation (Ishikawa et al., 1994a). Kondo et al. found the deposition site of inhaled Cr in the lung was the bronchial stroma, not the epithelium, and accumulated at higher levels in the bronchioles and subpleural areas of the lung (Kondo et al., 2003).

Little evidence of mutations in key oncogenes or tumor suppressor genes has been found in molecular studies in Cr-induced tumors. Ewis et al. found no point mutations at key positions in the Ha-ras and Ki-ras oncogenes in chromate-associated lung cancer samples (Ewis et al., 2001). This study suggests point mutation-activated Ras oncogene does not play a major role in the oncogenic mechanism of chromate-induced lung cancer. Kondo et al. found a lower rate of missense mutations in p53 in chromate lung cancer samples than in lung cancer patients who had not been exposed to chromate, and did not find base changes in p53 that are common in lung cancer (Kondo et al., 1997). Studies have found microsatellite instability and epigenetic changes in chromate lung cancer (Takahashi et al., 2005a; Kondo et al., 2006). Takahashi et al. found the majority of chromate-associated lung cancers exhibited two or more loci of microsatellite instability (MSI) compared with chromate-naïve lung cancer patients. In addition, the length of chromate exposure was associated with the incidence of MSI. This study suggests the carcinogenic mechanism of chromate lung cancer may be different from that of non-chromate lung cancer (Takahashi et al., 2005a).

Takahashi et al. found the frequency of replication errors in chromate lung cancer was very high, and the inhibition rate of DNA mismatch repair genes hMLH1 and hMSH2 proteins in chromate lung cancer was significantly higher than that in non-chromate lung cancer. This study demonstrates a strong correlation between inactivation of hMLH1 expression and microsatellite hyperinstability in chromate lung cancer and speculates that inhibition of hMLH1 protein causes genetic instability in chromate lung cancer (Takahashi et al., 2005a). Ali et al. found the methylation rates of CpG islands in APC, MGMT, and hMLH1 genes in chromate lung cancer were significantly higher than those in non-chromate lung cancer (Ali et al., 2011). Kondo et al found decreased expression and aberrant methylation of p16 in chromate lung cancer (Kondo et al., 2006). These studies suggest methylation of certain tumor suppressor genes may be associated with genomic instability in chromate lung cancer. In addition, one study found the expression of the anti-apoptotic protein surviving was decreased in small cell lung cancer type chromate lung cancer, but not P53 (Halasova et al., 2010). Pulmonary surfactant protein is important for normal lung function and clearance of dust from the upper respiratory tract (Griese, 1999). Ewis et al. found the chromate lung cancer group had significantly higher surfactant protein B variants (deletions/insertions) than the non-chromate lung cancer group, healthy individuals, and chromate workers without lung cancer (Ewis et al., 2006). The mutation of pulmonary surfactant protein B leads to damage of the pulmonary surfactant system and affects the clearance of chromium particles in the respiratory tract, which is considered to be related to the occurrence of lung cancer caused by chromate (Ewis et al., 2006).

Proposed mechanism of chromium-induced carcinogenesis

Research into the carcinogenic mechanism of Cr(VI) has been ongoing for decades since the IARC identified chromium and chromium compounds as carcinogens. The exact mechanism of Cr(VI) carcinogenesis and its details have not yet emerged. In the following sections, we discuss the key features that have been studied in these oncogenic drivers and the events that led to their development.

The role of physicochemical properties of Cr in Cr-induced carcinogenesis

The physicochemical properties of Cr play a crucial role in the mechanism of Cr(VI)-induced carcinogenesis. Uptake and metabolism are important aspects of Cr(VI) carcinogenicity. Studies have shown Cr(VI) compounds partially dissolve extracellularly to form metal cations and chromate oxyanions (Wise et al., 1993; Xie et al., 2004). Chromate is structurally similar to sulfate and phosphate, which makes it easy to enter cells through anion transport channels (Wiegand et al., 1985; Sehlmeyer et al., 1990; Alexander and Aaseth, 1995). Inside the cell, Cr(VI) is rapidly reduced to Cr(III), forming a stable complex with proteins and DNA, which causes high accumulation of metals in cells (Sehlmeyer et al., 1990). This metabolic process is performed by naturally occurring intracellular antioxidants such as cysteine, ascorbate and glutathione (Suzuki and Fukuda, 1990; Standeven and Wetterhahn, 1991; Standeven and Wetterhahn, 1992; Quievryn et al., 2001). Other potential intracellular Cr(VI) reducing agents include cytochrome P450 reductase, mitochondrial electron transport complexes, aldehyde oxidase,

and glutathione reductase (Mikalsen et al., 1989; Ryberg and Alexander, 1984; Banks and Cooke, 1986; Shi and Dalal, 1989). Reactive oxygen species released during the reduction process can cause oxidative damage to key molecules in cells, including DNA, RNA, proteins, and lipids (Leonard et al., 2004; Wang et al., 2011). Cr(V) and Cr(IV) are produced during the reduction process. The reactive intermediates directly interact with DNA to form Cr-DNA adducts (Snow and Xu, 1991; Bridgewater et al., 1994; Zhitkovich et al., 1995; Quievryn et al., 2002). It is generally accepted that the reduction process is a critical part of Cr(VI) carcinogenesis. However, if chromate particles are phagocytosed into cells, there appears to be no toxic effect as well as no apparent effect of the cation (Xie et al., 2004; Wise et al.,1993).

The solubility of Cr compounds is an important factor affecting the carcinogenicity of Cr. Epidemiological studies have shown insoluble chromate is more carcinogenic than soluble chromate, as evidenced by reduced lung cancer incidence among chromate workers after the removal of lime from the production process, thereby eliminating the production of insoluble calcium chromate (Davies et al., 1991). Experimental studies also support that the solubility of chromium affects its carcinogenic potential. Several studies have shown particulate Cr(VI) induces tumor formation in rat lungs when administered as intrabronchial particulates (Balansky et al., 2000; Levy and Venitt, 1986; Levy et al. 1986), but soluble Cr(VI) did not induce an increase in tumor formation (Levy et al., 1986). A cell experiment found particulate Cr(VI) induces tumor transformation in C3H/10T1/2 cells, while soluble Cr(VI) does not (Patierno et al., 1988).

Cr(VI)-induced DNA damage and chromosome instability

Cr(VI) has complex genotoxicity, which is characterized by damage to DNA bases and sugar-phosphate backbone (Tsapakos and Wetterhahn 1983, Gulanowski et al., 1992; Voitkun et al., 1998). The mechanism of Cr-induced formation of DNA damage can involve Cr-DNA interactions (direct), reactive oxygen species (ROS) (indirect) or carbon radicals (indirect) (Sugden and Stearns, 2000). Reduction of Cr(VI) can lead to the generation of various lesions, including oxidized bases, Cr-DNA base/phosphate adducts, protein-Cr-DNA cross-links (Cr-DPC), Asc-Cr-DNA plus complexes, DNA–DNA interstrand crosslinks and DNA strand breaks (Stearns and Wetterhahn, 1994; Stearns et al., 1994; Zhitkovich et al., 1996; Arakawa et al., 2000; Bridgewater et al., 1994; Casadevall and Kortenkamp, 1995; Casadevall et al., 1999; Stearns et al., 1995). DNA double strand breaks after Cr(VI) exposure are well documented (Qin et al., 2014; Xie et al., 2005; Wise et al., 2010).

If left unresolved or repair fails, DNA double strand breaks can result in chromosomal instability (Masuda and Takahashi, 2002). Chromosome instability is a hallmark of human tumors. Chromosomal instability is present in most lung cancers and has been detected in chromate-induced tumors (Maeng et al., 2004). Chromosomal instability can be a numerical change or a change in chromosome structure. This dissertation focuses on structural chromosomal instability.

Structural chromosomal instability

Structural chromosomal instability involves changes in the physical

structure of the genome, usually manifested as nucleotide deletions, chromosomal breaks, unequal exchanges of genetic material or translocations between two chromosomes (Albertson et al., 2003). Structural chromosomal instability has been studied in chromate workers. Conventional Giemsa staining and fluorescence in situ hybridization (FISH) have been used for chromosomal aberration analysis. Maeng et al. found blood Cr concentrations were statistically correlated with the frequency of chromatid exchange and the total frequency of chromosome/chromatid breaks and exchanges, as measured by Giemsa staining. Meanwhile, the frequency of translocations, insertions and acentric fragments detected by the FISH technique was significantly higher in Cr-exposed workers than in controls, also correlating with blood Cr concentrations (Maeng et al., 2004). Halasova et al. found total chromosomal aberrations were higher in exposed individuals than in controls among welders exposed to hexavalent chromium for a long time, and that the number of chromosomal types of breakage was almost twice as high in exposed individuals (Halasova et al., 2008). Moreover, Chromatid-type aberrations are positively correlated with blood chromium levels (Halasova et al., 2012).

Cell culture studies have provided substantial data supporting Cr(VI)-induced structural chromosomal instability. Chromosomal aberrations increase in a concentration-dependent manner in cultured cells after exposure to Cr (Wise et al., 2002; Wise et al., 2003; Wise et al., 2006a; Xie et al., 2005; Xie et al., 2009; Qin et al., 2014). Both particulate and soluble Cr(VI) cause chromosomal aberrations in cultured cells, as demonstrated by numerous studies. Chromosome

damage profiles in human lung cells were similar after exposure to lead chromate and sodium chromate, with chromatid lesions being the most common type. Aberrations become more complex with increasing concentrations, with damage to entire chromosomes such as isochromatid lesions, chromatid exchanges and dicentric chromosomes (Wise et al., 2002; Wise et al., 2006). Studies have found that chromosomal instability caused by soluble and particulate Cr(VI) is different. Chromosomal aberrations increased in human lung cells after 24 h exposure to sodium chromate but decreased over time after 48 h or 72 h exposure (Wise et al., 2006; Holmes et al., 2006). By contrast, in human lung cells exposed to particulate Cr(VI), such as lead chromate or zinc chromate, chromosomal aberrations increased with prolonged exposure (Wise et al., 2006; Holmes et al., 2006). However, another study found sodium chromate induced more chromosomal aberrations in human urothelial cells after 120 h exposure than 24 h exposure (Wise et al., 2016). Xie et al. demonstrated Cr(VI) can induce different levels of chromosome damage in different cell lines. This study found differences in chromosomal aberrations induced by particulate Cr(VI) exposure, but not after soluble Cr(VI) exposure (Xie et al., 2015). Although chromosomal aberrations caused by soluble or particulate chromium are not entirely consistent across cell lines and exposure times, these studies demonstrate chromium causes structural chromosomal instability. There are also differences in the chromosomal aberration potentials of different insoluble Cr(VI) compounds. The highest levels of chromosomal aberrations were found with zinc chromate, the lowest with lead chromate, while the effects of barium chromate were intermediate (Wise et al.,

2004; Wise et al., 2010).

Substantial evidence suggests Cr(VI)-induced carcinogenesis is driven by genomic instability. However, the exact mechanism is unclear. Chromosome instability appears to play a role in this complex molecular mechanism. This project focuses on the mechanisms of Cr(VI)-induced structural chromosomal instability, in particular the effect of Cr(VI) on high-fidelity DNA repair.

Mechanism of Cr-induced structural chromosome instability

Cr-induced DNA double strand breaks

DNA double strand breaks are the most dangerous DNA lesions that arise when two complementary strands of the DNA duplex are simultaneously damaged in proximity (within 10 base pairs) and physically dissociated from each another. Many exogenous DNA damaging agents, including anticancer chemotherapeutic drugs (Chen and Stubbe, 2005; Nowosielska and Marinus, 2005; Singh and Krishna, 2005) and ionizing radiation (IR) (Milligan et al., 1995), can cause DNA double strand breaks. Endogenous DNA double strand breaks generally result from DNA replication through single stranded lesions and mechanical stress (Aylon and Kupiec, 2004). These breaks can be indirectly produced through stalled or collapsed replication forks when replication forks encounter single strand breaks or DNA crosslinks (Friedberg et al., 2006). For a defined biological purpose, DNA double strand breaks also spontaneously occur in meiosis and V(D)J recombination to initiate recombination (Lieber et al., 2003).

Cr(VI) induces a spectrum of DNA damage that includes DNA single strand

breaks, Cr-DNA adducts and DNA-protein crosslinks (O'Brien et al., 2003). Although Cr(VI)-induced double strand breaks have not been investigated in vivo so far, a large number of cell culture studies have shown Cr(VI) induces the formation of double strand breaks (table 1.4). γ-H2AX foci formation and neutral comet assays are two methods that were used in these studies to measure DNA double strand breaks. H2AX, a histone protein, gets phosphorylated at Ser 139 in response to DNA double strand breaks (Fernandez-Capetillo et al., 2004). Phosphorylated H2AX forms foci at the sites of DSBs and the number of γ-H2AX foci closely correlates with the amount of expected DNA double strand breaks induced by IR (Rogakou et al., 1999). Another study observed a direct correlation between the number of γ-H2AX foci and DNA double strand breaks suggested each γ-H2AX focus may represent an individual break (Sedelnikova et al., 2002). Therefore, the formation of γ-H2AX foci is considered a quantitative marker of DNA double strand breaks. Walkman et al. reported potassium chromate induces a significant increase of γ-H2AX foci in HeLa cells (Wakeman et al., 2004). Ha et al. found γ-H2AX foci formation in sodium chromate treated human dermal fibroblasts (Ha et al., 2004). Xie et al. discovered lead chromate induces DNA double strand breaks in human lung cells (Xie et al., 2005). Particulate and soluble Cr(VI) compounds induced similar levels of DNA double strand breaks in human bronchial fibroblasts (Xie et al., 2005; Wise et al., 2010).

The mechanism by which Cr(VI) induces DNA double strand breaks is still unclear. Studies suggest Cr(VI)-induced DNA double strand breaks are produced through an indirect mechanism because DNA double strand breaks produced by

Cr(VI) are cell cycle stage-specific. These breaks appear in the late S phase or G2 phase, but not G1 phase indicating they occur as a consequence of DNA replication or repair in some way (Wakeman et al., 2004; Ha et al., 2004; Xie et al., 2009; Peterson-Roth et al., 2005; Reynolds et al., 2007). Wakeman et al. found short time (4 h) exposure to high concentrations of potassium chromate (up to 80 uM) induced γ-H2AX to appear in the S phase (Wakeman et al., 2004). Ha et al. found γ-H2AX appeared in S phase after 3 hours of 200uM sodium chromate exposure (Ha et al., 2004). However, Xie et al. found γ-H2AX to appear in the G2 phase after 24-hour exposure to low concentrations (0.2-0.5ug/cm^2) of zinc chromate (Xie et al., 2009). Cr-DNA adducts are the most commonly implicated form of Cr(VI)-induced DNA damage to precede the breaks thought to occur through a stalled replication fork (Holmes et al., 2008). It has been argued the breaks occur from the mishandling of Cr-DNA damage through mismatch repair (MMR) (Peterson-Roth et al., 2005; Reynolds et al., 2007; Reynolds et al., 2009). It is also possible that they manifest through the mishandling of single strand breaks that are frequently produced after Cr(VI) exposure. Such causes are consistent with the breaks being indirectly produced and with their cell cycle specificity.

Table 1.4 Cr(VI) Induces DNA Double Strand Breaks in human cell cultures.

Chemical	Concentration	Treat Time	Model System	Assays	Summary of Effects	Ref
Sodium chromate	3-6 uM	1-3 h	Normal human dermal fibroblasts	Neutral comet assay,	DNA double strand breaks are generated during Cr(VI) treatment. Cr(VI)-induced γ-H2AX production is S phase specific and is absent after serum starvation.	Ha et al., 2004
Potassium chromate	5-80 uM	30 min – 24 h	HeLa cells	Neutral comet assay, Immunostaining for γ-H2AX foci	Cr(VI) treated cells are typical “comet tails” characteristic of DNA strand breaks and Cr[VI] induced a significant increase of cells with γ-H2AX foci.	Wakeman et al., 2004
Lead chromate	0.1-5 ug/cm²	24 h	WTHBF-6 human lung fibroblasts	Neutral comet assay, Western blot analysis for pATM, Immunostaining for γ-H2AX foci	Cr(VI) induced DNA double strand breaks concentration-dependent increase, and actived ATM and γ-H2AX proteins.	Xie et al., 2005
Potassium chromate	0.2-5 uM	3 h	IMR90 human lung fibroblasts, human lung epithelial cells	Immunostaining for γ-H2AX, and 53BP1 foci in cyclin B1 expressing cells	Cr(VI)-induced DNA double strand breaks occurred in the G2 phase. Preloading ascorbate induced increases in γ-H2AX foci formation and micronucleus formation.	Reynolds et al., 2007
Lead chromate	0.1-1 ug/cm²	24 h	WTHBF-6 human lung fibroblasts	Neutral comet assay	Cr(VI) induced DNA double strand breaks concentration-dependent increase.	Xie et al., 2008

Zinc chromate	0.1-0.5 ug/cm²	24 h	WTHBF-6 human lung fibroblasts	Immunostain-ing for γ-H2AX, Flow cytometry for cell cycle analysis and γ-H2AX	Cr(VI) induced a G2 arrest. Cr(VI)-induced DNA double strand breaks occurred in the G2/M phase.	Xie et al., 2009
Barium chromate Lead chromate Zinc chromate Sodium chromate	0.01-1 ug/cm² 0.01-1 ug/cm² 0.1-0.5 ug/cm² 0.05-5 uM	24 h	WTHBF-6 human lung fibroblasts	Immunostain-ing for γ-H2AX	All chromium compounds caused concentration-dependent increases in DNA double-strand breaks. There were no significant differences in the ability of the chromium compounds to cause DNA double-strand breaks.	Wise et al., 2010
Zinc chromate	0.1-0.3 ug/cm²	24-120 h	WTHBF-6 human lung fibroblasts	Neutral Comet assay	Cr(VI) induces DNA double strand breaks in human lung cells in a concentration-dependent manner.	Qin et al., 2014
Potassium chromate	5-20 uM	3-6 h	H460 human lung epithelial cells; IMR90 normal human lung fibroblasts MEFs	WB for γ-H2AX, Immunostain-ing for γ-H2AX, 53BP1 and H3K9me3	Cr(VI) induced DNA double strand breaks increase in a concentration-dependent manner. Cr(VI)-induced DNA double strand breaks produced in the G2 phase and were located in euchromatic DNA.	DeLoughery et al., 2015
Sodium chromate	1-5 uM	24 and 120 h	HUC; hTERT-immortalized human urothelial cells	Immunostain-ing for γ-H2AX	Cr(VI) induced DNA double strand breaks increase in concentrationand time dependent manner.hTERT-status did not affect the extent of Cr-induced DNA damage.	Wise et al., 2016

DNA double strand break repair

Unrepaired or misrepaired DSBs can lead to the accumulation of total chromosomal rearrangements and mutations, leading to loss of genetic information. There are two main repair pathways for repairing DSBs: classical non-homologous end joining (c-NHEJ) and homologous recombination (HR). The choice of pathway depends mainly on the cell cycle stage and the presence of homologous sequences that can be used as templates for repair (Hustedt and Durocher, 2017). Classical non-homologous end joining (c-NHEJ) typically involves several iterative steps of DNA end-processing at a double strand break and ligates the broken ends back together, eliminating the requirement of a homologous template (Pannunzio et al., 2018). It is active throughout the cell cycle but is especially important during the G0 and G1 phases (Hustedt and Durocher, 2017). DSB ends joined by c-NHEJ may cause additions or losses of nucleotides, thus allowing a degree of genetic variability that is critical for physiological processes such as V(D)J and class-switching recombination (Bétermier et al., 2014; Pannunzio et al., 2018). In contrast, HR is generally a high-fidelity repair pathway because it utilizes homologous sequences as repair templates (Lisby and Rothstein, 2015). It functions only in the late S and G2 phases of the cell cycle when sister chromatids are available as repair templates (Hustedt and Durocher, 2017). In addition, there are two DNA repair pathways that can be used to repair double strand breaks that result in lower genomic fidelity, including single strand annealing (SSA) and alternative end joining (Alt-EJ). While both pathways are considered error-prone, they lead to different outcomes and thus their contributions

to genomic instability are unequal.

Homologous recombination repair

An early determinant of DSB repair pathway choice is DNA end resection—processing of DNA ends to generate 3' single strands, which are required for HR but inhibit c-NHEJ. At the initiation of HR repair, the ends of the double strand break are recognized and excised to form 3' single-stranded DNA (ssDNA) overhangs (Mladenov et al., 2016). Single-stranded DNA generated by excision of DSB ends provides substrates for the RAD51 filaments required for assembling strand invasion; in addition, the invaded 3' ends provide primers for repair synthesis of intact duplex templates. Initial processing of the ends involves the MRN complex, which includes MRE11, RAD50 and NBS1, and the CtIP protein. The MRN complex binds to the ends of the double strand break and resects the ends through the nuclease activity of MRE11 (Williams et al., 2007; Williams et al., 2008). CtIP stimulates the endonuclease activity of MRE11 in the MRN complex (Cannavo et al., 2014). After endonuclease cleavage, the resection proceeds in both directions. The exonuclease activity of MRN proceeds in the 3'-5' direction, while EXO1 and BLM/DNA2 nucleases catalyze long-range 5'-3' excision (Garcia et al., 2011; Shibata et al.,2013; Nimonkar et al., 2011).

ATM is activated by the MRN complex at the site of DNA damage and autophosphorylates at S1981 (Bakkenist and Kastan, 2003; Myler et al., 2017). ATM plays a key role in DNA repair by phosphorylating the C-terminal tail of histone variant H2AX on serine 139 (Burma et al., 2001). It also activates the

endonuclease activity of MRE11 by phosphorylating CtIP, which triggers DSB end resection (You et al., 2009). Single-stranded DNA generated by excision is subsequently coated with replication protein A (RPA), which is recruited to DSBs by CtIP (Sartori et al., 2007).

The invasion of 3' single-stranded DNA into the homologous duplex is the decisive step in HR. This process is guided by the strand-exchange recombinase RAD51. RAD51 is a DNA-dependent ATPase that forms nucleoprotein filaments with DNA, which is a homolog of the bacterial RecA protein (Shinohara et al., 1992). RPA-coated single-stranded DNA is a substrate for the recruitment of RAD51. RAD51 is recruited and loaded onto ssDNA while replacing RPA, forming a helical nucleoprotein filament responsible for recognizing homologous sequences and invading template DNA strands (Baumann et al., 1996; Sung and Robberson, 1995). This is a crucial step in HR repair. RAD51 filaments begin searching for homology in the other strand after binding to single-stranded DNA. The DNA strands invade at positions of homology, forming heteroduplex DNA junctions called D-loops (Sung et al., 2003; Renkawitz et al., 2014).

After nuclear filaments invade the donor duplex and subsequent D-loop formation, the repair uses the homologous sequence as a template for synthesis, leading to the formation of the Holliday junction (Constantinou et al., 2001). After Holliday junctions are resolved by resolvase proteins producing crossover or non-crossover products that are ligated, HR repair completes the accurate recovery of DNA double strand breaks (Heyer et al., 2004; Wyatt and West, 2014).

HR utilizes homologous sequences to repair DNA breaks, preventing structural chromosomal instability and maintaining high genomic fidelity. It is an error-free DNA double strand break repair mechanism.

Repair of Cr(VI)-induced DNA double strand breaks

c-NHEJ and HR repair are the main repair pathways to repair DNA double strand breaks. However, the mechanism of Cr(VI)-induced DNA double strand break repair remains incompletely defined. Bryant et al. found Cr(VI) causes DNA double strand breaks and triggers RAD51 foci formation and HR repair in Chinese hamster cells; in addition, HR repair protein XRCC3-deficient and BRCA2-deficient HR-deficient cells both were hypersensitive to Cr(VI) (Bryant et al., 2006). However, these authors did not detect c-NHEJ repair. In another study, Stackpole et al. found both RAD51C-deficient and XRCC3-deficient Chinese hamster cells had increased cytotoxicity and chromosomal aberrations after lead chromate exposure, relative to wildtype and cDNA-complemented cells (Stackpole et al., 2007). Camyre et al. found Ku80 deficiency does not affect chromate-induced cytotoxicity and chromosome damage in Chinese hamster ovary cells, suggesting c-NHEJ does not prevent Cr-induced chromosomal instability (Camyre et al., 2007). Tamblyn et al. found Mus81-deficient cells are more sensitive to the cytotoxic effects of Cr(VI) as well as Cr(VI)-induced growth arrest compared with wild-type cells. Mus81-deficient cells exhibited marked γ-H2AX elevation and displayed increased chromosome instability following Cr(VI) exposure compared with wild-type cells. Mus81 is one of the resolvases of Double Holliday junction

resolution of the HR repair pathway (Wyatt et al., 2013). Taken together, these studies demonstrate the importance of HR repair in the repair of Cr-induced DNA double strand breaks and in preventing Cr-induced structural chromosome instability in mammalian cells, whereas c-NHEJ does not prevent Cr-induced chromosome instability.

Cancer and whales

Peto's paradox

Cancer afflicts most vertebrates and appears to occur most frequently in mammals (Galis and Metz, 2003). The similarity of basic carcinogenetic mechanisms in mammals and the conservation of many tumor suppressor systems have enabled scientific research to model human disease using rodents and other mammals (Leroi et al., 2003). In the prediction of cancer risk, it is generally believed that the incidence of cancer is positively correlated with body size and age (Caulin and Maley, 2011). Cancer occurs when cells divide and mutate. Cell division is normal in organisms, as is somatic mutation. Most of the time, somatic mutations are either harmless or the body repairs them. If these mutations cannot be repaired, cancer may develop. Because cancer develops through the accumulation of somatic mutations, each proliferating cell is at risk of malignant transformation assuming that all proliferating cells have similar odds of mutation. Therefore, if an organism has more cells, i.e., more chances to initiate tumors, the likelihood of developing cancer should increase. Likewise, if an organism lives longer, its cells have more time to accumulate mutations. The likelihood of

carcinogenesis is therefore an increasing function of age, so an organism's lifetime cancer risk should also increase with its lifespan (Frank et al., 2007). If these assumptions hold, cancer incidence can be predicted by its positive correlation with body size and age (Caulin and Maley, 2011). However, it is well known that, at the cross-species level, larger organisms generally have longer lifespans (Speakman, 2005). In 1975, Peto et al. found at the species level, the incidence of cancer appears to be independent of the number of cells in an organism (Peto et al., 1975). For example, although whales have more cells than humans, cancer rates in whales are far lower than in humans (Nagy et al., 2007). If the probability of cancer throughout the cell is constant, then the incidence of cancer in whales should be higher than in humans. There appears to be no correlation between body size, longevity and cancer across species, with a lack of this relationship known as Peyto's paradox. In fact, cancer rates vary to some extent across mammalian species.

Whales and cancer

Whales are mammals that live in the ocean. The baleen whale suborder contains the largest and longest-lived mammals on earth. The blue whale (Balaenoptera musculus) included in this suborder is the largest mammal on earth. Baleen whales have long lifespans, most with an estimated lifespan of 80-100 years, and bowhead whales over 200 years (George et al., 1999). Despite their large size and longer lifespans compared with humans', baleen whales appear to have significantly lower rates of cancer than humans. Cancer rates in wild whales

are generally low (0.7%-2%) (Geraci et al., 1987; Newman and Smith, 2006). So far, reports of whale cancer are very limited, and the data available are from whale autopsy reports. The low number of reported cancers in whales may also be related to the longevity of whales. In 1987, Geraci et al. reported 14 tumors, including 6 papillomas, 5 leiomyomas, 2 adrenal adenomas, and one bronchial carcinoma, in more than 1800 free-range and captive cetaceans (Geraci et al., 1987). In 2006, a literature review by Newman and Smith documenting neoplasia in marine mammals revealed only 26 documented cases in baleen whales, including 11 in fin whales and 3 in humpback whales, 10 in blue whales, 1 in sei whales, and 1 in bowhead whales which reported lipoma in bowhead whale liver (Newman and Smith, 2006). Therefore, the large size and long lifespan of baleen whales, but a low incidence of cancer, reflects the Peto's paradox.

Potential mechanisms for evading cancer

The mechanisms by which baleen whales evade cancer are currently unclear. Blue whales with 1,000 times more cells than humans do not show an increased risk of cancer, suggesting that natural mechanisms can suppress cancer 1,000 times more effectively than found in human cells (Caulin and Maley, 2011). Peto suggested that evolution may be responsible for the differences in the rate of carcinogenesis in individual cells across species (Nunney, 2013). When individuals in a population are under selective pressure for cancer risk, the population has to evolve some cancer suppressors as an adaptation or suffer possible extinction (Tollis et al., 2017). Genomic analysis revealed that the African

elephant (*Loxodonta Africana*) genome contains 20 copies of the tumor suppressor gene TP53 (40 alleles), whereas humans have 1 copy of TP53 (2 alleles) (Abegglen et al., 2015). Blind mole rats, subterranean rodents with significant anti-cancer ability, have amino acid changes in p53 protein corresponding to mutations commonly found in human tumors, which weaken the apoptotic function of p53 in favor of a reversible cell cycle stasis (Ashur-Fabian et al., 2004; Avivi et al., 2005; Kato et al., 2003). A unique splice variant of heparanase with antitumor properties has also been identified in blind mole rats (Nasser et al., 2009). Recent studies have found evidence of some cancer-suppressing mechanisms in baleen whales. There is a large proportion of transposable elements (TEs) in the bowhead whale genome (~32%), especially the long-inserting nuclear element LINE-1 (Keane et al., 2015). Slow mutation rates are found in cetaceans, which may limit tumor cell generation and cancer progression (Tollis et al., 2019; Jackson et al., 2009). Sequencing of the bowhead whale genome identified specific mutations in ERCC1, a gene associated with cancer and aging, and gene duplications in PCNA, a gene associated with DNA repair, cell cycle, and aging (Keane et al., 2015). The turnover rate of tumor suppressor genes is nearly 2.4-fold higher in cetaceans than in most other mammals and highest in baleen whales, which may have favored the evolution of their anticancer resistance traits (Tejada-Martinez et al., 2021).

Chromosomal instability is one of the hallmarks of cancer. In some comparative studies of whale cells and human cells, it was found whale cells are more resistant to chromium-induced chromosomal instability than human cells (Li Chen et al., 2009a; Li Chen et al., 2009b; Li Chen et al., 2012; Wise et al., 2015).

Acute particulate Cr(VI) exposure produces less chromosomal instability in North Atlantic right whale (*Eubalaena glacialis*) lung fibroblasts compared with human lung fibroblasts (Li Chen et al., 2009a). Reduced Cr(VI)-induced chromosome instability was detected in sperm whale (*Physeter macrocephalus*) skin fibroblasts and fin whale (*Balaenoptera physalus*) skin fibroblasts compared with human skin fibroblasts (Li Chen et al., 2012; Wise et al., 2015). DNA repair is an important mechanism for maintaining chromosomal stability to prevent carcinogenesis. Genome analysis of bowhead whales identified gene duplications in the PCNA gene, which is involved in HR repair (Keene et al., 2015; Sebesta et al., 2013). High expression of HR repair genes was found in naked mole rats (*Heterocephalus glaber*), another long-lived species with a low incidence of cancer (MacRae et al., 2015). A recent study showed prolonged Cr(VI) exposure does not inhibit HR repair in North Atlantic right whale lung cells (Browning et al., 2017). Therefore, HR repair may be more efficient in whale cells and thus play an important role in counteracting Cr(VI)-induced chromosomal instability.

CHAPTER II

MATERIALS AND METHODS

Materials

Animals

12-week-old male and female Wistar rats (Envigo, Indianapolis, IN) were maintained under standard laboratory conditions. All animals were housed under a 12:12 hour light-dark cycle and provided food and water ad libitum. Animal procedures were approved by the Institutional Animal Care and Use Committee (IACUC) of University of Louisville, and followed the appropriate guidelines set forth by the American Veterinary Medical Association.

Cell lines

WTHBF-6 is an hTERT immortalized clonal cell line derived from human bronchial fibroblasts (Wise et al., 2004b). This cell line was developed by the Wise laboratory from primary lung fibroblasts derived from healthy lung tissue of a 67-year-old Caucasian man. Rat Lung Fibroblasts (RLF) (R506-05a) were purchased from Cell Applications (San Diego, CA), which are primary cells derived from normal rat lung. Bowhead whale primary lung fibroblasts (BHW200Lu) were utilized in this study. BHW200Lu is a primary cell line isolated from the lung of a subsistence-hunted bowhead whale in Barrow, Alaska.

Cell Culture

Dulbecco's Minimal Essential Medium and Ham's F12 (DMEM/F-12) 50:50 mixture, Dulbecco's phosphate buffered saline (PBS) 1X without calcium or magnesium, penicillin/streptomycin solution, glutagro supplement (200 mM), tissue culture dishes, flasks and plasticware were purchased from Corning (Corning, NY). Trypsin/EDTA (0.25%) and cosmic calf serum were purchased from Hyclone (Logan, Utah). Goat serum and sodium pyruvate (100 mM) were purchased from Lonza (Allendale, NJ). Rat fibroblast growth medium (R116-500), HBSS (062-100), Trypsin/EDTA (070-100), and Trypsin Neutralizing Solution (080-100) were purchased from Cell Applications (San Diego, CA).

Metal Preparation

Zinc chromate (CAS no. 13530-65-9; 99.7% purity) was purchased from Pfaltz and Bauer (Waterbury, Connecticut). Scintillation vials were purchased from Wheaton (Millville, NJ). Acetone was purchased from J.T. Baker (Philipsburg, NJ).

Antibodies

Anti-RAD51 antibody (sc-8349) was purchased from Santa Cruz (Dallas, TX). Anti-RAD51 antibody (PA5-27195) was purchased from Thermo Fisher (Carlsbad, CA). Anti-γ-H2AX antibody for immunofluorescence was purchased from Cell Signaling (Danvers, MA). Anti-cytokeratin antibody (C2931) was purchased from Sigma-Aldrich (St. Louis, MO). Anti-PMCA ATPase antibody (MA3-914) was purchased from Invitrogen (Grand Island, NY). Anti-γ-H2AX-

AF647 antibody (pS140) (560447) was purchased from BD Biosciences (Franklin Lakes, NJ). Fluorescent secondary antibodies were purchased from Life Technologies (Grand Island, NY).

Tissue embedding

Tissue Cassettes (18000-130) were purchased from VWR (Radnor, PA). Ethanol (2716) was purchased from Decon Labs (King of Prussia, PA). 10% neutral buffered formalin (16004-128) was purchased from VWR (Radnor, PA). Paraffin (39602004) was purchased from Leica (Deer Park, IL).

Hematoxylin and Eosin staining

Gill's Hematoxylin (3535-16) was purchased from Ricca Chemical Company (Arlington, TX) and Eosin (HT110116) was purchased from Sigma-Aldrich (St. Louis, MO). Xylene was purchased from Millipore (Billerica, MA). Permount mounting medium (17986-01) was purchased from Electron Microscopy Sciences (Hatfield, PA).

Immunofluorescence

Immunofluorescent staining of formalin-fixed paraffin embedded tissue samples.

The TrueBlack blocking buffer and background suppressor (23012) were purchased from Biotium (Fremont, CA). Sudan black B (0593) was purchased from VWR (Radnor, PA). Prolong Diamond Antifade Mountant with DAPI was purchased from Invitrogen (Grand Island, NY). Coverslips were purchased from

VWR (Randor, PA).

Immunofluorescent staining of cells.

Nunc Lab Tek II glass chamber slides were purchased from Thermo Fisher Scientific Inc. (Waltham, MA). FNC coating mix was purchased from AthenaFS (Baltimore, MD). 4% paraformaldehyde in PBS was purchased from Alfa Aesar (Ward Hill, MA) and Dulbecco's phosphate-buffered saline (10x) with magnesium and calcium was purchased from Corning (Corning, NY). Triton X-100 was purchased from Sigma-Aldrich (St. Louis, MO). Bovine serum albumin was purchased from EMD Millipore (Billerica, MA). Sodium azide was purchased from Amresco LLC (Solon, OH). Goat serum was purchased from Lonza (Allendale, NJ), and Prolong Gold Antifade Reagent with DAPI was purchased from Invitrogen (Grand Island, NY). Coverslips were purchased from VWR (Randor, PA).

Neutral Comet Assay

The comet assay electrophoresis system, lysis solution, comet slides, LM agarose and slide racks were purchased from Trevigen Inc. (Gaithersburg, MD). The dry bath incubator and slide warmer were purchased from Boekel Scientific (Feasterville, PA). Sodium chloride (NaCl), sodium acetate (NaOAc), glycine and the Millipore water system were purchased from EMD Millipore (Billerica, MA). Sodium hydroxide (NaOH), sodium dodecyl sulphate (SDS), hydrogen chloride (HCl), ammonium acetate and Tris(hydroxymethyl)aminomethane (Tris base), were purchased from J.T. Baker (Phillipsburg, NJ). Proteinase K was purchased

from Ameresco (Solon, OH). Ethylenediaminetetraacetic acid (EDTA) was purchased from Sigma-Aldrich (St. Louis, MO). Ethanol was purchased from Pharmco-AAPER (Hartford, CT). SYBR green was purchased from Life Science Tech (Grand Island, NY). The Comet IV software was purchased from Perceptive Instruments Ltd. (Edmunds, UK). Fluorescent microscopes were purchased from Olympus (Center Valley, PA).

Sister Chromatid Exchange

5-bromo-2'-deoxyuridine (BrdU) was purchased from Sigma-Aldrich (St. Louis, MO). Dulbecco's phosphate-buffered saline (10x) with magnesium and calcium was purchased from Corning (Corning, NY). Sodium chloride was purchased from EMD Millipore (Billerica, MA), and sodium citrate was purchased from J.T. Baker (Philipsburg, NJ). Hoechst 33258 pentahydrate was purchased from Invitrogen (Grand Island, NY).

Flow Cytometry

RNase A (BP2539100) was purchased from Fisher BioReagents (Hampton, New Hampshire). Mouse IgG1 kappa-AF647 Isotype (557714) was purchased from BD Biosciences (Franklin Lakes, NJ). Propidium Iodide (PI) (P3566) was purchased from Invitrogen (Eugene, Oregon). Rat serum was purchased from StemCell Technologies (Cambridge, Massachusetts).

Methods

Animal Models of Zinc Chromate Exposure

70 male and 70 female Wistar rats were utilized in our study. Twelve-week-old male and female Wistar rats were exposed to zinc chromate particles in saline solution or saline alone by oropharyngeal aspiration after brief 3% isoflurane (Henry Schein, 029405) anaesthesia. The rats were exposed to zinc chromate for 24 hours (Aim 1) or 90 days (Aim 2). In Aim 1, dose groups included 0, 0.2, 0.4, and 0.8 mg Cr/kg (body weight) with single administration for 24 hours. In Aim 2, dose groups included 0, 0.4, and 0.8 mg Cr/kg (body weight) once weekly administration repeated for 90 days. Animals were exposed for 24 hours or 90 days to evaluate the onset and persistence of the outcomes. At the end of each exposure time, animals were euthanized, and the lungs were isolated (Figure 2.1). The animal lungs in each group were used to measure chromium levels by ICP-MS. For 7 animals in each group, the isolated rat lungs fixed by formalin inflation were used for immunohistochemistry and H&E staining (Figure 2.2).

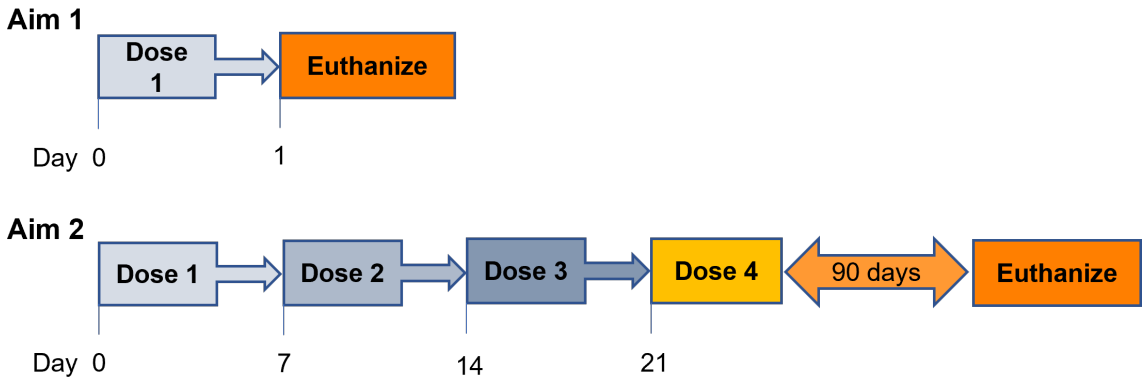

Figure 2.1. Single and repeated dosing regimens. In Aim 1, 12-week-old Wistar rats were treated with either 1 dose saline vehicle or zinc chromate and euthanized on Day 1. In Aim 2, 12-week-old Wistar rats were treated with once weekly administration for 90 days and then euthanized.

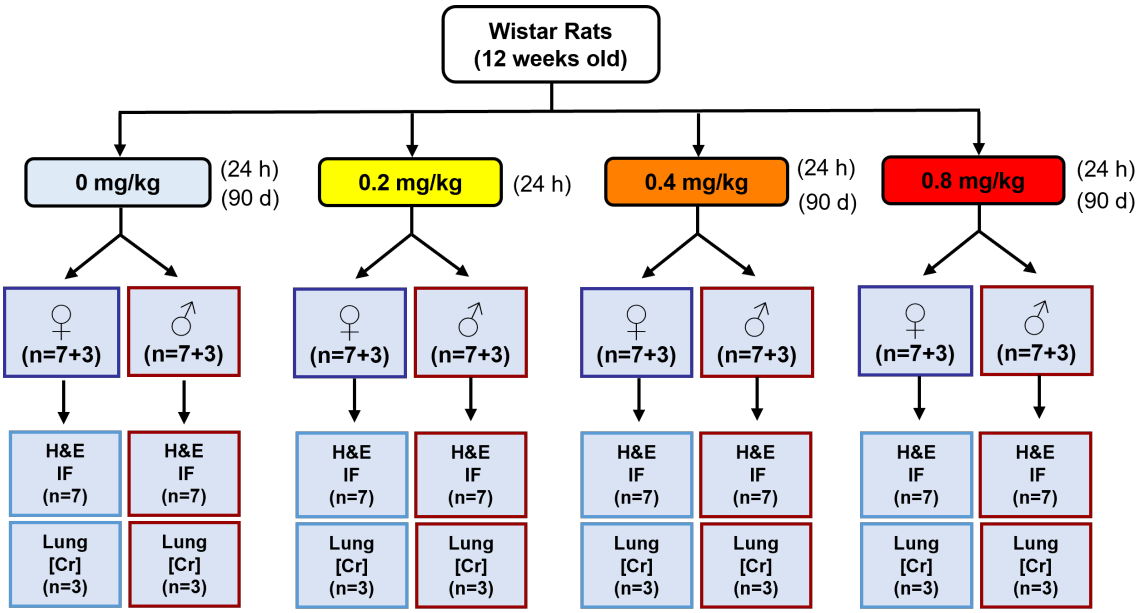

Figure 2.2. Rat grouping and outcomes examined. 12-week-old, male and female Wistar rats were treated with 0, 0.2, 0.4, or 0.8 mg Cr/kg (body weight) for 24 hours or 0, 0.4, or 0.8 mg Cr/kg (body weight) for 90 days. In every dose group, lung tissues from 7 rats were used for H&E staining and immunohistochemistry analysis, and lung tissues from 3 rats for zinc chromate accumulation measurements.

Sample collection

Upon euthanasia after intraperitoneal injection of a mixture of 90 mg/ml ketamine (University of Louisville Comparative Medicine Research Unit) and 10 mg/ml xylazine (Midwest Veterinary Supply), blood was collected and placed on ice. After perfusion with cold PBS, lungs were removed and sliced, and tissue was allocated for appropriate use. Samples for histology/immunohistochemistry were fixed with 10% neutral buffered formalin.

Preparation of lung sections for histology and immunohistochemistry

After fixation with 10% neutral buffered formalin for 24 hours, lung samples were stored in 75% ethanol for at least one hour and submitted to paraffin embedding (Table 2.1). After embedding, lung sections were cut at 5 microns on a microtome and affixed to slides.

Hematoxylin and eosin staining

Hematoxylin and eosin (H&E) staining provides a detailed representation of tissues with high-resolution for histopathological studies, thus allowing the identification of tissue abnormalities. H&E staining helps visualize otherwise transparent tissues under a microscope and is critical for tissue-based research in our Cr-exposed rat lung study. Lung sections were deparaffinized with xylene and rehydrated with an ethanol gradient to distilled water. Lung sections were then stained sequentially with Gill's Hematoxylin and eosin. After dehydration with an

ethanol gradient, coverslips were mounted with the Permount mounting medium (Table 2.2). The stained lung sections were analyzed by light microscopy.

Histological analysis

An Olympus light microscope with 10X, 20X and 40X objectives was used to analyze the amounts of macrophages and immune cells in H&E-stained rat lung tissue sections. We established a scoring system to analyze inflammation and determined the degree of inflammation according to this scoring system (Table 2.3). Each slide was scored based on the number and size of abnormal macrophages or inflammatory cells according to the scoring system.

Table 2.1. Paraffin embedding procedure.

75% Ethanol	60 minutes, 1x
85% Ethanol	60 minutes, 2x
95% Ethanol	60 minutes, 1x
95% Ethanol	Overnight at 4°C
100% Ethanol	30 minutes, 4x
1:1 Xylene: Ethanol	30 minutes, 1x
Xylene	30 minutes, 4x
Paraffin	30 minutes, 3x

Table 2.2. Hematoxylin and eosin staining steps.

Xylene	5 minutes, 2x
100% Ethanol	30 seconds, 2x
95% Ethanol	30 seconds, 2x
70% Ethanol	30 seconds, 1x
Distilled water	30 seconds, 1x
Gill's Hematoxylin	150 seconds, 1x
Distilled water	30 seconds, 1x
Acid Water Rinse	20 seconds, 1x
Distilled water	30 seconds, 1x
Bluing Reagent	40 seconds, 1x
Distilled water	30 seconds, 1x
80% Ethanol	40 seconds, 1x
Eosin	80 seconds, 1x
95% Ethanol	30 seconds, 1x
100% Ethanol	30 seconds, 4x
Xylene	5 minutes, 3x

Table 2.3. Macrophages and inflammatory cells scoring system.

Score	Condition
0	None
1	1-4 small areas
2	≥5 and <15 small areas
3	≥ 15 small or 1 moderate area
4	≥ 15 small and 1 moderate area
5	≥ 2 moderates plus any number of small areas
6	Widespread in ≥2 different pieces

The recorded “small area” indicated where macrophages or inflammatory cells are restricted to a limited, “small” area of the tissue. The “moderate” area is where macrophages or inflammatory cells appear in larger, contiguous sections of the tissue.

Cell culture

Cr(VI) is a human lung carcinogen. Epidemiological studies of chromate workers suggest that chromate-induced tumors are epithelial carcinomas, mainly squamous cell carcinomas (Hirose et al., 2002; Ishikawa et al., 1994a). Although squamous cell carcinoma originates in epithelial cells, Cr was found to accumulate in fibroblasts of the bronchial stroma rather than in epithelial cells (Kondo et al., 2003). These data suggest that fibroblasts accumulate Cr and may create a microenvironment for nearby epithelial cells that facilitates their transformation into cancer cells. Indeed, studies have shown fibroblasts play a key role in altering the cancer microenvironment by releasing growth factors, chemokines, and other carcinogenic components (Chen et al., 2014; Kalluri and Zeisberg, 2006).

Primary lung epithelial cells are difficult to use in culture because they rapidly reach replicative senescence. Thus, they cannot be maintained long enough for the exposure consistency required in this dissertation. The few immortalized lung epithelial cell lines that exist have abnormal karyotypes, making them unsuitable for chromosome instability studies. Our research considers the effect of Cr(VI) on chromosomes as the primary target of Cr(VI) exposure; therefore, currently available immortalized epithelial cells are not suitable for this work. Furthermore, as fibroblasts have been shown to be key targets of Cr(VI) exposure (Kondo et al., 2003), human bronchial fibroblasts (WTHBF-6) were used in this study (Wise et al., 2004b).

WTHBF-6 cells have normal growth parameters, a normal stable karyotype and cytotoxic and clastogenic responses to metals similar to primary cells (Wise

et al., 2004b). Cells were cultured as adherent monolayers in DMEM/F12 50:50, supplemented with 15% cosmic calf serum, 1% L-alanyl-L-glutamine, 1% penicillin/streptomycin, and 0.1 mM sodium pyruvate. Cells were maintained in a 5% CO_2-humidified environment at 37°C. They were fed every 48 h and sub-cultured at least once a week using 0.25% trypsin/1mM EDTA. All experiments were performed with logarithmically growing cells.

Rat lung fibroblasts (RLFs) were cultured as adherent monolayers in rat fibroblast growth medium. Cells were maintained in a 5% CO_2-humidified environment at 37°C. They were fed every 48 h and sub-cultured at least once a week. All experiments were performed on logarithmically growing cells.

BHW200Lu cells were utilized to study Cr(VI) genotoxicity in a species with a long life span and a low incidence of cancer. This cell line has a stable karyotype of 42 chromosomes. Cells were cultured as adherent monolayers in DMEM/F12 50:50, supplemented with 15% cosmic calf serum, 1% L-alanyl-L-glutamine, 1% penicillin/streptomycin, and 0.1 mM sodium pyruvate. Cells were maintained in a 5% CO_2-humidified environment at 33°C. They were fed every 72 h and sub-cultured at least once a week. All experiments were performed on logarithmically growing cells.

Treatment with particulate Cr(VI) compound

Insoluble Cr(VI) compounds are more carcinogenic than soluble Cr(VI) compounds, so particulate Cr(VI) compounds are considered to be the most toxic and carcinogenic (Levy et al., 1986; Levy and Venitt, 1986). In this dissertation, we

used zinc chromate as our representative Cr(VI) compound because it is the most potent form of particulate Cr(VI) (Wise et al., 2004a; Wise et al., 2010). Zinc chromate, a partially soluble particulate chromate compound that was shown alone by epidemiological studies to induce lung cancer (Kano et al., 1993). It has a wide range of industrial uses, especially as a rust inhibitor and pigment.

Zinc chromate was prepared according to our published methods (Xie et al., 2009) by washing twice with distilled water followed by two washes with acetone to remove all water soluble and organic components and allowing the particles to air dry. For treatment, zinc chromate was stirred in cold, sterile water on a stir plate at 4°C overnight and administered as a suspension of particles using a vortex. The particle size range of zinc chromate prepared using this method is between 0.2 and 2.3 um, with an average size of 1.7 um (Wise et al 2002). To account for treatment with a particulate compound, concentrations are expressed as ug/cm^2.

WTHBF-6 cells were treated at concentrations of 0.1-0.3 ug/cm^2 zinc chromate, rat lung cells were treated with 0.2 or 0.4 ug/cm^2 zinc chromate, and bowhead whale cells were treated with 0.1-0.4 ug/cm^2 zinc chromate. These concentrations are within the range of documented exposure levels (Danadevi et al., 2004; Ishikawa et al., 1994b). The cytotoxicity of these doses at various exposure times has been previously described (Holmes et al., 2010). While zinc chromate induces a time and concentration-dependent increase in cytotoxicity, plenty of cells survive the 120 h exposures (Holmes et al., 2010).

For animal treatment, zinc chromate was stirred in cold, sterile 0.9% sodium

chloride solution on a stir plate at 4°C overnight and administered as a suspension of particles using a vortex. The route of administration to animals was by oropharyngeal aspiration with zinc chromate suspension. The doses administered are as shown in Figure 1.1. This technique has been reported to avoid the loss of the dosing suspension in the gastrointestinal tract from swallowing by animals, thereby ensuring the most efficient delivery of the drug to the lungs (Rao et al., 2003). Vortex the zinc chromate solution for 10 s to suspend the particles before processing. Animals were removed from the chamber after brief anesthesia with 3% isoflurane. The nostrils were pinched, the tongue was squeezed out, and zinc chromate suspension or saline was instilled into the back of the animal's throat. After the animals took 6-7 deep breaths to ensure inhalation of the dosing suspension, the animals were returned to their cages.

Immunofluorescent staining

DNA damage response proteins, including γ-H2AX and RAD51, accumulate and/or modify near chromosomal DNA double strand breaks to form nuclear foci visible under a fluorescence microscope, which is helpful for the study of DNA damage and repair. Immunofluorescence was conducted as previously described with minor alterations (Xie et al., 2005).

Immunofluorescent staining of formalin-fixed paraffin embedded tissue samples

For γ-H2AX and RAD51 immunofluorescent staining, lung sections (5 microns thick) were rehydrated with xylene followed by incubation with an ethanol

gradient. 1 mM EDTA (pH 7.9) was used for antigen retrieval, which was performed in a vegetable steamer for 30 minutes, and slides were cooled at room temperature (RT) for 45 minutes. Slides were then rinsed 3 times for 5 minutes each with TBST. Slides were then blocked with TrueBlack blocking buffer for 15 minutes at room temperature and incubated with the primary antibody diluted with TrueBlack background suppressor overnight at 4°C. Anti-γ-H2AX antibody was used at 1:750, anti-RAD51 at 1:10000, anti-cytokeratin at 1:100, and anti-PMCA ATPase at 1:500. Next, slides were rinsed 3 times for 5 minutes each with TBST. Goat anti-rabbit Alexa Fluor 488 (1:500) and Goat anti-mouse Alexa Fluor 555 (1:500) were added to slides and incubated for 60 minutes at RT. Slides were then rinsed 3 times for 5 minutes with TBS. Next, slides were immersed in 3% Sudan black B with 70% ethanol for 20 minutes, followed by three washes with TBS for 5 minutes. The coverslips were mounted with DAPI. Nuclear foci were scored in 100 cells per concentration/time point by confocal microscopy.

Immunofluorescent staining of cells

For cells, immunofluorescence was conducted as previously described with minor alterations (Xie et al., 2005). Briefly, cells were seeded on glass chamber slides coated with FNC, allowed to re-enter logarithmic growth and treated with zinc chromate for either 24 or 120 h. At harvest, cells were fixed with 4% paraformaldehyde for 10 min, permeabilized with 0.2% Triton X-100 for 10 min and blocked with 10% goat serum in PBS for 1 h. For RAD51 foci, cells were fixed with 4% paraformaldehyde for 10 min, and permeabilized with 0.5% Triton X-100 for 30

mins. Cells were then incubated with anti-γ-H2AX (Cell Signaling 2577L; 1:100) or anti-RAD51 (Santa Cruz sc-8349; 1:200) antibodies at 4°C overnight, washed with PBS and incubated with Alexa Fluor 488 (1:2000) for 1 h. Cells were washed with PBS, and coverslips were mounted with DAPI. Nuclear foci were scored in 100 cells per concentration/timepoint by fluorescence microscopy. Results were expressed as the percentage of cells with >5 or >20 foci based on background levels such that negative controls had 5% or less of cells with this level. Images of 100 cells per concentration/timepoint were obtained under an Olympus microscope.

Confocal microscopy and image analysis

Confocal images were captured under an A1 confocal inverted Nikon Eclipse Ti microscope equipped with 20x and 100x Plan Fluor objectives. The acquired images were then denoised using the NIS-Elements software version AR 5.20.02. High magnification images (100x) were analyzed for foci counting. Region of interest (ROI) analysis was then conducted on images using the NIS-Elements software to measure signal intensity.

Neutral comet assay

The comet assay, also known as single-cell gel electrophoresis, is a method for measuring DNA strand breaks in eukaryotic cells. Under neutral and non-denaturing pH conditions, the intact DNA double helix remains supercoiled. In contrast, fragmented DNA resulting from double strand breaks can relax its

supercoiled structure and create differences in migration in an electrophoretic field. Therefore, the neutral comet assay allows the direct detection of DNA double strand breaks in individual cells.

The comet assay was performed as previously described (Xie et al., 2005) with some modifications. Briefly, logarithmically growing BHW200Lu cells were seeded into 6-well plates and treated with zinc chromate for 24 and 120 h after resting. After treatment, cells were washed, collected and resuspended in cold PBS. The cell suspension was then mixed with pre-warmed low-melting agarose at a 1:10 ratio and evenly spread onto comet slides, which were then placed on ice allowing cells to solidify. After complete solidification, cells were lysed by immersing the slides in freshly prepared lysis solution (2.5 M NaCl, 100 mM EDTA, 10 mM Tris, 1% SDS, pH 10) containing 1% Triton X-100 at 4°C for 30 minutes. Slides were then immersed in pre-warmed enzyme digestion solution (2.5 M NaCl, 100 mM EDTA, 10 mM Tris, pH 10) with 1 mg/ml proteinase k for 2 hours at 37°C. Electrophoresis was carried out at 21 V (1 V/cm) for 20 min in freshly prepared electrophoresis buffer (300 mM sodium acetate, 100 mM Tris, pH 9.0). Finally, slides were immersed in DNA precipitation buffer (0.15 M NH4Ac, ethanol) for 20 minutes followed by fixation with 70% ethanol and staining with SYBR green. All the steps described above were conducted under reduced light to prevent spurious DNA damage. Comet images were captured under an Olympus fluorescence microscope equipped with a SensiCam camera. Image analysis was carried out with the Comet Assay IV software (Perceptive Inc., UK). Tail intensity was adopted as a measurement to quantify DNA damage. One hundred randomly selected cells

were analyzed for each treatment. Each experiment was repeated three times.

Flow cytometry for cell cycle arrest and gamma-H2A.X staining

In order to examine cell cycle distribution and determine DNA double strand breaks during the cell cycle, flow cytometry for cell cycle analysis and gamma-H2A.X staining were used according to methods described by Huang and Darzynkiewicz (Huang and Darzynkiewicz, 2006). Briefly, cells were harvested after zinc chromate treatment and fixed with 4% paraformaldehyde for 15 minutes on ice. Cells were washed with 1x PBS and centrifuged at 300 x g for 4 minutes at room temperature and transferred to a new tube containing cold 70% ethanol. Samples were stored at -20°C for at least a week before analysis. After fixation and permeabilization, cells were washed with FACS Buffer (1x PBS, 10 mM sodium azide, 5% FBS). Cells were then blocked with 2% rat serum (StemCell Technologies) for 15 minutes followed by incubation with primary anti-γ-H2AX-AF647 (pS140) antibodies at the manufacturer's recommended amount of 0.5 µg per sample for 1 hour at room temperature. An isotype control sample was incubated with Mouse IgG1 kappa-AF647 Isotype antibody at the manufacturer's recommended concentration of 0.5 µg per sample for 1 hour at room temperature. Samples were washed with FACS buffer before incubation for 30 minutes in the dark with 1 mL PI staining solution. The PI staining solution was as follows per sample: 1 mL PBS, 1 mg RNase A and 5 µL PI [1 mg/mL in water] (Invitrogen, P3566). Samples were analyzed by flow cytometry (Attune NxT V6, ThermoFisher Scientific). Data were stratified by phase of the cell cycle based on PI fluorescence

into G1, S, and G2M phases. Within each phase of the cell cycle, DNA damage was quantified by calculating the percentage of cells staining positive for γ-H2AX normalized to control fluorescence. Data were expressed as the percentage of cells in each phase of the cell cycle and the percent γ-H2AX positive cells in each phase of the cell cycle normalized to control for each phase.

Sister chromatid exchange assessment

Sister chromatid exchanges (SCEs) were quantified as an indirect measure of HR repair activity. SCEs are the product of the exchange of homologous sequences between sister chromatids during the repair of a double strand break (Sonoda et al., 1999). SCEs form as a result of cross-over between the newly generated DNA strand and the template strand during the resolution of a Holiday Junction (Sonoda et al., 1999). While SCEs do not represent all HR resolution products, they serve as a useful indicator of HR repair.

BHW200Lu cells were seeded into 100-mm dishes, allowed to enter logarithmic growth and treated with 0-0.4 ug/cm^2 zinc chromate for 24 and 120 h. Cells were incubated concurrently with 0.6 ug/ml BrdU for two cell cycles prior to harvesting (72 h in the case of BHW200Lu cells). Following exposure, cells were harvested, prepared and dropped onto clean, wet slides according to the chromosome aberration protocol previously described. Slides were aged overnight or baked at 60°C for 1 h, soaked in 1x PBS for 5 min and stained with 0.5 ug/ml Hoechst 33258 pentahydrate solution for 10 min at room temperature. Excess solution was removed from the slides, followed by the addition of 25 ug/ml Hoechst

33258 pentahydrate solution and a glass coverslip. Coverslipped slides were incubated under 27 W fluorescent lights for 11 h in a humid chamber. At the end of this incubation, coverslips were washed off with distilled water and slides were incubated in pre-warmed 2x sodium chloride/sodium citrate solution for 15 min at 60°C. Finally, slides were washed with distilled water, stained with 4% Giemsa stain in Gurr's buffer and mounted. The total number of SCEs was obtained in fifty harlequin stained metaphases per concentration/timepoint.

Mitotic index

To determine whether cells accumulate during mitosis, the mitotic index was measured as previously described (Xie et al., 2008). Cells were seeded and treated with various concentrations of zinc chromate for 24 h or 120 h. After treatment, cells were harvested and incubated in 0.075 M KCl hypotonic solution for 10 min. Then, cells were fixed, and dropped on slides, which were uniformly stained with 5% Giemsa stain in Gurr's buffer. The mitotic index was determined as the number of mitotic cells per 5000 total relative to control cells by light microscopy. Three independent experiments were conducted.

Chromosomal aberration assay

Chromosomal aberrations were measured to determine clastogenicity according to our published methods (Wise et al., 2002). Briefly, cells were seeded and treated with various concentrations of zinc chromate for 24 or 120 h. Five hours prior to treatment end, 0.1 ug/ml demecolcine was added to arrest cells in

metaphase. Cells were then harvested, fixed, and dropped on slides as described in the sister chromatid exchange assay method. Finally, slides were stained with 5% Giemsa stain and scored for chromosome aberrations using previously defined criteria (Wise et al., 2002). One hundred metaphases were analyzed for each treatment, and three independent experiments were conducted.

Clonogenic survival assay

Cytotoxicity was determined by a clonogenic survival assay as previously reported (Wise et al., 2002). Cells were seeded and then treated for 24 h or 120 h with suspensions of zinc chromate. After treatment, cells were harvested, counted and reseeded at colony forming density (1000 cells in 100-mm plates). Cells were then allowed to grow to form colonies. The resulting colonies were fixed with 100% methanol, stained with crystal violet and counted. Each experiment was repeated at least three times.

Statistics

All data were expressed as mean ± standard error of the mean (SEM) from 3 experiments. In the animal study, simple linear regression was used to compare dose responses. In the animal study, two-way ANOVA was used when comparing different treatments, time points, lung regions, lung lobes, sexes, and cell types. In the cell culture study, two-way ANOVA was used when comparing different species, time points, and treatments. When comparing the means of two variables, two-way ANOVA with Dunnett multiple comparisons test was performed. Exposed

and unexposed groups were compared using one-way ANOVA. Statistical significance was determined at $p<0.05$.

CHAPTER III

RESULTS

Overview

Cr(VI) has been classified as a human lung carcinogen for decades, but the mechanism of Cr(VI)-induced cancer has not been fully elucidated. Chromosomal instability is a hallmark of lung cancer and is a driving event in Cr(VI)-induced lung cancer (Masuda and Takahashi 2002; Wise et al., 2018). Cr(VI)-induced structural chromosomal instability has been reported in epidemiologic studies focused on chromate workers and in numerous cell culture studies (Halasova et al., 2008; Halasova et al., 2012; Maeng et al., 2004; Qin et al., 2014; Xie et al., 2005; Xie et al., 2009; Wise et al., 2002; Wise et al., 2003; Wise et al., 2006). Unrepaired or misrepaired DNA double strand breaks are the primary mechanism for the formation of structural chromosomal instability. Numerous cell culture studies have shown that Cr(VI) induces the formation of DNA double strand breaks. The HR repair pathway without error repairing DNA double strand breaks prevents Cr(VI)-induced structural chromosomal instability and neoplastic transformation (Bryant et al., 2006; Stackpole et al., 2007; Xie et al., 2007). Recent studies have shown that acute Cr(VI) exposure increases HR repair activity in human lung cells whereas prolonged Cr(VI) exposure inhibits HR function (Xie et al. 2009, Qin et al. 2014, Browning et al. 2016). However, these outcomes were discovered in cell

culture experiments, and the effects of Cr(VI) in laboratory animals and in other wildlife species are currently unknown. Cr(VI)-induced double strand break and HR repair *in vivo* have not been investigated so far. Therefore, it is urgent and important to study Cr(VI)-induced double strand breaks and HR repair *in vivo* in experimental animal models. This project translates Cr(VI)-induced HR deficiency and chromosomal instability outcomes from human lung cells into experimental animals, human lung tumors, and whale cells.

Studies have found Cr(VI) induces DNA double strand breaks in many cell culture studies. Recent studies have shown acute Cr(VI) activates HR repair activity to repair increased DNA double strand breaks in human lung cells (Xie et al. 2009; Qin et al. 2014; Browning et al. 2016). Therefore, in Aim 1, we investigated DNA double strand breaks and HR repair activity in acute (24-hour) Cr(VI)-exposed rat lung tissue to test our hypothesis that acute exposure to particulate Cr(VI) induces DNA double strand breaks and induces HR repair *in vivo*.

Prolonged exposure in human lung cells was found to inhibit HR repair activity (Qin et al. 2014; Browning et al. 2016). Inhibition of HR repair results in structural chromosomal instability due to the failure of DNA double strand breaks to be repaired without errors. Therefore in Aim 2, we investigated DNA double strand breaks and HR repair activity in subchronic Cr(VI)-exposed rat lung tissue to test our hypothesis that subchronic exposure to particulate Cr(VI) induces DNA double strand breaks, but inhibits HR repair *in vivo*. Then we translated the outcomes into chromate workers' lung tumors to investigate the hypothesis that

Cr(VI)-induced DNA double strand break and HR repair inhibition continue to tumor formation.

Whales live in extreme environments and are exposed to high levels of Cr(VI) (Wise et al. 2019a; Wise et al., 2019b). They are long-lived species and exhibit a higher level of protection against cancer (de Magalhães, 2015; Keane et al., 2015). However, how whales evade carcinogenesis is unclear. Studies have shown that whale cells are more resistant to Cr(VI)-induced chromosome instability than human cells (Li Chen et al., 2009a; Li Chen et al., 2009b; Li Chen et al., 2012; Wise et al., 2015). However, no studies have investigated this mechanism of resistance to Cr(VI)-induced chromosomal damage. Therefore, Aim 3 in this project tests the hypothesis that whale cells exhibit a protective mechanism against Cr(VI)-induced chromosomal instability. We measured the effects of acute and prolonged Cr(VI) exposure on DNA double strand breaks, HR repair and structural chromosomal instability in bowhead whale lung cells. We then compared the effects of Cr(VI) exposure on whale and human cells.

The results for these three aims are presented in 3 parts, Aim 1, Aim 2 and Aim 3, as depicted in Figure 3.1. In Aim 1, we measured metal levels, lung histological changes, DNA double strand breaks and HR repair in 24-hour Cr(VI) exposure rat lungs. In Aim 2, we measured metal levels, lung histological changes, DNA double strand breaks and HR repair after 90-day Cr(VI) exposure. In Aim 2 we examined HR repair in chromate workers' lung tumor tissue slices. In Aim 3, we investigated Cr(VI)-induced DNA double strand breaks, and the effect of particulate Cr(VI) on HR repair in whale lung cells. Then we investigated cell cycle

profiles and determined in which cell cycle phase Cr(VI) caused DNA double strand breaks. After investigating chromosomal instability induced by Cr(VI) and its effect on HR repair in whale cells, we further contrasted the effects of Cr(VI) on chromosomal instability and HR repair in whale and human cells. All aims and objectives are detailed below.

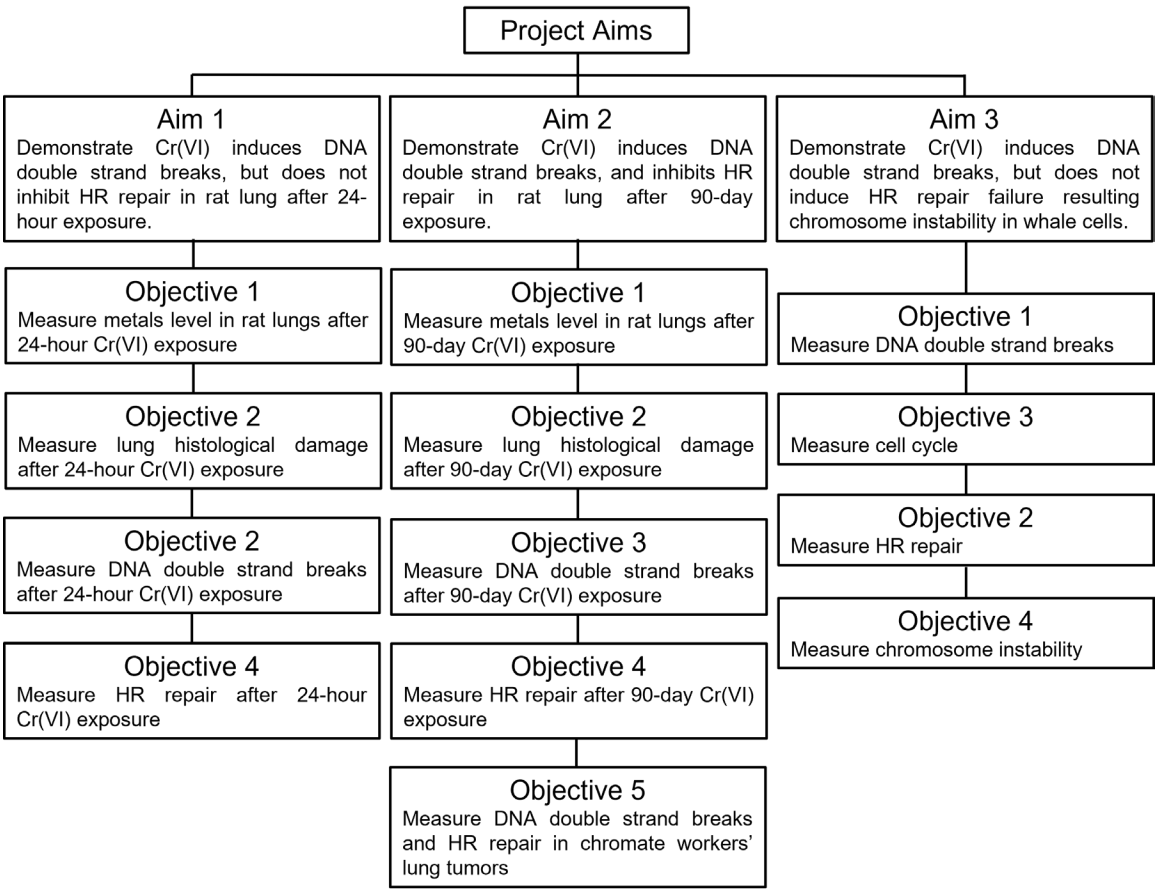

Figure 3.1. Organizational schematic of the research project.

Aim 1: Demonstrate particulate Cr(VI) induces DNA double strand breaks and HR repair in rat lung after 24-hour exposure.

BACKGROUND

Chromosomal instability is a major driver of Cr(VI) carcinogenesis (Chen et al., 2019; Rager et al., 2019; Wise et al., 2018). However, the mechanism of Cr(VI)-induced structural chromosomal instability remains largely unknown. Among the various forms of DNA damage induced by Cr(VI) compounds, DNA double strand breaks pose the greatest threat to genome integrity. If unrepaired or incorrectly repaired, DNA double strand breaks can lead to genomic instability and promote Cr(VI)-induced carcinogenesis. HR repair is a high-fidelity DNA double strand break repair pathway that repairs dangerous DNA double strand breaks in a manner that maintains genome stability. HR repair prevents Cr(VI)-induced chromosomal instability (Bryant et al., 2006; Gastaldo et al., 2007). Studies have shown that acute Cr(VI) exposure induces double strand breaks and increases HR repair activity in human lung cells (Xie et al., 2009; Qin et al., 2014; Browning et al., 2016). However, these data were all obtained in cell culture experiments, and it is not known whether the same outcomes can be seen in animals. Therefore, we investigated DNA double strand breaks and HR repair in rat lungs after acute Cr(VI) exposure.

RESULTS

Chromium accumulation in the Lung

The main organ impacted by Cr(VI) is the lungs. Inhalation exposure of Cr(VI) particulates is the predominant mode of exposure in chromium workers. Therefore, we exposed rats to zinc chromate particles in saline solution by oropharyngeal aspiration in this study. Since we aim to study the effects of chromium on rat lungs, we first needed to determine whether chromium reaches and accumulates in the lungs. We measured Cr levels in rat lung tissue by ICP-MS.

After 24-hour Cr(VI) exposure, we found Cr accumulation in rat lung tissue (Figure 3.2). Cr levels in the rat lungs increased in a dose-dependent manner (linear regression analysis: $p<0.0001$) (Figure 3.3). After 24-hour exposure to 0 (saline), 0.2, 0.4, and 0.8 mg/kg zinc chromate, the average Cr levels in whole lung tissues were 0.120, 3.295, 6.147, and 16.145 mg Cr/kg lung tissue, respectively. The 0.8 mg/kg zinc chromate treatment group was significantly increased in Cr level compared with the saline group ($p<0.0001$) (Figure 3.2).

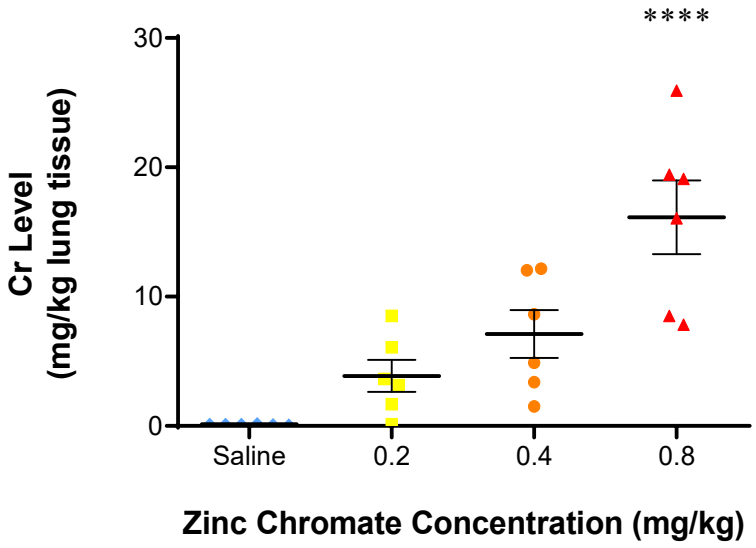

Figure 3.2. Cr levels in whole rat lungs after 24-hour exposure. Cr levels (relative to saline) increased with dose after 24-hour zinc chromate exposure. The 0.8 mg/kg zinc chromate group had significantly higher levels than the saline group. Error bar = standard error of the mean. Statistically different from the control (saline) group: ****p<0.0001.

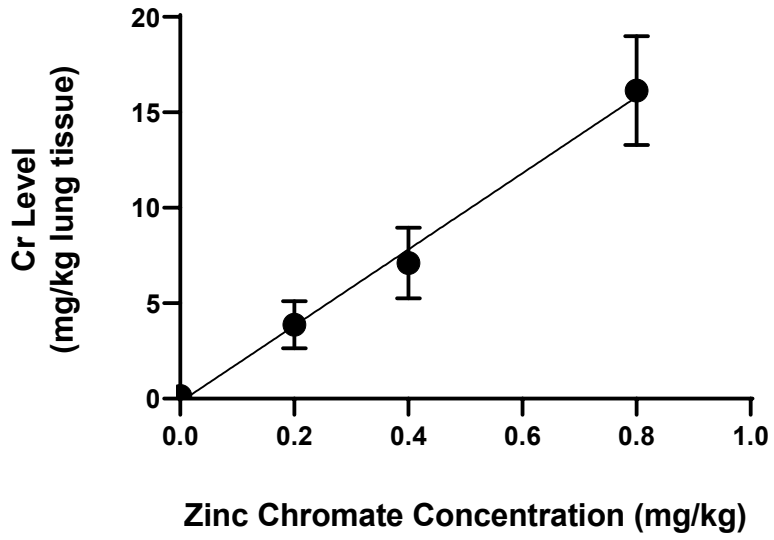

Figure 3.3. Cr levels in whole rat lungs after 24-hour exposure shown with a linear regression line. This figure shows a linear correlation between these 4 variables: saline, 0.2 mg/kg, 0.4 mg/kg and 0.8 mg/kg zinc chromate. The *p* value is <0.0001.

When airborne particles are inhaled into the airways, most particles are removed by mucociliary clearance by macrophage phagocytosis (Lippmann et al.,1980). A small fraction is redistributed and remains within the lung tissue (Oberholster, 1988). The deposition and removal of particles in the respiratory tract occur in a non-uniform manner. Therefore, we investigated the specific distribution of zinc chromate particles in both the left and right lungs of rats. We found Cr levels increased in a dose-dependent manner in both the left and right lungs, after 24-hour zinc chromate exposure (Figure 3.4). After 24-hour exposure to 0 (saline), 0.2, 0.4, and 0.8 mg/kg zinc chromate, the average Cr levels in left rat lungs were 0.011, 0.359, 1.091, and 1.163 mg Cr/kg lung tissue, respectively. In right rat lungs, after 24-hour exposure to 0 (saline), 0.2, 0.4, and 0.8 mg/kg zinc chromate, the average Cr levels were 0.072, 3.423, 5.773, and 14.556 mg Cr/kg lung tissue, respectively. The elevation of Cr levels in the right lung was statistically significant, after 24-hour 0.4 and 0.8 mg/kg zinc chromate exposures (*p<0.05 and ****p<0.0001, respectively). Compared with Cr levels in the left lung, there was a statistically significant increase in chromium deposition in the right lung (p<0.0001).

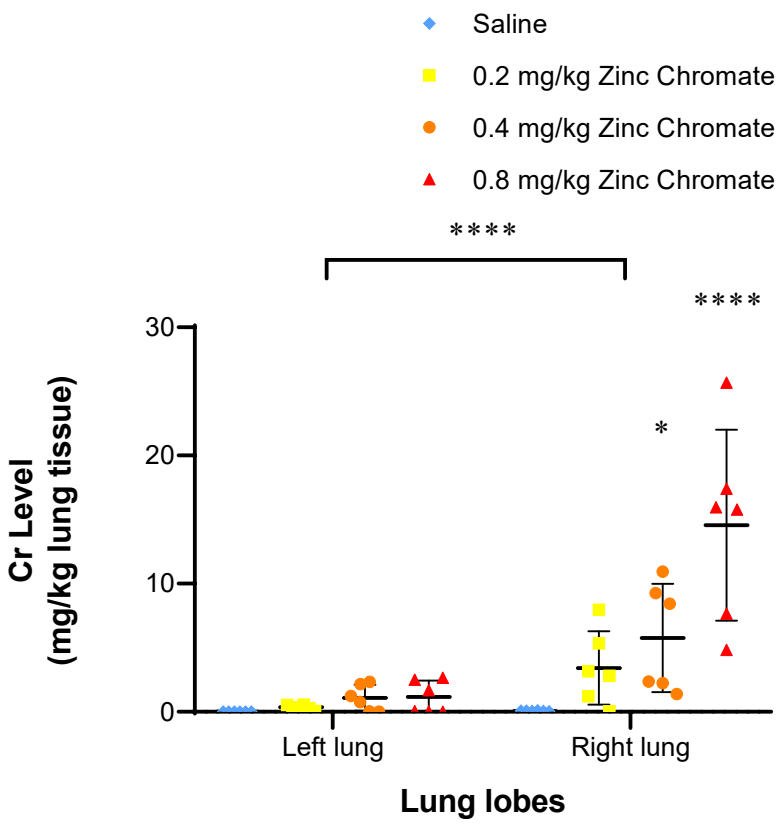

Figure 3.4. Cr levels in left rat lungs vs. right rat lungs after 24-hour exposure. This figure shows Cr levels increased in a dose-dependent manner in the left and right lungs. Cr-induced level increases were statistically significant in the right lung. Cr levels in right rat lungs were significantly increased compared with left rat lungs. Error bar = standard error of the mean. Statistically different from the control (saline) group: *p<0.05, ****p<0.0001.

The left lung of the rat has only one lobe, and the right lung has four lobes, including the superior, middle, inferior, and accessory lobes. We further determined the distribution of Cr in each lung lobe. Cr levels increased in a dose-dependent manner in each individual rat lung lobe after 24-hour zinc chromate exposure (Figure 3.5). For example, after 24-hour exposure to 0 (saline), 0.2, 0.4, and 0.8 mg/kg zinc chromate, the average Cr levels in the right inferior lobe were 0.027, 1.273, 3.630, and 4.578 mg Cr/kg lung tissue, respectively. The elevation of Cr levels in the right inferior lobe was statistically significant, after 24-hour 0.4 and 0.8 mg/kg zinc chromate exposures (***p<0.001 and ****p<0.0001, respectively). We also found Cr levels significantly increased in the right accessary lobe after 24-hour 0.8 mg/kg zinc chromate exposure (****p<0.0001). However, the increase in Cr concentration in the bronchial tree was significantly less pronounced than in other lobes after acute exposure (*p<0.05) (Figure 3.6). This outcome suggests that chromium was inhaled and deposited into the distal airways in the rat lungs.

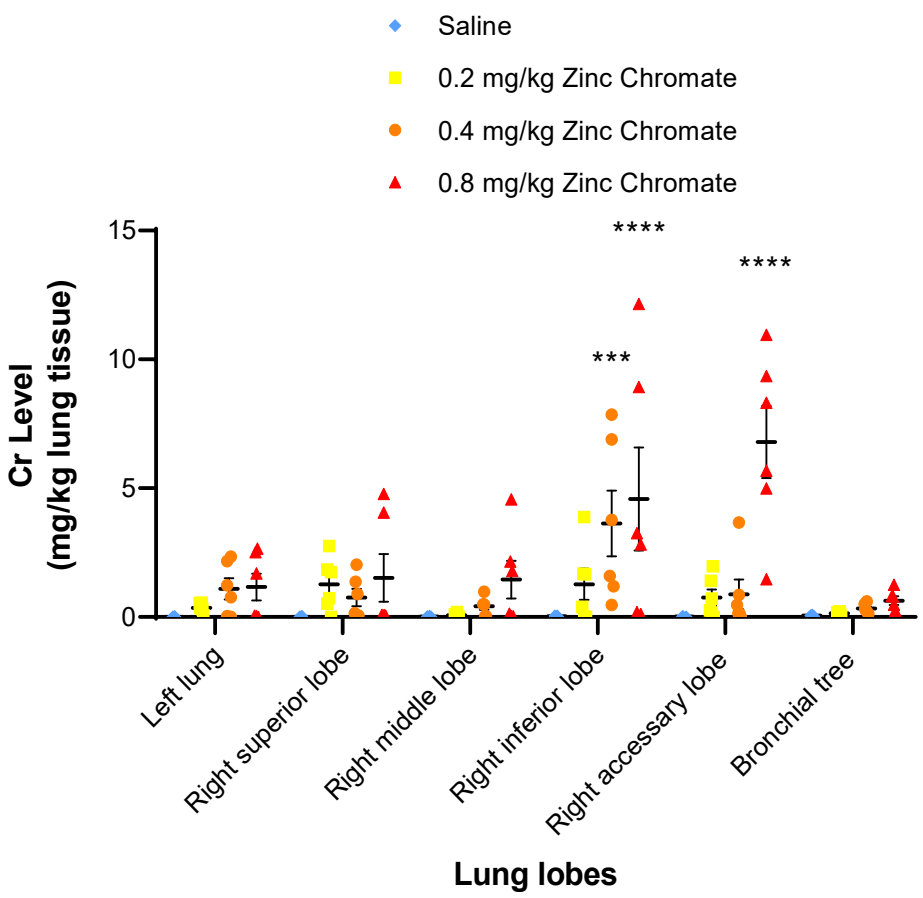

Figure 3.5. Cr distribution in individual rat lung lobes after 24-hour zinc chromate exposure. Cr levels increased in a dose-dependent manner in each individual rat lung lobe. In the right inferior lobe and right accessary lobes, Cr levels were significantly higher than in the saline group. Error bar = standard error of the mean. Statistically different from the control (saline) group: ***p<0.001, ****p<0.0001.

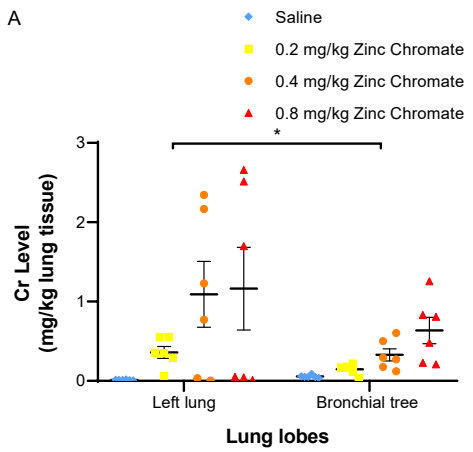
A
Saline
0.2 mg/kg Zinc Chromate
0.4 mg/kg Zinc Chromate
0.8 mg/kg Zinc Chromate
*
Cr Level (mg/kg lung tissue)
3
2
1
0
Left lung
Bronchial tree
Lung lobes

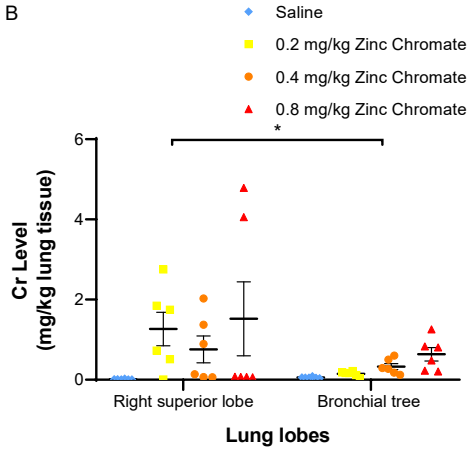
B
Saline
0.2 mg/kg Zinc Chromate
0.4 mg/kg Zinc Chromate
0.8 mg/kg Zinc Chromate
*
Cr Level (mg/kg lung tissue)
6
4
2
0
Right superior lobe
Bronchial tree
Lung lobes

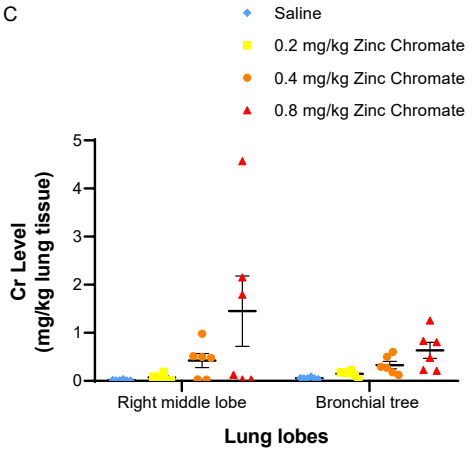
C
Saline
0.2 mg/kg Zinc Chromate
0.4 mg/kg Zinc Chromate
0.8 mg/kg Zinc Chromate
Cr Level (mg/kg lung tissue)
5
4
3
2
1
0
Right middle lobe
Bronchial tree
Lung lobes

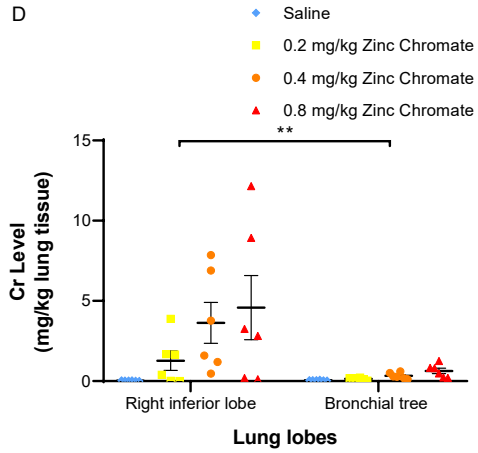
D
Saline
0.2 mg/kg Zinc Chromate
0.4 mg/kg Zinc Chromate
0.8 mg/kg Zinc Chromate
**
Cr Level (mg/kg lung tissue)
15
10
5
0
Right inferior lobe
Bronchial tree
Lung lobes

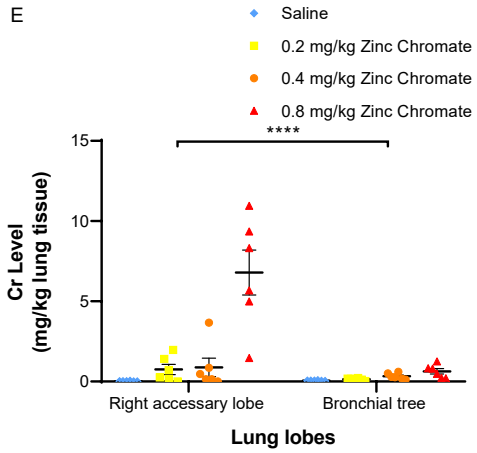
E
Saline
0.2 mg/kg Zinc Chromate
0.4 mg/kg Zinc Chromate
0.8 mg/kg Zinc Chromate
****
Cr Level (mg/kg lung tissue)
15
10
5
0
Right accessary lobe
Bronchial tree
Lung lobes

Figure 3.6. Cr distribution in the bronchial tree vs. other lung lobes after 24-hour zinc chromate exposure. Cr level elevation was statistically significantly less pronounced in the bronchial tree than in the other lung lobes. A. Elevation of Cr levels in bronchial tree vs. left lung (*p<0.05). B. Elevation of Cr levels in bronchial tree vs. right superior lobe (*p<0.05). C. Elevation of Cr levels in bronchial tree vs. right middle lobe. D. Elevation of Cr levels in bronchial tree vs. right inferior lobe (**p<0.01). E. Elevation of Cr levels in bronchial tree vs. right accessory lobe (****p<0.0001). Error bar = standard error of the mean.

Lung Histological Change

Repeated exposure to Cr(VI) induces lung damage and inflammation. Beaver et al. found that a single nasal aspiration exposure to zinc chromate particles caused lung tissue damage and inflammation that persisted for up to 21 days in mice (Beaver et al., 2009). We therefore investigated Cr(VI)-induced lung histological changes by H&E staining before investigating Cr(VI)-induced DNA damage. We found infiltration of inflammatory cells in the alveolar area after 24-hour Cr(VI) exposure. Inflammatory cells accumulated around the alveoli and terminal airways (Figure 3.7). In the group exposed to saline for 24 h, the main cell types aggregated in the alveolar region were macrophages. While exposed to zinc chromate for 24 hours, various inflammatory cells were gathered around the alveolar area and terminal airways, mainly neutrophils. Cr(VI)-induced inflammatory cells aggregated around the alveolar area and terminal airways showed a slightly increasing trend after 24-hour exposure (Figure 3.8).

Since the cell types of inflammatory cell aggregation after acute exposure differed between saline and Cr(VI) exposures, we investigated macrophage aggregation and non-macrophage aggregation separately. We found macrophage aggregation did not differ between groups after acute exposure, whereas non-macrophage inflammatory cells increased significantly with increasing zinc chromate doses after acute Cr(VI) exposure (Figure 3.9). These data suggest the inflammatory response to acute chromium exposure is dominated by the aggregation of non-macrophages, including neutrophils and lymphocytes.

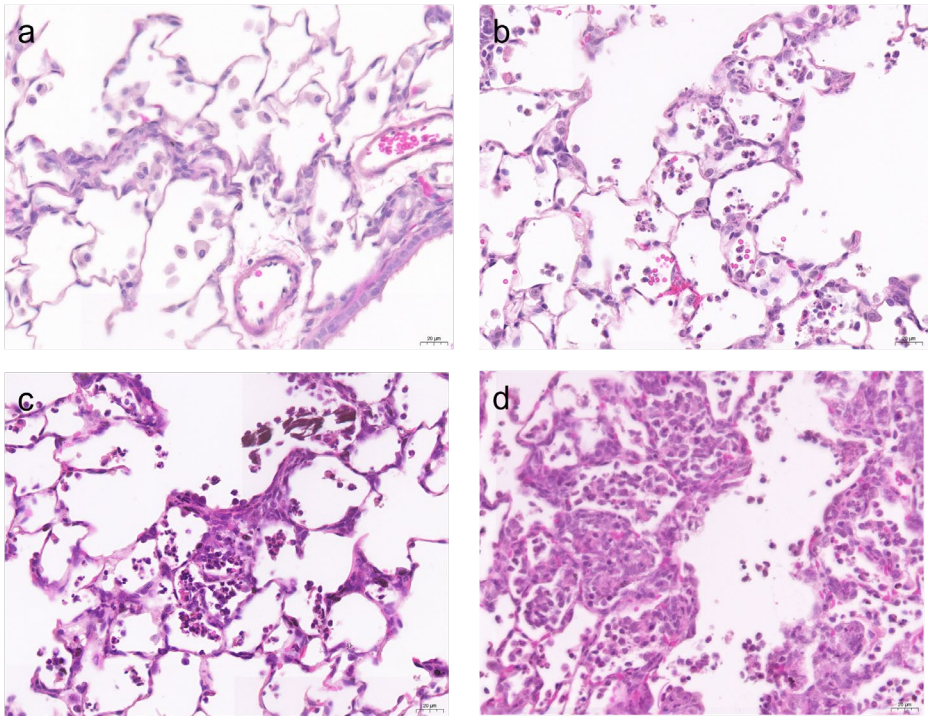

Figure 3.7. Cr(VI) induces inflammation in rat lung after 24-hour exposure. a. Macrophages accumulate in the alveolar region after 24-hour exposure to saline. b. Neutrophils and lymphocytes accumulate in the alveolar region after 24-hour exposure to 0.2 mg/kg zinc chromate. c. Many neutrophils and lymphocytes accumulate in the alveolar region after 24-hour exposure to 0.4 mg/kg zinc chromate. d. Many neutrophils and lymphocytes accumulate in the alveolar region after 24-hour exposure to 0.8 mg/kg zinc chromate. Magnifications for a - d are x400.

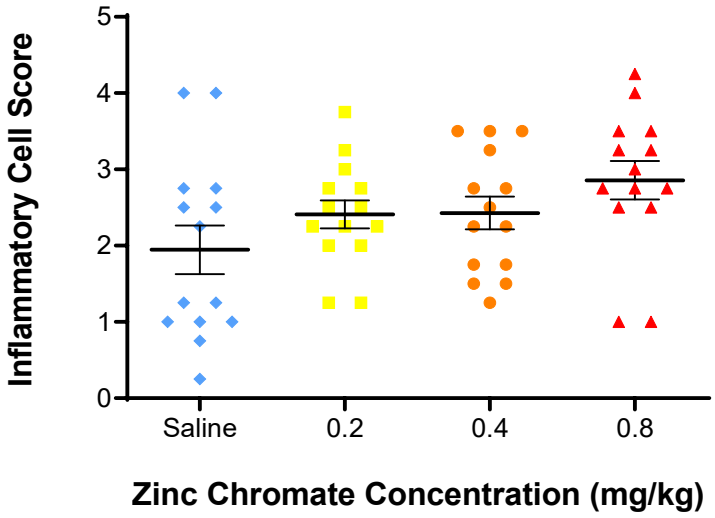

Figure 3.8. Cr(VI) induces inflammatory cell aggregation in the rat lung after 24-hour exposure. Inflammatory cell aggregation increased after 24-hour exposure to zinc chromate compared with saline exposure. Inflammatory cells were scored according to Table 1.3. Error bar = standard error of the mean.

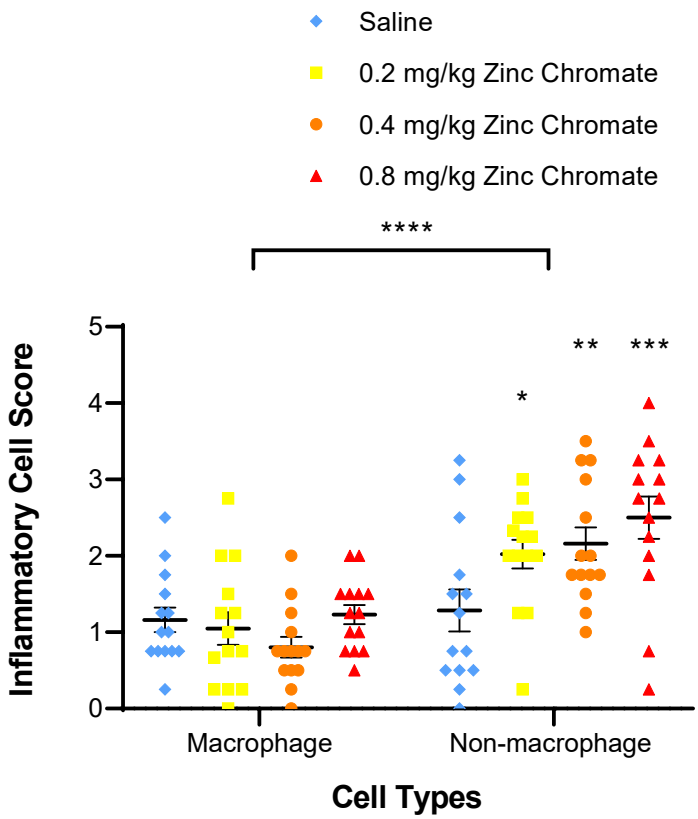

Figure 3.9. Cr induced non-macrophage inflammatory cell aggregation in rat lung after 24-hour exposure. This graph shows macrophage aggregation and non-macrophage inflammatory cell aggregation are different after acute exposure (****p<0.0001). Macrophage aggregation did not differ between groups after 24-hour exposure, whereas non-macrophage inflammatory cells were significantly increased after 24-hour zinc chromate exposure. Cr(VI)-induced non-macrophage inflammatory cell aggregations were significantly increased in a dose-dependent manner after exposure to 0.2, 0.4 and 0.8 mg/kg zinc chromate (*p<0.05, **p<0.01, ***p<0.001).

DNA Double Strand Breaks

Histone H2AX is phosphorylated at Ser 139 in response to DNA double strand breaks (Fernandez-Capetillo et al., 2004). The number of phosphorylated H2AX foci forming at double strand break sites can represent the number of DNA double strand breaks (Rogakou et al., 1999; Sedelnikova et al., 2002). Therefore, the formation of γ-H2AX foci is considered a quantitative marker of DNA double strand breaks. Although numerous cell culture studies have shown that Cr(VI) induces the formation of double strand breaks, Cr(VI)-induced double strand breaks in vivo have not been investigated so far. In the present study, we detected the formation of γ-H2AX foci in Cr(VI)-exposed rat lungs by immunofluorescence. We found Cr(VI) induced γ-H2AX foci formation in rat lungs after 24-hour zinc chromate exposure (Figure 3.10). We investigated γ-H2AX foci formation in different lung sites. Cr(VI)-induced γ-H2AX foci formation increased in a dose-dependent manner in bronchioles. Specifically, after 24-hour exposure to 0 (saline), 0.2, 0.4, and 0.8 mg/kg zinc chromate in bronchioles, the percent of cells with γ-H2AX foci were 8.1, 20.2, 25.9, and 30.4%, respectively. There were statistically significant γ-H2AX foci formation increases in bronchioles after exposure to 0.4 and 0.8 mg/kg zinc chromate (**p<0.01 and ***p<0.001, respectively) (Figure 3.11). However, after 24-hour exposure to zinc chromate, there was a slight increase in γ-H2AX foci formation in the alveoli. In bronchioles, the formation of γ-H2AX foci caused by Cr(VI) was more pronounced than in alveoli (****p<0.0001) (Figure 3.11).

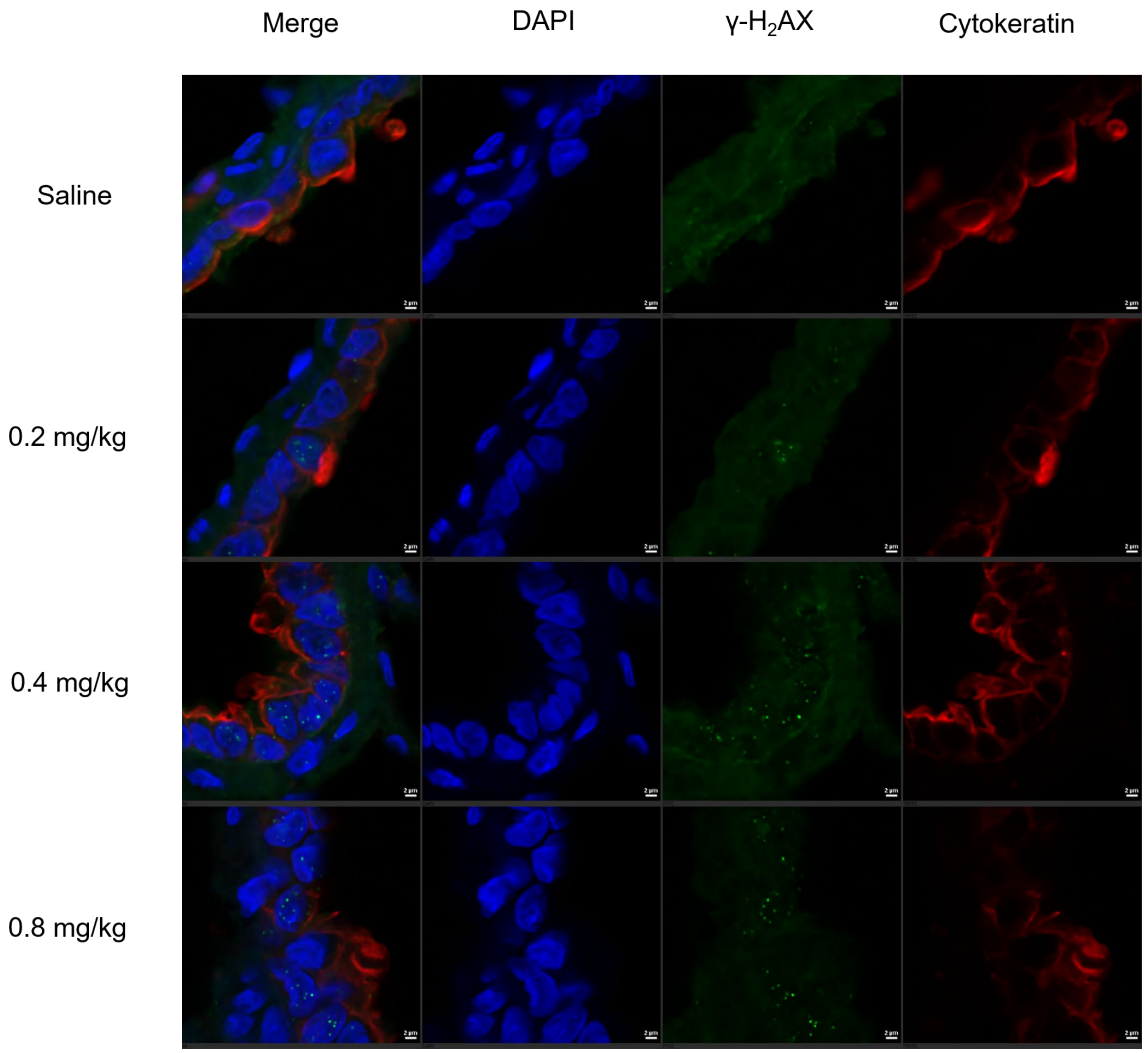

Figure 3.10. Particulate Cr(VI) induces DNA double strand breaks in the rat lung. Representative images of γ-H2AX foci are shown. First column, merged image; second column, DAPI staining; third column, γ-H2AX foci staining; fourth column, staining for cytokeratin, a marker of epithelial cells.

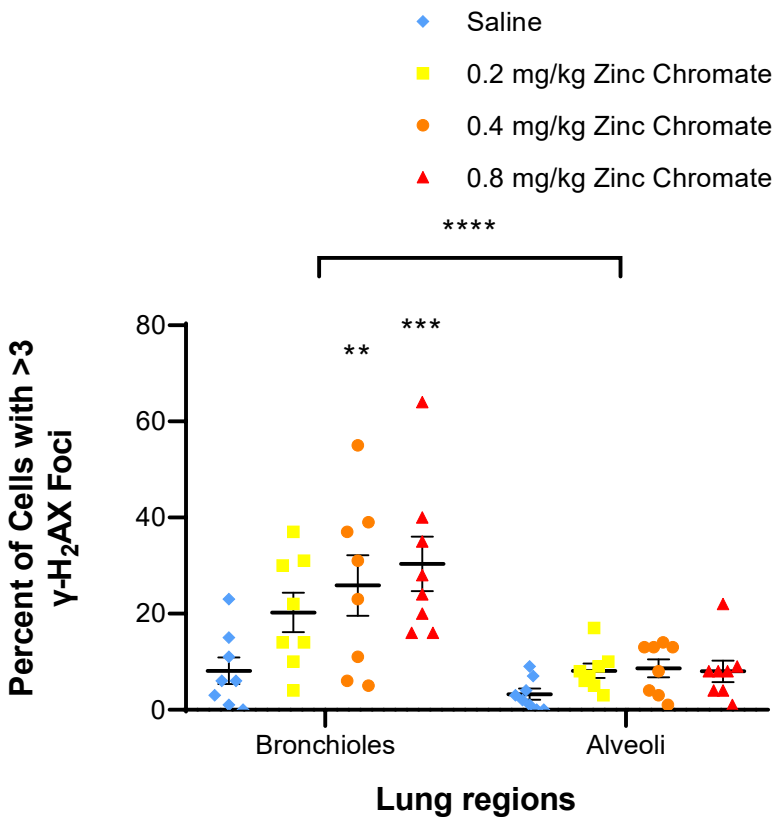

Figure 3.11. Comparison of γ-H2AX foci formation after 24-hour zinc chromate exposure within and between groups of different lung regions. Cr(VI)-induced γ-H2AX foci formed in both the bronchiolar and alveolar regions. γ-H2AX foci formation in bronchioles increased with zinc chromate dose. After exposure to 0.4 and 0.8 mg/kg zinc chromate, γ-H2AX foci formation in bronchioles was significantly increased (**p<0.01, ***p<0.001). The formation of γ-H2AX foci in the alveoli was slightly increased after 24-hour exposure to zinc chromate. Cr(VI)-induced γ-H2AX foci formation showed statistically significant differences between bronchioles and alveoli (****p<0.0001). Error bar = standard error of the mean.

Epidemiological studies of chromate workers found that chromate-induced tumors are epithelial carcinomas, mainly squamous cell carcinomas (Hirose et al., 2002; Ishikawa et al., 1994a). Since squamous cell carcinomas originate from epithelial cells, we further investigated Cr(VI)-induced DNA double strand breaks in rat lung epithelial and non-epithelial cells. We also investigated the bronchiolar and alveolar regions of the lung. As a result, we found few γ-H2AX foci formed in bronchiolar non-epithelial cells after 24-hour zinc chromate exposure, whereas γ-H2AX foci formation in bronchiolar epithelial cells increased with Cr dose. Specifically, after 24-hour exposure to 0 (saline), 0.2, 0.4, and 0.8 mg/kg zinc chromate in bronchiolar epithelial cells, the rats of cells with γ-H2AX foci were 5.1%, 7.8%, 12.1%, and 12.9%, respectively. γ-H2AX foci formation in bronchiolar epithelial cells was significantly increased after exposure to 0.4 and 0.8 mg/kg zinc chromate (*p<0.05) (Figure 3.12). In bronchioles, Cr(VI)-induced γ-H2AX foci formation was almost exclusively in epithelial cells (****p<0.0001) (Figure 3.12).

We found that γ-H2AX foci formation in alveolar non-epithelial cells was almost unchanged after 24-hour Cr(VI) exposure compared with saline exposure, whereas γ-H2AX foci formation in alveolar epithelial cells increased with Cr(VI) dose (Fig. 3.13). When comparing alveolar non-epithelial and epithelial cells, we found that Cr(VI)-induced γ-H2AX foci formation was predominantly in epithelial cells (****p<0.0001) (Figure 3.13).

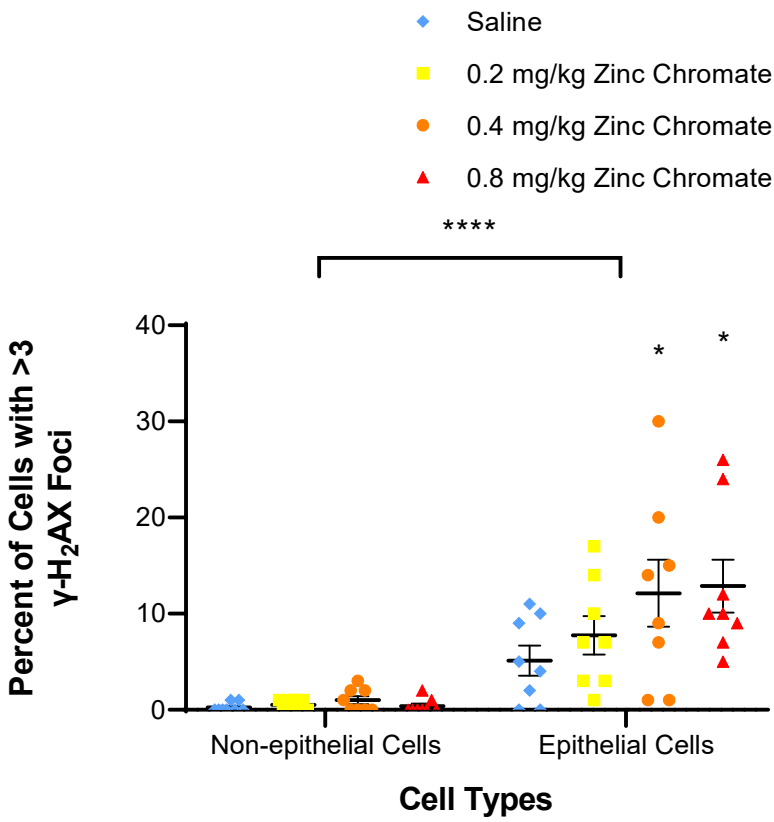

Figure 3.12. Comparison of γ-H2AX foci formation in bronchioles after 24-hour exposure to zinc chromate within and between groups of non-epithelial and epithelial cells. Few γ-H2AX foci formed in bronchiolar non-epithelial cells after 24 hours of zinc chromate exposure, whereas γ-H2AX foci formation in bronchiolar epithelial cells increased with Cr(VI) doses. γ-H2AX foci formation in bronchiolar epithelial cells was significantly increased after exposure to 0.4 and 0.8 mg/kg zinc chromate (*p<0.05). In bronchioles, Cr(VI)-induced γ-H2AX foci formation was significantly different between non-epithelial and epithelial cells (****p<0.0001).

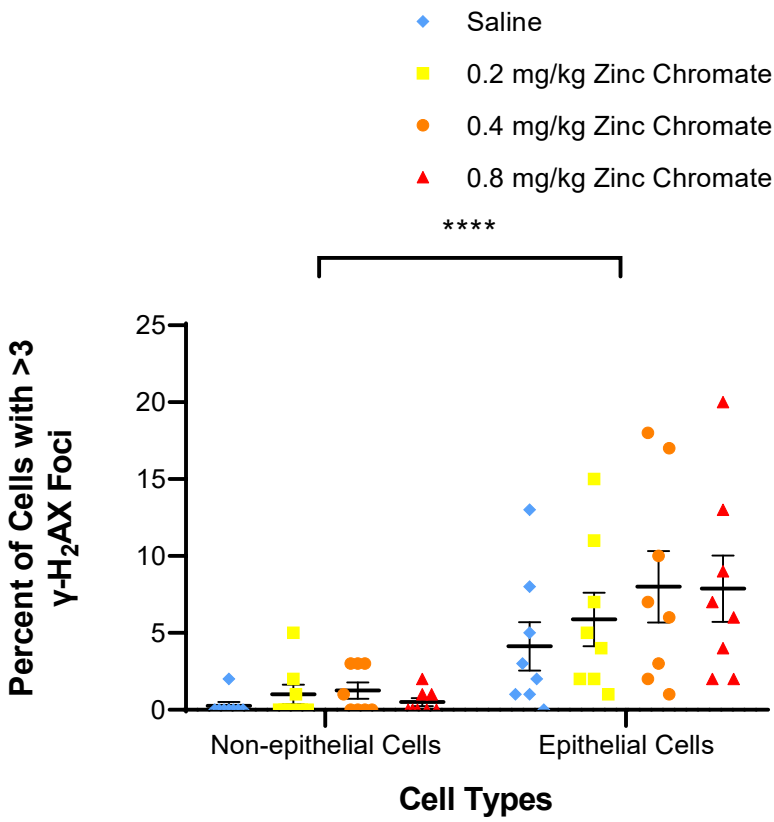

Figure 3.13. Comparison of γ-H2AX foci formation in alveoli after 24-hour exposure to zinc chromate within and between groups of non-epithelial and epithelial cells. γ-H2AX foci formation in alveolar non-epithelial cells was almost unchanged compared to saline exposure, whereas γ-H2AX foci formation in alveolar epithelial cells increased with Cr(VI) dose. Cr(VI)-induced γ-H2AX foci formation was significantly different between alveolar non-epithelial and epithelial cells (****p<0.0001).

HR Repair

HR repair is the accurate repair of DNA double strand breaks using undamaged sister chromatids as a template to maintain the integrity of the genome (Van et al. 2001). Recombinase RAD51, a key repair protein in HR repair, binds single-stranded DNA and forms nuclear filaments that play a key role in HR by guiding strand exchange and homology searching (Filippo et al., 2008; Li et al., 2008). Our previous study found that acute particulate Cr(VI) activates HR repair to prevent Cr(VI)-induced DNA double strand breaks, whereas prolonged particulate Cr(VI) inhibits HR repair by targeting RAD51 (Qin et al., 2014; Browning et al., 2016). We therefore investigated RAD51 expression to assess HR repair in rat lungs after 24-hour zinc chromate exposure by immunofluorescence. We found that Cr(VI) induced RAD51 foci formation in rat lungs following 24-hour zinc chromate exposure (Figure 3.14). We next investigated RAD51 foci formation in different lung sites. Cr(VI)-induced RAD51 foci formation increased in a dose-dependent manner in bronchioles. Specifically, after 24-hour exposure to 0 (saline), 0.2, 0.4, and 0.8 mg/kg zinc chromate in the bronchioles, the rates of cells with RAD51 foci were 9.1, 11.1, 17.75, and 24.63, respectively. RAD51 foci formation in bronchioles was significantly increased after exposure to 0.8 mg/kg zinc chromate (***p<0.001) (Figure 3.15). However, after 24-hour exposure to zinc chromate, there was no increase in RAD51 foci formation in the alveoli compared to the saline-exposed group. Cr(VI)-induced RAD51 foci formation after 24-hour zinc chromate exposure was significantly different in the bronchioles and alveoli (****p<0.0001) (Figure 3.15).

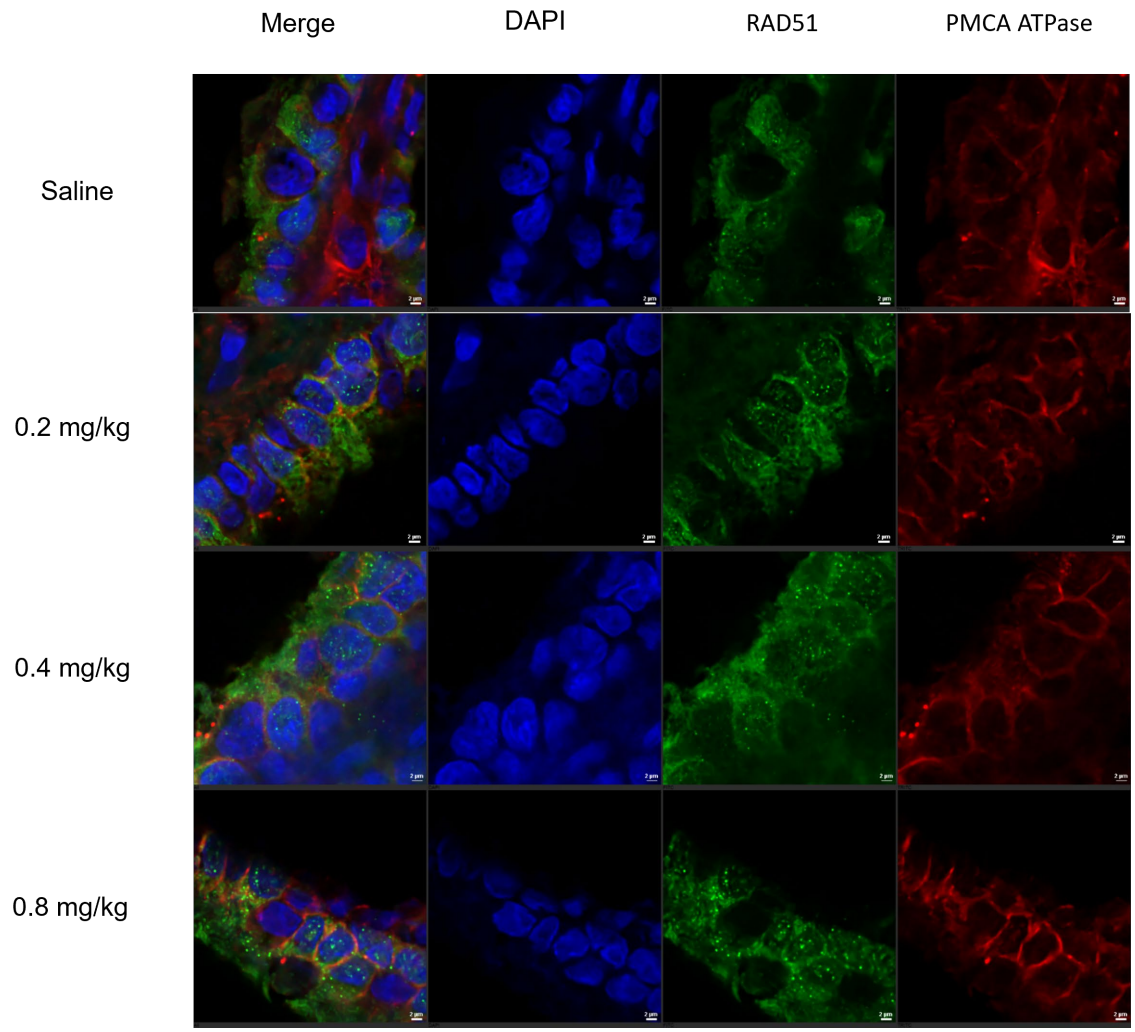

Figure 3.14. Particulate Cr(VI) induces RAD51 foci formation in the rat lung. Representative images of RAD51 foci are shown. First column, merged image; second column, DAPI staining; third column, RAD51 foci staining; fourth column, staining for PMCA ATPase, a marker of the cell membrane.

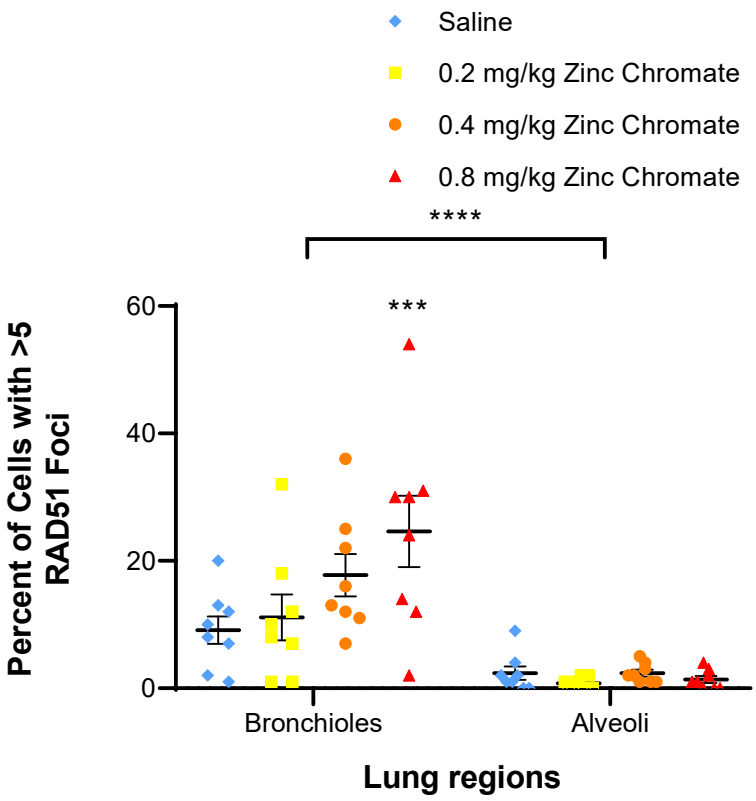

Figure 3.15. Comparison of RAD51 foci formation after 24-hour zinc chromate exposure within and between groups of different lung regions. RAD51 foci formation was increased in bronchioles in a dose-dependent manner after 24-hour exposure, and was significantly increased after exposure to 0.8 mg/kg zinc chromate (***p<0.001). After 24-hour exposure to zinc chromate, there was no increase in RAD51 foci formation in alveoli compared with the saline-exposed group. Cr(VI)-induced RAD51 foci formation was significantly different in bronchioles and alveoli after 24-h zinc chromate exposure (****p<0.0001). Error bar = standard error of the mean.

Sex differences

There are gender differences in the incidence of lung cancer among non-smoking patients. Women who do not smoke have higher rates of lung cancer than men. Therefore, we investigated whether there are differences in lung Cr levels, lung histological changes, DNA double strand breaks, and HR repair between female and male rats.

Chromium Uptake

We investigated potential differences in Cr levels in the lungs of female and male rats after 24-hour zinc chromate exposure. We found Cr levels increased in a dose-dependent manner in either left or right lung lobe, female or male rat (Figure 3.16). We compared left and right lung Cr levels within sex groups. We found Cr levels were higher in the right lung than in the left within the same sex group (Figure 3.16). For example, within the female group, after 24-hour exposure to 0 (saline), 0.2, 0.4, and 0.8 mg/kg zinc chromate, the mean levels of Cr in the left lung were 0.010, 0.417, 0.678, and 1.456 mg Cr/kg lung tissue, respectively; these values in the right lung were 0.087, 3.997, 7.244, and 19.685 mg Cr/kg lung tissue, respectively. In the right lung of female rats, there were statistically significant increases following exposure to 0.4 and 0.8 mg/kg zinc chromate (*p<0.05 and ****p<0.0001, respectively). In the female rat group, dose-dependent increases in Cr levels were statistically significant in the right lung when compared to the left lung (****p<0.0001). In the male rat group, after 24-hour zinc chromate exposure at 0 (saline), 0.2, 0.4 and 0.8 mg/kg, the mean levels of Cr in the left lung were

0.0127, 0.301, 1.505 and 1.163 mg Cr/kg lung tissue, respectively, versus 0.072, 3.423, 5.773 and 14.556 mg Cr/kg lung tissue in the right lung, respectively. There was a statistically significant increase after exposure to 0.8 mg/kg zinc chromate (**p<0.01). Likewise, there was a statistically significant increase in Cr levels in the right lung compared with the left lung in the male rat group (**p<0.01). The difference between the left and right lungs in female rats was statistically more significant (Figure 3.16). Changes in Cr level deposition were also statistically different between sexes (*p<0.05) (Figure 3.16).

We then investigated the distribution of Cr in each lung lobe by sex. We found dose-dependent increases in Cr levels in all lobes, in both females and males, with the exception of the left lung, right superior lobe, and the right inferior lobe of male rats (Figure 3.17). The Cr levels in the lung lobes were not similar to those in the corresponding lung lobes in different sex groups. For example, in the right superior lung of female rats, Cr concentrations increased with Cr(VI) dose, but in the right superior lung of male rats, Cr concentrations instead decreased compared with 0.2 mg/kg after 24-hour exposure to 0.4 and 0.8 mg/kg zinc chromate. In the right inferior lung of female rats, there was a statistically significant increase in Cr concentration after 24-hour exposure to 0.4 and 0.8 mg/kg zinc chromate (*p<0.05, ****p<0.0001), whereas in the right inferior lung of male rats, the concentration was only statistically significant after 24-hour exposure to 0.4 mg/kg zinc chromate (*p<0.05). However, the Cr level decreased after 24-hour exposure to 0.8 mg/kg zinc chromate compared with 0.4 mg/kg exposure. Although there was a dose-dependent increase in Cr concentration with statistical

significance after 24-hour exposure to 0.8 mg/kg zinc chromate, in the right accessory lobe of both female and male rats (****p<0.0001). There was considerable variability in Cr levels after exposure to 0.8 mg/kg zinc chromate in male rats. In the right middle lobe, the trend of increasing Cr concentration with increasing dose was similar in both sex groups. Therefore, we selected the middle lobe of the rat lung for subsequent immunofluorescence studies. In addition, we found that in the female rat group, the distribution of Cr in different lung lobes was significantly different (****p<0.0001). Moreover, there were statistically significant differences in the distribution of Cr in each lobe between the different sex groups (*p<0.05).

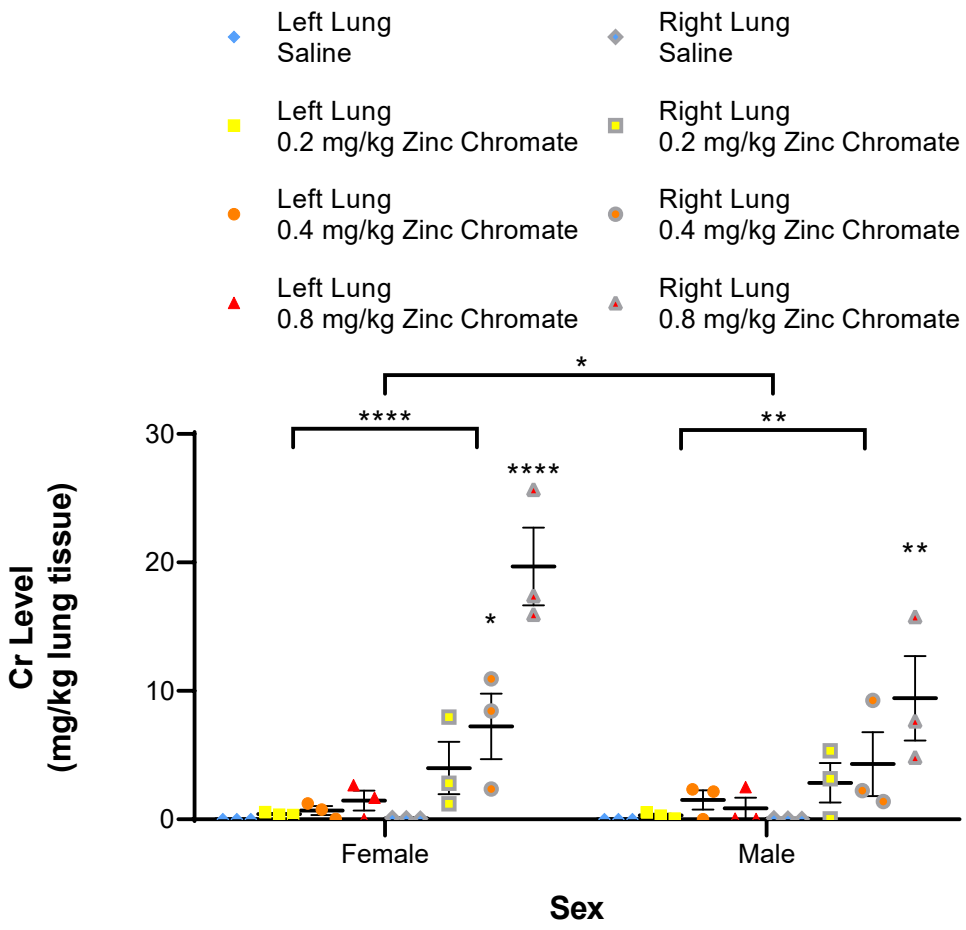

Figure 3.16. Comparison of Cr levels in the left and right lungs of rats after exposure for 24 hours within and between groups of different sexes. Cr levels increased dose-dependently in either left or right lung, female or male rat. In the same sex group, the right lung had higher Cr content than the left lung. In the right lung of the female group, there were statistically significant increases following 24-hour exposure to 0.4 and 0.8 mg/kg zinc chromate (*p<0.05, ****p<0.0001). In the female rat group, there was a statistically significant dose-dependent increase in Cr levels in the right lung compared with the left lung (****p<0.0001). There was also a statistically significant increase in Cr levels in the right lung of the male rat group compared with the left lung (**p<0.01). Among groups, there was a

statistically significant increase (**p<0.01) in the right lungs of male rats exposed to 0.8 mg/kg zinc chromate for 24 hours. Changes in Cr deposition were also statistically different between sexes (*p<0.05). Error bar = standard error of the mean.

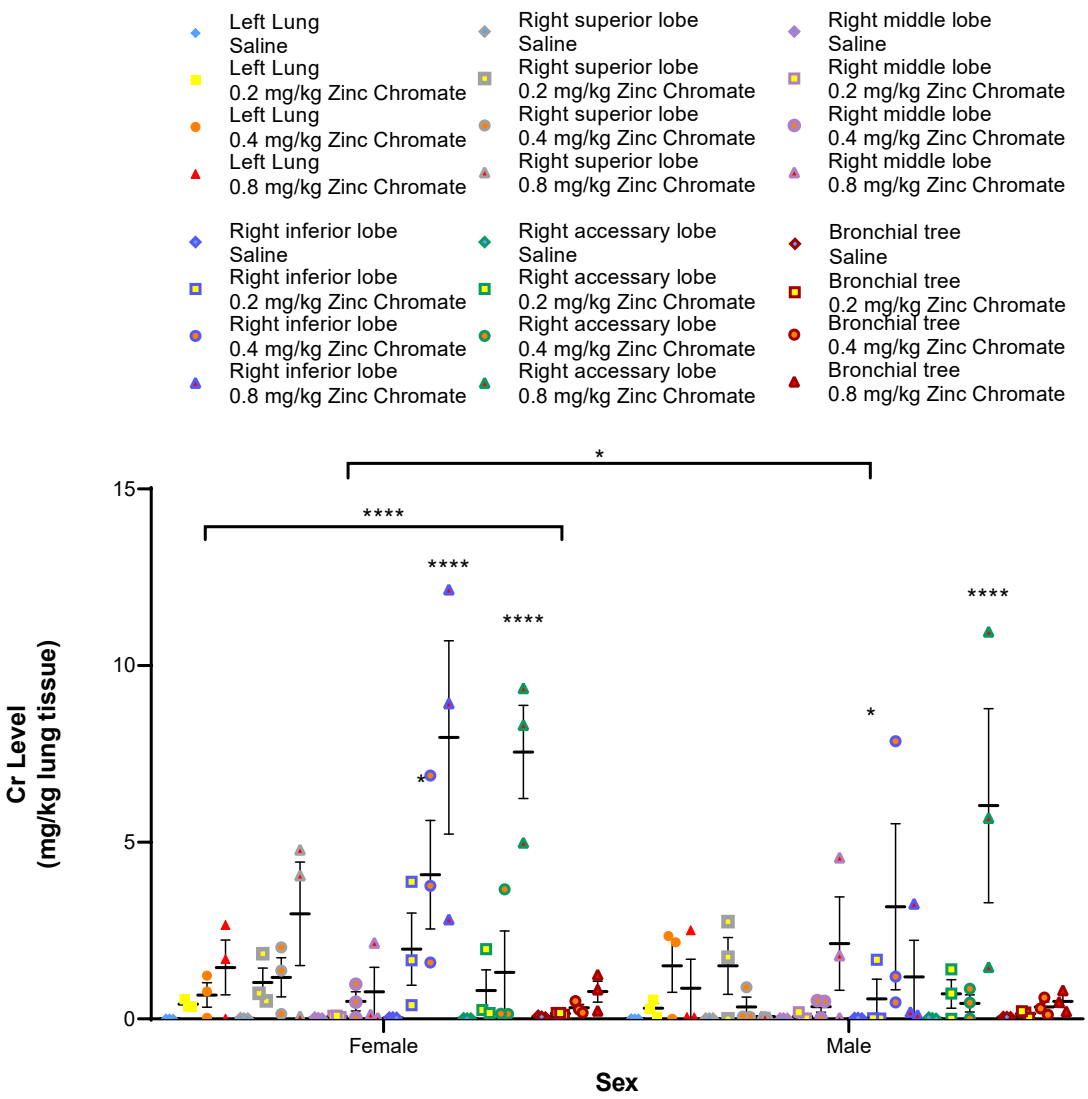

Figure 3.17. Comparison of Cr distribution in lung lobes after exposure for 24 hours within and between groups of different sexes. The graph shows a dose-dependent increase in Cr content in all lung lobes, including in females and males, except the left, right upper, and right lower lobes of male rats. The distribution of Cr in lung lobes of different sex groups was different from those of the corresponding lung lobes. In the right lower lung of female rats, Cr concentrations were significantly increased after 24-hour exposure to 0.4 and 0.8 mg/kg zinc chromate (*p<0.05 and

****p<0.0001, respectively), while in male rats of the right lower lung, they were significantly different after 24-hour 0.4 mg/kg zinc chromate exposure (*p<0.05). In the right accessory lobe of female and male rats, there were statistically significant increases in Cr concentrations after 24-hour exposure to 0.8 mg/kg zinc chromate (****p<0.0001). In the female rat group, the distribution of Cr in different lung lobes was significantly different (****p<0.0001). There were statistically significant differences in Cr distribution in each lobe between the different sex groups (*p<0.05). Error bar = standard error of the mean.

Lung Histological Change

We next investigated potential differences in inflammatory cell aggregation in the lungs of female and male rats. We found aggregation of inflammatory cells in the lungs of female rats was significantly more pronounced after 24-hour exposure to zinc chromate than to saline exposure (Figure 3.18). Inflammatory cell scores significantly increased after 24-hour exposure to 0.2 and 0.8 mg/kg zinc chromate (*p<0.05 and **p<0.01, respectively). However, 24-hour exposure to zinc chromate in male rats resulted in a slightly greater degree of inflammatory cell aggregation in the lungs than in the saline-exposed group (Figure 3.18). There were statistically significant differences in inflammatory cell aggregation between the different sex groups (****p<0.0001).

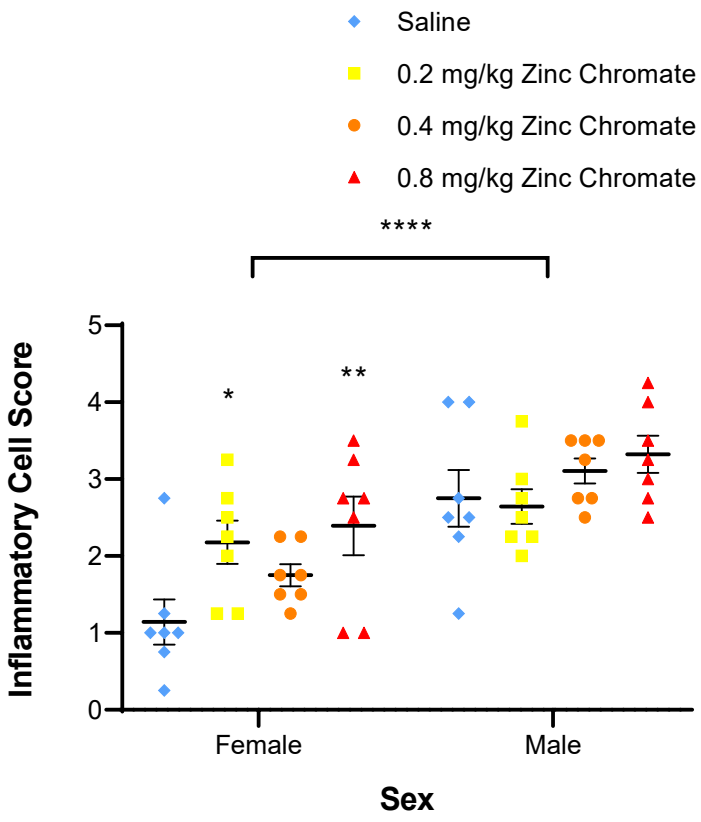

Figure 3.18. Comparison of inflammatory cell aggregation after exposure for 24 hours within and between groups of different sexes. Inflammatory cell aggregation in the lungs of female rats was more pronounced after 24-hour exposure to zinc chromate compared with the saline group. Inflammatory cell scores were significantly increased after exposure to 0.2 and 0.8 mg/kg zinc chromate for 24 hours (*p<0.05, **p<0.01). 24-hour exposure to zinc chromate in male rats resulted in slightly higher levels of inflammatory cell aggregation in the lungs than in the saline-exposed group. Inflammatory cell aggregation was statistically different between the female and male groups (****p<0.0001). Error bar = standard error of the mean.

DNA Double Strand Breaks

We then investigated γ-H2AX foci formation in bronchioles and alveoli by sex. We found that in bronchioles, γ-H2AX foci formation increased with zinc chromate dose in both female and male rats (Figure 3.19). Cr(VI)-induced foci formation was not statistically different between sex groups in bronchioles. In alveoli, γ-H2AX foci formation in male rats all increased with zinc chromate dose but not in female rats (Fig. 3.20). γ-H2AX foci formation was significantly increased in male rats after 24h zinc chromate exposure (*p<0.05). Comparing γ-H2AX foci formation in alveoli between sex groups, there were some differences in Cr(VI)-induced γ-H2AX foci formation, although the difference was not statistically significant.

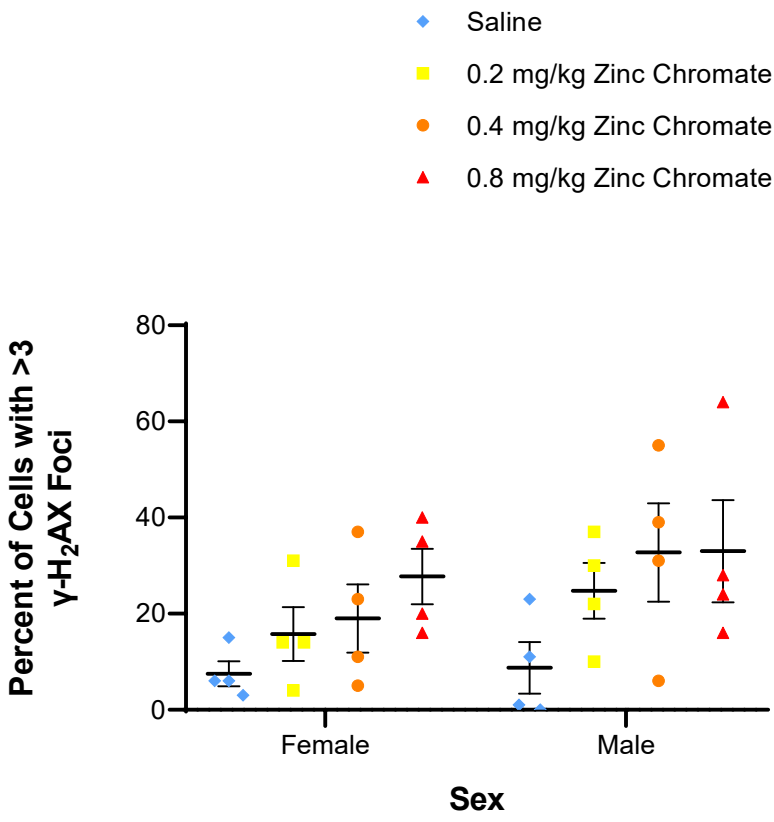

Figure 3.19. Comparison of γ-H2AX foci formation in bronchioles after 24-hour exposure to zinc chromate within and between groups of different sexes. There were dose-dependent increases in foci formation in female and male rats following 24-hour exposure to zinc chromate. When comparing bronchioles between sex groups, no statistical differences in Cr(VI)-induced foci formation were found. Error bar = standard error of the mean.

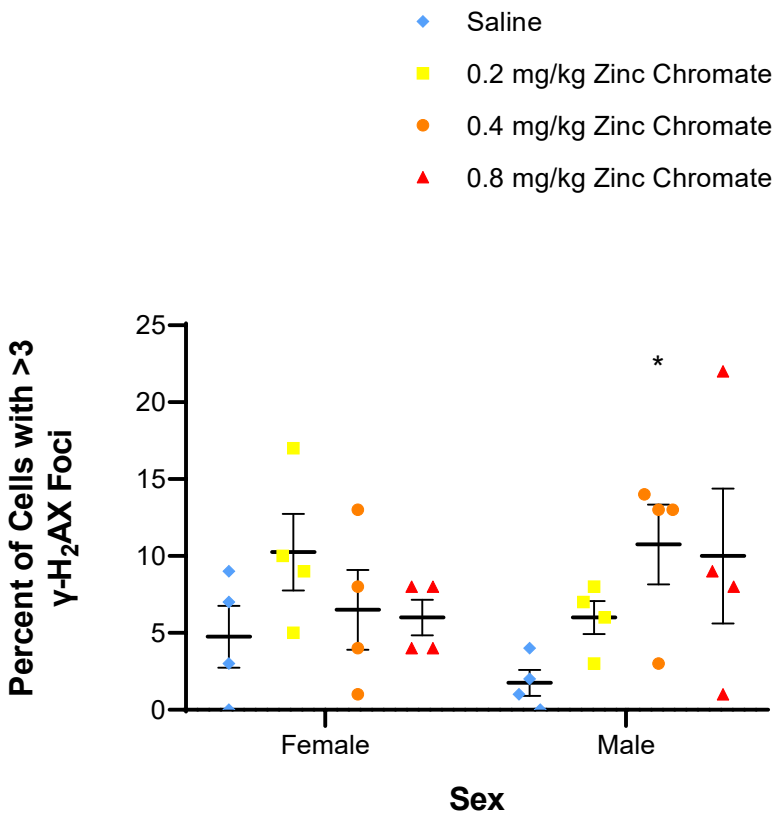

Figure 3.20. Comparison of γ-H2AX foci formation in alveoli after 24-hour exposure to zinc chromate within and between groups of different sexes. γ-H2AX foci formation in alveoli increased with zinc chromate doses in male rats, but not in female rats. γ-H2AX foci formation was significantly increased in male rats after 24-hour exposure to zinc chromate (*p<0.05). Cr(VI)-induced γ-H2AX foci formation was not statistically different between the sex groups in alveoli. Error bar = standard error of the mean.

HR Repair

We also studied RAD51 foci formation in bronchioles and alveoli by sex. We found that in bronchioles, RAD51 foci formation increased with zinc chromate doses in female and male rats (Figure 3.21). When comparing the sex groups for Cr(VI)-induced RAD51 foci formation in bronchioles, no statistical differences were found. In alveoli, RAD51 foci formation increased with zinc chromate doses in male rats, but not in female rats (Figure 3.22). When comparing different sex groups in alveoli, there were some differences in Cr(VI)-induced RAD51 foci formation, although they were not statistically significant.

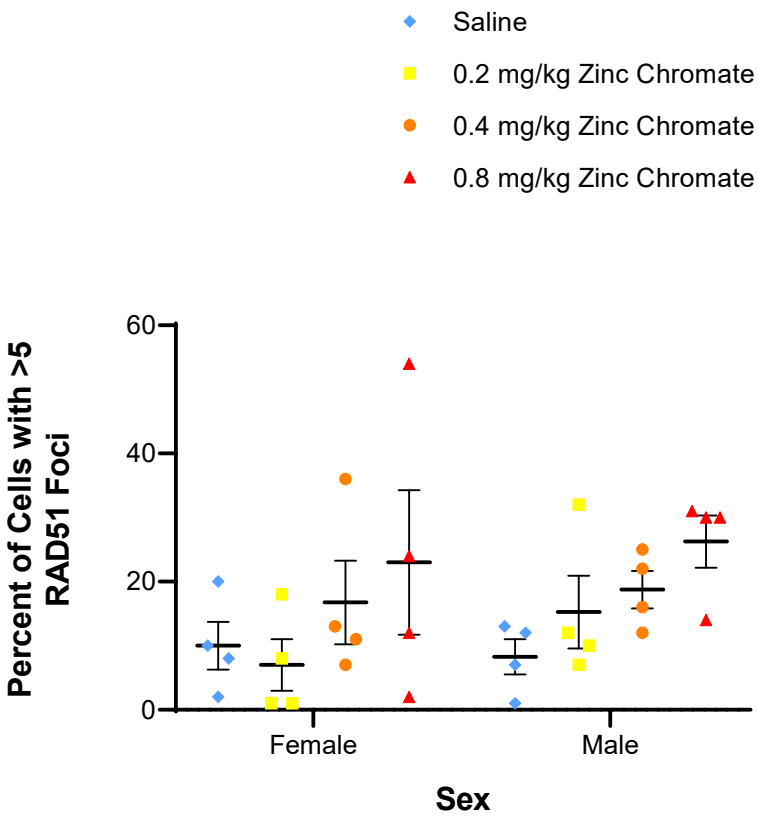

Figure 3.21 Comparison of RAD51 foci formation in bronchioles after 24-hour exposure to zinc chromate within and between groups of different sexes. RAD51 foci formation increased with zinc chromate dose in female and male rats in bronchioles after 24-hour exposure. When comparing the sex groups in bronchioles, no significant differences in Cr(VI)-induced RAD51 foci formation were found. Error bar = standard error of the mean.

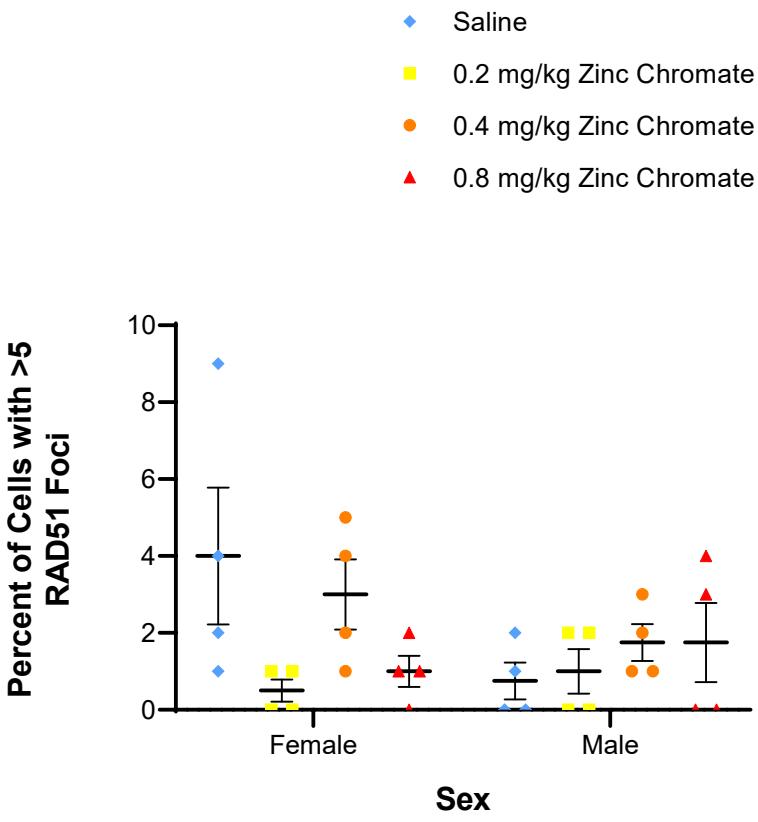

Figure 3.22. Comparison of RAD51 foci formation in alveoli after 24-hour exposure to zinc chromate within and between groups of different sexes. RAD51 foci formation in alveoli in female rats was not increased after Cr(VI) exposure compared with the saline-exposed group. RAD51 foci formation in male rats increased with zinc chromate dose in alveoli. Cr(VI)-induced RAD51 foci formation was not significantly different between sex groups in the alveoli. Error bar = standard error of the mean.

Accumulation of Other Metals

Zinc Levels

Because we treated the rats with zinc chromate, we also measured zinc levels in the rat lungs. Zinc is an essential trace element for the human body. It can pass through the cell membrane both inside and outside the cell according to the needs of the cell. We found that zinc levels in rat lung tissue did not increase with dose after 24-hour zinc chromate exposure (Figure 3.23). For example, after 24-hour exposure to 0 (saline), 0.2, 0.4, and 0.8 mg/kg zinc chromate, the mean levels of zinc in the whole lung were 98.792, 86.435, 91.2, and 121.655, respectively. Mean whole lung zinc levels were even lower in the 0.2 and 0.4 treatment groups than in the saline group. Combined with Cr data in the whole rat lung, a dose-dependent accumulation of Cr was confirmed in the rat lung. After entering the cell, hexavalent chromium is reduced to trivalent chromium, which easily binds to intracellular macromolecules and then is too large to pass through the membrane and return to the outside of the cell. However, the transport of zinc inside and outside the cell membrane is bidirectional due to cellular requirements.

We then investigated the distribution of zinc levels in the left and right lungs of rats, respectively. After 24-hour exposure, zinc levels in the left rat lung exposed to zinc chromate were not higher than those of rats exposed to saline (Figure 3.24). However, after exposure to 0.4 mg/kg and 0.8 mg/kg zinc chromate for 24 hours, respectively, the levels of zinc in the right rat lung were higher than those of the saline group (Figure 3.24). There was a statistically significant increase after exposure to 0.8 mg/kg zinc chromate ($*p<0.05$). Zinc levels were significantly

higher in the right lung than in the left lung (****p<0.0001). Combined with Cr data, more zinc chromate particles accumulated in the right lung of rats.

We further assessed zinc distribution in each lung lobe. After 24-hour exposure to zinc chromate, zinc levels did not change consistently in each rat lung lobe (Figure 3.25). Zinc levels were increased in the right inferior and accessary lung lobes, whereas zinc levels were decreased in the left lung lobe, right superior lung lobe and bronchial tree after 24-hour exposure to zinc chromate. Zinc levels in the right middle lung lobe slightly increased after 0.8 mg/kg zinc chromate exposure and decreased after 0.2 and 0.4 mg/kg zinc chromate exposures. After 24-hour 0.8 mg/kg zinc chromate exposure, zinc levels in the right accessory lobe were significantly increased (****p<0.0001). Significantly lower metal levels in the bronchial tree found in the Cr data than in other lobes were not found in the zinc data.

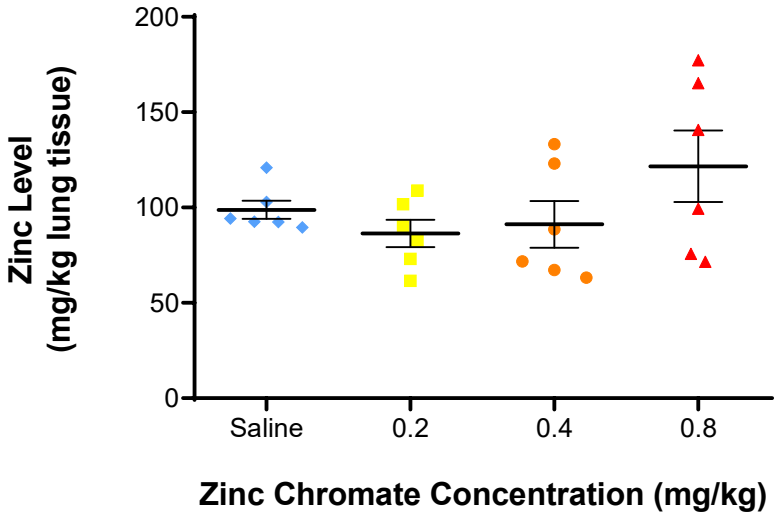

Figure 3.23. Zinc levels in whole rat lungs after 24-hour exposure. Zinc levels in the whole lung tissue of rats did not increase in a dose-dependent manner compared to the saline group after 24-hour exposure to zinc chromate.

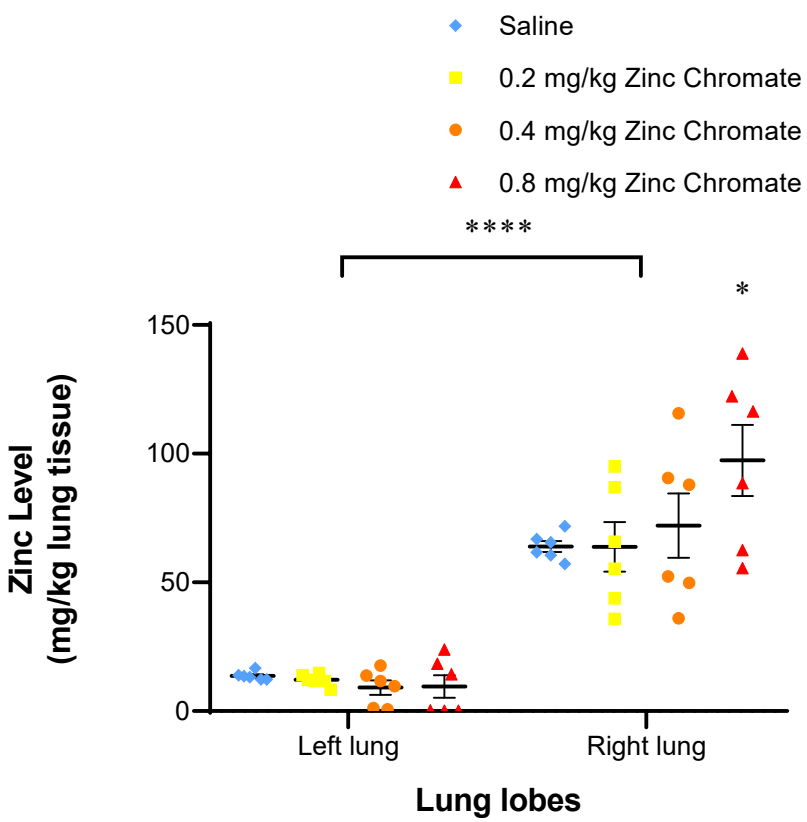

Figure 3.24. Zinc levels in the left and right rat lungs after 24-hour exposure. Zinc levels in the left lung of rats did not increase after 24-hour exposure to zinc chromate. However, after exposure to 0.4 mg/kg and 0.8 mg/kg zinc chromate for 24 hours, respectively, zinc levels in the right lung of rats increased. There was a statistically significant increase after exposure to 0.8 mg/kg zinc chromate (*p<0.05). Zinc levels were significantly higher in the right lung compared with the left lung (****p<0.0001). Error bar = standard error of the mean.

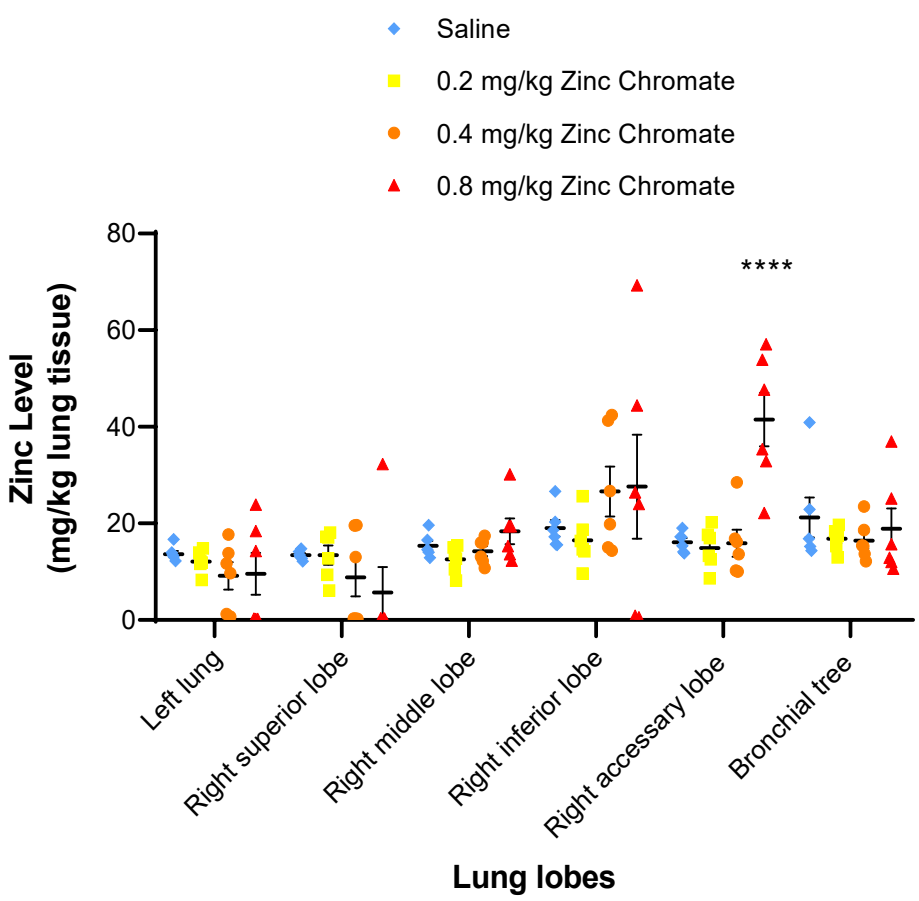

Figure 3.25. Zinc distribution in each individual rat lung lobe after 24-hour zinc chromate exposure. This figure shows changes in zinc levels in each rat lung lobe were not consistent after 24-hour exposure to zinc chromate. Zinc levels were increased in the right middle lung and right accessory lung, whereas zinc levels were decreased in the left lung, right upper lung, and bronchial tree. Zinc levels in the right middle lung slightly increased after 0.8 mg/kg zinc chromate exposure and decreased after 0.2 and 0.4 mg/kg zinc chromate exposures. Zinc levels in the right appendage were significantly increased after 24-hour 0.8 mg/kg zinc chromate exposure (****p<0.0001). Error bar = standard error of the mean.

Iron Uptake

We investigated iron levels in rat lungs. We found iron levels did not increase but instead slightly decreased in rat lung tissue after 24-hour exposure to zinc chromate (Figure 3.26). For example, after 24-hour zinc chromate exposure at 0 (saline), 0.2, 0.4, and 0.8 mg/kg, mean whole lung iron levels were 177.497, 150.513, 119.59, and 175.933, respectively. Mean whole lung zinc levels were even lower in the 0.2 and 0.4 treatment groups than in the saline group. Combined with Cr and zinc level data in the whole rat lung, a dose-dependent accumulation of chromium in the rat lungs was further confirmed.

We further investigated iron distribution in each lung lobe. After 24-hour exposure to zinc chromate, iron levels in each rat lung lobe tended to decrease except for a slight increase in the bronchial tree (Figure 3.28). Iron levels in the left and right lower lungs were significantly reduced after 24-hour exposure to 0.4 mg/kg zinc chromate ($*p<0.05$). Iron levels in the bronchial tree were higher than in other lobes.

There is a certain relationship between the metabolism of different metals such as iron, zinc, copper and chromium in the body, and their interactions are either antagonistic or synergistic (Staniek and Wójciak, 2018). Staniek and Wójciak found that CR(III) supplementation reduces iron levels in the kidneys of rats in the recommended iron diet group (Staniek and Wójciak, 2018). We therefore investigated whether chromium exposure affects functional iron levels in rat lungs. We used the ratio of iron content to Cr content to assess functional iron levels in rat lungs. We found functional iron levels were significantly reduced after 24-hour

zinc chromate exposure (Figure 3.29). Specifically, after 24-hour exposure to 0 (saline), 0.2 mg/kg, 0.4 mg/kg and 0.8 mg/kg zinc chromate, iron to Cr ratios in rat lungs were 11701, 3254, 1326 and 1428, respectively. These data suggest that Cr exposure affects iron metabolism in rats.

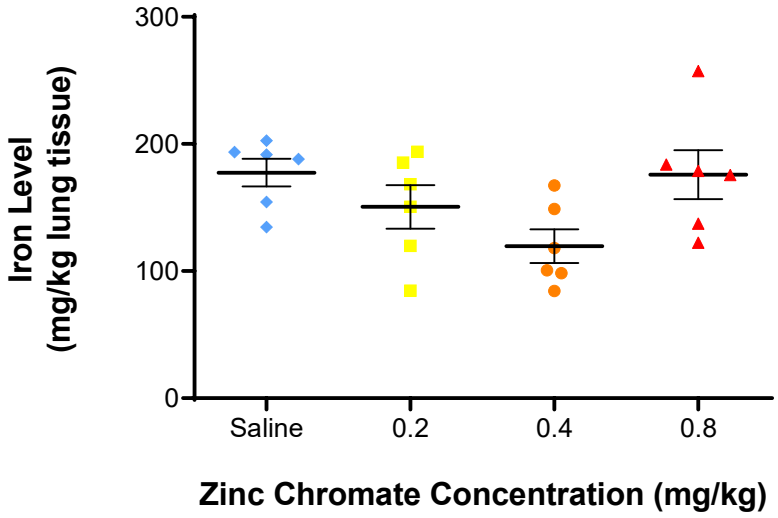

Figure 3.26. Iron levels in the whole rat lungs after 24-hour exposure. Iron levels in the rat lung tissue decreased after 24-hour exposure to zinc chromate. Mean whole-lung iron levels were lower than those of the saline group after 24-hour zinc chromate exposure at 0.2 and 0.4 mg/kg. Error bar = standard error of the mean.

We then investigated the distribution of iron levels in the left and right lungs of rats, respectively. After 24-hour exposure, iron levels in both the left and right lungs of rats exposed to zinc chromate were not higher than those of rats exposed to saline (Figure 3.27). Iron levels were significantly higher in the right lung than in the left lung (****p<0.0001).

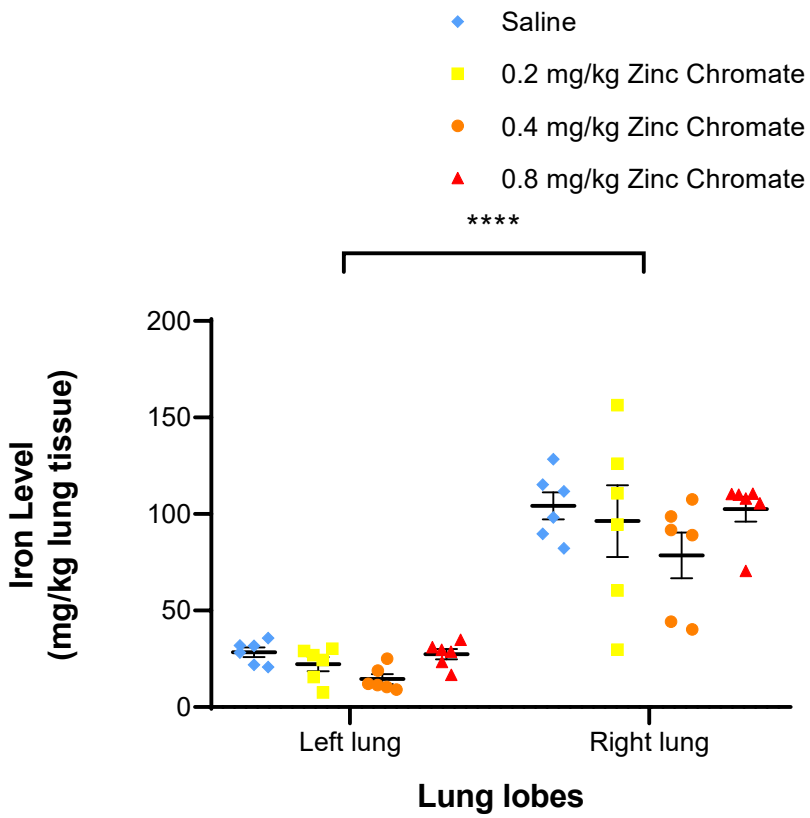

Figure 3.27. Iron levels in the left and right rat lungs after 24-hour exposure. This figure shows iron levels in both the left and right lungs of rats were no higher than in saline-exposed rats after 24-hour zinc chromate exposure. Iron levels were statistically significantly higher in the right lung when compared to the left lung (****p<0.0001). Error bar = standard error of the mean.

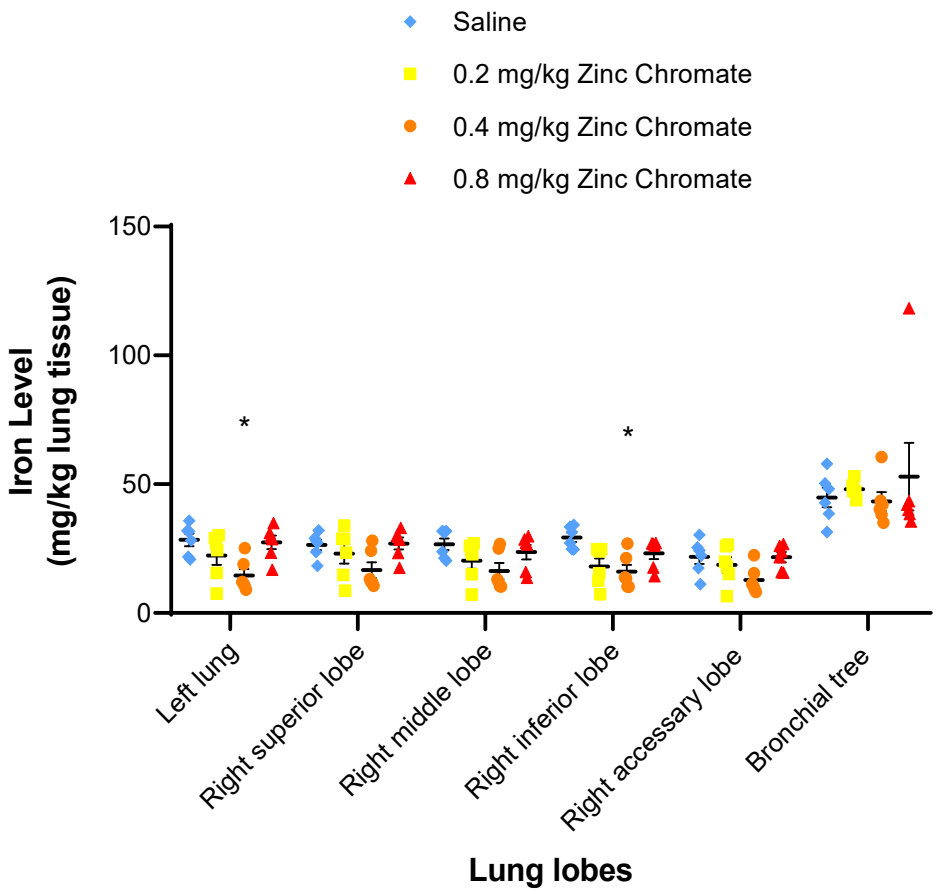

Figure 3.28. Iron distribution in individual rat lung lobes after 24-hour zinc chromate exposure. Iron levels in each rat lobe decreased except for a slight increase in the bronchial tree after 24-hour exposure to zinc chromate. Iron levels in the left lung and right inferior lung lobe were significantly decreased after 24-hour exposure to 0.4 mg/kg zinc chromate (*p<0.05). The iron levels were higher in the bronchial tree than in other lobes. Error bar = standard error of the mean.

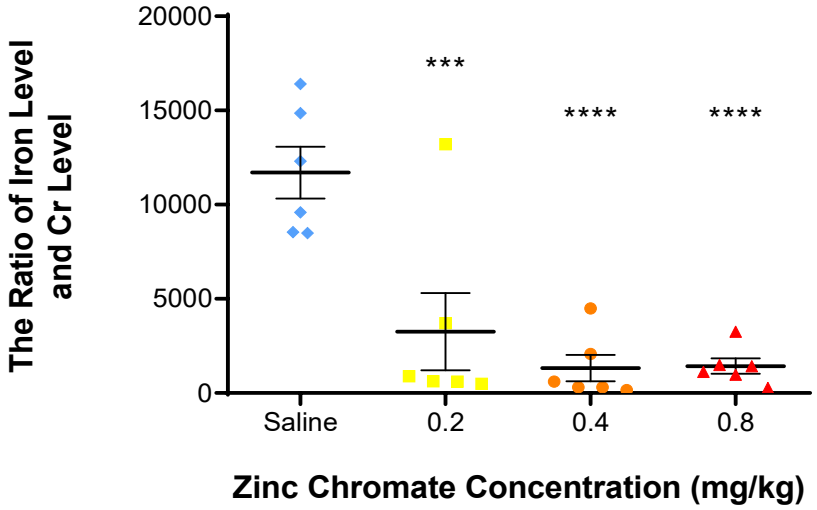

Figure 3.29. Functional iron levels in the rat lung after 24-hour zinc chromate exposure. Functional iron levels decreased after 24-hour zinc chromate exposure. After 24-hour exposure to 0.2 mg/kg, 0.4 mg/kg and 0.8 mg/kg zinc chromate, respectively, the ratios of iron to Cr in the lungs of rats were significantly lower than those of the saline group (****p*=0.001, *****p*=0.001).

SUMMARY

Cr has been listed as a lung carcinogen for decades, but the carcinogenic mechanism of chromium remains unclear. We found in a previous cell culture study that acute Cr(VI) causes DNA double strand breaks and activates HR repair to protect Cr(VI)-induced chromosomal instability. However, these effects have not been verified in animal experiments. We therefore performed corresponding studies in the lungs of rats after acute Cr(VI) exposure.

In this aim, we found a dose-dependent increase in rat lung Cr levels after 24-hour zinc chromate exposure. Chromium accumulation was more pronounced in the right lung than in the left lung. Furthermore, when Cr concentrations in each lung lobe were examined separately, we found that Cr concentration increase in the bronchial tree after acute exposure was significantly less pronounced than in other lobes. These results indicate that Cr(VI) was inhaled and deposited into the distal airways of the rat lung.

Cr(VI)-induced lung histological changes were investigated by H&E staining, and we found inflammatory cell infiltration in the alveolar region after 24-hour Cr(VI) exposure. Inflammatory cells accumulated around the alveoli and terminal airways. In the group exposed to saline for 24 hours, the predominant cell type that aggregated in the alveolar region was macrophages. After 24-hour exposure to zinc chromate, various inflammatory cells, mainly neutrophils, aggregated in the alveolar region and around the terminal airways. After 24-hour exposure, Cr(VI)-induced inflammatory cells clustered around the alveolar areas and terminal airways with a slight increasing trend.

We detected γ-H2AX foci formation in Cr(VI)-exposed rat lungs by immunofluorescence. We found that Cr(VI) induced γ-H2AX foci formation in rat lungs 24- hours after zinc chromate exposure. Cr(VI)-induced γ-H2AX foci formation was increased in bronchioles in a dose-dependent manner. γ-H2AX foci formation caused by Cr(VI) was more pronounced in bronchioles than in alveoli. Moreover, Cr(VI)-induced γ-H2AX foci were formed almost exclusively in epithelial cells, both in bronchiolar and alveolar regions.

We also investigated RAD51 to assess HR repair in rat lungs following 24-hour zinc chromate exposure by immunofluorescence. The results showed Cr(VI) induced RAD51 foci formation in rat lungs after 24-hour exposure to zinc chromate. Cr(VI)-induced RAD51 foci formation increased in a dose-dependent manner in bronchioles. However, there was no increase in RAD51 foci formation in alveoli compared with the saline group. After 24-hour zinc chromate exposure, Cr(VI)-induced RAD51 foci formation was more pronounced in bronchioles than in alveoli.

Comparing different sex groups, we found higher lung levels of Cr in female rats than in male rats. However, acute inflammatory response to Cr(VI) exposure was stronger in male rats than in female rats in terms of lung histology. There were no significant gender differences in the formation of γ-H2AX foci and RAD51 foci.

Aim 2: Demonstrate particulate Cr(VI) induces DNA double strand breaks, inhibits HR repair in the rat lung after 90-day exposure.

BACKGROUND

The HR repair pathway can repair dangerous DNA double strand breaks to prevent Cr(VI)-induced chromosomal instability (Bryant et al., 2006; Gastaldo et al., 2007). However, these data were found in cell culture experiments, and it is not known whether the same results can be seen in animals. In Aim 1, we found acute Cr(VI) induced DNA double strand breaks and HR repair active in rat lung. Cell cultured studies have shown prolonged Cr(VI) exposure induces HR dysfunction by inhibiting RAD51 (Qin et al., 2014; Browning et al., 2016). We therefore investigated DNA double strand breaks and HR repair in rat lungs following subchronic Cr(VI) exposure. We exposed rats to zinc chromate single dose weekly for 90-day and then investigated metal levels, lung histological changes, DNA double strand breaks, and HR repair in rat lungs.

RESULTS

Chromium Accumulation in Lung

After 90 days of oropharyngeal inhalation exposure of rats to zinc chromate, we evaluated whether chromium reached and accumulated in the lungs. We measured Cr levels in rat lung tissue by ICP-MS. Cr accumulation was detected in rat lung tissue (Figure 3.30). We observed dose-dependent increases in Cr levels following 90-day exposure with 0, 0.4, and 0.8 mg/kg zinc chromate (linear

regression analysis: $p<0.0001$) (Figure 3.31). After 90-day exposure to 0 (saline), 0.4, and 0.8 mg/kg zinc chromate, average Cr levels in whole lung tissues were 0.1560, 12.50, and 12.42 mg Cr/kg lung tissue, respectively. Cr levels were significantly higher than the saline group after exposure to 0.4 and 0.8 mg/kg zinc chromate. (***$p<0.001$) (Figure 3.30).

The deposition and removal of inhaled particles in the respiratory tract occur in an uneven manner. We next investigated the specific distribution of zinc chromate particles in both the left and right lungs of rats. We found after 90-day exposure to zinc chromate, Cr levels in the left and right lungs increased in a dose-dependent manner (Figure 3.32). After 90-day exposure to 0 (saline), 0.4 and 0.8 mg/kg zinc chromate, mean Cr levels in the left lungs of rats were 0.008, 1.607, and 1.838 mg Cr/kg lung tissue, respectively, and in the right lung of rats, they are 0.104, 10.67 and 10.22 mg Cr/kg lung tissue. After 90-day 0.4 and 0.8 mg/kg zinc chromate exposures, there were statistically significant increases in Cr levels in the right lung (****$p<0.0001$). In the 0.8 mg/kg treatment group, Cr accumulation in the right lung was not higher than that of the 0.4 mg/kg treatment group. Cr levels were significantly increased in the right lung compared with the left lung ($p<0.0001$).

As for the 24-hour exposure study, we further investigated the distribution of Cr in the lung lobes of each rat after 90-day zinc chromate exposure. After 90-day exposure to zinc chromate, Cr levels in each rat lung lobe increased in a dose-dependent manner (Figure 3.33). For example, after 90-day exposure to saline, 0.4 and 0.8 mg/kg zinc chromate exposure, mean Cr levels in the right superior

lobe were 0.017, 7.003 and 2.864 mg Cr/kg lung tissue, respectively. After 90-day 0.4 and 0.8 mg/kg zinc chromate exposures, there were statistically significant increases in right superior lobe Cr levels (****p<0.0001, *p<0.05). We also found Cr levels in the right accessory lobe were significantly increased after 90-day 0.8 mg/kg zinc chromate exposure (**p<0.01). However, the increase in Cr concentration in the bronchial tree after 90-day exposure was significantly lower than in other lobes (*p<0.05) (Fig. 3.34). This result indicates particulate Cr(VI) was inhaled and deposited into the distal airways of the rat lungs after 90-day exposure.

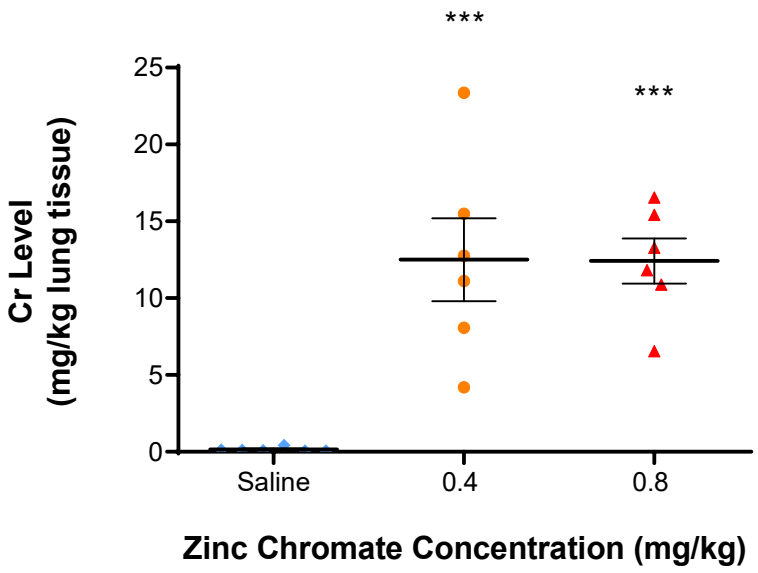

Figure 3.30. Cr levels in whole rat lungs after 90-day exposure. Cr levels increased after 90-day zinc chromate exposure. There were dose-dependent increases in Cr levels following 90-day exposure with 0 (saline), 0.4, and 0.8 mg/kg zinc chromate (linear regression analysis: $p<0.0001$). Compared with the saline-exposed group, Cr levels were significantly increased after exposure to 0.4 and 0.8 mg/kg zinc chromate (***$p<0.001$). Error bar = standard error of the mean.

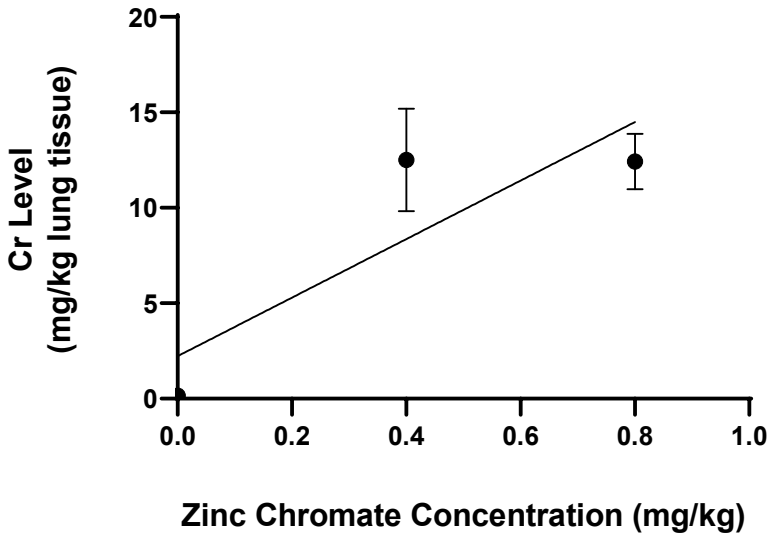

Figure 3.31. Cr levels in whole rat lungs after 90-day exposure shown with regression line. There was a linear correlation between these 3 groups, including 0 (saline), 0.4 mg/kg and 0.8 mg/kg zinc chromate (p=0.0009).

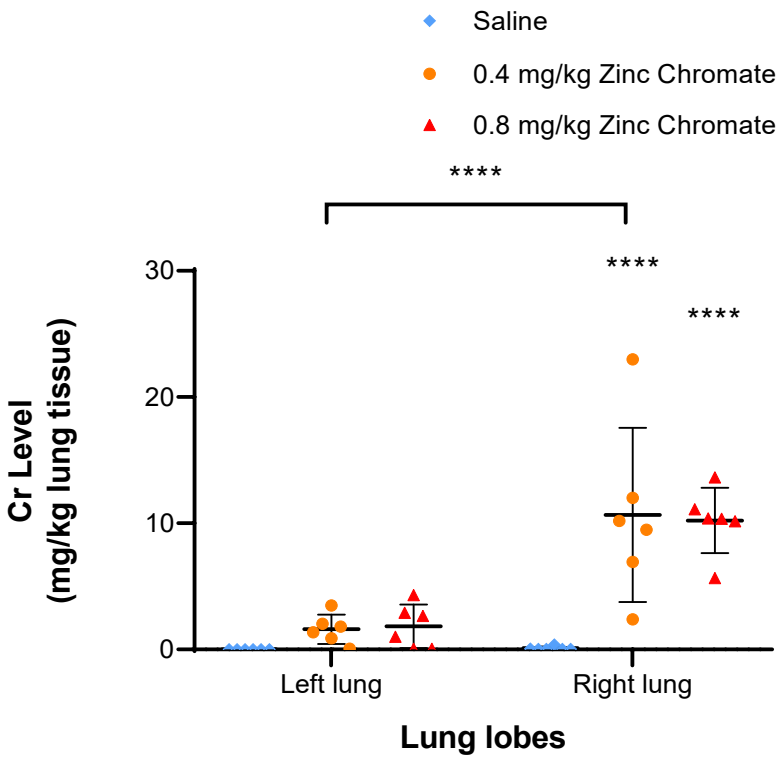

Figure 3.32. Cr levels in the left rat lung vs. right rat lung after 90-day exposure. Cr levels increased in a dose-dependent manner in the left and right lungs (linear regression analysis: left lung $p<0.05$ and right lung $p<0.01$). Cr level increases were statistically significant in the right lung (****$p<0.0001$). Cr levels were significantly increased in the right rat lung compared with the left rat lung (****$p<0.0001$). Error bar = standard error of the mean.

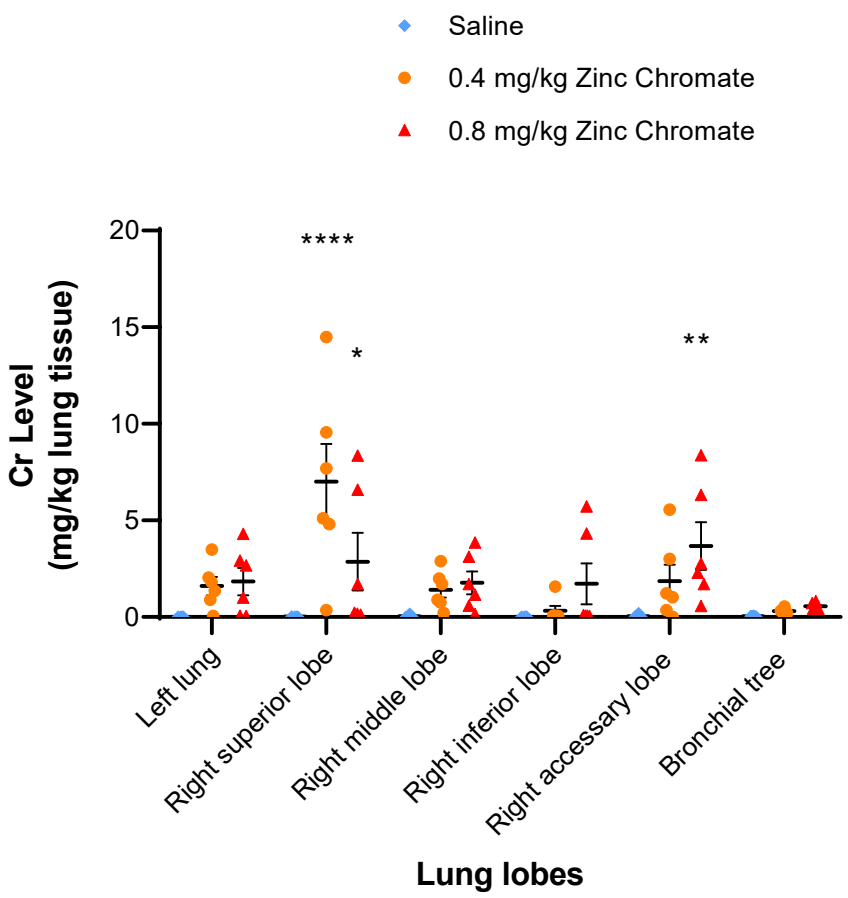

Figure 3.33. Cr distribution in each individual rat lung lobe after 90-day zinc chromate exposure. Cr levels in each rat lung lobe increased in a dose-dependent manner after 90-day exposure to zinc chromate. Right upper lobe Cr levels were significantly increased after 90-day zinc chromate exposure at 0.4 and 0.8 mg/kg (****p<0.0001 and *p<0.05, respectively). Cr levels in the right accessory lobe were significantly increased after 90-day 0.8 mg/kg zinc chromate exposure (**p<0.01). Error bar = standard error of the mean.

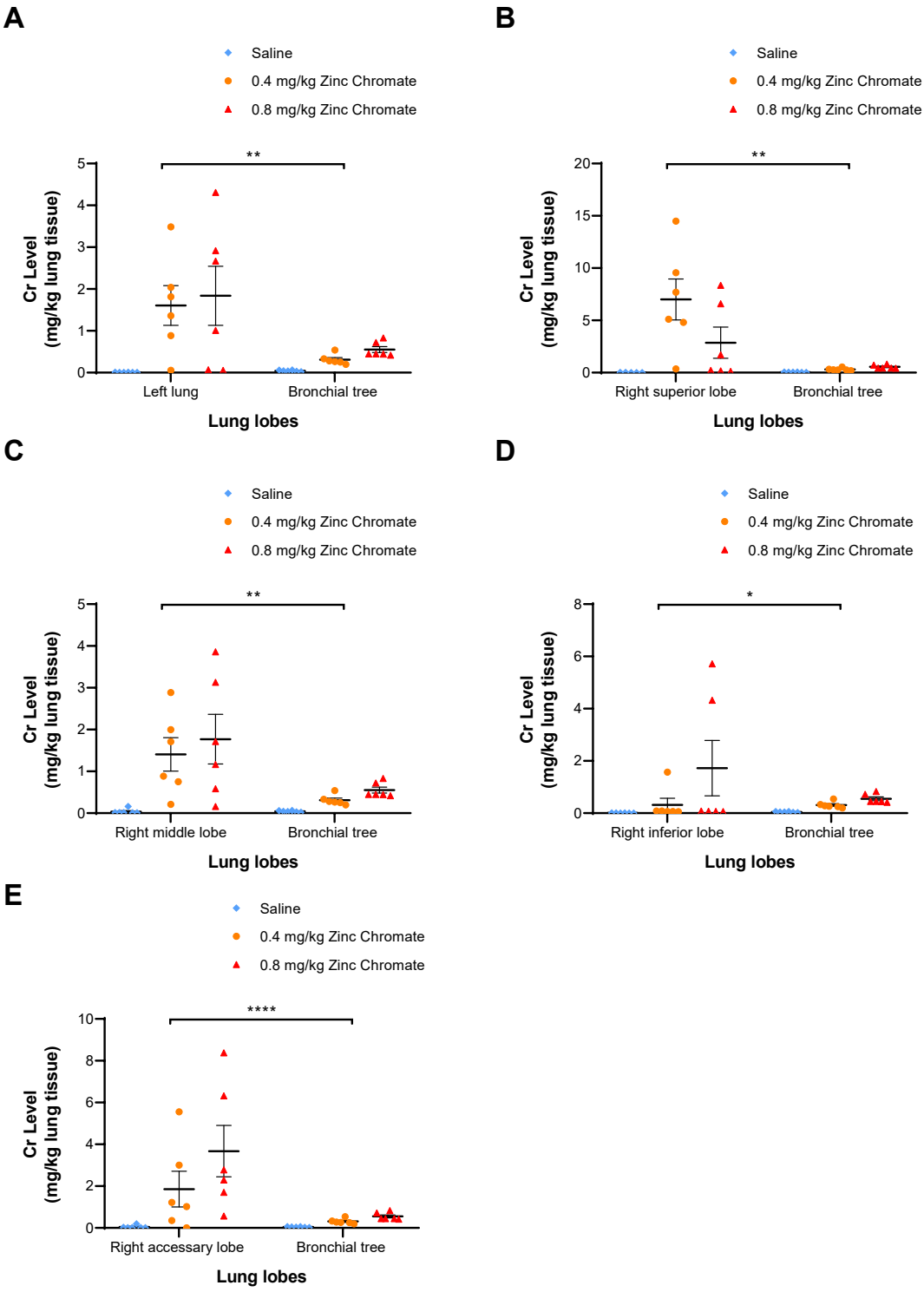
A
Saline
0.4 mg/kg Zinc Chromate
0.8 mg/kg Zinc Chromate
Cr Level (mg/kg lung tissue)
**
Left lung
Bronchial tree
Lung lobes
B
Saline
0.4 mg/kg Zinc Chromate
0.8 mg/kg Zinc Chromate
Cr Level (mg/kg lung tissue)
**
Right superior lobe
Bronchial tree
Lung lobes
C
Saline
0.4 mg/kg Zinc Chromate
0.8 mg/kg Zinc Chromate
Cr Level (mg/kg lung tissue)
**
Right middle lobe
Bronchial tree
Lung lobes
D
Saline
0.4 mg/kg Zinc Chromate
0.8 mg/kg Zinc Chromate
Cr Level (mg/kg lung tissue)
*
Right inferior lobe
Bronchial tree
Lung lobes
E
Saline
0.4 mg/kg Zinc Chromate
0.8 mg/kg Zinc Chromate
Cr Level (mg/kg lung tissue)
****
Right accessary lobe
Bronchial tree
Lung lobes

Figure 3.34. Cr distribution in the bronchial tree and other lung lobes after 90-day zinc chromate exposure. Cr level elevation was significantly less pronounced in the bronchial tree than in the other lung lobes. A. Cr level elevation in the bronchial tree vs. left lung (**p<0.01). B. Cr level elevation in the bronchial tree vs. right superior lobe (**p<0.01). C. Cr level elevation in the bronchial tree vs. right middle lobe (**p<0.01). D. Cr level elevation in the bronchial tree vs. right inferior lobe (*p<0.05). E. Cr level elevation in the bronchial tree vs. right accessory lobe (****p<0.0001). Error bar = standard error of the mean.

Lung Histological Change

We investigated Cr(VI)-induced lung histological changes following 90-day zinc chromate exposure by H&E staining. We found macrophage aggregation and lymphocyte aggregation in the alveolar region after 90-day Cr exposure. Macrophages accumulated mainly around the alveoli and terminal airways (Figure 3.35). Lymphocytes were mainly in the alveolar interstitium, and the alveolar wall was thickened. A large number of necrotic cells were seen in the alveoli. Thickening of the blood vessel wall was seen in the lungs of Cr(VI)-exposed rats (Figure 3.35). Cr(VI)-induced macrophage aggregation around the alveolar areas and terminal airways, and increased with Cr dose after 90-day exposure to zinc chromate (Fig. 3.36).

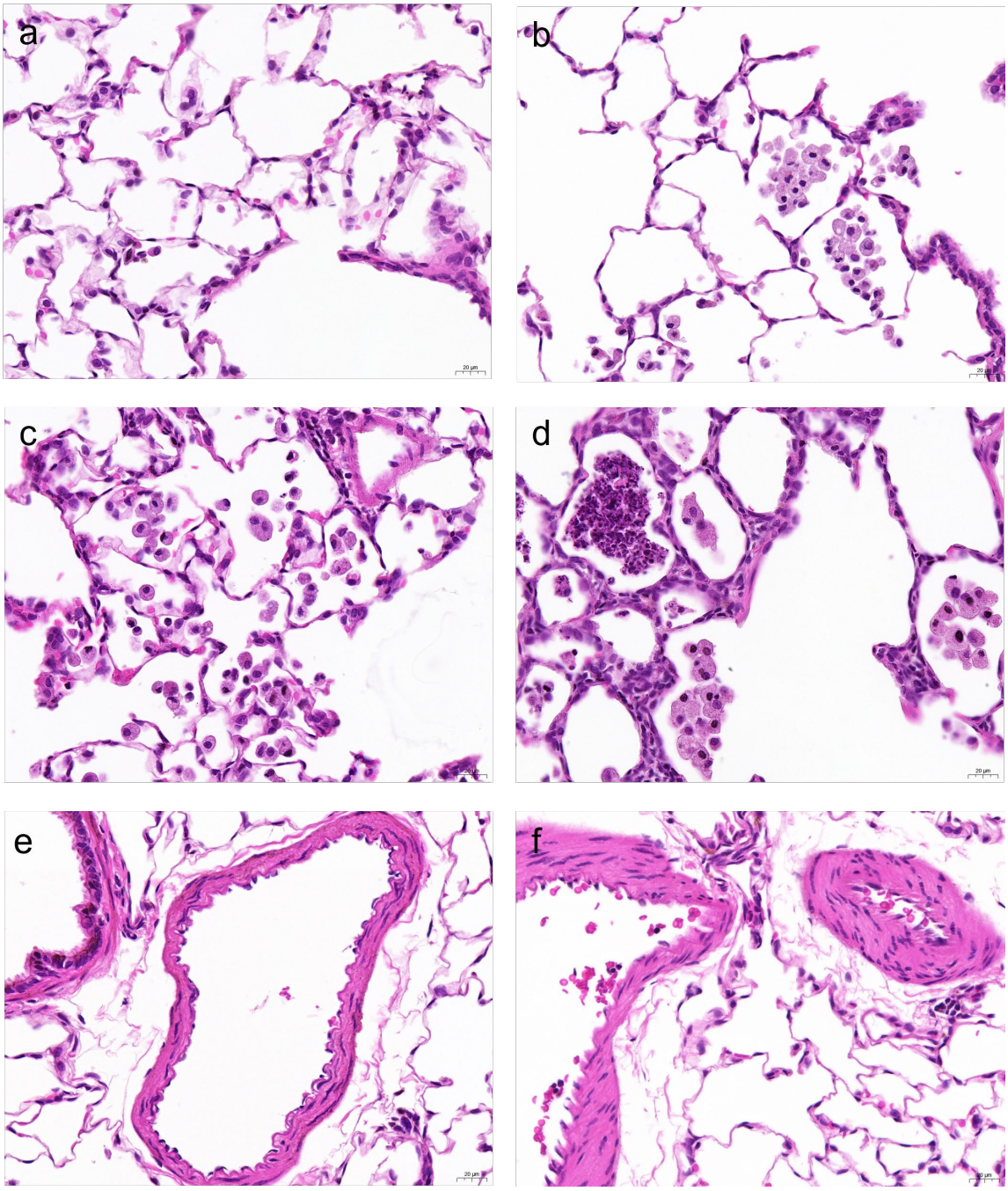

Figure 3.35. Cr(VI) induces inflammation and vascular wall changes in the rat lung after 90-day exposure. a. Few macrophages accumulated in the alveolar region after 90-day exposure to saline. b. Some macrophages accumulated in the alveolar region after 90-day exposure to 0.4 mg/kg zinc chromate. c. A great

number of macrophages accumulated in the alveolar region after 90-day exposure to 0.8 mg/kg zinc chromate. d. Many necrotic cells and macrophages in the alveoli, with alveolar wall thickening. e. Normal blood vessels in the rat lung after 90-day exposure to saline. f. Blood vessel wall thickening in the rat lung after 90-day 0.8 mg/kg zinc chromate exposure. Magnification in a-f: x400.

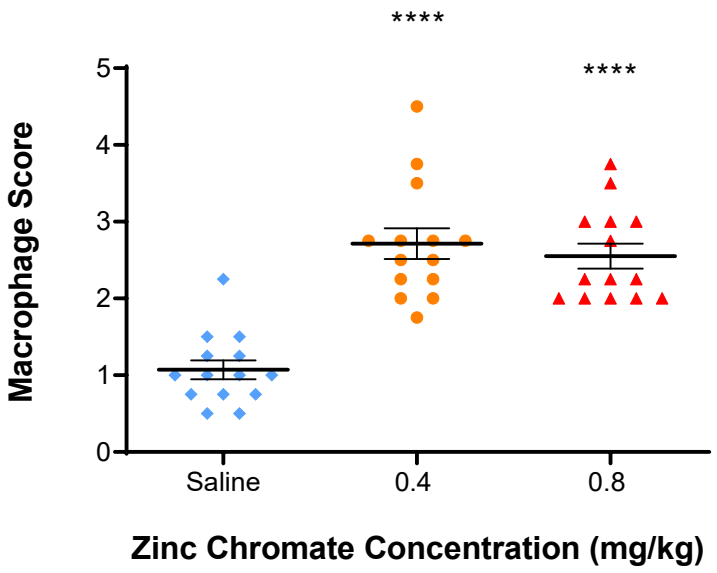

Figure 3.36. Cr induces macrophage aggregation in the rat lung after 90-day exposure. Macrophage aggregation increased after 90-day exposure to zinc chromate compared with saline exposure. After 90-day exposure to 0.4 and 0.8 mg/kg zinc chromate, there were statistically significant increases in macrophage scores (*****p<0.0001). Macrophages were scored according to Table 1.3. Macrophages and inflammatory cells scoring system. Error bar = standard error of the mean.

DNA Double Strand Break

Having established that particulate Cr(VI) was inhaled and deposited and caused histological changes in rat lungs, we next examined the formation of γ-H2AX foci in Cr-exposed rat lungs by immunofluorescence. We found Cr(VI) induced γ-H2AX foci formation in rat lungs after 90-day zinc chromate exposure (Figure 3.37). We also studied γ-H2AX foci formation in different lung sites. Cr(VI)-induced γ-H2AX foci formation was increased in a dose-dependent manner in bronchioles and alveoli. Specifically, after exposure to 0 (saline), 0.4, and 0.8 mg/kg zinc chromate for 90 days in bronchioles, the rates of cells with γ-H2AX foci were 4.63%, 21.88%, and 22.50%, respectively. After exposure to 0.4 and 0.8 mg/kg zinc chromate, γ-H2AX foci formation in bronchioles were significantly increased (**p<0.01) (Fig. 3.38). Meanwhile, after 90-day exposure to zinc chromate, γ-H2AX foci formation was slightly increased in alveoli. Cr(VI)-induced γ-H2AX foci formation was more significant in bronchioles than in alveoli after 90-day zinc chromate exposure (*p<0.05) (Fig. 3.38).

In acute Cr(VI)-exposure rats, we found Cr(VI)-induced DNA double strand breaks mostly in epithelial cells. We further investigated Cr(VI)-induced DNA double strand breaks in both epithelial and non-epithelial cells, by measuring γ-H2AX foci formation, after exposure to 90-day zinc chromate. We also measured γ-H2AX foci formation in different regions of the lung, i.e., bronchiolar and alveolar regions. We found few γ-H2AX foci formed in bronchiolar non-epithelial cells after 90-day zinc chromate exposure, whereas γ-H2AX foci formation in bronchiolar epithelial cells increased with Cr(VI) dose. Specifically, after exposure to 0 (saline),

0.4 and 0.8 mg/kg zinc chromate for 90 days, the rates of cells with γ-H2AX foci in bronchiolar epithelial cells were 2.25%, 10.38%, and 12.50%, respectively. γ-H2AX foci formation in bronchiolar epithelial cells was significantly increased after exposure to 0.4 and 0.8 mg/kg zinc chromate (**p<0.01 and ****p<0.0001, respectively) (Figure 3.39). In bronchioles, there was a statistically significant difference in Cr(VI)-induced γ-H2AX foci between epithelial and non-epithelial cells. This data demonstrates Cr(VI)-induced γ-H2AX foci in bronchioles formed almost exclusively in epithelial cells (****p<0.0001) (Fig. 3.39).

We also observed little changes in γ-H2AX foci formation in alveolar non-epithelial cells after 90-day Cr exposure compared with saline exposure, whereas γ-H2AX foci formation in alveolar epithelial cells increased with Cr(VI) dose (Fig. 3.40). Specifically, the rates of cells with γ-H2AX foci in alveolar epithelial cells were 4.50%, 8.38% and 12.00% after 90-day 0 (saline), 0.4 and 0.8 mg/kg zinc chromate exposures, respectively. γ-H2AX foci formation in alveolar epithelial cells was significantly increased after exposure to 0.8 mg/kg zinc chromate (**p<0.01) (Figure 3.40). When comparing alveolar non-epithelial cells and epithelial cells, Cr(VI)-induced γ-H2AX foci formation was significantly different (****p<0.0001) (Figure 3.40). These data suggest Cr(VI)-induced γ-H2AX foci formation in the alveoli are almost exclusively formed in epithelial cells.

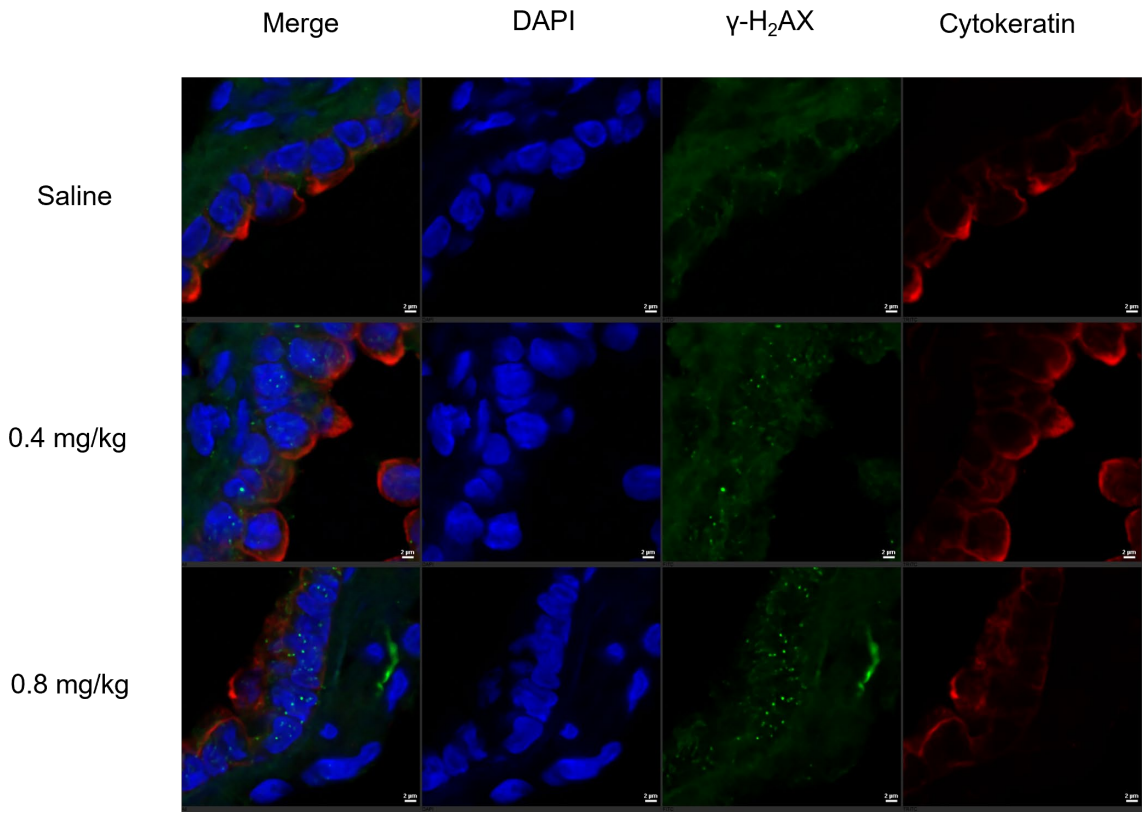

Figure 3.37. Particulate Cr(VI) induces DNA double strand breaks in the rat lung after 90-day exposure. Representative images of γ-H2AX foci are shown. First column, merged image; second column, DAPI staining; third column, γ-H2AX foci staining; fourth column, staining of cytokeratin, a marker of epithelial cells.

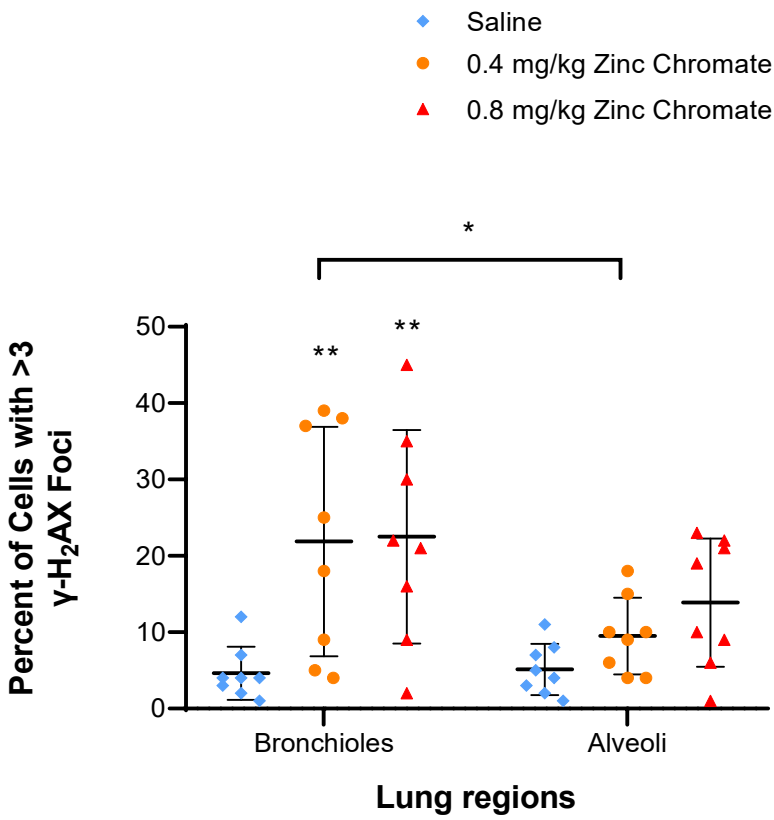

Figure 3.38. Comparison of γ-H2AX foci formation after 90-day zinc chromate exposure within and between groups of different lung regions. Cr(VI)-induced γ-H2AX foci formation in both bronchioles and alveoli. γ-H2AX foci formation in bronchioles increased with zinc chromate dose. γ-H2AX foci formation in bronchioles was significantly increased after exposure to 0.4 and 0.8 mg/kg zinc chromate (**p<0.01). γ-H2AX foci formation in alveoli was slightly increased after 90-day exposure to zinc chromate. Cr(VI)-induced γ-H2AX foci formation showed statistically significant differences between bronchioles and alveoli (*p<0.05). Error bar = standard error of the mean.

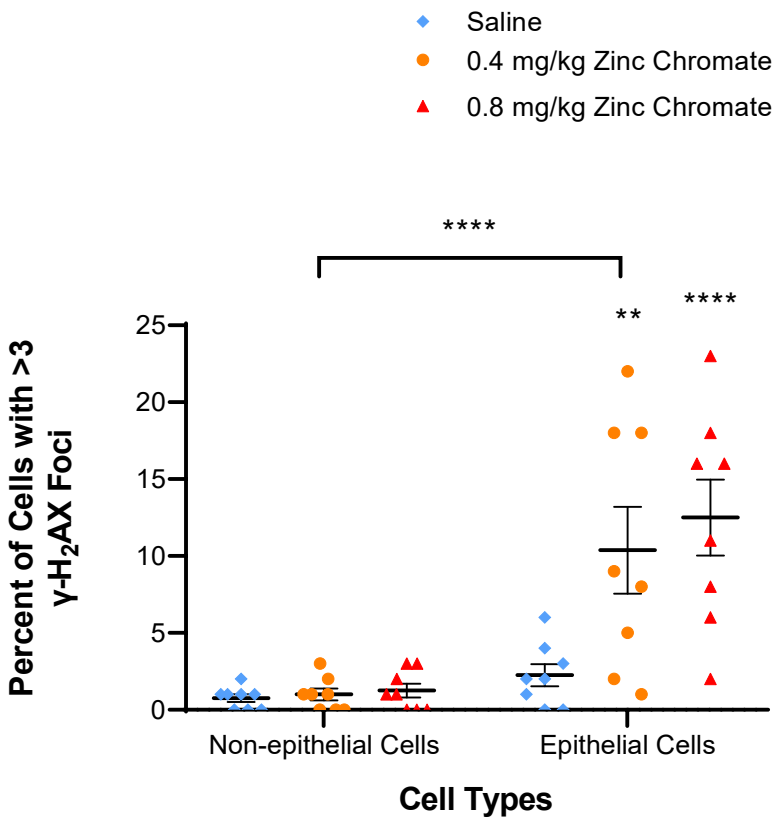

Figure 3.39. Comparison of γ-H2AX foci formation in bronchioles after 90-day exposure to zinc chromate within and between groups of non-epithelial and epithelial cells. After 90-day zinc chromate exposure, few γ-H2AX foci formed in bronchiolar non-epithelial cells, whereas γ-H2AX foci formed in bronchiolar epithelial cells increased with Cr(VI) dose. γ-H2AX foci formation in bronchiolar epithelial cells was significantly increased after exposure to 0.4 and 0.8 mg/kg zinc chromate (**p<0.01 and ****p<0.0001, receptively). Cr(VI)-induced γ-H2AX foci formation in bronchioles was significantly different between non-epithelial and epithelial cells after 90-day zinc chromate exposure (****p<0.0001).

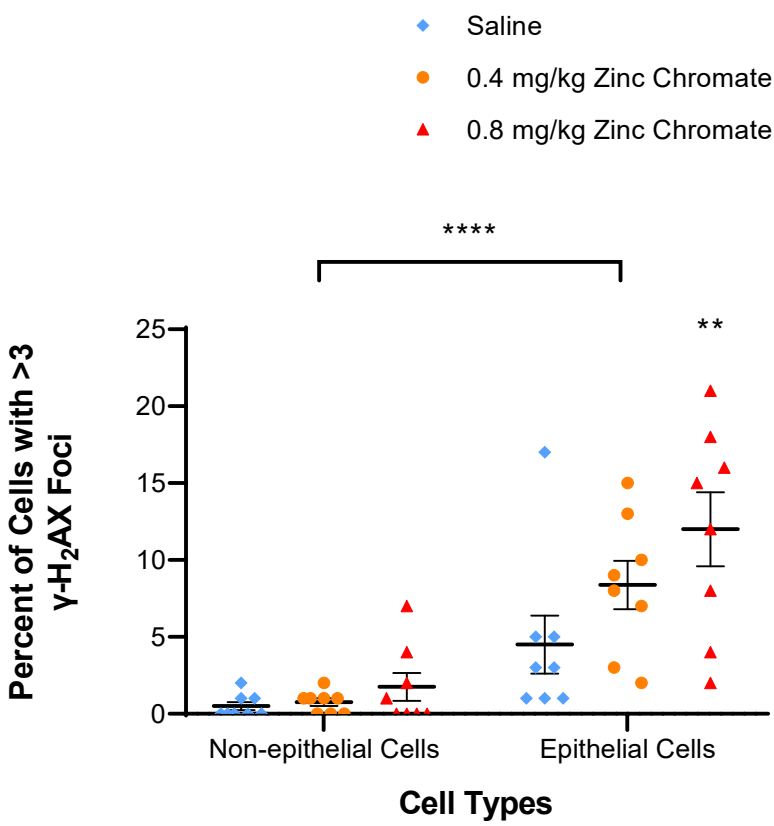

Figure 3.40. Comparison of γ-H2AX foci formation in alveoli after 90-day exposure to zinc chromate within and between groups of non-epithelial and epithelial cells. γ-H2AX foci formation in alveolar non-epithelial cells was almost unchanged compared with saline exposure, whereas γ-H2AX foci formation in alveolar epithelial cells increased with Cr(VI) dose. γ-H2AX foci formation in alveolar epithelial cells was significantly increased after exposure to 0.8 mg/kg zinc chromate (**p<0.01). Cr(VI)-induced γ-H2AX foci formation was significantly different when comparing alveolar non-epithelial and epithelial cells after 90-day exposure to zinc chromate (****p<0.0001).

HR Repair

Broken DNA duplexes are repaired without error by HR repair. Our previous study found acute particulate Cr(VI) activates HR repair to prevent Cr(VI)-induced DNA double strand breaks, whereas prolonged particulate Cr(VI) inhibits HR repair by targeting RAD51, the key enzyme in HR repair (Qin et al., 2014; Browning et al.; 2016). We found HR repair activation in the lungs of rats acutely exposed to zinc chromate. Therefore, it is imperative to investigate HR after subchronic Cr(VI) exposure. We investigated RAD51 to assess HR repair in rat lungs after 90-day zinc chromate exposure by immunofluorescent staining. We found Cr(VI) inhibited RAD51 foci formation in rat lungs after 90-day exposure to zinc chromate (Figure 3.41). Next, we investigated RAD51 foci formation in different lung sites. Cr(VI)-induced RAD51 foci formation was reduced in a dose-dependent manner in bronchioles. Specifically, after 90-day exposure to 0 (saline), 0.4 and 0.8 mg/kg zinc chromate in bronchioles, the rates of cells with RAD51 foci were 20.00%, 11.94% and 9.313%, respectively. RAD51 foci formation in bronchioles were significantly reduced after exposure to 0.4 and 0.8 mg/kg zinc chromate (*p<0.05, **p<0.01) (Figure 3.42). However, after 90-day exposure to zinc chromate, RAD51 foci formation in alveoli was slightly reduced compared with the saline-exposed group. After 90-day zinc chromate exposure, Cr(VI)-induced RAD51 foci formation was statistically different between bronchioles and alveoli (****p<0.0001) (Figure 3.42). These data indicate Cr(VI)-induced RAD51 inhibition is more obvious in the bronchiolar region than in the alveolar region.

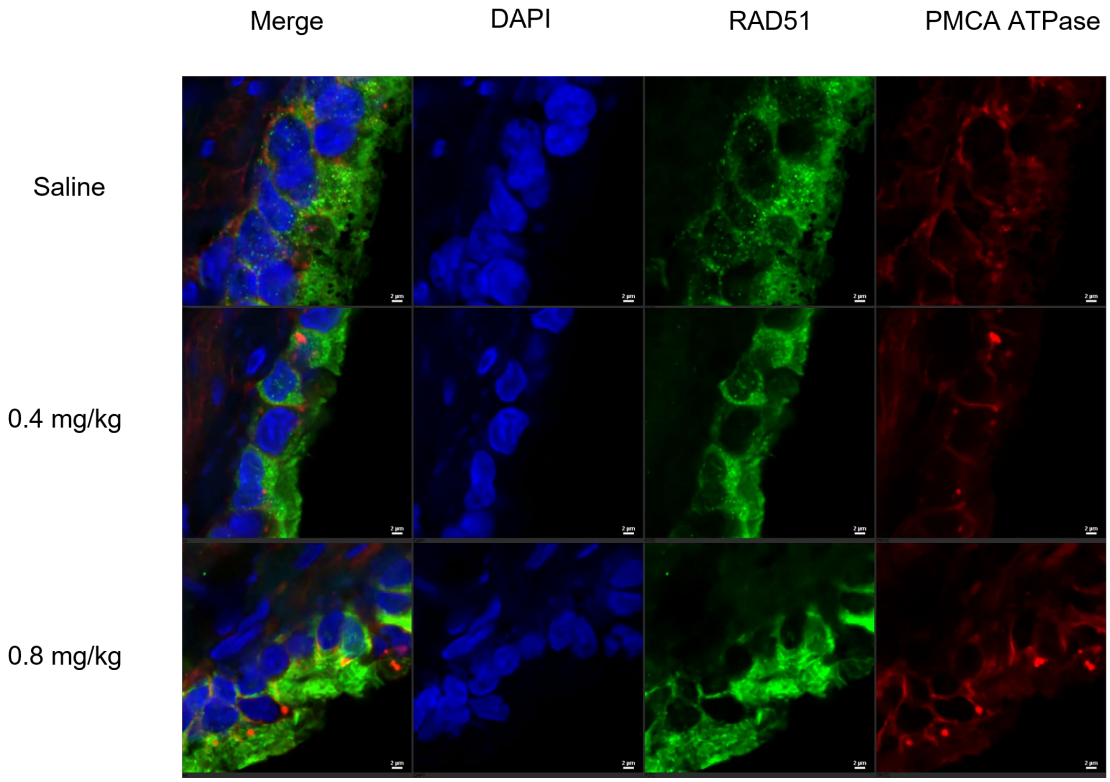

Figure 3.41. Particulate Cr(VI) reduces RAD51 foci formation in the rat lung after 90-day exposure. Representative images of RAD51 foci are shown. First column, merged image; second column, DAPI staining; third column, RAD51 foci staining; fourth column, staining of PMCA ATPase, a marker of the cell membrane.

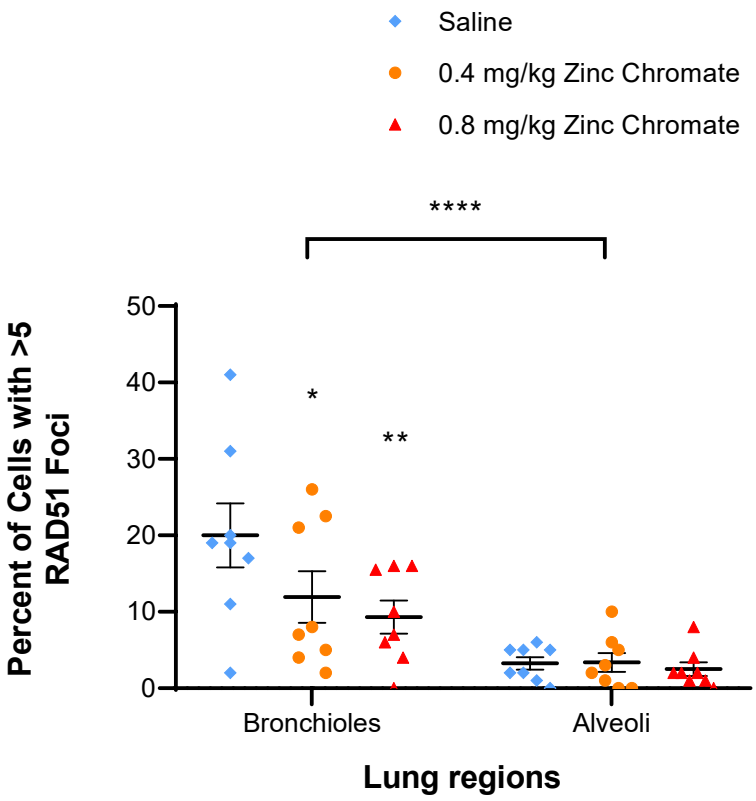

Figure 3.42. Comparison of RAD51 foci formation after 90-day zinc chromate exposure within and between groups of different lung regions. RAD51 foci formation was decreased in bronchioles in a dose-dependent manner after 90-day Cr(VI) exposure. RAD51 foci formation in bronchioles was significantly decreased after exposure to 0.4 and 0.8 mg/kg zinc chromate (*p<0.05 and **p<0.01, respectively). After 90-day exposure to 0.4 mg/kg zinc chromate, there was no decrease in the formation of RAD51 foci in alveoli compared to the saline-exposed group. However, there was a slight decrease in RAD51 foci formation in alveoli after 90-day exposure to 0.8 mg/kg zinc chromate. Cr(VI)-induced RAD51 foci formation was significantly different between bronchioles and alveoli after 90-day zinc chromate exposure (****p<0.0001). Error bar = standard error of the mean.

Sex differences

We investigated whether there were differences in lung Cr levels, lung histological changes, DNA double strand breaks, and HR repair in female and male rats after 90-day zinc chromate exposure.

Chromium Levels

We investigated whether there were differences in Cr levels in the lungs of female and male rats after 90-day exposure to zinc chromate. First, we investigated left and right lung Cr levels by sex. We found Cr levels increased in the left or right lung after 90-day exposure to zinc chromate in both females and males (Figure 3.41). We compared left and right lung Cr levels within the sex groups. We found in the same-sex group, Cr content in the right lung was higher than that of the left lung (Figure 3.43). For example, in the female group, after 90-day exposure to 0 (saline), 0.4 and 0.8 mg/kg zinc chromate, mean Cr levels in the left lung were 0.007, 2.062 and 1.332 mg Cr/kg lung tissue, respectively. After 90-day exposure to 0 (saline), 0.4 and 0.8 mg/kg zinc chromate, the mean levels of Cr in the right lung were 0.049, 7.111 and 9.881 mg Cr/kg lung tissue, respectively. In the right lung of female rats, there were statistically significant increases following exposure to 0.4 and 0.8 mg/kg zinc chromate (*p<0.05 and **p<0.01, respectively). In the female rat group, there was a statistically significant dose-dependent increase in Cr levels in the right lung compared with the left lung (**p<0.01). In the male rat group, mean Cr levels in the left lung after 90-day exposure to zinc chromate at 0 (saline), 0.4 and 0.8 mg/kg were 0.008, 1.152 and

2.344 mg Cr/kg lung tissue, respectively. After 90-day exposure to 0 (saline), 0.4 and 0.8 mg/kg zinc chromate, the mean levels of Cr in the right lung were 0.160, 14.22 and 10.56 mg Cr/kg lung tissue, respectively. There were statistically significant increases after exposure to 0.4 and 0.8 mg/kg zinc chromate (***p<0.001 and **p<0.01, respectively). Likewise, there was a statistically significant increase in Cr levels in the right lung compared with the left lung in the male rat group (***p<0.001). Comparing the sex groups, changes in Cr levels were not significantly different between the sexes (Figure 3.44).

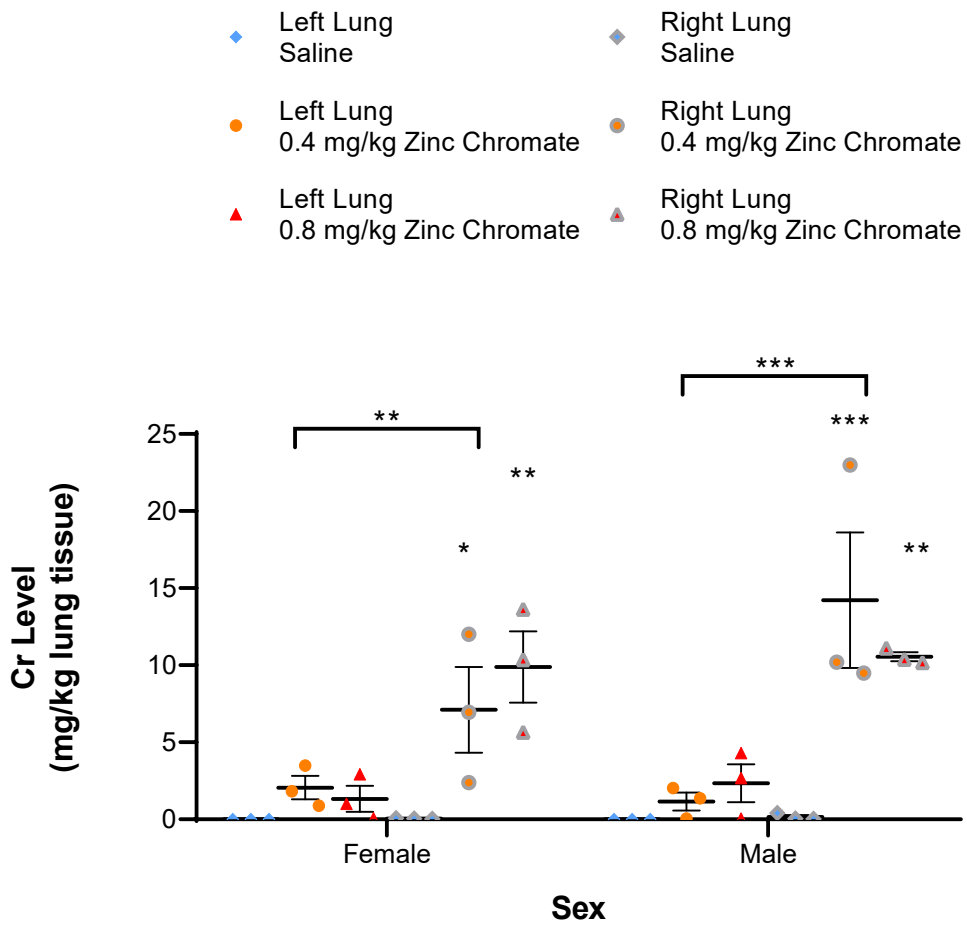

Figure 3.43. Comparison of Cr levels in the left and right lungs of rats after exposure for 90-day within and between groups of different sexes. Cr levels increased in both the left and right lungs, in female and male rats. In the same sex group, the right lung had higher Cr content than the left lung. In the right lung of the female group, there were statistically significant increases following 90-day exposure to 0.4 and 0.8 mg/kg zinc chromate (*p<0.05 and **p<0.01, respectively). In the female rat group, there was a statistically significant dose-dependent increase in Cr levels in the right lung compared with the left lung (**p<0.01). There was also a statistically significant increase in Cr levels in the right lung of the male rat group compared with the left lung (***p<0.001). In addition, there were

statistically significant increases (***p<0.001 and **p<0.01, respectively) in the right lung of male rats exposed to 0.4 and 0.8 mg/kg zinc chromate for 90 days. Changes in Cr levels were not statistically different between the different sex groups. Error bar = standard error of the mean.

We then investigated Cr distribution in each lung lobe by sex. We found dose-dependent increases in Cr levels in all lobes in females and males, except for the right upper lobe in male rats and the left and right upper lungs in female rats (Figure 3.42). Cr distribution in lung lobes of different sex groups was different from that of corresponding lung lobes. For example, in the right inferior lung of female rats, Cr levels increased with Cr(VI) dose, but in the right inferior lung of male rats, Cr levels did not change after 90-day exposure to 0.4 and 0.8 mg/kg zinc chromate compared with saline exposure. In the right superior and accessary lung lobes, changes in Cr levels after 90-day exposure to 0.4 and 0.8 mg/kg zinc chromate were more pronounced in males than in females, although no statistically significant differences were found. In the right middle lobe, the trends of increasing Cr concentration with Cr(VI) dose were similar in different sex groups. Therefore, we selected the middle lobe of the rat lung for subsequent immunofluorescence studies. Furthermore, we found Cr distribution in different lung lobes was statistically different in the male rat group (**p<0.01). However, there was no statistically significant difference in Cr distribution in each lobe between the different sex groups.

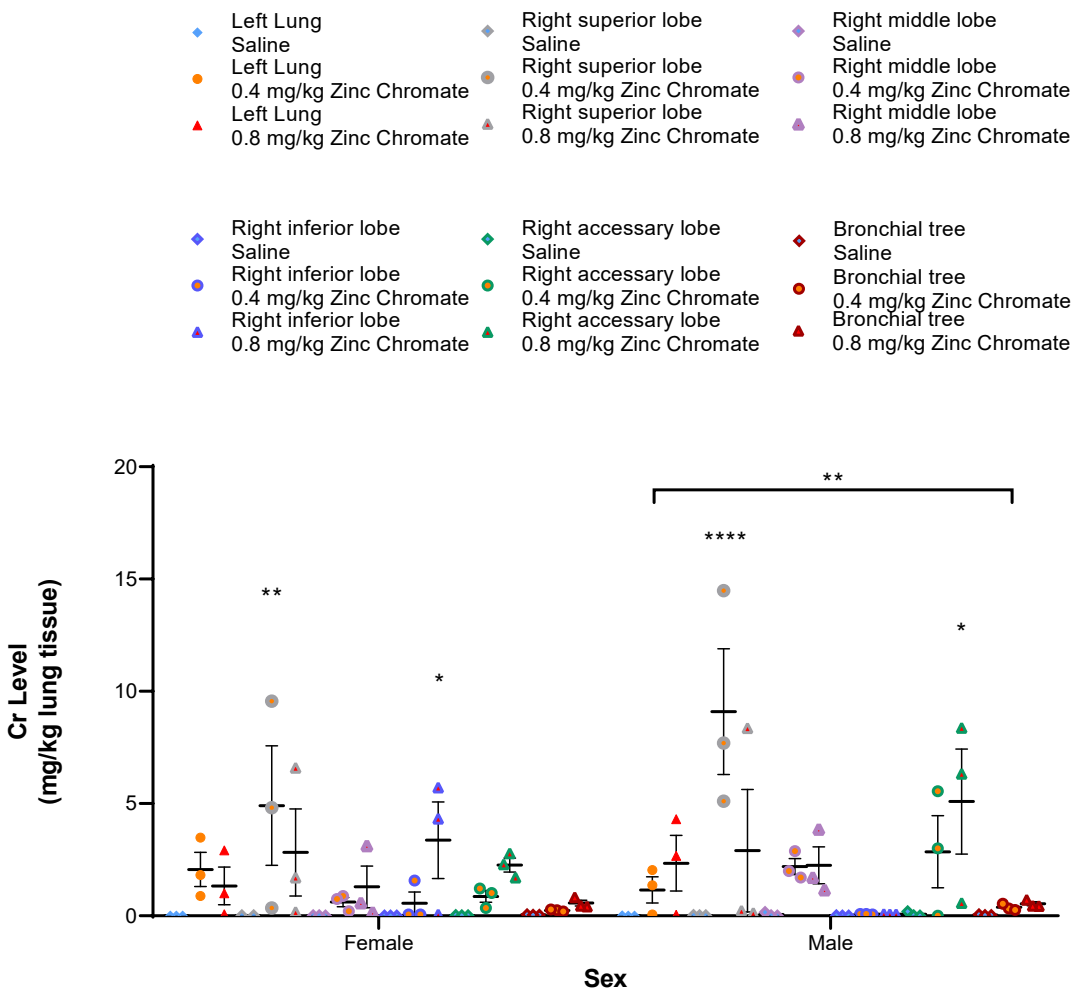

Figure 3.44. Comparison of the distribution in each lung lobe after exposure for 90 days within and between groups of different sexes. Dose-dependent increases in Cr levels in all lobes in females and males were found, except the right upper lobe in male rats, and the left and right upper lungs in female rats. Cr distribution in lung lobes in different sex groups was different from those of corresponding lung lobes. In the right lower lung of female rats, Cr levels increased with zinc chromate doses, but in the right lower lung of male rats, Cr levels did not change with increasing doses. In the right upper and accessary lung lobes, changes in Cr levels after 90-day exposure to 0.4 and 0.8 mg/kg zinc chromate were more obvious in male rats

than in female rats, although no statistically significant differences were found. In the right middle lobe, the trends of increasing Cr concentration with Cr(VI) dose were similar in the different sex groups. In addition, Cr distribution in different lung lobes in the male rat group were statistically different (**p<0.01). There were no statistically significant differences in Cr distribution in each lobe between the different sex groups. Error bar = standard error of the mean.

Lung Histological Change

We next investigated whether there were differences in macrophage aggregation in the lungs of female and male rats. We found the aggregations of macrophages in the lungs of female and male rats were increased after 90-day exposure to zinc chromate compared to exposure to saline (Figure 3.45). For example, after 90-day exposure to saline, 0.4 and 0.8 mg/kg zinc chromate, the lung macrophage scores of female rats were 1.071, 2.607 and 2.464, respectively. After 90-day exposure to saline, 0.4 and 0.8 mg/kg zinc chromate, male rat lung macrophage scores were 1.071, 2.821 and 2.643, respectively. After 90-day exposure to 0.4 and 0.8 mg/kg zinc chromate, there were significant increases in lung macrophage scores in both male and female rats (****$p<0.0001$). There were no statistically significant differences in macrophage aggregation between the sex groups.

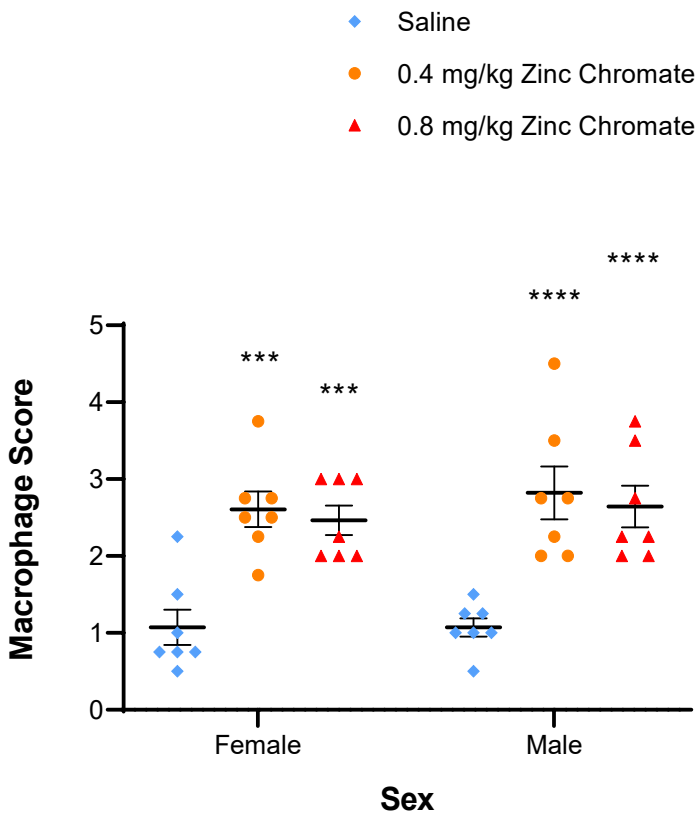

Figure 3.45. Comparison of macrophage aggregation after exposure for 90 days within and between groups of different sexes. Macrophage aggregation scores in female and male rat lungs were increased after 90-day exposure to zinc chromate. Macrophage scores were significantly increased after exposure to 0.4 and 0.8 mg/kg zinc chromate for 90 days (***p<0.001 and ****p<0.0001, respectively). Comparing the sex groups, there were no statistically significant differences in macrophage aggregation scores between female and male rats. Error bar = standard error of the mean.

DNA Double Strand Breaks

We then investigated γ-H2AX foci formation in bronchioles and alveoli by sex after 90-day zinc chromate exposure. We found in bronchioles, γ-H2AX foci formation was increased in female and male rats following zinc chromate exposure (Fig. 3.46). Specifically, the formation of γ-H2AX foci in female rats increased with zinc chromate dose, although not significantly. After 90-day 0.8 mg/kg zinc chrome exposure, γ-H2AX foci formation was increased in male rats compared with saline exposure but was not higher than in the 0.4 mg/kg group. Comparing the sex groups for bronchioles, no statistically significant differences in Cr(VI)-induced foci formation were found. In alveoli, γ-H2AX foci formation increased with zinc chromate dose in both female and male rats (Figure 3.47). γ-H2AX foci formation was significantly increased in female rats after exposure to 0.8 mg/kg zinc chromate for 90 days (*p<0.05). Comparing the sex groups for alveoli, there were some differences in Cr(VI)-induced γ-H2AX foci formation, although they were not statistically significant.

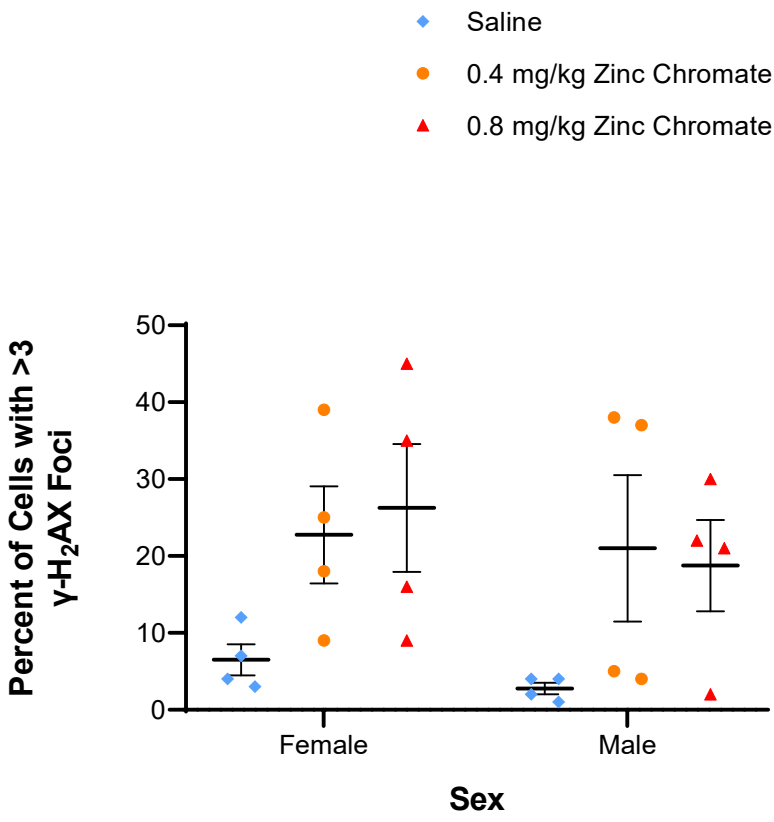

Figure 3.46. Comparison of γ-H2AX foci formation in bronchioles after 90-day exposure to zinc chromate within and between groups of different sexes. γ-H2AX foci formation was increased in the bronchioles of female and male rats following 90-day exposure to zinc chromate. Comparing the sex groups for bronchioles, no statistically significant differences in Cr(VI)-induced foci formation were found. Error bar = standard error of the mean.

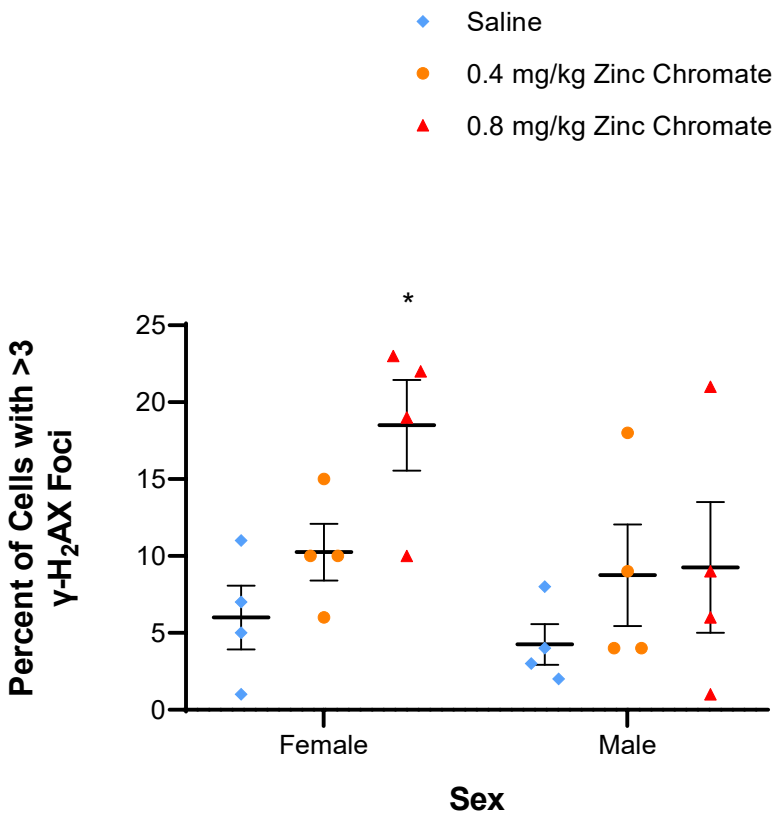

Figure 3.47. Comparison of γ-H2AX foci formation in alveoli after 90-day exposure to zinc chromate within and between groups of different sexes. γ-H2AX foci formation in alveoli increased with zinc chromate dose in both female and male rats. γ-H2AX foci formation was significantly increased in female rats after 90-day exposure to zinc chromate (*p<0.05). Cr(VI)-induced γ-H2AX foci formation was not statistically different between the sex groups in alveoli. Error bar = standard error of the mean.

HR Repair

We investigated RAD51 foci formation in bronchioles and alveoli by sex. We found in bronchioles, RAD51 foci formation decreased with increasing zinc chromate dose in female and male rats (Figure 3.48). Cr(VI)-induced reduction in RAD51 foci formation in bronchioles was somewhat different, although not statistically different, between the sex groups. In the alveoli of male rats, RAD51 foci formation decreased with increasing zinc chromate dose, which was not found in female rats (Figure 3.49). Comparing the different sex groups for alveoli, there were some differences in Cr(VI)-induced RAD51 foci formation, although they were not statistically significant.

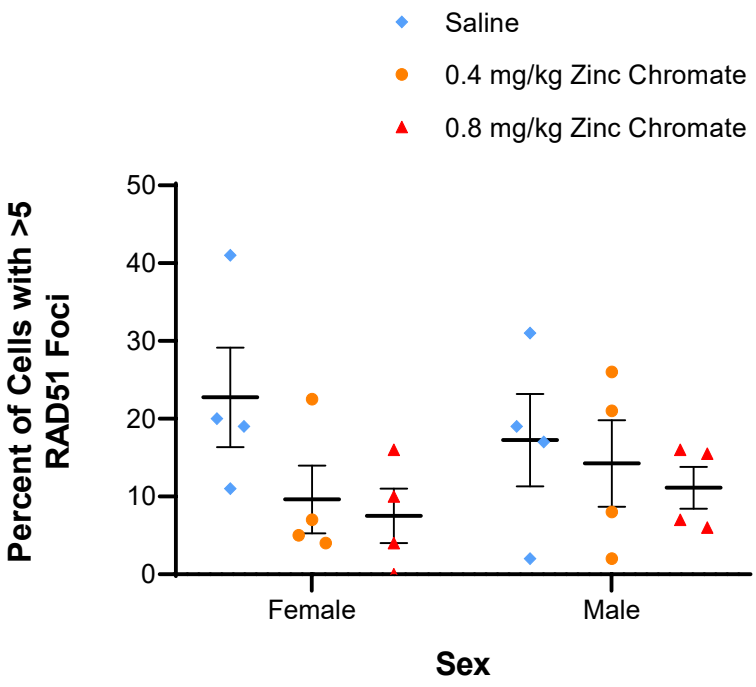

Figure 3.48 Comparison of RAD51 foci formation in bronchioles after 90-day exposure to zinc chromate within and between groups of different sexes. RAD51 foci formation decreased with zinc chromate dose in female and male rats in bronchioles after 24 h exposure. Comparing the sex groups for bronchioles, no statistically significant differences in Cr(VI)-induced RAD51 foci formation were found. Error bar = standard error of the mean.

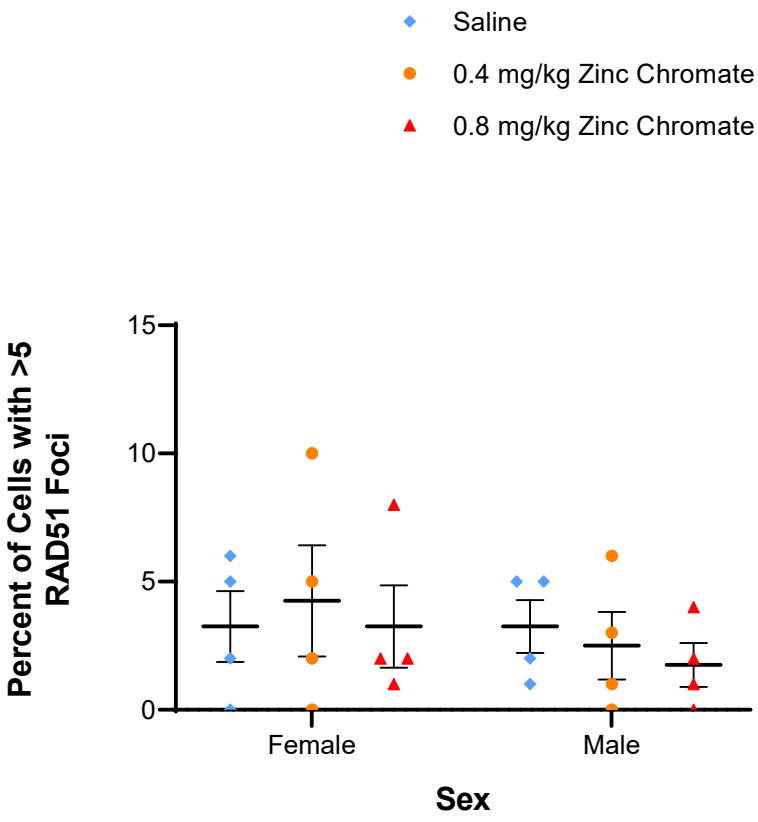

Figure 3.49. Comparison of RAD51 foci formation in alveoli after 90-day exposure to zinc chromate within and between groups of different sexes. RAD51 foci formation in the alveoli of female rats was not decreased after Cr(VI) exposure compared to the saline group. RAD51 foci formation in male rats decreased with increasing zinc chromate dose in the alveoli. Cr(VI)-induced RAD51 foci formation was not statistically different between the sex groups for alveoli. Error bar = standard error of the mean.

Accumulation of Other Metals

Zinc Levels

We measured zinc levels in rat lungs after 90-day exposure to zinc chromate. We found zinc levels in rat lung tissue increased with increasing dose after 90-day exposure to zinc chromate (Figure 3.50). For example, after 90-day 0 (saline), 0.4 and 0.8 mg/kg zinc chromate exposure, mean whole lung zinc levels were 66.90, 72.51 and 82.51, respectively. Combined with the data on Cr levels in the whole rat lung, a dose-dependent accumulation of zinc chromate in the rat lung was demonstrated.

We next investigated the distribution of zinc levels in both the left and right lungs of rats. After 90-day exposure, zinc levels in the left lung of rats exposed to zinc chromate were not higher than those of rats exposed to saline (Fig. 3.51). However, after 90-day exposure to 0.4 mg/kg and 0.8 mg/kg of zinc chromate, respectively, the levels of zinc in the right lung of rats were higher than those of the saline group (Fig. 3.51). There was a statistically significant increase after exposure to 0.8 mg/kg zinc chromate (**p<0.01). Zinc levels were significantly higher in the right lung than in the left lung (****p<0.0001). Combined with the Cr data, more zinc chromate particles accumulated in the right lung of the treated rats.

We further investigated the distribution of zinc in each lung lobe. After 90-day exposure to zinc chromate, zinc levels in each rat lung lobe did not change with zinc chromate dose except for increases in the right upper lung, right lower lung, and bronchial tree (Figure 3.52). After 90-day 0.8 mg/kg zinc chromate exposure, zinc levels in the right upper and lower lung lobes were significantly

increased (*p<0.05). Significantly lower levels of Cr in the bronchial tree found in the 90-day Cr(VI) exposure data compared with other lobes were not found in the zinc data.

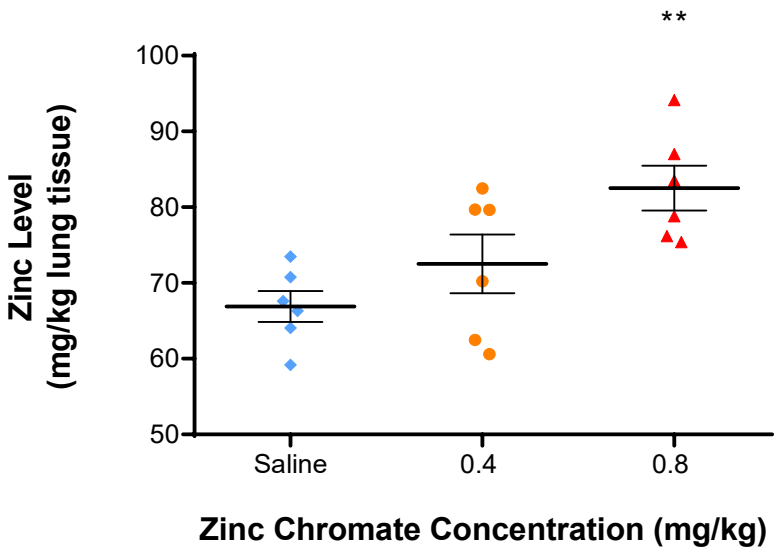

Figure 3.50. Zinc levels in whole rat lungs after 90-day exposure. Zinc levels in the whole lung tissue of rats increased in a dose-dependent manner compared to the saline group after 90-day exposure to zinc chromate. Zinc levels were significantly higher after 90-day exposure to 0.8 mg/kg of zinc chromate compared with the saline-exposed group (**p<0.01). Error bar = standard error of the mean.

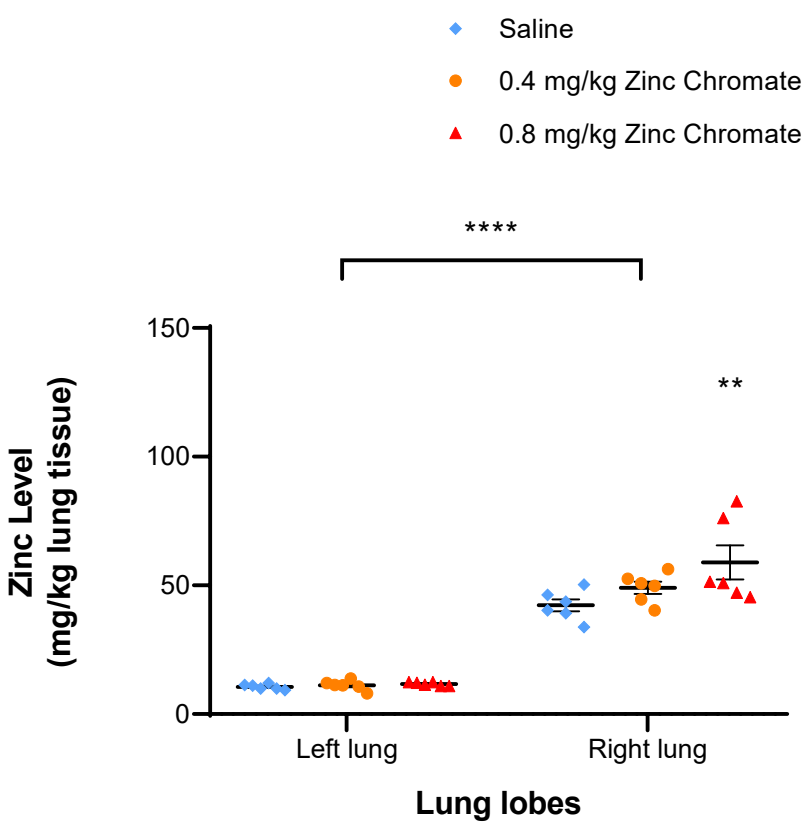

Figure 3.51. Zinc levels in rat left lung vs. right lung after 90-day exposure. Zinc levels in the left lung of rats did not increase after 90-day exposure to zinc chromate, whereas zinc levels in the right lung increased with zinc chromate dose. There was a statistically significant increase after exposure to 0.8 mg/kg zinc chromate in the right lung (*p<0.05). Zinc levels were significantly higher in the right lung than in the left lung (****p<0.0001). Error bar = standard error of the mean.

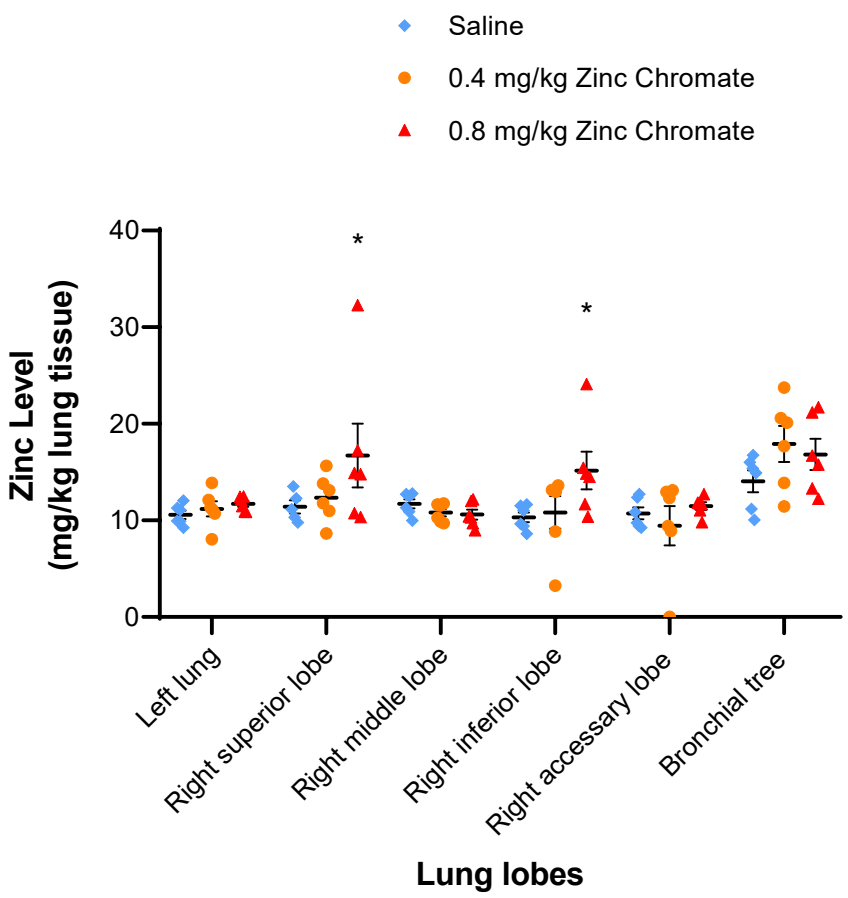

Figure 3.52. Zinc distribution in each individual rat lung lobe after 90-day zinc chromate exposure. Zinc levels in each rat lung lobe did not change after 90-day exposure to zinc chromate except for increases in the right upper lung lobe, right lower lung lobe and bronchial tree. Zinc levels in the right upper and lower lung lobes were significantly increased after 90-day 0.8 mg/kg zinc chromate exposure (*p<0.05). Error bar = standard error of the mean.

Iron Levels

We investigated iron levels in rat lungs. We found a slight increase in iron levels in rat lung tissue after 90-day exposure to zinc chromate (Figure 3.53). For example, after 90-day 0 (saline), 0.4 and 0.8 mg/kg zinc chromate exposure, mean whole lung iron levels were 101.2, 115.3 and 131.4 mg Iron/kg lung tissue, respectively. Combined with the data on Cr and zinc levels in the whole rat lung, it is further confirmed there is a dose-dependent accumulation of Cr in the rat lung.

We then investigated the distribution of iron levels in the left and right lungs of rats, respectively. After 90-day exposure to zinc chromate, iron levels in the left lung did not change compared to saline exposure. Iron levels in the right lung of rats exposed to zinc chromate were higher than those of the saline-exposed group (Figure 3.54). Iron levels were significantly higher in the right lung than in the left lung (****p<0.0001).

We next investigated the distribution of iron in each lung lobe. After 90-day exposure to zinc chromate, iron levels in each rat lung lobe did not change with zinc chromate dose, except for increases in the right lower lung lobe and bronchial tree (Figure 3.55). Iron levels in the bronchial tree were significantly increased after 90-day zinc chromate exposure at 0.4 and 0.8 mg/kg (***p<0.001 and **p<0.01, respectively). Iron levels were higher in the bronchial tree than in other lobes.

We further investigated whether subchronic Cr(VI) exposure affects functional iron levels in rat lungs. We found a significant decrease in functional iron levels after 90-day zinc chromate exposure (Figure 3.56). Specifically, after 90-day exposure to 0 (saline), 0.4 mg/kg, and 0.8 mg/kg zinc chromate, iron-to-Cr ratios

in rat lungs were 7318, 413.7, and 497.2, respectively. These data suggest subchronic Cr(VI) exposure affects iron metabolism in rats.

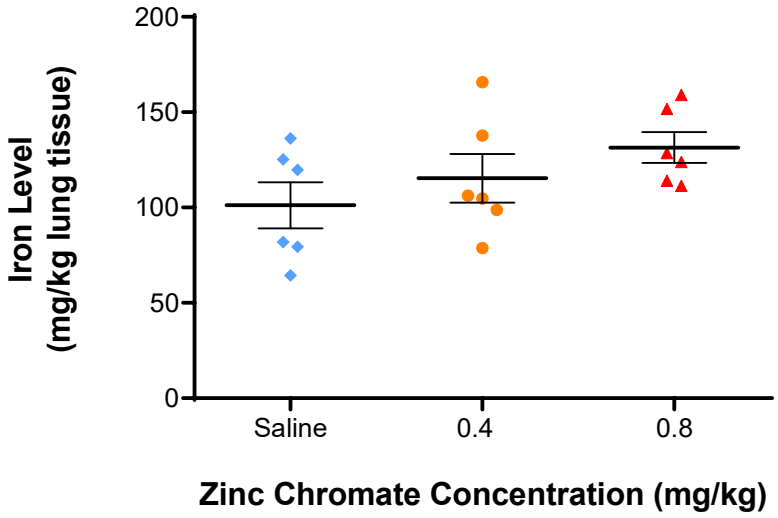

Figure 3.53. Iron levels in whole rat lungs after 90-day exposure. Iron levels in rat lung tissue slightly increased after 90-day exposure to zinc chromate. Whole lung iron levels were not significantly different between the Cr(VI)- and saline-exposed groups. Error bar = standard error of the mean.

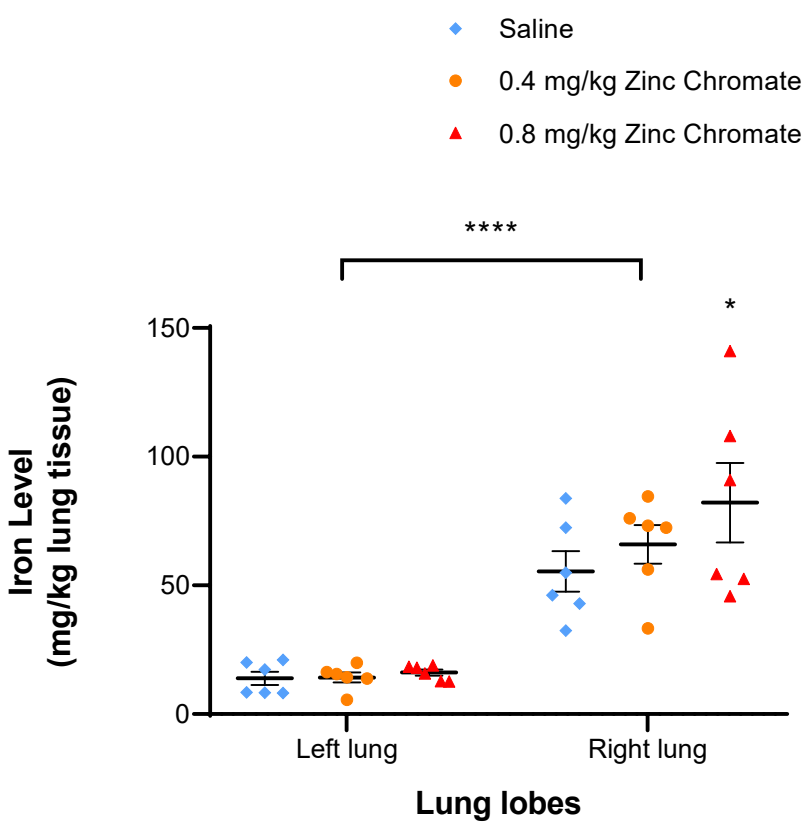

Figure 3.54. Iron levels in rat left lung vs. right lung after 90-day exposure. Iron levels were unchanged in the left lung but elevated in the right lung after 90-day exposure to zinc chromate. Iron levels were significantly higher in the right lung of rats exposed to 0.8 mg/kg zinc chromate compared with the saline group (*p<0.05). There was a statistically significant difference in iron levels between the left and right lungs (****p<0.0001). Error bar = standard error of the mean.

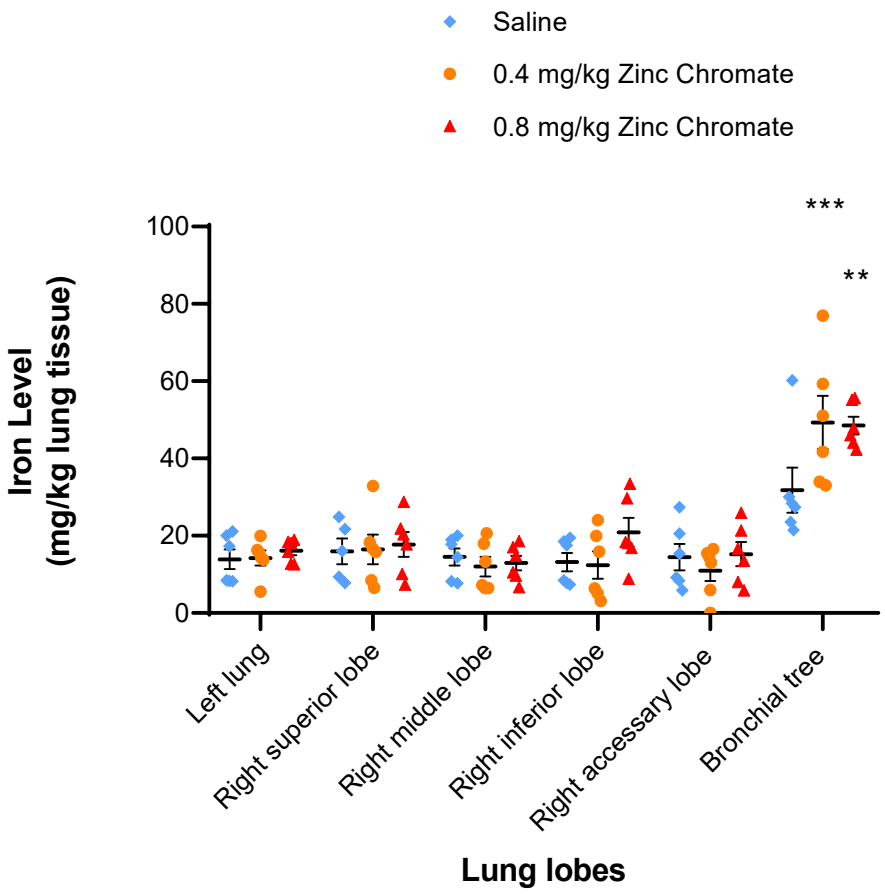

Figure 3.55. Iron distribution in individual rat lung lobes after 90-day zinc chromate exposure. Iron levels in each rat lung lobe did not change with zinc chromate dose after 90-day exposure to zinc chromate, except for increases in the right lower lung lobe and bronchial tree. Iron levels in the bronchial tree were significantly increased after 90-day zinc chromate exposure at 0.4 and 0.8 mg/kg (***p<0.001 and **p<0.01, respectively). Comparing lung lobes, iron levels were higher in the bronchial tree compared with other lobes. Error bar = standard error of the mean.

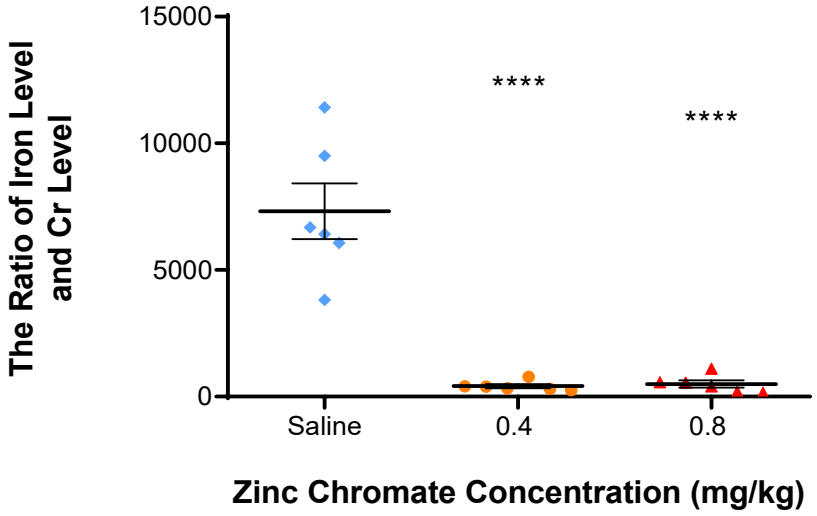

Figure 3.56. Functional iron levels in rat lungs after 90-day zinc chromate exposure. Functional iron levels were significantly reduced after 90-day zinc chromate exposure. After 90-day exposure to 0.4 mg/kg and 0.8 mg/kg zinc chromate, the ratios of iron to Cr in the lungs of rats were significantly lower versus the saline group (****p<0.001).

Comparison of acute and subchronic exposures

After we completed our investigations in rats with different exposure times, we compared the levels of Cr, the extent of DNA damage, and the effect of Cr(VI) on HR repair after acute and subchronic exposures.

Chromium Levels

Comparing Cr levels in rat lungs between acute and subchronic exposures, we found at 0.4 mg/kg zinc chromate, Cr levels in the lungs of rats were higher with subchronic exposure than with acute exposure. However, at 0.8 mg/kg zinc chromate, Cr levels in the lungs were lower after subchronic exposure than in the acute exposure group, and even did not exceed the levels of subchronic exposure at 0.4 mg/kg zinc chromate (Figure 3.57). A possible reason is that there is a Cr uptake saturation capacity at high dose after subchronic exposure. We therefore investigated the relative concentrations of Cr in tissues, expressed as a relative concentration P value (Weber, 1983). We found in the acute exposure group, the change in P value did not vary significantly between doses, whereas in the subchronic exposure group, the P value for exposure to 0.8 mg/kg zinc chromate was lower than that for exposure to 0.4 mg/kg zinc chromate (Figure 3.58). These data suggest after subchronic exposure to zinc chromate, Cr levels in the lung tissue could reach saturation. When Cr levels were investigated separately in the left and right lungs, Cr levels in the left lung did not differ significantly after different exposure times. In the right lung, the differences in Cr levels after different exposure times were similar to total Cr levels (Figure 3.59).

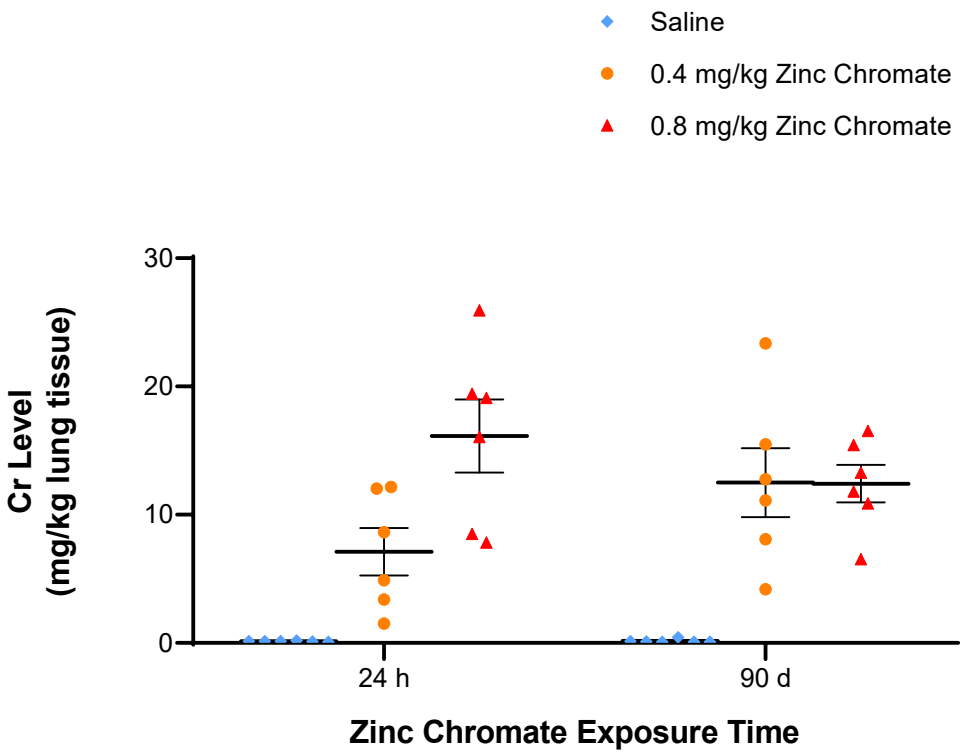

Figure 3.57. Comparison of total Cr levels after different zinc chromate exposure times. Cr levels in the lungs of rats after subchronic exposure were higher than those of the acute exposure group at 0.4 mg/kg zinc chromate. When exposed to 0.8 mg/kg zinc chromate, Cr levels were lower in the subchronic exposure group than in the acute exposure group, and even lower than in the 0.4 mg/kg zinc chromate group of the same time point.

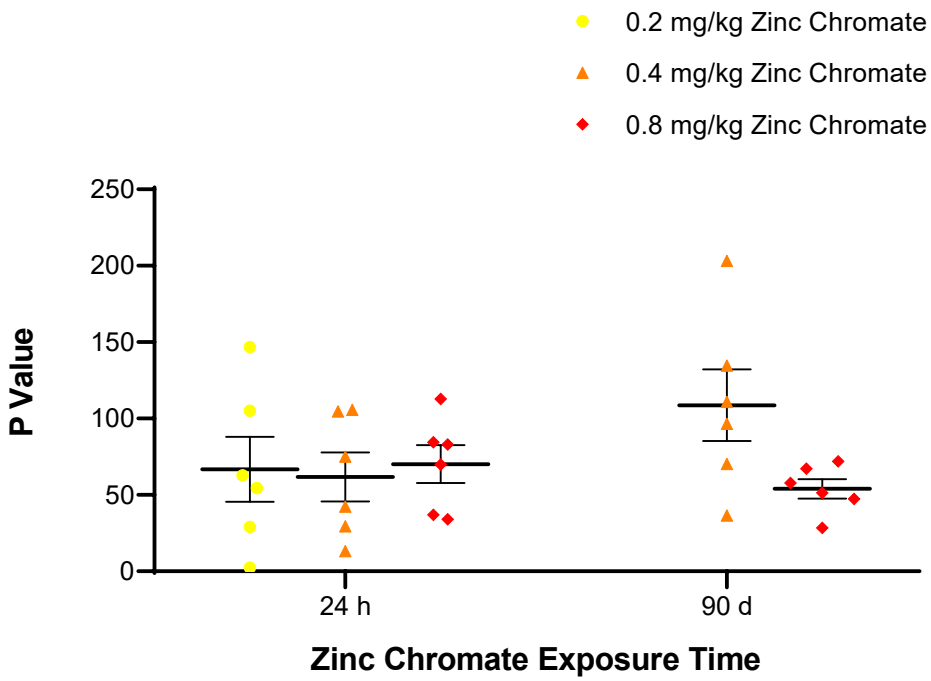

Figure 3.58. Comparison of the relative concentration of Cr in the lung tissue at different zinc chromate exposure times. The relative concentration of Cr in the tissue was expressed as a relative concentration P value: P = (Cr levels in tissue/wet organ weight) / (administered Cr dose/animal weight at sacrifice). P values were different within groups with different zinc chromate exposure times. Changes in P values were not significantly different between dosed concentrations in the 24-hour exposure group. In the subchronic exposure group, the P value was lower for 0.8 mg/kg zinc chromate exposure than for 0.4 exposure (p=0.0999).

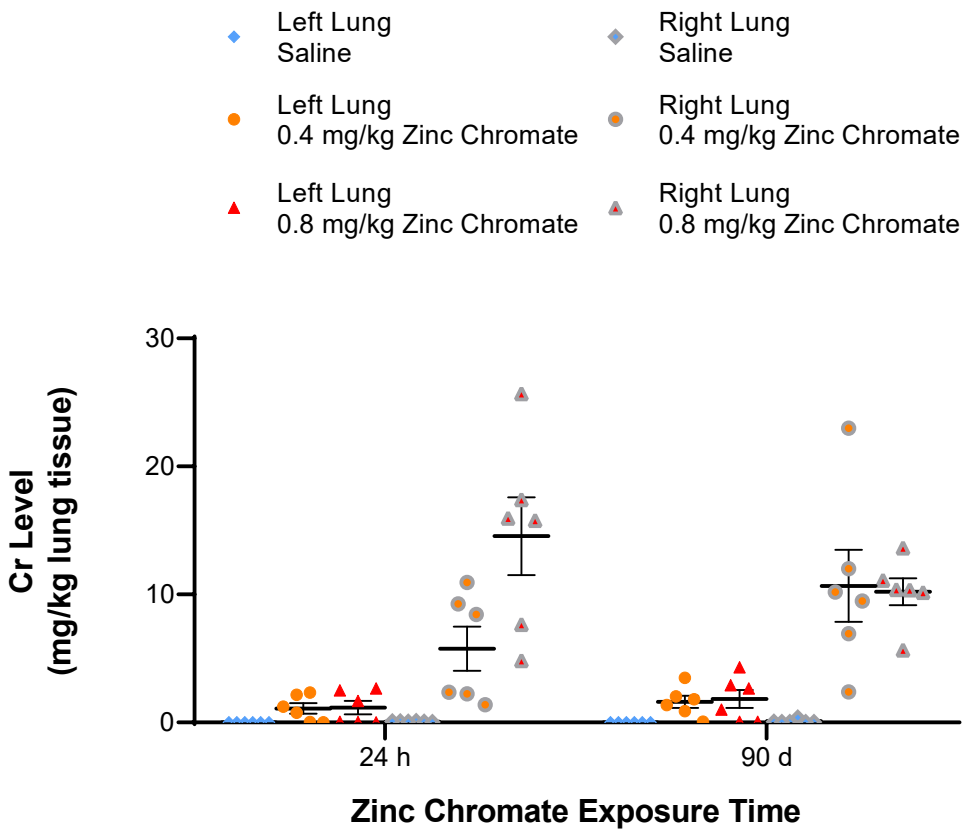

Figure 3.59. Comparison of Cr levels in left and right lungs after different zinc Cr exposure times. Cr levels in the left lung did not differ significantly after different exposure times. In the right lung, when exposed to 0.4 mg/kg zinc chromate, the subchronic exposure group had higher lung Cr levels than the acute exposure group. At 0.8 mg/kg zinc chromate, Cr levels were lower in the subchronic exposure group than in the acute exposure group.

DNA double strand breaks

We compared Cr(VI)-induced DNA double strand breaks between acute and subchronic exposures. We found Cr(VI)-induced γ-H2AX foci formation was slightly higher in bronchioles after acute exposure compared with subchronic exposure (Figure 3.60). However, in alveoli, Cr(VI)-induced γ-H2AX foci formation in the subchronic group increased with zinc chromate dose, while in the acute group, high doses of zinc chromate did not increase γ-H2AX foci formation compared with low doses (Figure 3.60).

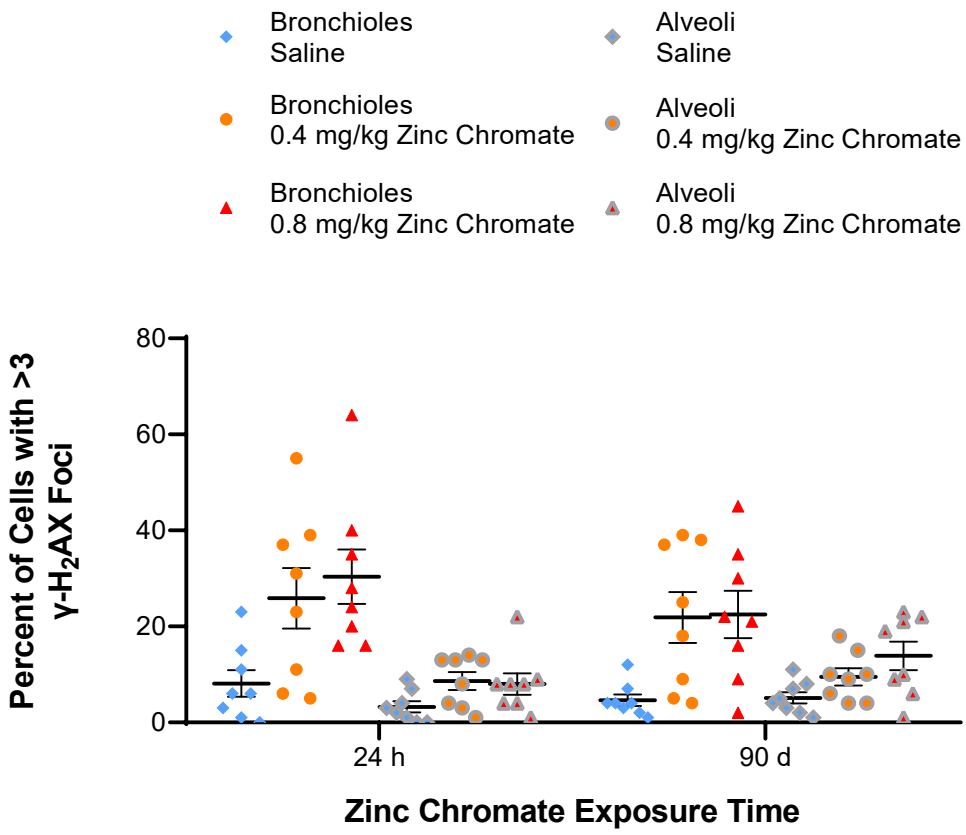

Figure 3.60. Comparison of Cr(VI)-induced DNA double strand breaks in bronchioles and alveoli after different zinc chromate exposure times. In bronchioles, Cr(VI)-induced γ-H2AX foci formation was slightly higher in the 24-hour exposure group than in the 90-day group. In the alveolar region, Cr(VI)-induced γ-H2AX foci formation increased with zinc chromate dose in the 90-day exposure group, while 24-hour exposure to 0.8 mg/kg zinc chromate did not increase γ-H2AX foci formation compared with 0.4 mg/kg zinc chromate exposure for the same time.

HR repair

We next compared changes in HR repair following zinc chromate exposure between the acute and subchronic groups. We found in bronchioles, different exposure times elicited completely different responses to HR repair. Specifically, RAD51 foci formation increased with dose after acute zinc chromate exposure, while decreasing with increasing dose with subchronic zinc chromate exposure (Figure 3.59). This result indicated Cr(VI) activated HR repair after acute exposure, whereas subchronic exposure to Cr(VI) inhibited HR repair. In addition, in alveoli, RAD51 foci formation did not change after zinc chromate exposure and did not differ between groups at different exposure times (Figure 3.61).

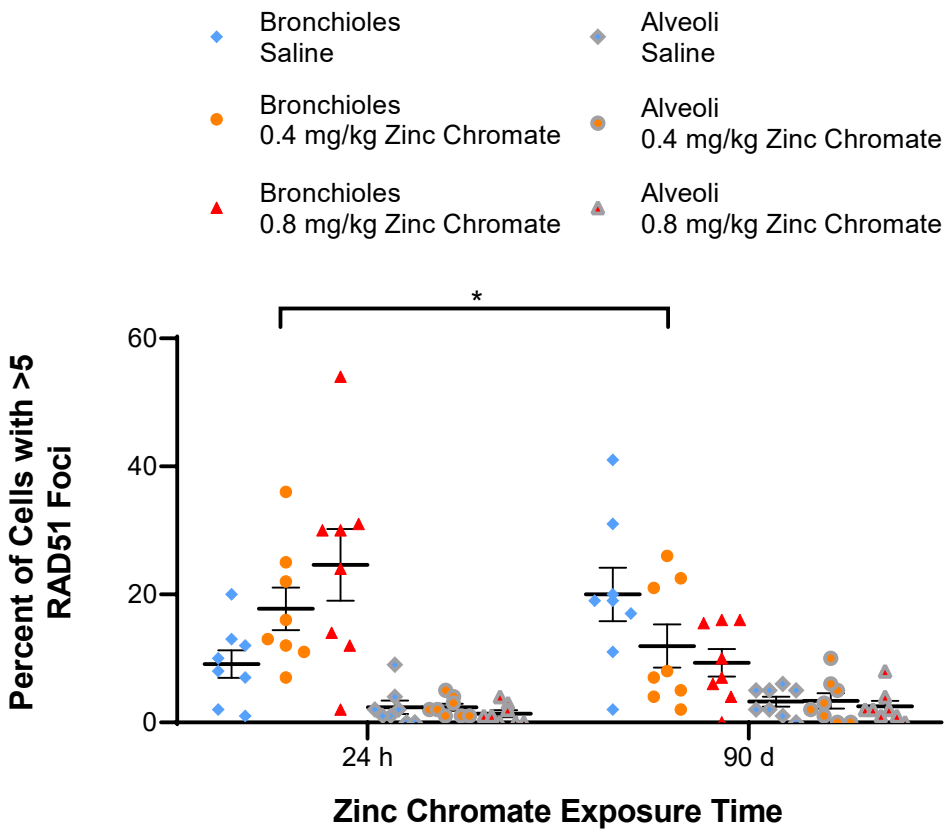

Figure 3.61. Comparison of changes in HR repair in bronchioles and alveoli after different zinc chromate exposure times. In bronchioles, RAD51 foci formation increased with dose after 24-hour zinc chromate exposure but decreased with increasing dose with 90-day zinc chromate exposure. In alveoli, RAD51 foci formation did not change after zinc chromate exposure and showed no difference between groups with different exposure times. *p<0.05.

Chromate-associated Lung Cancers' study

Epidemiological studies have found high rates of lung cancer among chromate workers. Kondo et al. reported the pathological type of chromium-related lung tumors is mainly squamous cell carcinoma. They found accumulation of Cr(VI) particles at lung bifurcations during bronchoscopy of chromate workers and pathological examination of lung tumors. We investigated DNA double strand breaks and HR repair in lung tumor tissue sections from these chromate workers to further clarify whether chromium-induced DNA double strand breaks and HR repair inhibition persist to tumor formation. The three lung tumors investigated in this project were all squamous cell carcinomas. The lung tissue used as a control group was the corresponding normal adjacent lung tissue samples from the same patients. Normal lung tissue structure, including normal bronchial and normal alveolar areas, can be seen in the lung tissue of the control group (Figure 3.62). The tissue of the lung tumor lost the normal lung structure, which was replaced with a tumor-shaped cell mass. Keratin pearls and intercellular bridges were visible within the cell mass (Figure 3.62).

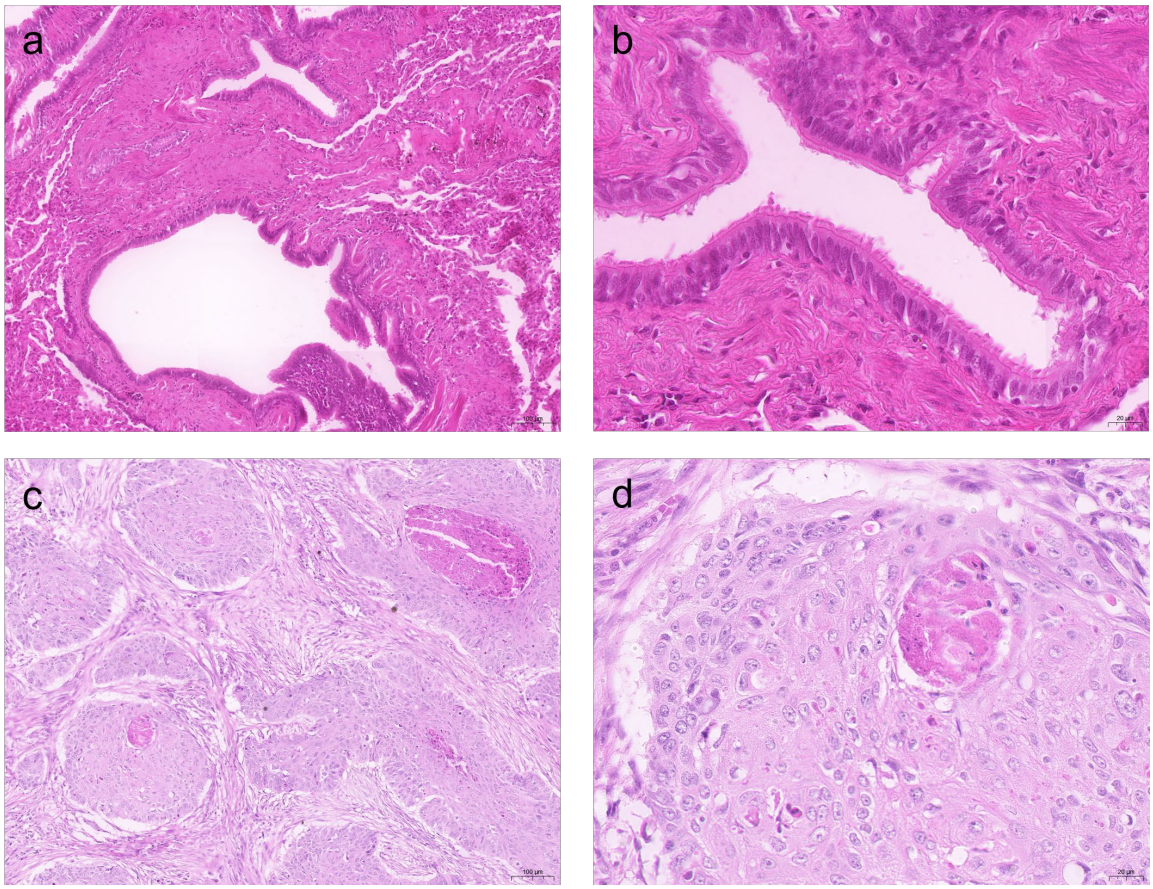

Figure 3.62. Morphological characteristics of chromium-related lung cancer in H&E-stained tissue sections. a. and b. Normal lung tissue adjacent to the tumor in the same lung cancer patient. Normal lung tissue structure including bronchioles and alveoli can be seen. Magnifications for a and b are ×100 and x400, respectively. c. and d. Lung cancer tissue without normal lung tissue structure. Keratin pearls and intercellular bridges are visible within the cell mass. Magnifications for c and d are ×100 and x400, respectively.

DNA Double Strand Breaks

By immunofluorescence, we investigated γ-H2AX foci formation in chromate workers' lung tumor tissue sections to determine whether Cr(VI)-induced DNA double strand breaks persist into tumor formation. We detected γ-H2AX foci in tumor tissue cells (Fig. 3.63), and γ-H2AX foci formation was significantly increased in tumor tissue cells compared with normal adjacent lung tissue (Fig. 3.64). This data suggests Cr(VI) causes DNA double strand breaks that persist through tumor formation rather than being transient.

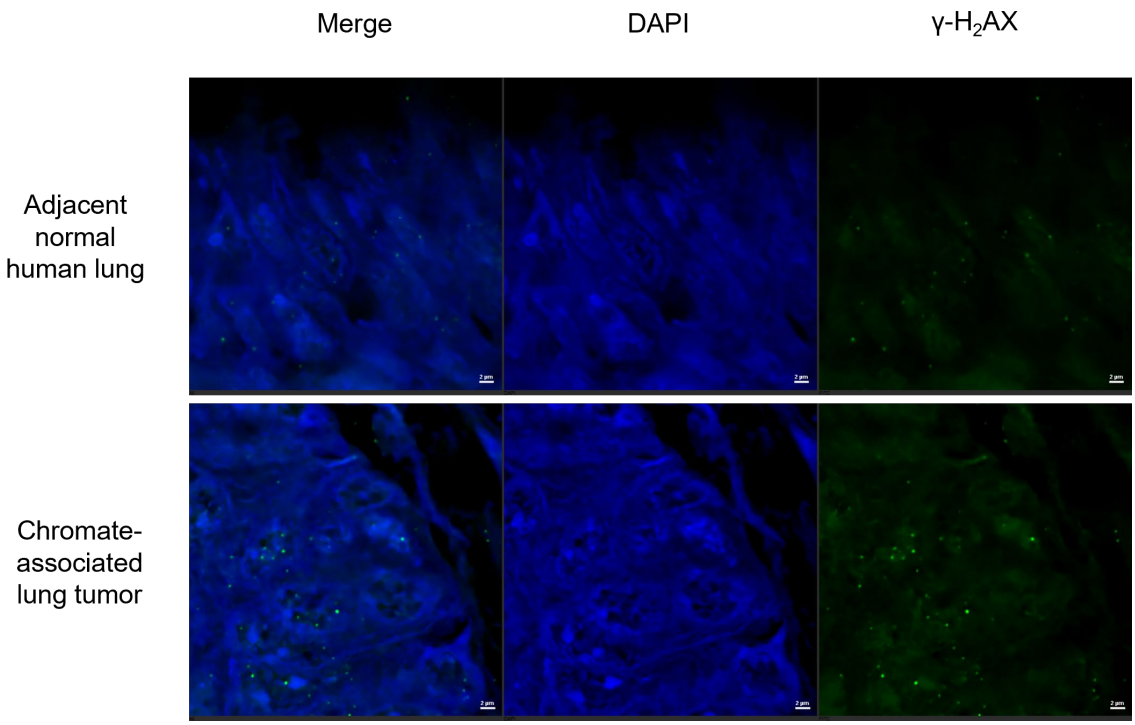

Figure 3.63. Cr(VI)-induced γ-H2AX foci in chromate worker lung tumor tissue. Green dot signals in the nucleus are γ-H2AX foci.

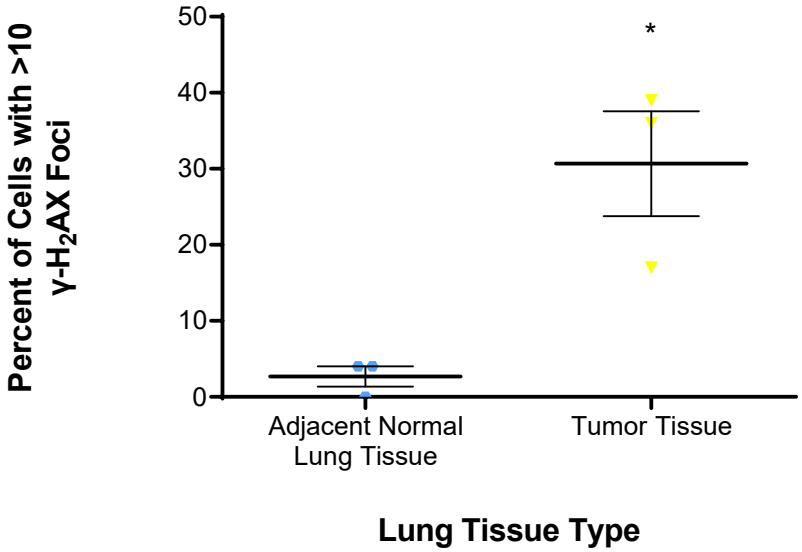

Figure 3.64. Cr(VI)-induced DNA double strand breaks in chromate worker lung tumor tissue. γ-H2AX foci formation was significantly increased in tumor tissue cells compared with normal adjacent lung tissue (p<0.05). Error bar = standard error of the mean.

HR repair

We next investigated RAD51 foci formation in chromate worker lung tumor tissue sections to determine whether Cr(VI)-induced HR deficiency persists into tumor formation. We found more RAD51 foci in the nucleus of normal adjacent lung tissue, whereas RAD51 foci were almost invisible in the nucleus of tumor tissue (Fig. 3.65). We then performed ROI analysis of nuclei on the images acquired by confocal microscopy. We found the signal intensity of RAD51 was lower in tumor tissue than in normal adjacent lung tissue (Fig. 3.66). These data suggest Cr(VI) causes HR defects that persist into tumor formation rather than being transient.

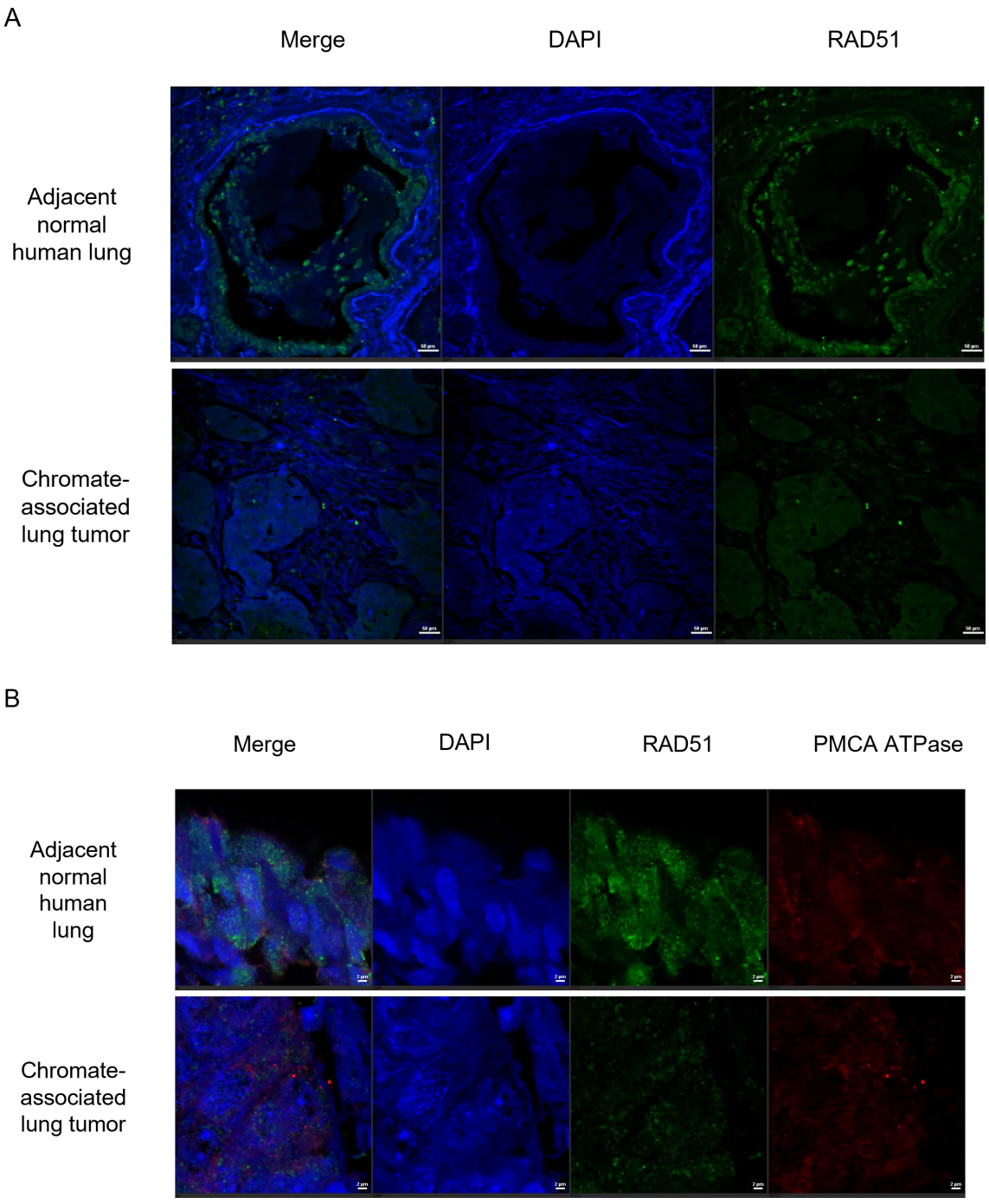

Figure 3.65. RAD51 foci in normal adjacent lung and tumor tissues from a chromate worker's lung. Green dot signals in the nucleus are RAD51 foci. Red

signals reflect PMCA ATPase expression. Magnifications for A and B are ×200 and x1000 with x3 digital zoom, respectively.

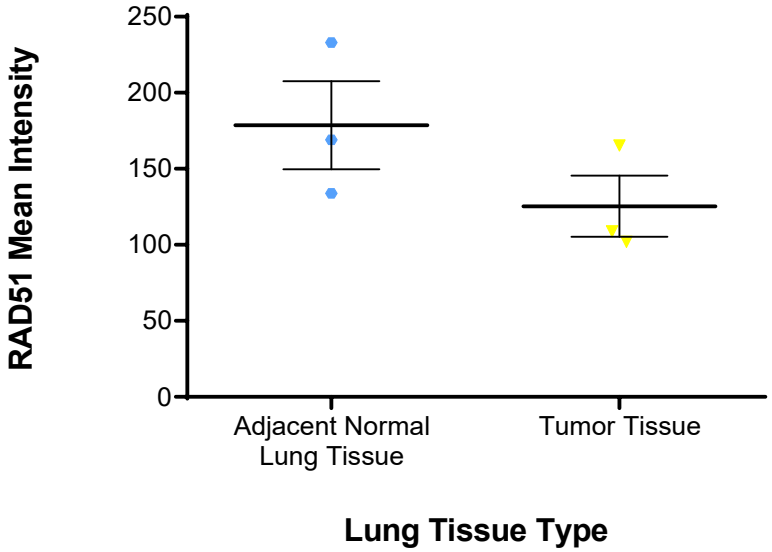

Figure 3.66. Cr(VI)-induced HR deficiency in chromate worker lung tumor tissue. The mean signal intensity of RAD51 was lower in the tumor tissue than in normal adjacent lung tissue (p=0.2059). Image analysis was performed with the nucleus as the region of interest, on 100 intact, non-overlapping and random nuclei.

SUMMARY

In this aim, we found Cr accumulated in rat lung tissue in a dose-dependent manner after 90-day zinc chromate exposure. Cr levels in the left and right lungs both increased in a dose-dependent manner. Cr levels were significantly elevated in the right lung compared with the left lung. We also found Cr dose elevation was significantly lower in the bronchial tree after 90-day exposure than in other lobes. This result indicates particulate Cr(VI) was inhaled and deposited into the distal airways of the rat lung after 90-day exposure.

Cr(VI)-induced lung histological changes were investigated by H&E staining. We found macrophage aggregation and lymphocyte aggregation in the alveolar region after 90-day Cr exposure. A large number of necrotic cells could be seen in alveoli. Vascular wall thickening was observed in the lungs of Cr(VI)-exposed rats. Cr(VI)-induced macrophage aggregation was found around the alveolar region and terminal airways, and increased with Cr dose after 90-day zinc chromate exposure.

We also found after 90-day zinc chromate exposure, Cr(VI) induced γ-H2AX foci formation in rat lungs, which increased in a dose-dependent manner in bronchioles and alveoli. γ-H2AX foci formation caused by Cr was more pronounced in bronchioles than in alveoli. Cr(VI)-induced γ-H2AX foci formed almost exclusively in bronchioles and alveolar epithelial cells after 90-day zinc chromate exposure.

We next investigated RAD51 foci to assess HR repair in rat lungs after 90-day zinc chromate exposure by immunofluorescence. We found Cr(VI) inhibited RAD51 foci formation in rat lungs after 90-day zinc chromate exposure. Cr(VI)-

induced RAD51 foci formation was reduced in a dose-dependent manner in bronchioles and slightly in alveoli. These data suggest Cr(VI)-induced RAD51 inhibition is more pronounced in the bronchiolar region than in the alveolar region.

When comparing the sex groups, we found changes in Cr deposition did not differ significantly between the sexes. There was also no statistically significant difference in macrophage accumulation in the lungs of female and male rats. In bronchioles and alveoli, there were some differences in Cr(VI)-induced γ-H2AX foci formation in different sex groups, although they were not statistically significant. Cr(VI)-induced γ-H2AX foci formation was higher in the female rat group than in the male rat group. Comparing sex groups for bronchioles and alveoli, subchronic Cr(VI)-induced RAD51 foci formation somewhat differed, although the differences were not statistically significant.

We found significantly increased γ-H2AX foci formation and decreased RAD51 foci formation in chromium-associated lung tumor tissue. This result confirms Cr(VI)-induced DNA double strand breaks and HR deficiency persist into tumor formation rather than being transient effects.

Aim 3: Demonstrate particulate Cr(VI) induces DNA double strand break, but does not induce HR repair failure resulting in chromosomal instability in whale lung cells.

BACKGROUND

Cr(VI) is a global pollutant and environmental toxicant. To understand how Cr(VI) affects health, it is important to consider multiple perspectives by using the One Environmental Health approach. One Environmental Health, a specific subset of One Health, is a research strategy focused on the study of toxicants, aiming to incorporate human health, wildlife health, and ecosystem health in order to establish a more comprehensive understanding of global health (Pérez and Wise 2018). The whale model was included as a part of the One Environmental Health Approach to investigate Cr(VI) carcinogenesis across species, because whales live in an extreme environment and are exposed to a high level of Cr(VI) (Wise et al., 2019a; Wise et al., 2019b). This type of analysis is performed to determine how two species with different environmental adaptations respond differently to toxicant exposure. Whales represent humans in the ocean, which means they are our closest marine relatives. Whales are long-lived species and exhibit a higher level of protection from cancer (de Magalhães, 2015; Keane et al., 2015). For example, bowhead whales (*Balaena mysticetus*) live for over 200 years. The longevity of this species while living in an extreme environment strongly suggests the existence of effective mechanisms conferring resistance to cancer caused by environmental carcinogens (Seim et al., 2014; Keane et al., 2015; Ma and Gladyshev, 2017). However, how whales evade carcinogenesis is unknown. Studies show whale cells

are more resistant to Cr(VI)-induced chromosome instability than human cells (Li Chen et al., 2009a; Li Chen et al., 2009b; Li Chen et al., 2012; Wise et al., 2015). A recent study showed prolonged Cr(VI) exposure does not inhibit HR repair in North Atlantic Right Whale lung cells (Browning et al., 2017). Thus, HR repair may play an important role in the increased Cr(VI) resistance observed in whale cells. However, no more data are available investigating HR repair activity after Cr(VI) exposure in whale cells. Therefore, investigating the effect of Cr(VI) in whale cells may shed light on how to prevent Cr(VI)-induced chromosome instability.

Our previous studies found Cr(VI) exposure caused DNA double strand breaks while inhibiting HR repair, resulting in chromosomal instability in human lung cells (Browning et al., 2016; Qin et al., 2014; Wise et al., 2003; Wise et al., 2002; Xie et al., 2009). In Aim 1 and Aim 2, we found Cr(VI) exposure caused DNA double strand breaks in rat lung tissue, and we also observed the inhibition of HR repair by subchronic Cr(VI) exposure. Cr(VI)-induced HR repair inhibition was demonstrated in Cr(VI)-related lung tumors, that is, Cr(VI)-induced HR repair inhibition persisted into tumor formation. Therefore in Aim 3, we translated these outcomes in whale lung cells to further complement our understanding of the mechanism of Cr(VI)-induced chromosomal instability.

RESULTS

DNA Double Strand Breaks

Cr(VI)-induced DNA damage has been shown to result in DNA double strand breaks (DSBs) in human cells (Xie et al.,2008; Xie et al.,2009; Kost et al.;

2012, Qin et al.,2014; Wise et al., 2016). We measured the ability of Cr(VI) to induce DNA double strand breaks in bowhead whale lung cells by the neutral comet assay and immunofluorescent analysis of γ-H2AX foci formation. We found particulate Cr(VI) induced a concentration-dependent increase in comet tail formation measured as tail intensity (Figure.3.67 A). Specifically, exposure to 0.1, 0.2, 0.3 and 0.4 ug/cm² zinc chromate resulted in 149.1, 182.9, 205.9 and 216.8% tail intensity increases, respectively, relative to control bowhead whale cells after acute exposure and 136.4, 162.1, 177.1 and 192.0% after prolonged exposure, respectively.

Induction of double strand breaks triggers phosphorylation of histone H2A.X on Ser 139, forming foci at the sites of DNA double strand break. The formation of γ-H2AX foci is considered a quantitative marker of DNA double strand breaks (Rogakou et al., 1999; Sedelnikova et al., 2002). We found particulate Cr(VI) induced γ-H2AX foci formation in bowhead whale lung cells (Figure.3.67 B), and γ-H2AX foci formation increased in a concentration-dependent manner (Figure.3.67 C). Specifically, the percent of cells with γ-H2AX foci increased from a control value of 11% to 26, 33, 42 and 51 % after 24-hour exposure to 0.1, 0.2, 0.3 and 0.4 ug/cm² zinc chromate, respectively, and from a control value of 6% to 20, 27, 45 and 41% after 120-hour exposure, respectively.

In human cells, Cr(VI)-induced DNA double strand breaks occur indirectly and only manifest in the late S phase or G2 phase after 24-hour exposure (Wakeman et al., 2004; Ha, et al., 2004; Zhang et al., 2001; O'Brien et al., 2002; Reynolds et al., 2007; Xie et al., 2009; Holmes et al., 2010). In order to understand

in which cell cycle phase Cr(VI)-induced DNA double strand breaks occur, we detected γ-H2AX in various cell cycle phases by flow cytometry. Based on the difference in cellular DNA content, we divided the cells into G1, S, and G2/M phases. Through gating analysis of γ-H2AX and DNA content distribution, the percentages of γ-H2AX expressed cells in each phase of the cell cycle were estimated. We found DNA double strand breaks occurred in the S and G2/M phase in bowhead whale lung cells (Figure.3.67 D and E). Specifically, after 24-hour exposure to zinc chromate, the proportions of γ-H2AX-positive bowhead whale lung cells in the S and G2/M phases were higher than that of the G1 phase in the high-concentration Cr(VI) exposure group (Figure.3.67 D). This phenomenon was more pronounced after 120-hour exposure. We found Cr(VI)-induced DNA double strand breaks occurred in the S and G2/M phases with increasing zinc chromate concentrations in bowhead whale lung cells (Figure.3.67 E).

A

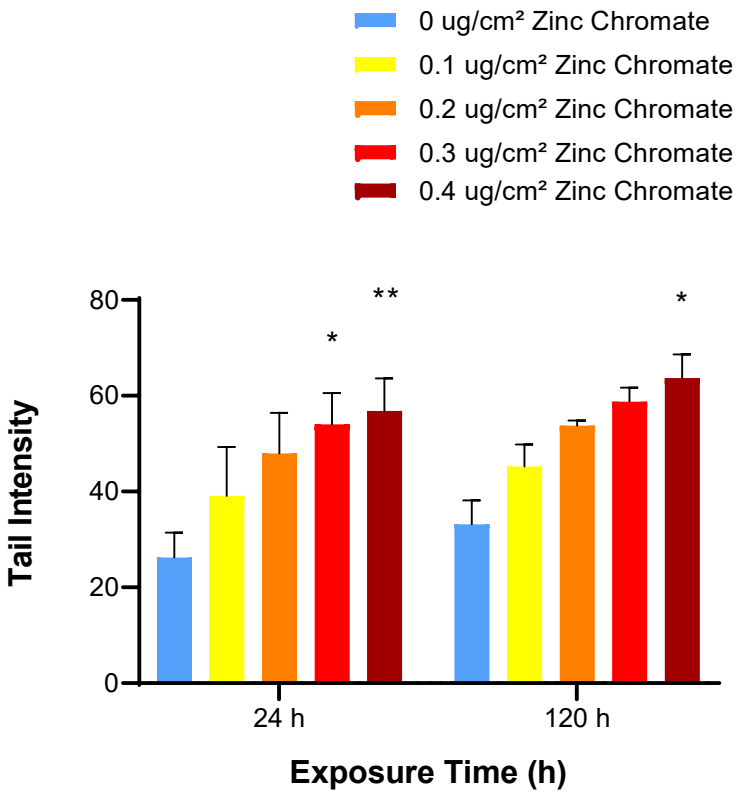
0 ug/cm² Zinc Chromate
0.1 ug/cm² Zinc Chromate
0.2 ug/cm² Zinc Chromate
0.3 ug/cm² Zinc Chromate
0.4 ug/cm² Zinc Chromate
Tail Intensity
80
60
40
20
0
*
**
*
24 h
120 h
Exposure Time (h)

B

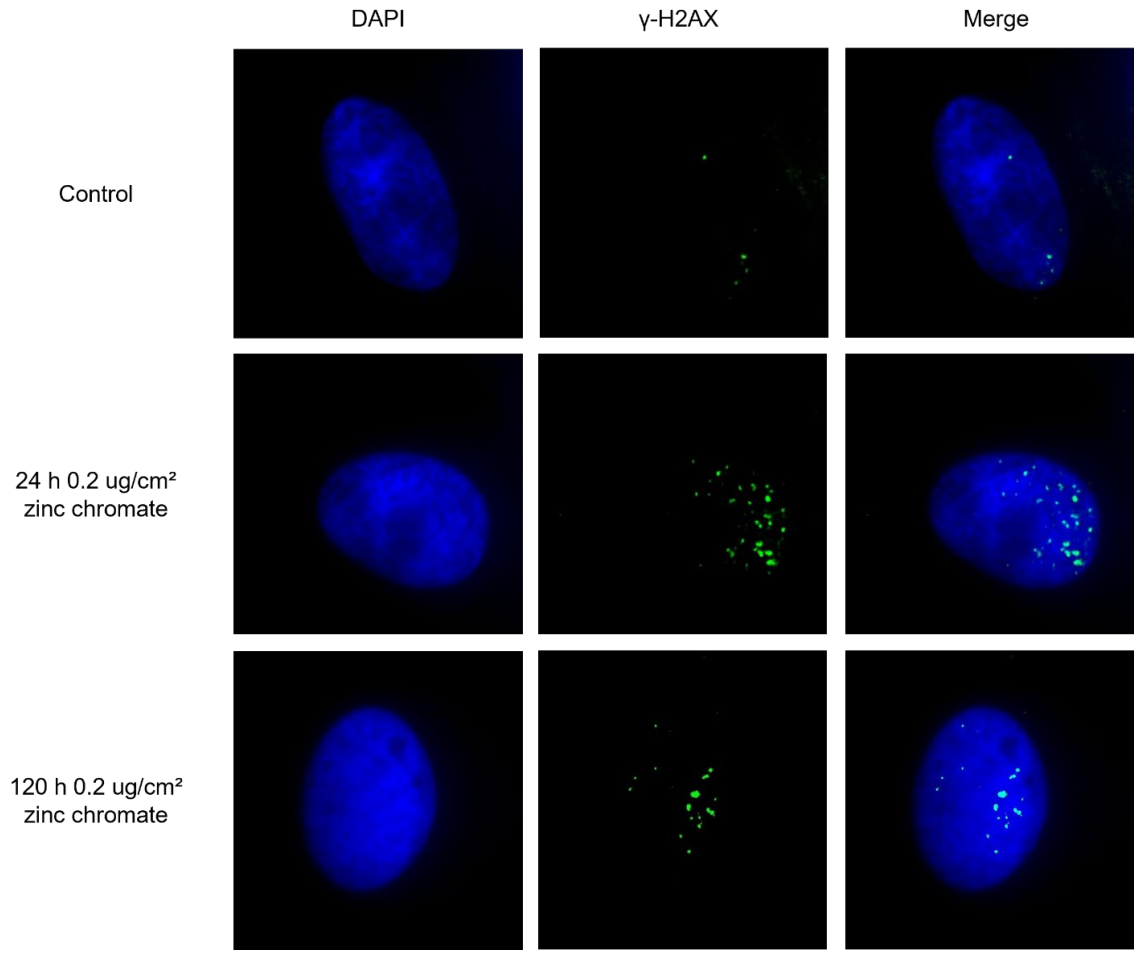
DAPI
γ-H2AX
Merge
Control
24 h 0.2 ug/cm²
zinc chromate
120 h 0.2 ug/cm²
zinc chromate

C

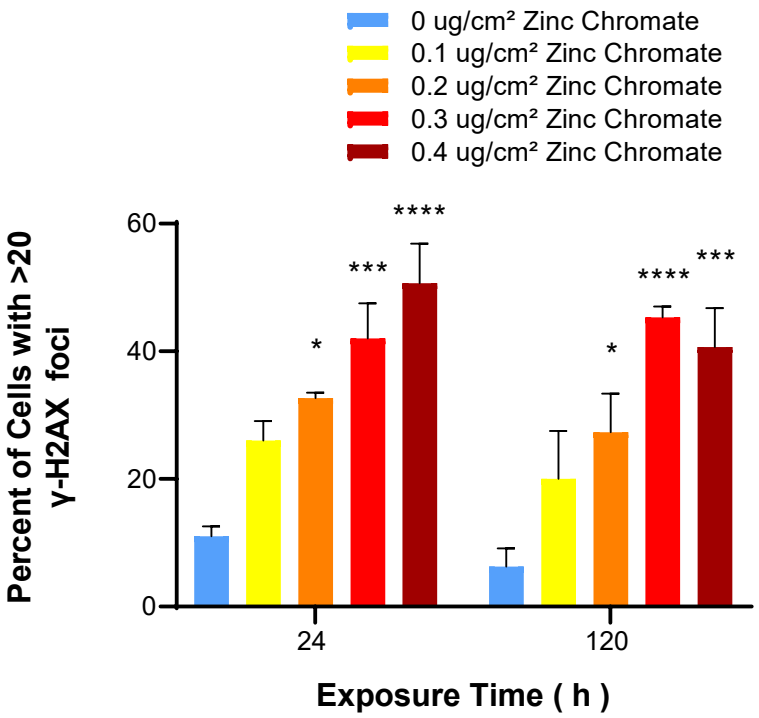
0 ug/cm² Zinc Chromate
0.1 ug/cm² Zinc Chromate
0.2 ug/cm² Zinc Chromate
0.3 ug/cm² Zinc Chromate
0.4 ug/cm² Zinc Chromate
Percent of Cells with >20 γ-H2AX foci
60
40
20
0
*
***
****
*
****
***
24
120
Exposure Time (h)

D

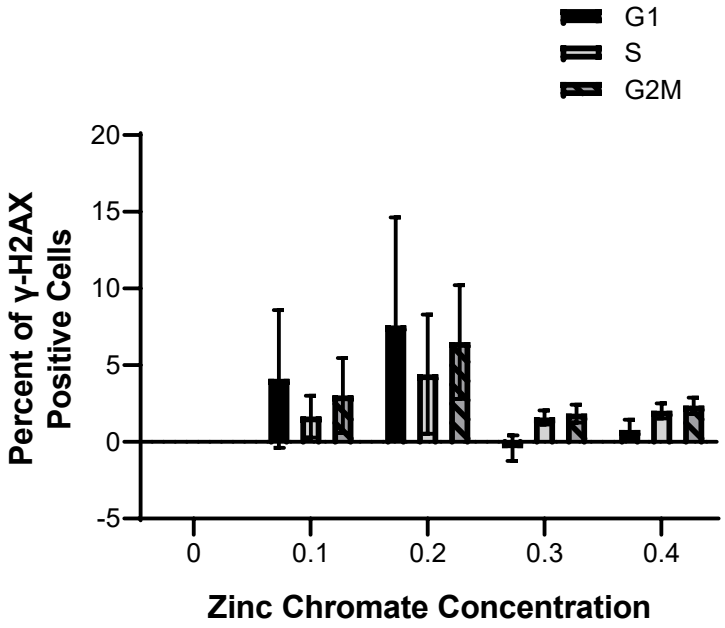
G1
S
G2M
20
15
10
5
0
-5
Percent of γ-H2AX Positive Cells
0
0.1
0.2
0.3
0.4
Zinc Chromate Concentration

E

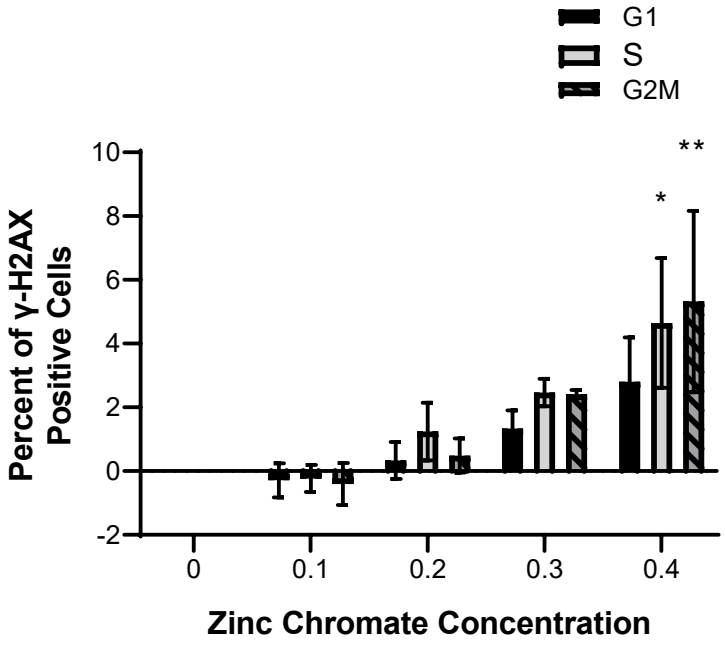
G1
S
G2M
10
8
6
4
2
0
-2
*
**
Percent of γ-H2AX Positive Cells
0
0.1
0.2
0.3
0.4
Zinc Chromate Concentration

Figure.3.67. Cr(VI) induces DNA double strand breaks in bowhead whale lung cells. Cr(VI) induced DNA double strand breaks in bowhead whale lung cells as measured by the neutral comet assay, immunofluorescent signal count for γ-H2AX foci and flow cytometry. **A)** Cr(VI) induced DNA double strand breaks as measured by the neutral comet assay. Comet tail intensity, reflecting double-strand DNA breaks, was significantly increased compared with the control group after exposure to 0.3 and 0.4 ug/cm² zinc chromate for 24 hours and 0.4 ug/cm² zinc chromate for 120 hours (*p<0.05 and **p<0.01, respectively). Comparing groups with different exposure times, no statistically significant difference was found. **B)** Representative images of γ-H2AX foci in bowhead whale lung cells. The first column is DAPI stained nuclear image, the second one is the respective γ-H2AX foci image, and the third one is the merged image. **C)** Cr(VI)-DNA double strand breaks in bowhead whale lung cells measured by γ-H2AX foci count obtained by immunofluorescence. γ-H2AX foci formation increased in a concentration-dependent manner after both 24-hour and 120-hour zinc chromate exposures. γ-H2AX foci formation significantly increased after 24 and 120 hours of treatment with 0.2, 0.3 and 0.4 ug/cm² zinc chromate (*p<0.05, ***p<0.001, ****p<0.0001). Comparing groups with different exposure times, no statistically significant difference was found. **D)** Cr(VI)-induced DNA double strand breaks occurred in S and G2/M phases in bowhead whale lung cells after 24-hour Cr(VI) exposure. 24-hour high Cr(VI) concentration induced the proportions of γ-H2AX-positive whale lung cells in the S phase and G2/M phases. **E)** Cr(VI)-induced DNA double strand breaks occurred in the S and G2/M phases in bowhead whale lung cells after 120-

hour Cr(VI) exposure. The proportions of γ-H2AX-positive whale lung cells in the S phase and G2/M phase were higher than that of the G1 phase after 120-hour Cr(VI) exposure. After exposure to 0.3 ug/cm² zinc chromate, the proportions of γ-H2AX-positive whale lung cells in the S phase and G2/M phase were significantly higher than control values (*p<0.05).

Cell Cycle Profile

When DNA damage occurs within the cell, the cell undergoes a DNA damage response. The DNA damage response is a network of cellular pathways that sense, signal, and repair DNA damage, including cell cycle arrest, activation of DNA repair networks, and apoptosis (Zhou and Elledge, 2000). If DNA damage is detected at cell cycle checkpoints, cell cycle arrest occurs activating repair mechanisms to repair DNA damage. Since Cr(VI)-induced G2 arrest was observed in our laboratory and others s (O'Brien et al., 2002; Reynolds et al., 2007; Xie et al., 2009; Holmes et al., 2010), we tested whether Cr(VI) induces G2 arrest after prolonged exposure in bowhead whale lung cells. We measured cell cycle profiles by flow cytometry. There were not obviously increased bowhead whale lung cells in G2/M after 24-hour or 120-hour zinc chromate exposure (Figure.3.68 A, B, and C). Since the data obtained by flow cytometry is the sum of the percentages of cells in the G2 and M phases, we do not know the actual proportions of cells in the G2 and M phases, separately. We therefore measured the mitotic index in whale lung cells to determine whether cells accumulate during mitosis. We found there were decreases of bowhead whale lung cells in mitosis in a concentration-dependent manner after 24-hour and 120-hour zinc chromate exposure (Figure.3.68 D and E). Taken together, no obvious increase of cells in G2/M combined with a reduction in mitotic cells indicated Cr(VI) induced G2 phase arrest in whale cells, which was not detectable by flow cytometry.

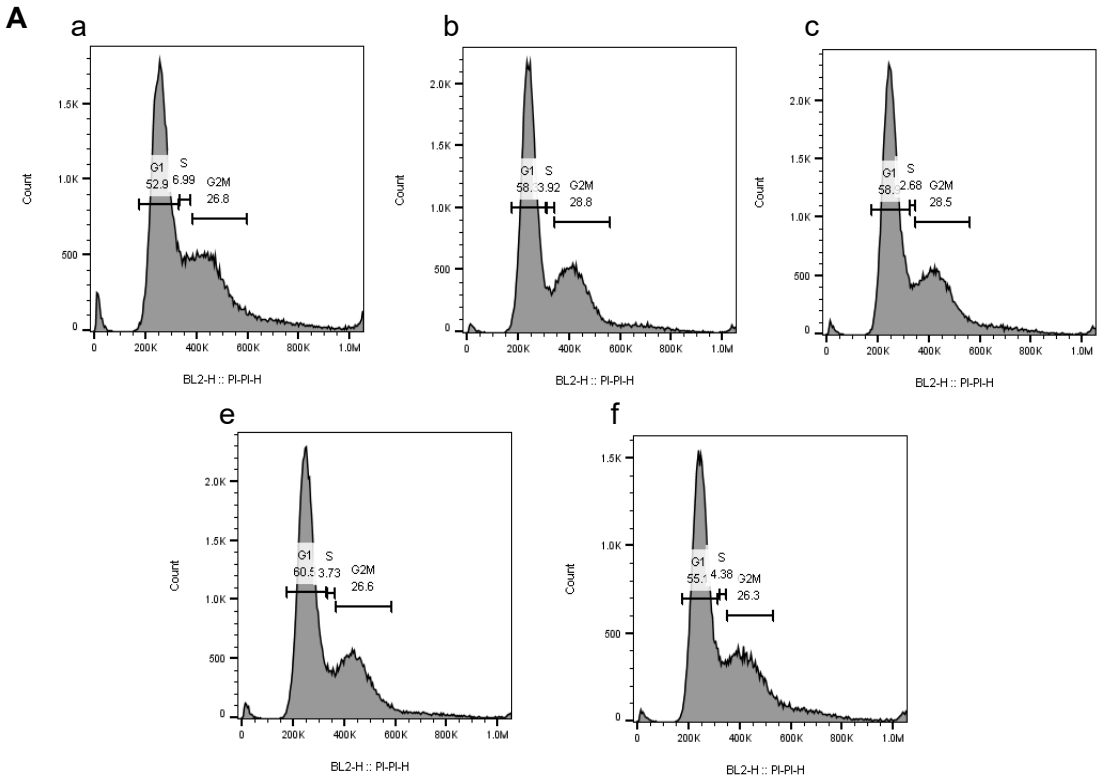
A
a
b
c
e
f
Count
BL2-H :: PI-PI-H
G1
S
G2M
52.9
6.99
26.8
58.
3.92
28.8
58.
2.68
28.5
60.5
3.73
26.6
55.
4.38
26.3

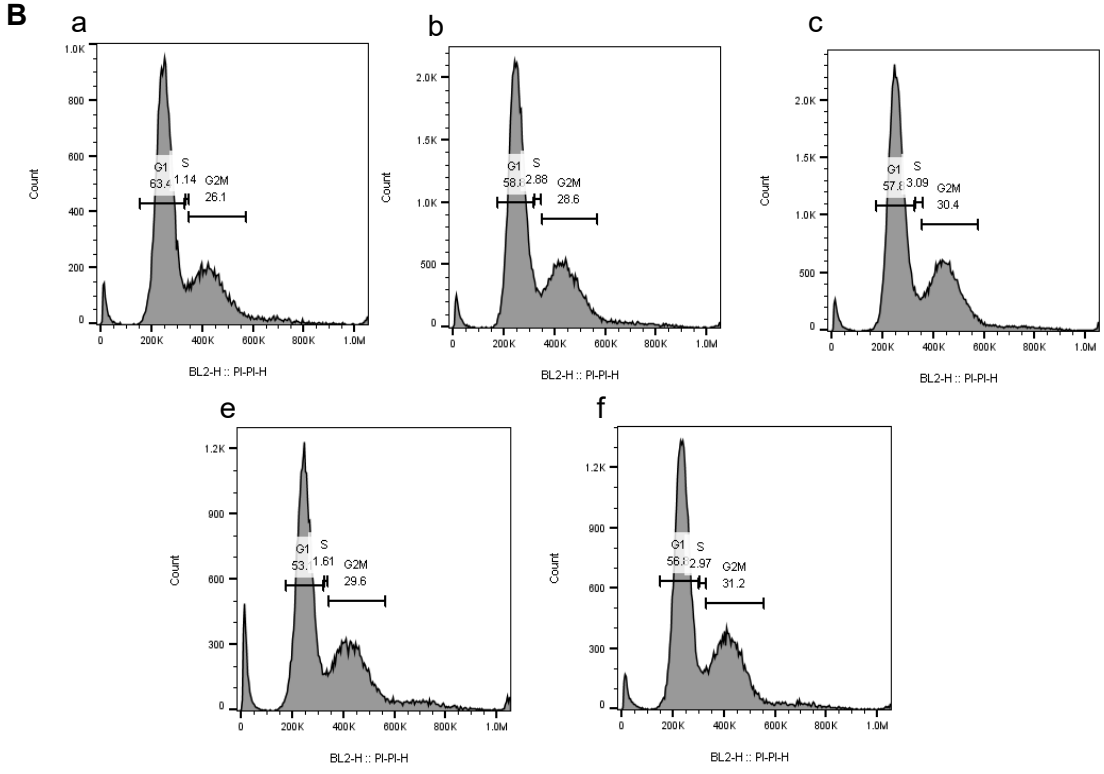
B
a
b
c
e
f
Count
BL2-H :: PI-PI-H
G1
S
G2M
63.
1.14
26.1
58.
2.88
28.6
57.
3.09
30.4
53.
1.61
29.6
56.
2.97
31.2

D

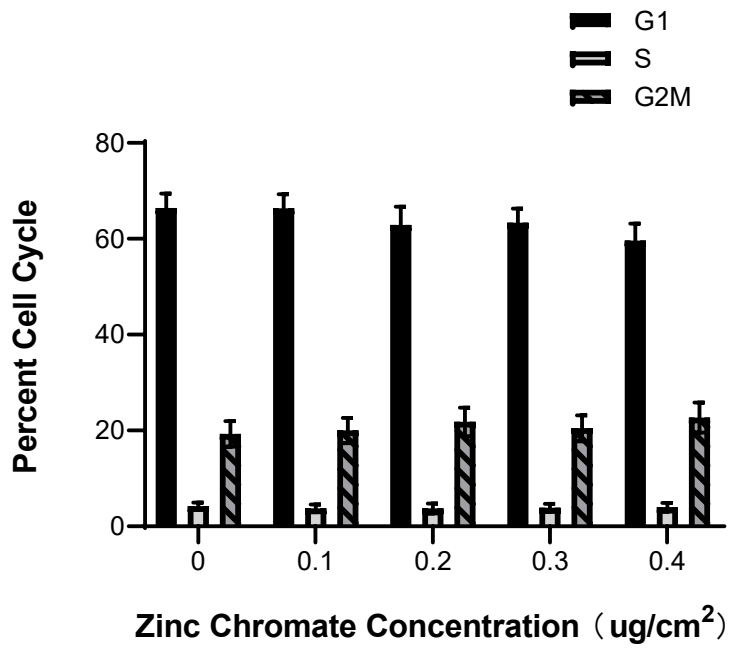
G1
S
G2M
80
60
40
20
0
Percent Cell Cycle
0
0.1
0.2
0.3
0.4
Zinc Chromate Concentration（ug/cm2）

E

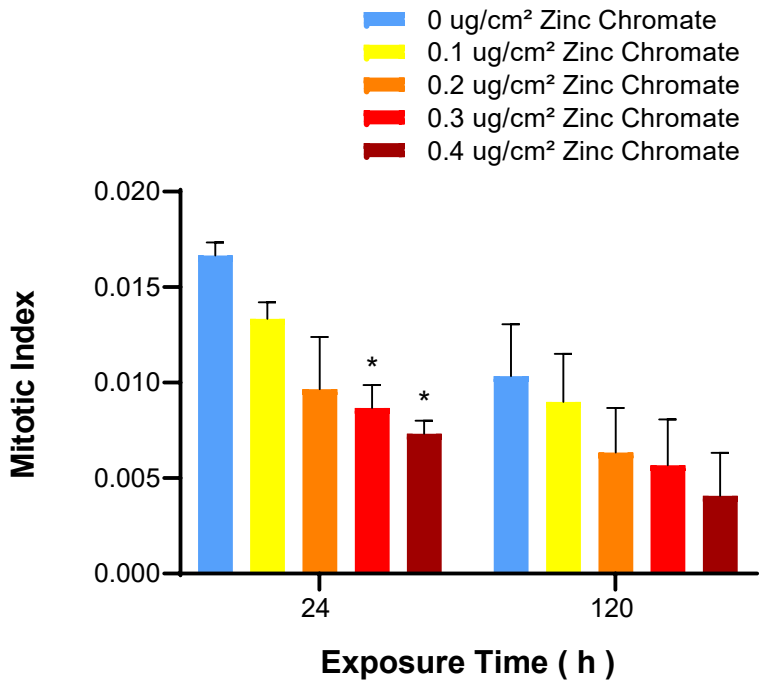
0 ug/cm² Zinc Chromate
0.1 ug/cm² Zinc Chromate
0.2 ug/cm² Zinc Chromate
0.3 ug/cm² Zinc Chromate
0.4 ug/cm² Zinc Chromate
0.020
0.015
0.010
0.005
0.000
Mitotic Index
*
*
24
120
Exposure Time (h)

Figure.3.68. Cr(VI)-induced G2 phase arrest in whale lung cells. Cr(VI) induced G2 arrest in bowhead whale lung cells. **A)** Cell cycle profiles after 24-hour zinc chromate exposure in the whale lung cells. **B)** Cell cycle profiles after 120-hour zinc chromate exposure in the whale lung cells. **C)** The percentage of cells in the G2/M phase did not increase after 24-hour zinc chromate exposure. **D)** The percentage of cells in the G2/M phase did not increase after 120-hour zinc chromate exposure. **E)** Cr(VI) induced mitotic index decreases of bowhead whale lung. There were decreases of bowhead whale lung cells in mitosis in a concentration-dependent manner after 24-hour and 120-hour zinc chromate exposure. After 24-hour exposure, 0.3 and 0.4 ug/cm² zinc chromate significantly decreased the numbers of bowhead whale lung cells in mitosis (*p<0.05).

HR Repair

HR repair is the accurate repair of DNA double strand breaks using undamaged sister chromatids as a template to maintain genome integrity (Van et al. 2001). Our previous studies found prolonged particulate Cr(VI) inhibits HR repair by targeting RAD51 (Qin et al., 2014; Browning et al., 2016). HR repair protects against Cr(VI)-induced DNA double strand breaks, and we have shown prolonged particulate Cr(VI) induced almost equal amounts of DNA double strand breaks in human lung cells and bowhead whale lung cells. Therefore, we evaluated HR repair in particulate Cr(VI) treated bowhead whale lung cells by sister chromatid exchange assay. Sister chromatid exchange is the result of the crossover between sister chromatids in the resolution step of HR and is quantified as a measure of HR repair activity. We found particulate Cr(VI) induced a significant concentration-dependent increase in sister chromatid exchange formation after both 24-hour and 120-hour exposure (Figure.3.69 A). Specifically, 24-hour exposure to 0, 0.1, 0.2, 0.3 and 0.4 ug/cm² zinc chromate induced an average of 0.05, 0.12, 0.16, 0.21 and 0.23 sister chromatid exchanges per chromosome, respectively; and 120-hour exposure induced an average of 0.07, 0.12, 0.18,0.21 and 0.22 sister chromatid exchanges per chromosome, respectively (Figure.3.69 A).

RAD51, the recombination enzyme, is a key protein of the HR repair pathway. Upon induction of DNA double strand breaks, RAD51 is recruited and localizes to the nucleus (Essers et al., 2002). Then we measured RAD51 foci formation to confirm HR repair is functional in whale cells following particulate Cr(VI) exposure (Figure.3.69 B). We found Cr(VI) induced a significant increase in

RAD51 nuclear foci formation (Figure.3.69 C). Specifically, the percent of cells with RAD51 foci increased from a control value of 12 to 20, 25, 27 and 29% after 24-hour exposure to 0.1, 0.2, 0.3 and 0.4 ug/cm² zinc chromate and from a control value of 8 to 13, 21, 24 and 27% after 120-hour exposure, respectively. All these data suggest HR repair is functional in bowhead whale cells after zinc chromate exposure.

A

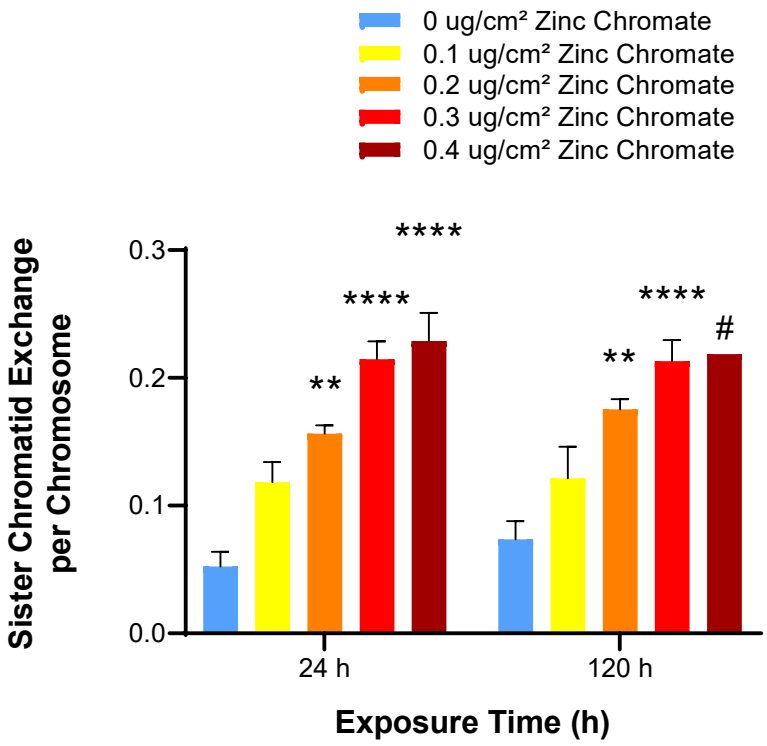
0 ug/cm² Zinc Chromate
0.1 ug/cm² Zinc Chromate
0.2 ug/cm² Zinc Chromate
0.3 ug/cm² Zinc Chromate
0.4 ug/cm² Zinc Chromate
Sister Chromatid Exchange per Chromosome
0.3
0.2
0.1
0.0
****
****
**
**
****
#
24 h
120 h
Exposure Time (h)

B

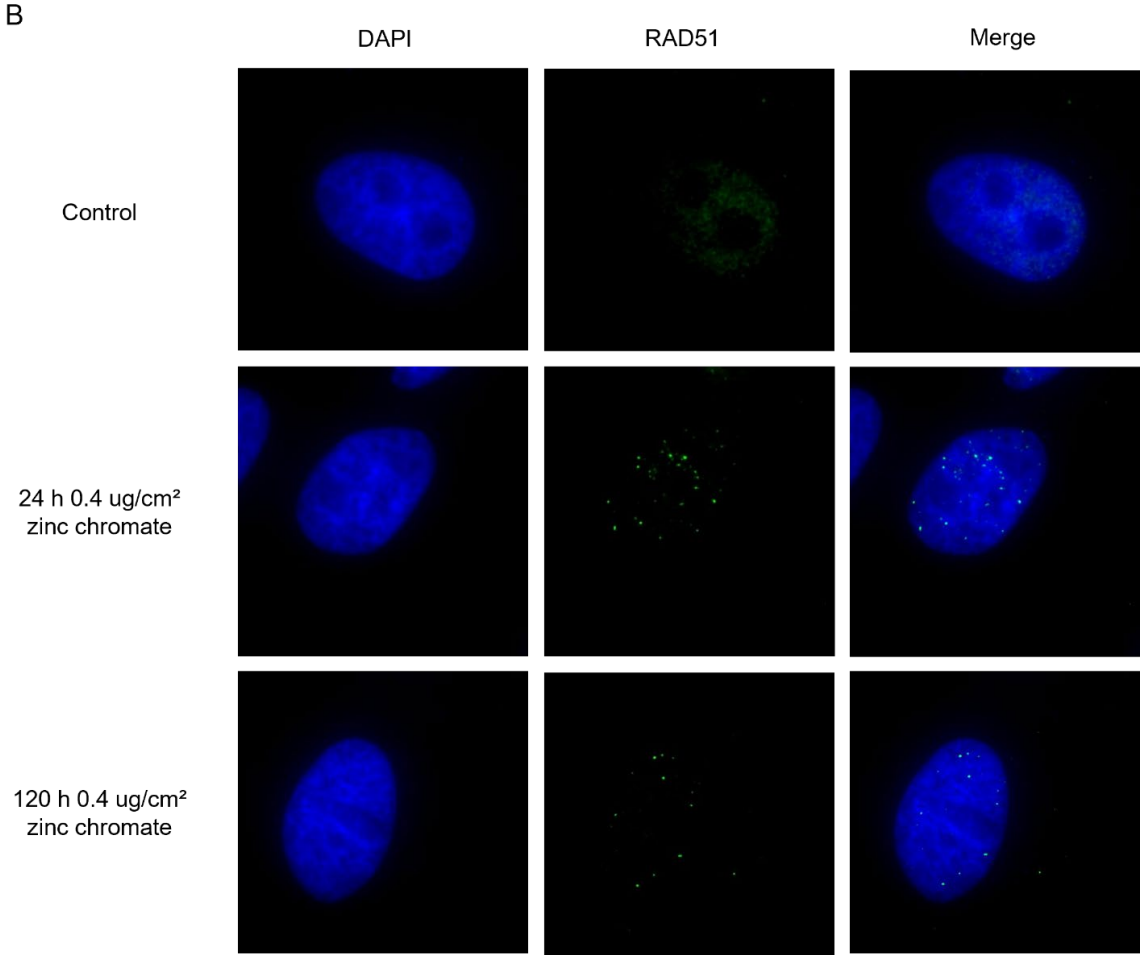
DAPI
RAD51
Merge
Control
24 h 0.4 ug/cm²
zinc chromate
120 h 0.4 ug/cm²
zinc chromate

C

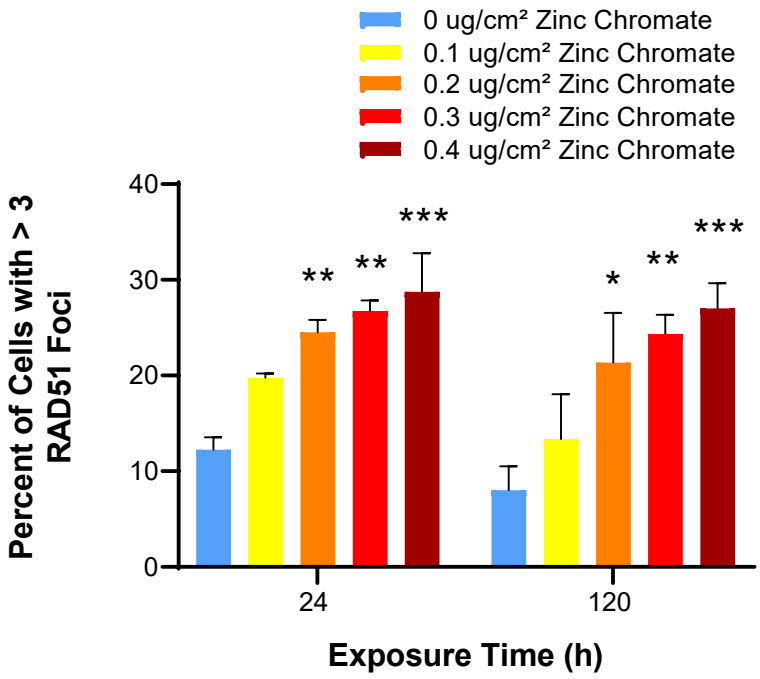

Figure.3.69. Cr(VI)-induced HR repair active in bowhead whale cells. HR repair remained functional in bowhead whale cells after zinc chromate exposure as measured by the sister chromatid exchange assay and immunofluorescent analysis of RAD51 foci formation. **A)** HR repair measured by the sister chromatid exchange assay. SCE significantly increased in a concentration-dependent manner after 24-hour and 120-hour zinc chromate exposures. 24-hour exposure to 0.2, 0.3 and 0.4 ug/cm² zinc chromate induced a significant increase in SCE compared with the control group (**p<0.01 or ****p<0.0001). 120-hour exposure to 0.2 and 0.3 ug/cm² zinc chromate induced a significant increase in SCE compared with the control group (**p<0.01 and ****p<0.0001, respectively). # show 1 experiment data, there were no metaphases in the other two experiments. **B)** Representative images of RAD51 foci in bowhead whale lung cells. First column,

DAPI staining; second column, RAD51 foci staining; third column, merged image. **C)** RAD51 foci formation was significantly increased in a concentration-dependent manner after 24-hour and 120-hour zinc chromate exposures. 24-hour exposure to 0.2, 0.3 and 0.4 ug/cm² zinc chromate induced significant increases in RAD51 foci formation compared with controls (**p<0.01 or ***p<0.001). Exposure to 0.2, 0.3 and 0.4 ug/cm² zinc chromate for 120 hours significantly increased RAD51 nuclear foci formation compared with controls (*p<0.05, **p<0.01, ***p<0.001).

Chromosome instability

If DNA double strand breaks are not repaired or are improperly repaired, they can lead to structural chromosome instability. We measured chromosome damage in bowhead whale lung cells. For the chromosomal damage study, we used two chromosomal damage measures. One measure is the percentage of metaphases with damage, which determines the frequency of damaged cells. Another measure was the total aberration per 100 metaphases to measure the extent of damage within the cell. The difference between the two genotoxicity measures indicates that the number of cells with multiple aberrations is increasing. We found chromosome damage increased in a concentration-dependent manner in bowhead whale lung cells after both 24-hour and 120-hour exposure to zinc chromate (Figure 3.70). Cr(VI) did not increase the number of cells with multiple aberrations in bowhead whale lung cells. However, Cr(VI)-induced chromosome damage did not increase further after 120-hour exposure than after 24-hour exposure. This result indicates Cr(VI) exposure did not induce chromosomal instability in whale lung cells.

A

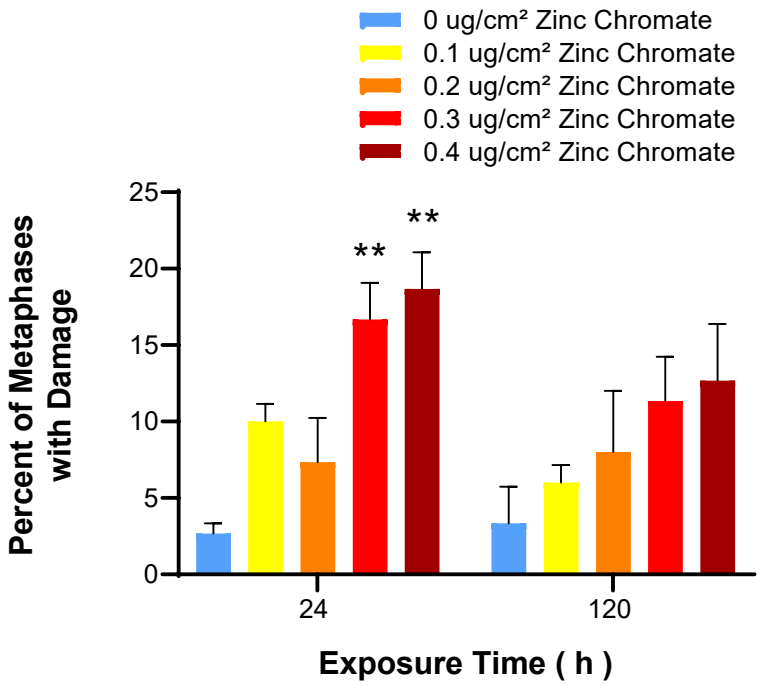
0 ug/cm² Zinc Chromate
0.1 ug/cm² Zinc Chromate
0.2 ug/cm² Zinc Chromate
0.3 ug/cm² Zinc Chromate
0.4 ug/cm² Zinc Chromate
Percent of Metaphases with Damage
25
20
15
10
5
0
**
**
24
120
Exposure Time (h)

B

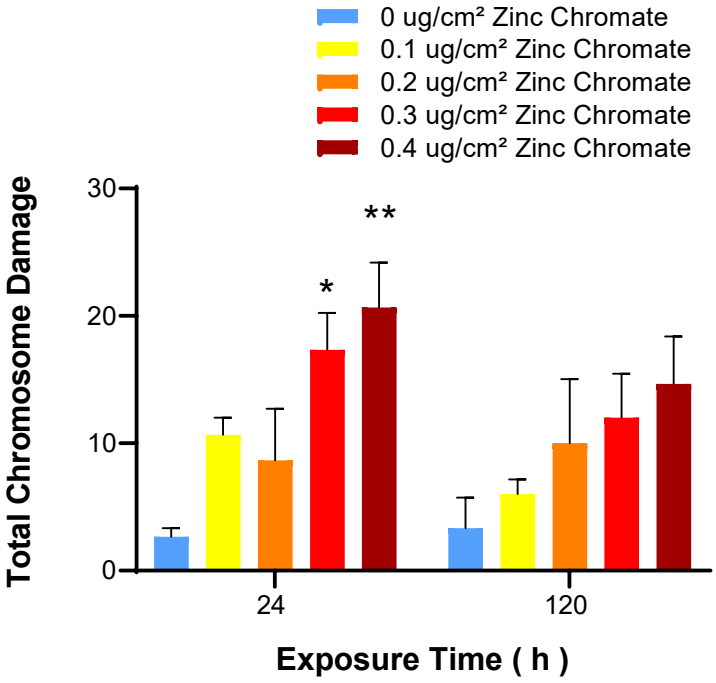
0 ug/cm² Zinc Chromate
0.1 ug/cm² Zinc Chromate
0.2 ug/cm² Zinc Chromate
0.3 ug/cm² Zinc Chromate
0.4 ug/cm² Zinc Chromate
Total Chromosome Damage
30
20
10
0
*
**
24
120
Exposure Time (h)

Figure.3.70. Cr(VI) does not induce chromosome instability in whale lung cells. Chromosome damage was increased in a concentration-dependent manner after 24-hour and 120-hour zinc chromate exposures. **A)** The percentages of metaphases with damage were increased in a concentration-dependent manner after 24-hour and 120-hour zinc chromate exposures. 24-hour exposure to 0.3 and 0.4 ug/cm² zinc chromate induced significant increases in chromosome damage compared with controls (**p<0.01). After 120-hour exposure to zinc chromate, chromosome damage did not surpass that of 24-hour exposure. **B)** Total chromosome damage was increased in a concentration-dependent manner after 24-hour and 120-hour zinc chromate exposures. 24-hour exposure to 0.3 and 0.4 ug/cm² zinc chromate induced significant increases in chromosome damage compared with controls (*p<0.05 and **p<0.01, respectively). At 120-hour exposure to zinc chromate, total chromosome damage did not surpass that of 24-hour exposure.

Cytotoxicity

Because prolonged Cr(VI) does not induce chromosome instability in bowhead whale lung cells, we hypothesized bowhead whale lung cells may avoid Cr(VI)-induced cytotoxicity. Thus, we measured Cr(VI)-induced cytotoxicity in bowhead whale lung cells. We found zinc chromate induced concentration-dependent cytotoxicity in bowhead whale lung cells (Figure 71).

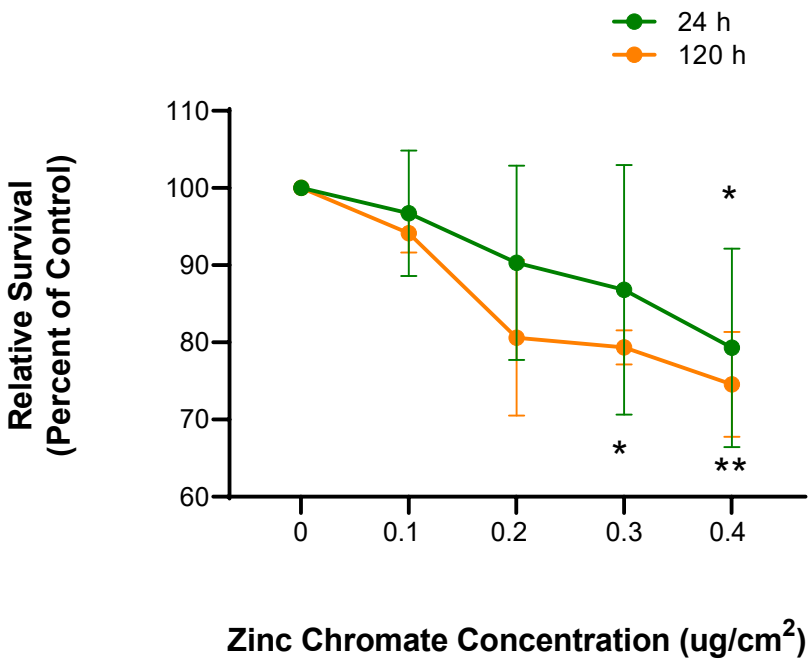

Figure.3.71. Cr(VI)-induced cytotoxicity in bowhead whale lung cells. Cr(VI) induced cytotoxicity in bowhead whale lung cells in a concentration manner after 24-hour and 120-hour exposures. After 24-hour exposure to 0.4 ug/cm², cell survival was significantly decreased compared with the control group (*p<0.05). After 120-hour exposure to 0.3 and 0.4 ug/cm², cell survival was significantly decreased compared with the control group (*p<0.05 and **p<0.01, respectively).

Comparisons with human lung cells and rat lung cells

Next, we compared Cr(VI)-induced DNA double strand breaks, HR repair inhibition, chromosomal instability, and cytotoxicity in lung cells of different species. We used lung fibroblasts for all three species as whale epithelial cells have not been successfully cultured and human lung epithelial cell lines are all aneuploid. The reason why we added some rat lung cell comparisons is to clarify whether differences found between human lung cells and whale lung cells reflect whale specific outcomes.

Cr(VI)-DNA double strand break

We compared the ability of Cr(VI) to induce DNA double strand breaks in bowhead whale lung cells, human lung cells and rat lung cells, using neutral comet assay. We found Cr(VI)-induced similar DNA double strand breaks levels in all three species' cell lines (Figure 3. 72 A). Because in human cells the breaks all occur in the late S/G2 phase and not in the G1 phase, we compared the profiles of DNA double strand breaks in the cell cycle between bowhead whale lung cells and human lung cells using flow cytometry. We found with increasing zinc chromate concentrations in human lung cells, more DNA double strand breaks occurred in S and G2/M phases (Figure 3. 72 B and C). The proportion of γ-H2AX-positive human lung cells in the S phase was higher after 24-hour Cr(VI) exposure and 120-hour Cr(VI) exposure (Figure 3. 72 B). However, in bowhead whale lung cells, Cr(VI)-induced DNA double strand breaks were found in the S phase and G2/M phase in the high-concentration exposure group (Figure 3.72 C). Overall, the

data show for both whale and human lung cells, Cr(VI)-induced DNA double strands occurred in S or G2.

A

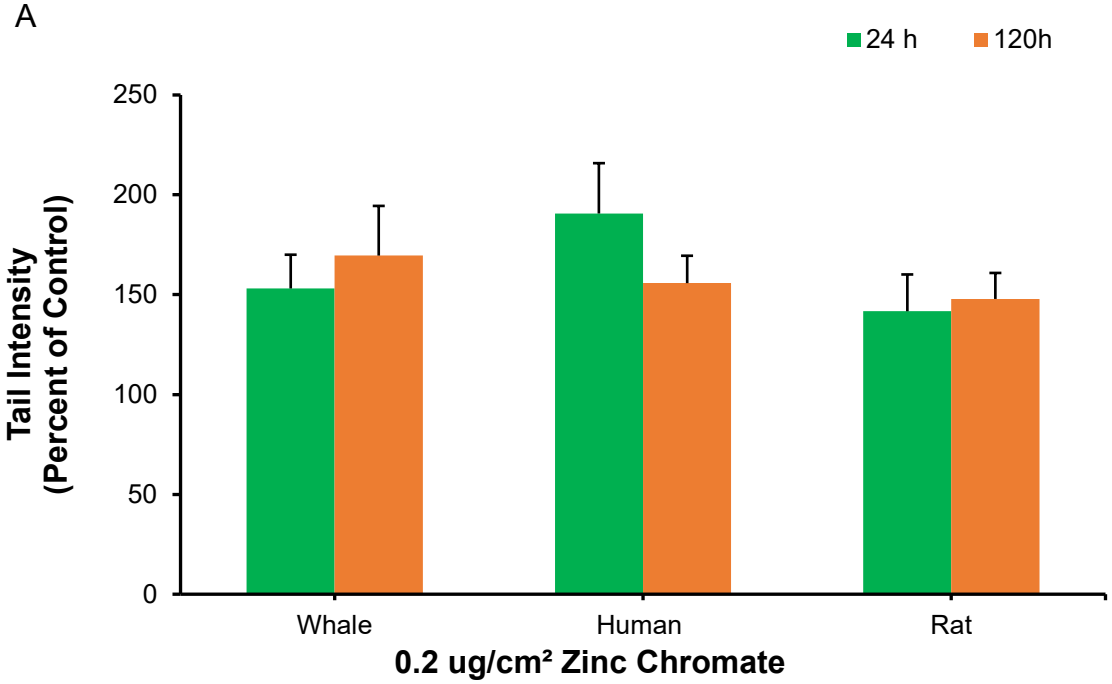
24 h
120h
250
200
150
100
50
0
Tail Intensity
(Percent of Control)
Whale
Human
Rat
0.2 ug/cm² Zinc Chromate

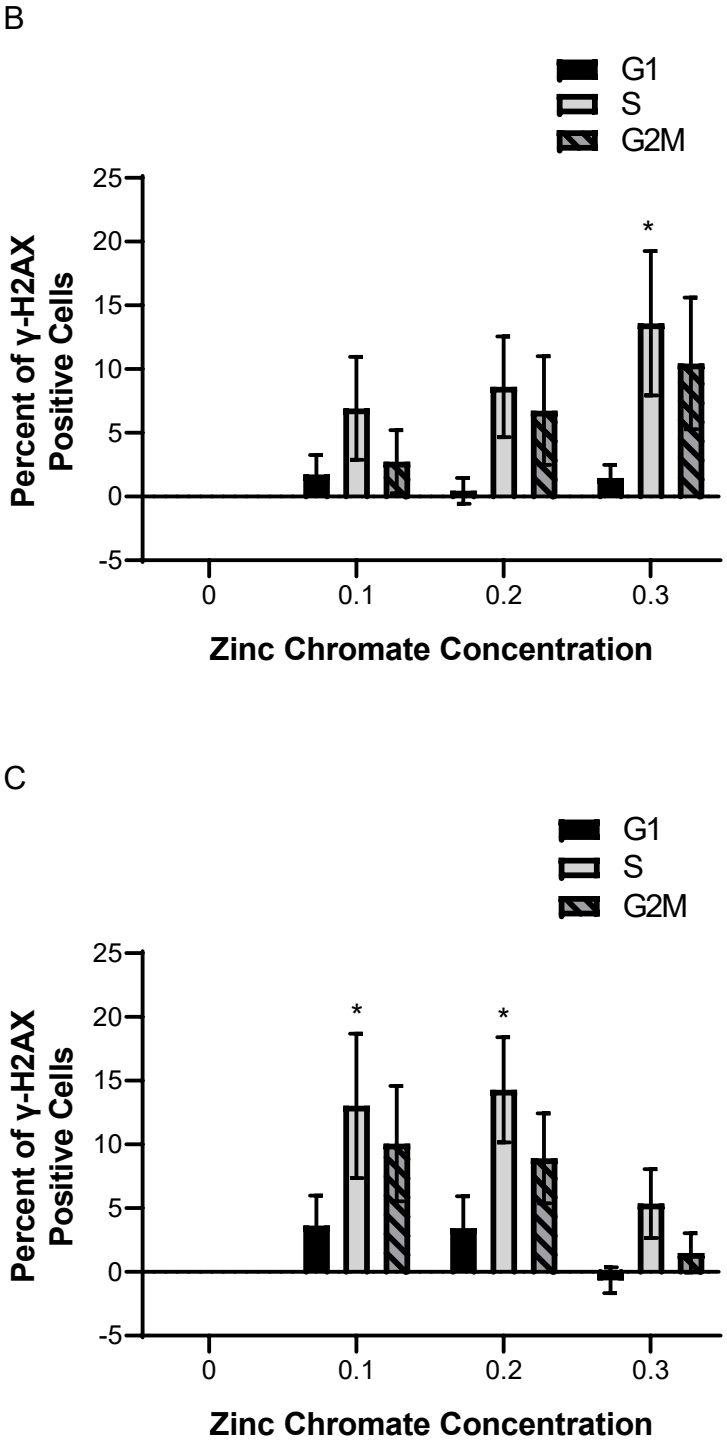

Figure.3.72. Comparison of Cr(VI)-induced DNA double strand breaks in human lung cells, rat lung cells and bowhead whale lung cells. **A)** The intensity of comet tails produced in human lung cells, rat lung cells and bowhead whale lung cells

were similar after 0.2 ug/cm² zinc chromate exposure. After 24-hour exposure, Cr(VI)-induced comet tail intensity was slightly higher in human lung cells, but after 120-hour exposure, Cr(VI)-induced comet tail intensities in the three species' cell lines were pretty close. **B)** and **C)** show Cr(VI)-induced DNA double strand breaks occur in the S and G2/M phases in human lung cells. **B)** The proportions of H2AX-positive human lung cells in the S and G2/M phases were higher than those of the G1 phase after 24-hour Cr(VI) exposure. After exposure to 0.3 ug/cm² zinc chromate, the proportion of H2AX-positive human lung cells in the S phase was significantly higher than the control value (*p<0.05). **C)** The proportions of H2AX-positive human lung cells were higher in the S and G2/M phases compared with the G1 phase after 120-hour Cr(VI) exposure. After exposure to 0.1 and 0.2 ug/cm² zinc chromate, the proportions of H2AX-positive human lung cells in the S phase were significantly higher than the control value (*p<0.05).

Cr(VI)-induced cell cycle arrest

When DNA damage is detected by cell cycle checkpoints, cell cycle arrest occurs, and repair mechanisms are activated to repair DNA damage. It is well established that Cr(VI) induces a G2 arrest in human lung cells after acute exposure, but chronic exposures have not been considered. Above, we reported, for bowhead whale lung cells, after prolonged exposure Cr(VI)-induced a G2 arrest that is not obvious from flow cytometry. Here we show prolonged zinc chromate exposure induced a G2/M arrest in a concentration-dependent manner in human lung cells (Figure.3.73). Our previous study has examined chromium-induced changes in the mitotic index of human lung cells and found that zinc chromate induces a concentration-dependent decrease in the number of mitotic cells (Xie et al., 2009). Thus considered altogether, particulate Cr(VI) induced a G2 arrest in human and whale lung cells after both acute and prolonged exposures.

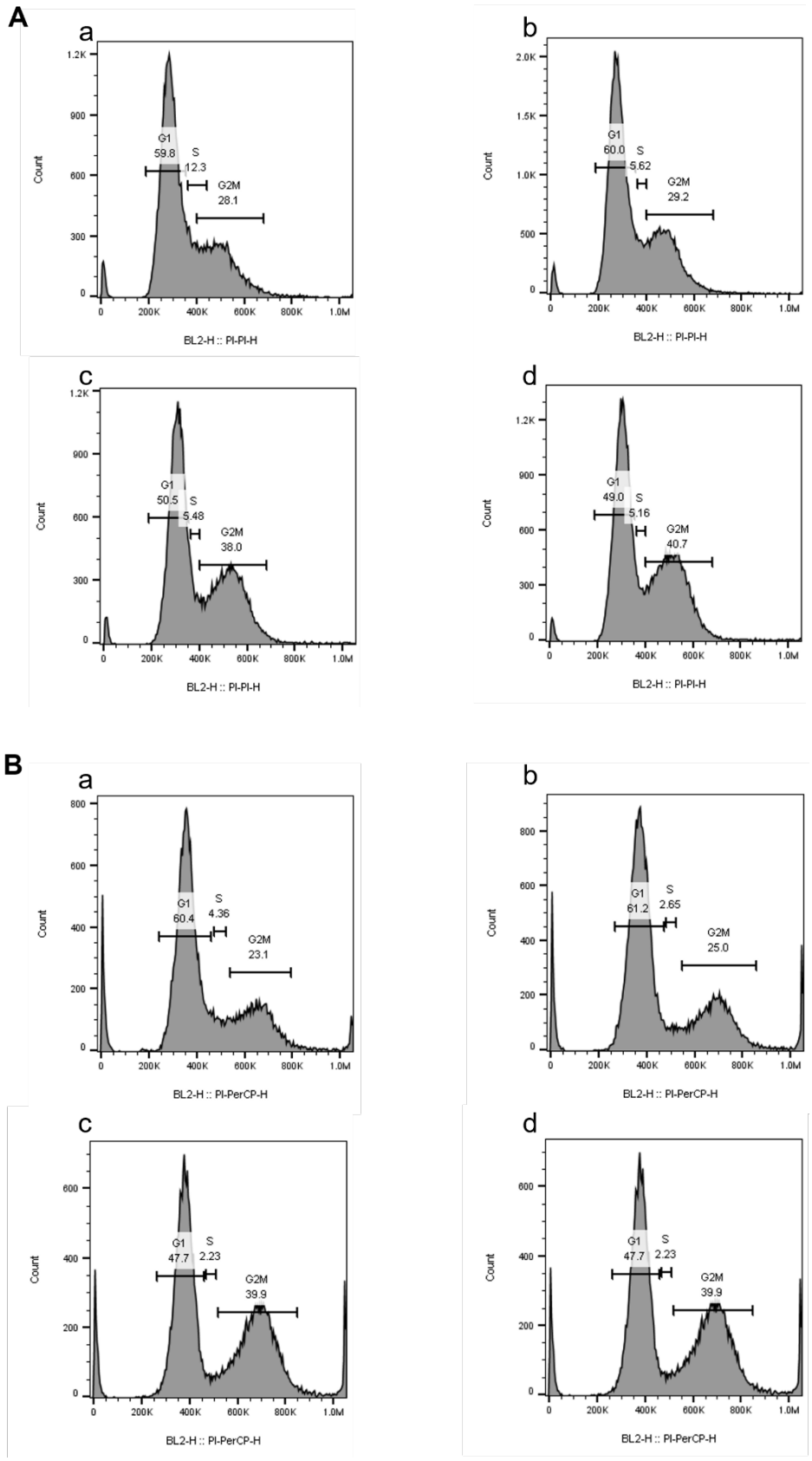
A
a
G1
59.8
S
12.3
G2M
28.1
Count
BL2-H :: PI-PI-H
b
G1
60.0
S
5.62
G2M
29.2
Count
BL2-H :: PI-PI-H
c
G1
50.5
S
5.48
G2M
38.0
Count
BL2-H :: PI-PI-H
d
G1
49.0
S
5.16
G2M
40.7
Count
BL2-H :: PI-PI-H
B
a
G1
60.4
S
4.36
G2M
23.1
Count
BL2-H :: PI-PerCP-H
b
G1
61.2
S
2.65
G2M
25.0
Count
BL2-H :: PI-PerCP-H
c
G1
47.7
S
2.23
G2M
39.9
Count
BL2-H :: PI-PerCP-H
d
G1
47.7
S
2.23
G2M
39.9
Count
BL2-H :: PI-PerCP-H

C

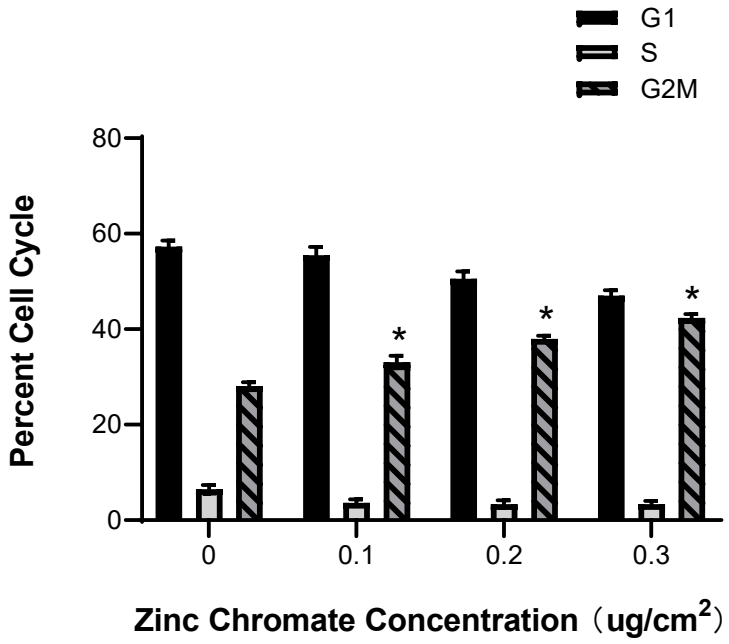
G1
S
G2M
80
60
40
20
0
Percent Cell Cycle
*
*
*
0
0.1
0.2
0.3
Zinc Chromate Concentration（ug/cm2）

D

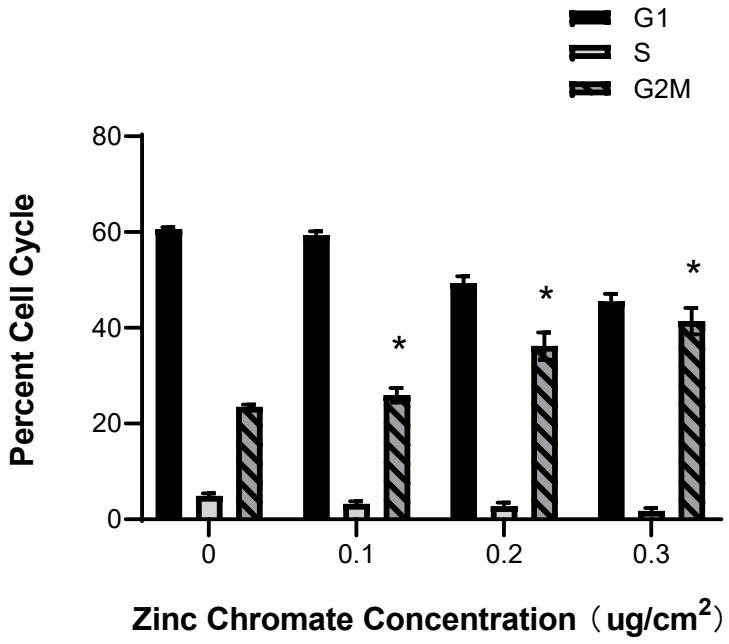
G1
S
G2M
80
60
40
20
0
Percent Cell Cycle
*
*
*
0
0.1
0.2
0.3
Zinc Chromate Concentration（ug/cm2）

Figure.3.73. Cr(VI) induces G2/M phase arrest in human lung cells. Cr(VI) induces G2/M arrest in a concentration-dependent manner in human lung cells. **A)** and **B)** are cell cycle profiles in human lung cells. **A)** Cell cycle profiles after 24-hour zinc chromate exposure in the human lung cells. **B)** Cell cycle profiles after 120-hour zinc chromate exposure in the human lung cells. **C)** and **D)** show the changes of the percentage of human lung cells in cell cycle phases after Cr(VI) exposure. **C)** The percentage of cells in the G1 phase decreased while those of cells in the G2/M phase increased with increasing Cr(VI) concentration after 24-hour zinc chromate exposure. Exposure to 0.1, 0.2 and 0.3 ug/cm² zinc chromate resulted in significantly higher percentages of cells in G2/M than the control value (*p<0.05). **D)** The percentage of cells in the G1 phase decreased while those of cells in the G2/M phase increased with increasing Cr(VI) concentration after 120-hour zinc chromate exposure. Exposure to 0.1, 0.2 and 0.3 ug/cm² zinc chromate induced significant increases in the percentages of cells in the G2/M phase compared with control cells (*p<0.05).

Cr(VI)-induced HR repair inhibition

HR repair prevents Cr(VI)-induced DNA double strand breaks. We have shown that Cr(VI) induces similar numbers of DNA double strand breaks in human lung cells, rat lung cells, and bowhead whale lung cells. We compared changes in Cr(VI)-induced HR repair in lung cells of these different species. Comparing HR repair function in human lung cells, rat lung cells, and bowhead whale lung cells by measuring RAD51 foci formation, we found Cr(VI) induced HR repair after acute exposure, but inhibited HR after prolonged exposure in rat and human lung cells. Notably, and in contrast, Cr(VI) did not inhibit HR repair, after prolonged exposures in whale lung cells (Figure 3.74 B).

To clarify this finding, we considered HR repair in whale and human lung cells using the sister chromatid exchange assay. Consistent with the RAD51 foci data, after acute exposure to 0.2 ug/cm² zinc chromate, sister chromatid exchanges increased in both human and whale lung cells, but after 120-hour exposure, they were significantly reduced in human lung cells, but were not affected in bowhead whale lung cells (Figure 3.74 A). Taken altogether, these data show whale lung cells escape Cr(VI)-induced repair inhibition.

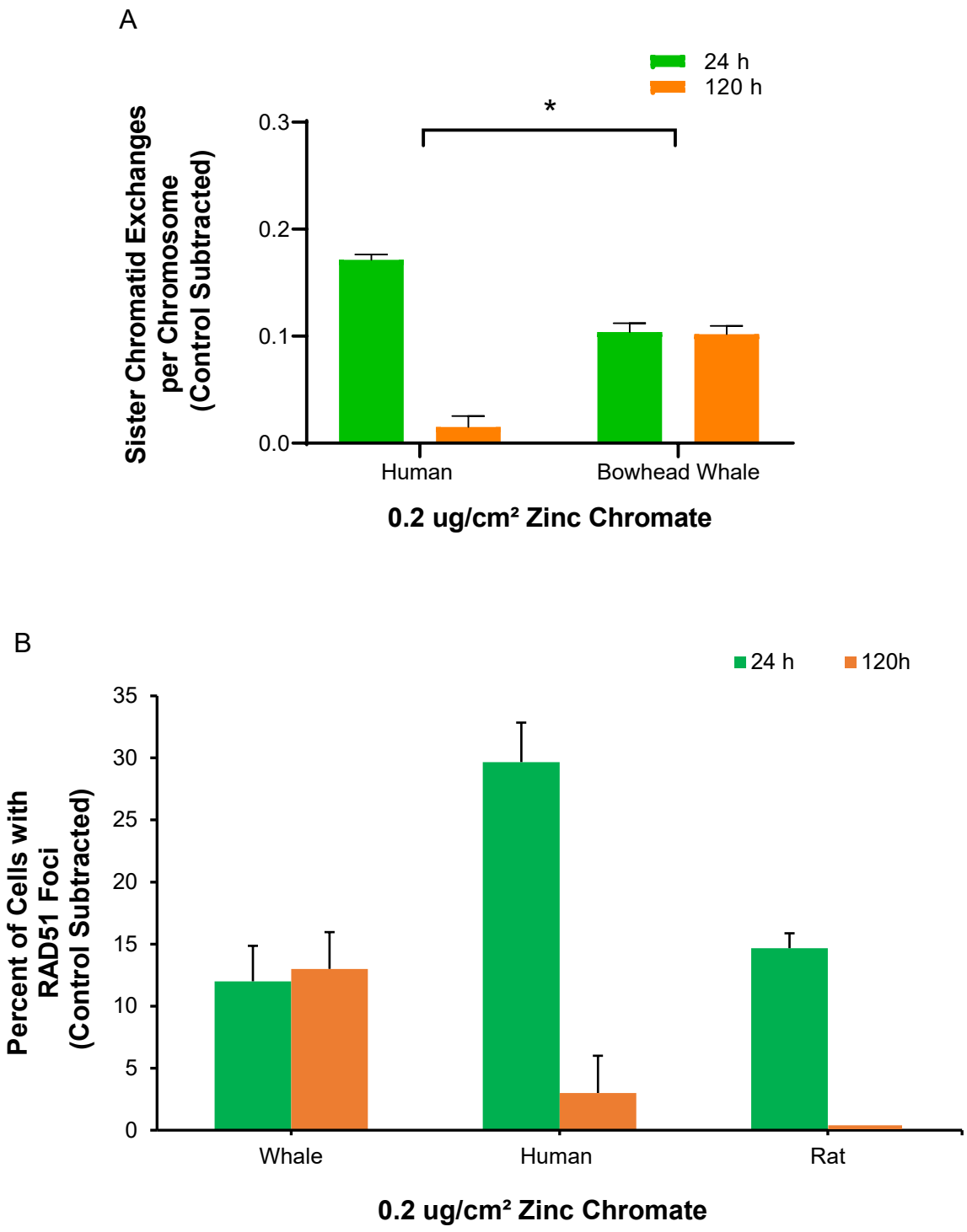

Figure.3.74. Comparison of Cr(VI)-induced HR repair changes in human lung cells, rat lung cells and bowhead whale lung cells. Cr(VI)-induced HR repair changes

were different in these three species' cell lines. **A)** Comparison of Cr(VI)-induced sister chromatid exchanges between human lung cells and bowhead whale lung cells. This figure shows the difference of 0.2 ug/cm² zinc chromate induced sister chromatid exchanges between human lung cells and bowhead whale lung cells. In human lung cells, Cr(VI)-induced sister chromatid exchanges were much less abundant in the 120-hour exposure group compared with the 24-hour exposure group. In bowhead whale lung cells, Cr(VI)-induced sister chromatid exchanges in the 120-hour exposure group were similar to the 24-hour exposure group. **B)** RAD51 foci information produced in those three species' cell lines were different after 0.2 ug/cm² zinc chromate exposure. After 24-hour exposure, Cr(VI)-induced RAD51 foci information was less pronounced in rat and whale lung cells compared with human lung cells. However, after 120-hour exposure, Cr(VI)-induced RAD51 foci information decreased in human and rat lung cells but still increased in bowhead whale lung cells.

Cr(VI)-induced chromosome instability

If HR repair is inhibited, cells will sort to other DNA repair pathways, which are low fidelity repair pathways. Improperly repaired DNA double strand breaks can lead to structural chromosomal damage and cause chromosome instability. We compared Cr(VI) -induced chromosomal instability in whale lung cells and human lung cells. We found higher percentages of metaphases with damage in human lung cells than in bowhead whale lung cells after 24-hour and 120-hour Cr(VI) exposure (Figure 3.75 A). The total amount of chromosome damage in human lung cells was significantly higher after 120-hour Cr(VI) exposure than that after 24-hour Cr(VI) exposure (Figure 3.75 B). However, in bowhead whale lung cells, the total chromosome damage after 120-hour Cr(VI) exposure was lower than that after 24-hour Cr(VI) exposure. These data indicate Cr(VI) induces chromosomal instability in human lung cells, but not in bowhead whale lung cells.

A

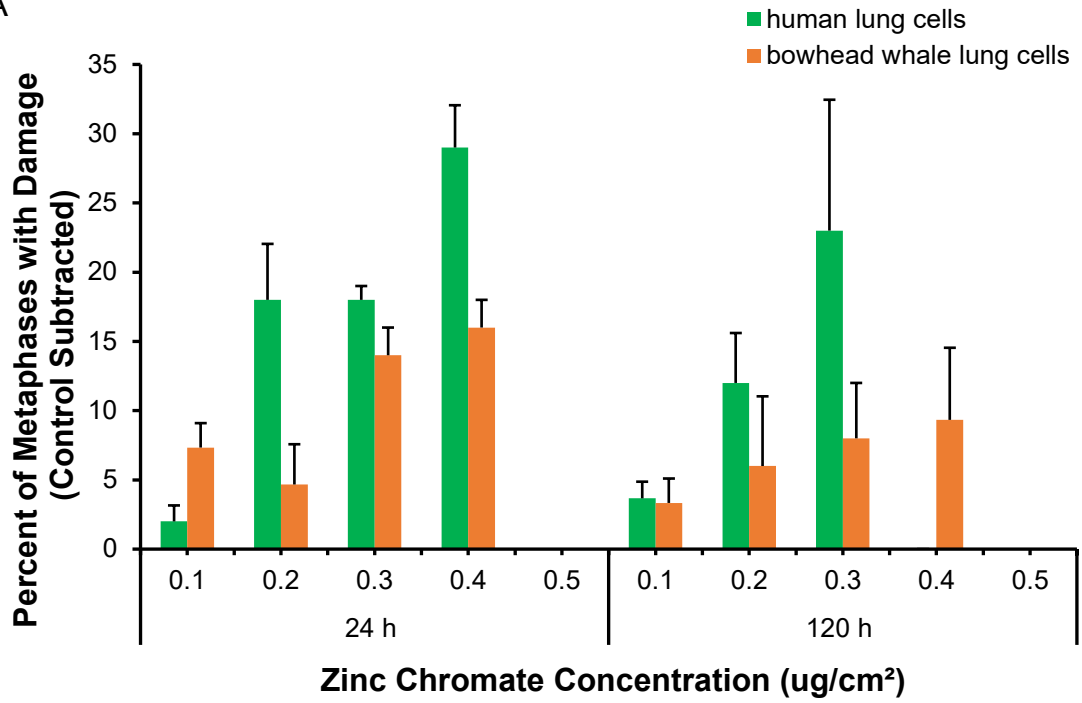
human lung cells
bowhead whale lung cells
Percent of Metaphases with Damage (Control Subtracted)
35
30
25
20
15
10
5
0
0.1
0.2
0.3
0.4
0.5
0.1
0.2
0.3
0.4
0.5
24 h
120 h
Zinc Chromate Concentration (ug/cm²)

B

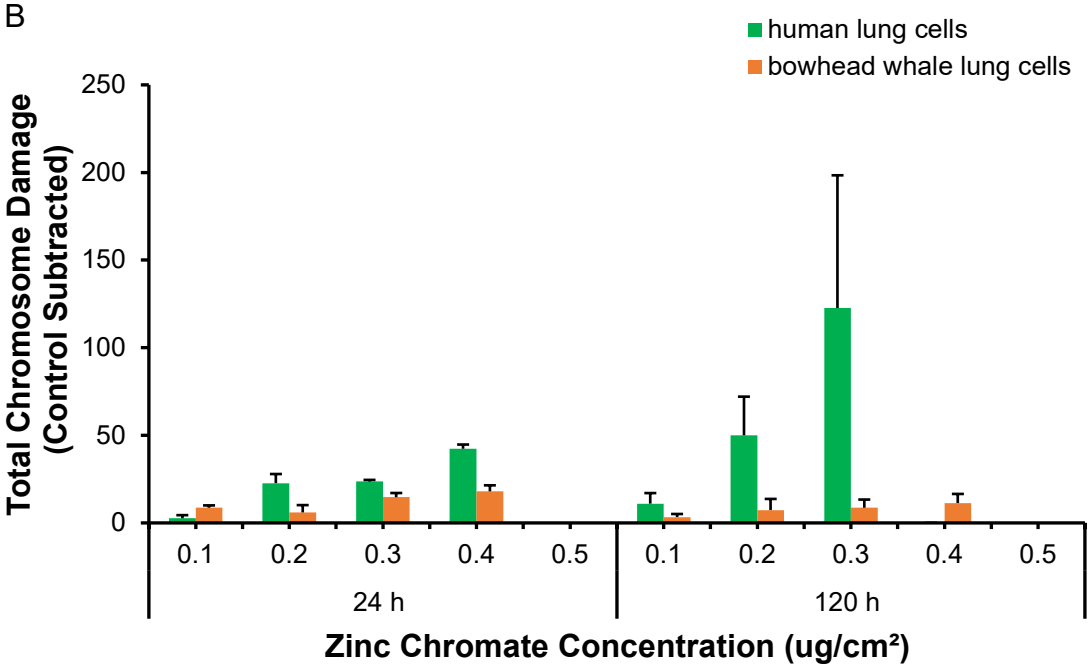
human lung cells
bowhead whale lung cells
Total Chromosome Damage (Control Subtracted)
250
200
150
100
50
0
0.1
0.2
0.3
0.4
0.5
0.1
0.2
0.3
0.4
0.5
24 h
120 h
Zinc Chromate Concentration (ug/cm²)

Figure.3.75. Comparison of Cr(VI)-chromosome instability in human lung cells and bowhead whale lung cells. Cr(VI)-induced chromosomal instability differed in these two types of lung cells. **A)** The comparison of the percentage of mid-term damage in human lung cells and bowhead whale lung cells after Cr(VI) exposure. The percentage of metaphase with damage was higher in human lung cells than in bowhead whale lung cells after both 24-hour and 120-hour Cr(VI) exposure. **B)** The comparison of total chromosomal damage in human lung cells and bowhead whale lung cells after Cr(VI) exposure. In human lung cells, total chromosomal damage was significantly higher after 120-hour Cr(VI) exposure than after 24-hour Cr(VI) exposure; however, in bowhead whale lung cells, total chromosomal damage was lower after 120-hour Cr(VI) exposure compared with 24-hour Cr(VI) exposure.

Cr(VI)-Induced Cytotoxicity

Given whale cells have better HR and avoid chromosome instability, we hypothesized these differences would manifest as less Cr(VI)-induced cell death. Indeed, when we compared Cr(VI)-induced cytotoxicity in human lung cells and bowhead whale lung cells, we found more bowhead whale lung cells survive than human lung cells at the same zinc chromate concentration and exposure time (Figure 3.76).

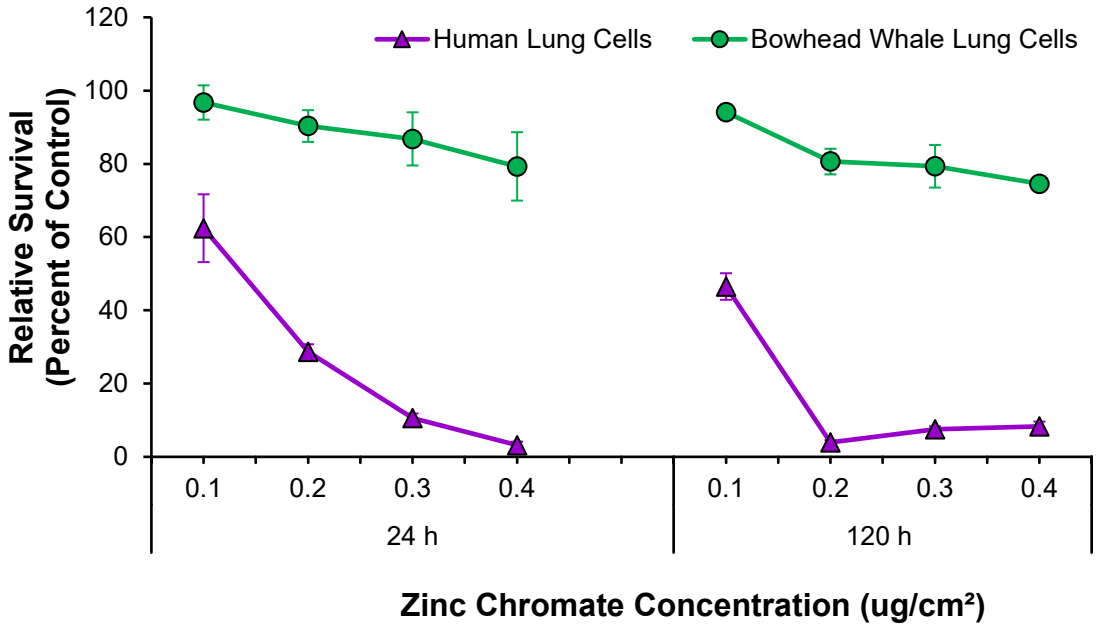

Figure.3.76. Comparison of Cr(VI)-induced cytotoxicity between human lung cells and bowhead whale lung cells. Whale lung cells were more resistant to Cr(VI)-induced cytotoxicity than human lung cells. The viability of cells in both cell lines decreased with concentration after 24-hour and 120-hour zinc chromate exposures. Bowhead whale lung cells had much higher survival rates than human lung cells at the same zinc chromate concentration and exposure time.

Summary

In Aim 3, in order to further complement our understanding of the mechanism of Cr(VI)-induced chromosomal instability, we translated to whale lung cells the outcomes of Cr(VI)-induced DNA double strand breaks, affecting HR repair, and causing chromosomal instability that we found in human lung cells. We found Cr(VI) induces DNA double strand breaks, G2 arrest, HR repair, chromosome damage and cell death in whale cells after both acute and prolonged exposures. Thus, Cr(VI) exposure is a potential health concern for whales.

We also compared outcomes in whale and human lung cells. We found Cr(VI) induced equal amounts of DNA double strand breaks in bowhead and human whale lung cells after prolonged exposure. This outcome indicates Cr(VI) has the same clastogenic potency in both species at these doses. We also found Cr(VI) induced HR after acute exposure in both species indicating HR is a key response pathway. However, prolonged Cr(VI) exposures inhibited HR repair in human cells, but whale cells escaped this repair inhibition. Subsequently and consequently, there was no chromosome instability in the whale cell and less cell death, while the human lung cells incurred Cr(VI)-induced chromosome instability and increased cell death. We also found by comparing key select outcomes in rat cells, that the whale outcomes were likely specific to whale cells, as outcomes in rat cells were similar to those in human cells.

CHAPTER IV

DISCUSSION

Overview

Cr(VI)-induced chromosome instability plays a key role in the mechanism of Cr(VI) carcinogenesis (Masuda and Takahashi 2002; Wise et al., 2018). Studies have found chromosome instability in chromium-associated lung tumors. Numerous studies have reported Cr(VI) causes various forms of DNA damage (Qin et al., 2014; Xie et al., 2005; Xie et al., 2009; Wise et al., 2002; Wise et al., 2003; Wise et al., 2006). Double-strand breaks in these lesions are particularly lethal. The presence of unrepaired or misrepaired DNA double-strand breaks is the primary mechanism responsible for the structural instability of chromosomes. HR repair is a high-fidelity DNA double-strand break repair mechanism that is critical for preventing structural chromosome instability (Bryant et al., 2006; Stackpole et al., 2007). Cell culture experiments have shown metals, including Cr(VI), cadmium, lead, arsenic, and nickel, induce DNA double-strand breaks, and HR repair has been shown to be the pathway to repair these DNA breaks (Bryant et al., 2006; Gastaldo et al., 2007; Helleday et al., 2000; Stackpole et al., 2007). When HRrepair is inhibited, the odds of high-fidelity repair of cells are reduced, resulting in the increased incidence of chromosome instability.

Our studies have demonstrated Cr(VI) causes DNA double-strand breaks and Cr(VI) has different effects on HR repair at different exposure times. Following acute exposure, Cr(VI) induces HR repair to repair Cr(VI)-induced DNA double-strand breaks. However, after prolonged exposure, Cr(VI) causes defects in HR repair and DNA double-strand breaks cannot be effectively repaired, resulting in chromosome instability (Browning et al., 2016; Qin et al., 2014; Wise et al., 2003; Wise et al., 2002; Xie et al., 2009). However, these results were derived from cultured cells, and no studies have investigated Cr(VI)-induced DNA damage and HR repair in experimental animals; in addition, there is no corresponding study of HR repair in chromium-associated lung tumors. Thus, this project translates Cr(VI)-induced DNA double-strand breaks and HR repair inhibition found in human lung cells into experimental rats and chromium-associated human lung tumors, and goes a step further, studying environmental toxicants in different species. The results will help better explore the carcinogenic mechanisms of metals, and these results were further translated into whale lung cells.

In Aim 1, we tested whether acute Cr(VI) exposure causes DNA double-strand breaks and activates HR repair. We found acute Cr(VI) exposure induced the formation of γ-H2AX and RAD51 foci in the rat lung, which were evident in the bronchi. Cr(VI)-induced γ-H2AX foci and RAD51 foci formation increased in a concentration-dependent manner. Whether in bronchioles or alveoli, Cr(VI)-induced γ-H2AX foci formation almost exclusively occurred in epithelial cells.

In Aim 2, we tested whether subchronic Cr(VI) exposure inhibits HR repair. In addition, HR repair was investigated in chromium-associated lung tumor tissue.

We found subchronic Cr(VI) exposure also induced an increase in γ-H2AX foci formation in rat lungs in a concentration-dependent manner. However, subchronic Cr(VI) exposure reduced RAD51 foci formation. These data indicate HR repair is inhibited after subchronic Cr(VI) exposure. We also showed chromium-associated human lung tumor tissues had more Cr(VI)-induced DNA double-strand breaks, and HR repair was inhibited in these tumor tissues.

In Aim 3, we translated our findings in human and rat lung cells into whale cells. Cr(VI)-induced DNA double-strand breaks, HR repair, and Cr(VI)-induced chromosome damage were investigated. We found Cr(VI) exposure induces DNA double strand breaks in whale lung cells with a similar amount of breaks as in human lung cells. Prolonged Cr(VI) exposure did not inhibit HR repair in whale lung cells, and thus Cr(VI) did not cause chromosome instability in whale lung cells.

Below, we discuss the data supporting these conclusions in detail.

Cr(VI)-induced DNA double-strand break in normal rat lung tissue, normal human lung tissue and human lung tumors

Our study found particulate Cr(VI) induced DNA double-strand breaks in rat lungs after acute and subchronic exposures, and in both human lung tumors and adjacent normal human lung tissue isolated from former chromate workers. This study is the first to report Cr(VI) exposure induces DNA double-strand break in animals and humans. The outcomes are consistent with numerous cell culture studies have found Cr(VI) is toxic to DNA, causing DNA double-strand breaks (Ha et al., 2004; Wakeman et al., 2004; Xie et al., 2005; Reynolds et al., 2007; Xie et

al. 2009; Qin et al., 2014; DeLoughery et al., 2015). The particulate Cr(VI)-induced DNA double-strand breaks increased in a concentration-dependent manner in rat lung after acute and subchronic exposures. These observations are consistent with findings from cell culture studies that showed similar results in human lung cells after acute and prolonged particulate Cr(VI) exposure (Xie et al., 2005; Xie et al., 2009; Qin et al., 2014). Thus, our study successfully translates Cr(VI)-induced DNA double-strand break to experimental animals.

The findings that Cr(VI)-induced DNA double-strand breaks in human lung tumors demonstrate particulate Cr(VI)-induced DNA double strand break persist into tumor formation long after exposure has ceased, rather than being a transient and early phenomenon. Such an outcome is consistent with cell culture studies showing Cr(VI)-induced changes persist in cells long after exposure has ceased and that these changes are heritable at a cellular level (Wise et al., 2018). No other studies have considered DNA double-strand breaks in Cr(VI) -related lung tumors. High γ-H2AX expression has been reported in other tumors. A study reported high expression of γ-H2AX in non-small cell lung cancers with unknown contributing factors (Mattaios et al., 2013). γ-H2AX has been also studied in multiple other cancer types as an indicator for the detection of DNA double-strand breaks, including breast, colon, ovarian, and cervical cancer (Mei et al., 2015; Nagelkerke et al., 2011; Sedelnikova et al., 2011; Brustmann et al., 2011). γ-H2AX is highly expressed in these tumor tissues. However, these studies detected γ-H2AX by immunohistochemistry, rather than observing γ-H2AX foci by tissue immunofluorescent staining.

Taken together, Cr(VI)-induced DNA double strand break is found in cultured cells, experimental animals, normal human lung tissue and human lung tumors, and establishes Cr(VI)-induced DNA double strand break as a crucial lesion in Cr(VI) carcinogenesis.

Cr(VI)-induced DNA double-strand break differs in bronchioles and alveoli

We observed differences in particulate Cr(VI)-induced double-strand breaks in different lung regions. In bronchioles, Cr(VI)-induced DNA double-strand breaks were prominent, while they were much lower in the alveoli. This outcome is consistent with key observations about Cr(VI)-induced tumors. For example, our result is consistent with findings from pathological studies that show Cr(VI)-associated lung tumors are mostly squamous cell carcinomas, which originate from the bronchial epithelium with very little tumor formation in the alveolar region (Ewis et al., 2001; Ewis et al., 2006; Ishikawa Y et al., 1994a; Ishikawa Y et al., 1994b; Kondo et al., 1997). in addition, premalignant lesions of the bronchial epithelium were found in studies of rats chronically exposed to particulate Cr(VI). Levy et al. found premalignant lesions (dysplasia, and squamous metaplasia) and squamous cell carcinoma in rat bronchial epithelium exposed to particulate Cr(VI) for over 2 years (Levy et al., 1986). Takahashi et al. found premalignant lesions in the bronchial epithelium of rats after exposure to strontium chromate particles inserted in the bronchus for 9 months (Takahashi et al., 2004). A pathology report of Kondo et al. on fiberoptic bronchoscopy biopsies of chromium workers indicated premalignant lesions in the bronchial epithelium, and the detected accumulation of

Cr increased significantly with the progression of bronchial epithelial malignancy (Kondo et al., 2003).

Our findings that Cr(VI) causes DNA double-strand breaks primarily in bronchioles are consistent with reports that Cr(VI) causes premalignant lesions in the bronchial epithelium. A study reported differences in the amounts of radiation-induced DNA double strand breaks between bronchioles and alveoli. Indeed, Ochola et al. found more γ-H2AX foci formed in bronchial cells than in alveoli in radiation-irradiated mouse lung tissue (Ochola et al., 2019). However, unlike our findings, radiation-induced γ-H2AX foci were more formed in basal cells than in apical cells of the epithelium. Therefore, this finding further illustrates the importance of Cr(VI)-induced DNA double strand break in the mechanism of Cr(VI) carcinogenesis. Our findings provide supporting evidence for Cr(VI)-induced carcinogenesis in the bronchial epithelium.

Cr(VI)-induced DNA double-strand break in epithelial cells

We found Cr(VI) induced DNA double strand breaks almost exclusively in epithelial cells in the rat lung. No other report on Cr(VI)-induced DNA double strand breaks in epithelial cells in the lung tissue has been published. These findings contrast with cell culture studies which show Cr(VI)-induced DNA double-strand break both occur in lung epithelial cells and lung fibroblasts (Xie et al., 2005; Xie et al., 2009; Qin et al., 2014; Reynolds et al., 2007; DeLoughery et al., 2015). The explanation for this contrast is that in these cell culture studies, each lung cell type is studied independently and grown under specific culture conditions. They were

not considered as multiple types of cells grown in co-culture. Our result is consistent with the findings from pathological studies that show Cr(VI) -associated lung tumors are mostly squamous cell carcinomas, which originate from the bronchial epithelial cells (Ewis et al., 2001; Ewis et al., 2006; Ishikawa Y et al., 1994a; Ishikawa Y et al., 1994b; Kondo et al., 1997). The finding of epithelial cells as the main cell type of Cr(VI)-induced DNA double strand breaks in the rat lung provides strong evidence that Cr(VI) targets the bronchial epithelium.

Cr(VI)-induced HR repair active in rat lung after acute exposure

We found particulate Cr(VI)-induced HR repair was active in the rat lung after acute exposure. This report is the first to consider HR repair in Cr(VI) exposed animals. Our finding is consistent with the findings from cell culture studies, which report HR repair is induced active and RAD51 increased after acute Cr(VI) exposure (Bryant et al., 2006; Qin et al., 2014; Browning et al., 2016). These findings mean the translation of Cr(VI)-induced HR repair activation from cell culture work to experimental animals is successful.

Cr(VI)-induced HR repair inhibition in rat lung and human lung tumor

We observed subchronic particulate Cr(VI) exposure suppressed HR repair, manifested as loss of RAD51 foci, in the rat lung tissue and in both human lung tumors and adjacent normal human lung tissue isolated from former chromate workers. This finding is also the first report of Cr(VI)-induced HR repair inhibition in animal lung tissue and human lung tissue. Our findings are consistent with cell

culture studies showing loss of HR repair and RAD51 function after prolonged Cr(VI) exposure (Qin et al., 2014; Browning et al., 2016). Thus, we successfully translated Cr(VI)-induced inhibition of HR repair to experimental animals, normal human lung tissue and human lung tumors.

We found Cr(VI)-induced HR repair inhibition in human lung tumors. There are no other reports of Cr(VI)-induced HR repair inhibition in human lung tumors. Some studies considered HR repair in other lung tumors. A recent study evaluating Cancer Genome Atlas (TCGA) data showed 53% of lung adenocarcinomas and 51% of squamous cell lung cancers have somatic alterations in at least one gene for HR repair or Fanconi anemia (Saiama et al., 2014). Takenaka et al performed immunohistochemical detection of RAD51 in 41 NSCLC surgical specimens, and found RAD51 expression could be significantly detected in squamous cell carcinoma, and poorly differentiated carcinoma (Takenaka et al., 2007). These data are inconsistent with our study, which suggests loss of RAD51 may be specific to Cr(VI)-induced lung tumors or perhaps metal-induced lung tumors. Such a hypothesis is consistent with observations from a prospective study of Cr(VI) workers which reported increased methylation levels of RAD51 CpG sites in peripheral venous blood samples from chromate workers compared to a control group (Hu et al., 1987). Our findings also demonstrate Cr(VI)-induced HR repair inhibition persists long after exposure and into the tumorigenic stage, which is consistent with cell culture studies showing Cr(VI)-induced changes persist in cells long after exposure has ceased and that these changes are heritable at a cellular level (Wise et al., 2018).

Taken together, our findings establish Cr(VI)-induced HR repair inhibition is a key mechanism that drives the Cr(VI) carcinogenetic mechanism.

Cr(VI)-induced DNA double strand break and HR repair inhibition has sex difference

We found female and male rats responded differently to Cr(VI)-induced DNA double strand break and HR repair changes. After subchronic particulate Cr(VI) exposure, Cr(VI)-induced DNA double strand breaks were more numerous in female rats than in male rats, and Cr(VI)-induced HR repair inhibition was more obvious in female rats than in male rats. These results indicate that Cr(VI) induces more DNA double-strand breaks and enhanced HR inhibition in female rats than in male rats. This study is the first study to discover sex differences in Cr(VI)-induced DNA double strand breaks and HR repair inhibition and these findings are consistent with observations that non-smoking women have a higher incidence of lung cancer than non-smoking men.

In fact, sex differences in terms of incidence and survival are striking in many cancer types not associated with the reproductive system (Sung et al., 2021). The reasons for these differences are unclear, but in addition to the environment and lifestyle, sex hormones may play a role. Differences in sex steroid hormone levels may therefore contribute to differences in cancer susceptibility between men and women. Sex hormones have been found to regulate DNA repair, with positive or negative regulation of HR repair (Wengner et al., 2020; Bowen et al., 2015; Wilk et al., 2012). So far, research on the role of sex on DNA repair has been

inconclusive. A study found women have a reduced ability to repair tobacco-induced DNA damage using nucleotide excision repair (NER) (Wei et al., 2000), and reduced NER activity was associated with an increased risk of lung cancer (Spitz et al., 2003). Our study found HR repair, which is used to repair DNA double-strand breaks in female rats, was significantly reduced after Cr(VI) exposure compared with male rats, suggesting that sex hormones may be involved in the regulation of Cr(VI) inhibition of HR repair.

Oropharyngeal Aspiration Rat Model Established

In this study, we successfully established an oropharyngeal aspiration rat model to study particulate Cr(VI) carcinogenesis. We found Cr was inhaled into rat lungs and accumulated in each lung lobe after both acute and subchronic exposures. We observed the outcomes of Cr(VI)-induced DNA double strand break and HR repair changes in rat lung tissues. Ours is the first study to apply oropharyngeal aspiration to a rat model for studying Cr(VI). This mode of administration has been used in two recent studies of mice considering the effects of chronic repeated calcium chromate exposure (Zeidler-Erdely et al., 2020; Wang et al., 2022). One study exposed A/J mice to iron sesquioxide or calcium chromate through oropharyngeal aspiration once per week for 26 weeks and found increased incidence of tumors compared with the control group (Zeidler-Erdely et al., 2020). The other study exposed A/J mice to calcium chromate once per week for 26 weeks via oropharyngeal aspiration and found total RNA m6A levels in chromate-exposed mouse lungs were significantly higher than in the vehicle group and

METTL3 protein levels were drastically increased in chromate-caused mouse lung tumors (Wang et al., 2022). These two mouse studies combined with our rat study indicate oropharyngeal aspiration is a useful tool for studying Cr(VI) carcinogenesis. We successfully translated the outcomes found in cell culture studies to experimental animals through this model.

Whales Are Resistant to Cr(VI)-Induced HR Repair Deficiency and Chromosome Instability

Few studies have examined the response of whale lung cells to Cr(VI) exposure. This study is the first to investigate Cr(VI)-induced DNA double-strand breaks and HR repair in bowhead whale cells and the first one to compare the effects of Cr(VI) exposure in human lung cells, rat lung cells, and bowhead whale lung cells.

We found Cr(VI) causes DNA double-strand breaks in bowhead whale lung cells with the similar amount as in human lung cells. Meaza et al. reported that Cr induces DNA double-strand breaks in fin whales' skin cells by the neutral comet assay (Meaza et al., 2021). Our finding is consistent with this report

We found the canonical DNA break response to acute and prolonged exposure to Cr(VI) in whale cells. Similar amounts of breaks formed, the cells arrested in G2 and HR repair was induced consistent with a G2 arrest. Whale lung cell response to Cr(VI)-induced DNA double strand breaks was similar to the human lung cell response after acute exposure, but was notably different after prolonged exposure. Specifically, prolonged particulate Cr(V) exposure induced

HR repair in bowhead whale lung cells, but our previous reports in human lung cells showed prolonged exposure inhibited HR repair (Qin et al., 2014; Browning et al., 2016). Our data in bowhead whale cells is consistent with data on North Atlantic right whale lung cells that found similar SCE levels after acute and chronic SCE exposure (Browning et al., 2017). These findings suggest whales are resistant to Cr(VI)-induced HR suppression. Such a conclusion is consistent with our observations that Cr(VI): 1) caused a weaker G2 arrest, 2) did not cause chromosomal instability and 3) showed lower cytotoxicity in bowhead whale cells. Li Chen et al. found sperm whale skin cells are also resistant to acute Cr(VI)-induced cytotoxicity and clastogenicity and show less cytotoxicity and genotoxicity than the human skin cells (Li Chen et al., 2012).

It is interesting to note that Cr(VI)-induced G2 arrest in bowhead whale lungs was not as pronounced as in human lung cells, or even detectable by flow cytometry. This study is the first to investigate cell cycle profiles in whale cells and the first report to compare Cr(VI)-induced G2 arrest in different species. It is possible that the differences in G2 arrest may reflect some technical artifact in the measurements or that the assay lack precision. However, it is also possible that this result confirms that the efficiency and capacity of HR repair in whale lung cells are superior to that in human lung cells. Perhaps, G2 arrest is less pronounced in the whale cells because the repair for the breaks or the underlying lesions is more efficient.

Taking together, bowhead whale lung cells are resistant to Cr(VI)-induced HR repair deficiency, resulting in no chromosome instability and more cells

surviving after Cr(VI) exposure. These outcomes mean Cr(VI)-induced HR repair deficiency resulting in chromosome instability is the core driver in Cr(VI) carcinogenesis. These findings shed an important light to explore the mechanism of how whales avoid cancer.

Conclusion of this study's findings

We successfully translated Cr(VI)-induced DNA double strand break and HR repair inhibition from cells to experimental animals, normal human lung tissue, and Cr(VI)-associated human lung tumors. Our findings established a mechanism for Cr(VI)-induced DNA double strand break and HR repair inhibition in Cr(VI) carcinogenesis. The translated data in whale lung cells strongly confirm Cr(VI)-induced HR repair deficiency resulting in chromosome instability is the core driver in Cr(VI) carcinogenesis.

FUTURE DIRECTIONS

The data presented in this project study help to explore the mechanism of Cr(VI)-induced carcinogenesis. It is the first study to investigate DNA double-strand breaks and HR repair in experimental animal lung tissue, normal human lung tissue, and human lung tumors. We translated Cr(VI)-induced DNA double-strand breaks and HR repair inhibition to subchronically exposed rat lungs and chromium-related lung tumors. These data generate many new ideas and hypotheses for future research.

We found HR repair inhibition in Cr-associated human lung tumors. With only three tumors analyzed, there is a need to investigate HR repair in more Cr(VI)-associated lung tumors. In addition, it would be interesting to consider HR repair in lung tumors unrelated to Cr(VI). This effort will be a valuable future direction. Already based on a preliminary analysis of RNA-seq data from large cohorts of patients from the TCGA project, RAD51 expression actually increases in most lung squamous cell carcinomas in general. Thus, this analysis combined with our findings suggests Cr(VI)-induced RAD51 decrease may indeed be specific to Cr(VI)-induced lung cancer.

Translational data in whale lung cells strongly confirm that Cr(VI)-induced HR repair deficiency leading to chromosomal instability is a core driver of Cr(VI) carcinogenesis. This outcome makes it necessary to investigate chromosomal

instability in experimental animal lung tissue, normal human lung tissue, and human lung tumors. We will investigate chromosomal instability using fluorescence immune in situ hybridization. Wise et al. found structural chromosomal instability in some specific chromosomes in chronically exposed human lung cells (Wise et al., 2018). We will investigate chromosomal instability in lung tissue after chromium exposure using fluorescent in situ hybridization. The translation of chromium-induced chromosomal instability into experimental animal lung tissue and human lung tumors will be carried out.

REFERENCES

Abegglen, L. M., Caulin, A. F., Chan, A., Lee, K., Robinson, R., Campbell, M. S., ... & Schiffman, J. D. (2015). Potential mechanisms for cancer resistance in elephants and comparative cellular response to DNA damage in humans. *Jama*, *314*(17), 1850-1860.

ACGIH. (2011). Guide to occupational exposure values. Cincinnati, OH: American Conference of Governmental Industrial Hygienists, Publication No. 0389.

Agency for Toxic Substances and Disease Registry (ATSDR). (2000). Case studies in environmental medicine: Chromium toxicity. U.S. Department of Health and Human Services. Course SS3048.

Agency for Toxic Substances and Disease Registry (ATSDR). (2011). Case Studies in Environmental Medicine (CSEM) Chromium Toxicity.

Agency for Toxic Substances and Disease Registry (ATSDR). (2012). A toxicological profile for chromium. U.S. Department of Health and Human Services.

Albertson, D. G., Collins, C., McCormick, F., & Gray, J. W. (2003). Chromosome aberrations in solid tumors. *Nature genetics*, *34*(4), 369-376.

Alderson, M. R., Rattan, N. S., & Bidstrup, L. (1981). Health of workmen in the chromate-producing industry in Britain. *British journal of industrial medicine*, *38*(2), 117.

Alderson, M. R., Rattan, N. S., & Bidstrup, L. (1981). Health of workmen in the chromate-producing industry in Britain. *British journal of industrial medicine*, *38*(2), 117.

Alexander, J., & Aaseth, J. (1995). Uptake of chromate in human red blood cells and isolated rat liver cells: the role of the anion carrier. *Analyst*, *120*(3), 931-933.

Ali, A. H., Kondo, K., Namura, T., Senba, Y., Takizawa, H., Nakagawa, Y., Toba, H., Kenzaki, K., Sakiyama, S., & Tangoku, A. (2011). Aberrant DNA methylation of some tumor suppressor genes in lung cancers from workers with chromate exposure. *Molecular carcinogenesis*, *50*(2), 89–99.

Arakawa, H., Ahmad, R., Naoui, M., & Tajmir-Riahi, H. A. (2000). A Comparative Study of Calf Thymus DNA Binding to Cr (III) and Cr (VI) Ions: evidence for the guanine N-7-chromium-phosphate chelate formation. *Journal of Biological Chemistry*, *275*(14), 10150-10153.

Ashur-Fabian, O., Avivi, A., Trakhtenbrot, L., Adamsky, K., Cohen, M., Kajakaro, G., ... & Rechavi, G. (2004). Evolution of p53 in hypoxia-stressed Spalax mimics human tumor mutation. *Proceedings of the National Academy of Sciences*, *101*(33), 12236-12241.

Avivi, A., Ashur-Fabian, O., Amariglio, N., Nevo, E., & Rechavi, G. (2005). p53: A Key Player in Tumoral and Evolutionary Adaptation: A Lesson from the Israeli Blind Subterranean Mole Rat. *Cell Cycle*, *4*(3), 368-372.

Aylon, Y., & Kupiec, M. (2004). DSB repair: the yeast paradigm. *DNA repair*, *3*(8-9), 797–815.

Azad, N., Iyer, A. K. V., Wang, L., Lu, Y., Medan, D., Castranova, V., & Rojanasakul, Y. (2010). Nitric oxide–mediated Bcl-2 stabilization potentiates malignant transformation of human lung epithelial cells. *American journal of respiratory cell and molecular biology*, *42*(5), 578-585.

Baetjer, A. M. (1950). Pulmonary Carcinoma in Chromate-Workers. II. Incidence on Basis of Hospital Records. *Arch. Indust. Hyg. & Occupational Med.*, *2*(5), 505-16.

Bakkenist, C. J., & Kastan, M. B. (2003). DNA damage activates ATM through intermolecular autophosphorylation and dimer dissociation. *Nature*, *421*(6922), 499-506.

Balansky, R. M., D'Agostini, F., Izzotti, A., & De Flora, S. (2000). Less than additive interaction between cigarette smoke and chromium(VI) in inducing clastogenic damage in rodents. *Carcinogenesis*, *21*(9), 1677–1682.

Banks, R. B., & Cooke Jr, R. T. (1986). Chromate reduction by rabbit liver aldehyde oxidase. *Biochemical and biophysical research communications*, *137*(1), 8-14.

Barceloux D. G. (1999). Chromium. *Journal of toxicology. Clinical toxicology*, *37*(2), 173–194.

Barnhart, J. (1997). Occurrences, uses, and properties of chromium. *Regulatory toxicology and pharmacology*, *26*(1), S3-S7.

Baumann, P., Benson, F. E., & West, S. C. (1996). Human Rad51 protein promotes ATP-dependent homologous pairing and strand transfer reactions in vitro. *Cell*, *87*(4), 757-766.

Beaver, L. M., Stemmy, E. J., Schwartz, A. M., Damsker, J. M., Constant, S. L., Ceryak, S. M., & Patierno, S. R. (2009). Lung inflammation, injury, and proliferative response after repetitive particulate hexavalent chromium exposure. *Environmental health perspectives*, *117*(12), 1896-1902.

Bétermier, M., Bertrand, P., & Lopez, B. S. (2014). Is non-homologous end-joining really an inherently error-prone process?. *PLoS genetics*, *10*(1), e1004086.

Bielicka, A., Bojanowska, I., & Wisniewski, A. (2005). Two Faces of Chromium-Pollutant and Bioelement. *Polish Journal of environmental studies*, *14*(1).

Birk, T., Mundt, K. A., Dell, L. D., Luippold, R. S., Miksche, L., Steinmann-Steiner-Haldenstaett, W., & Mundt, D. J. (2006). Lung cancer mortality in the German chromate industry, 1958 to 1998. *Journal of Occupational and Environmental Medicine*, 426-433.

Bowen, C., Zheng, T., & Gelmann, E. P. (2015). NKX3.1 Suppresses TMPRSS2-ERG Gene Rearrangement and Mediates Repair of Androgen Receptor-Induced DNA Damage. *Cancer research*, *75*(13), 2686–2698.

Bragt, P. C., & van Dura, E. A. (1983). Toxicokinetics of hexavalent chromium in the rat after intratracheal administration of chromates of different solubilities. *The Annals of occupational hygiene*, *27*(3), 315–322.

Bridgewater, L. C., Manning, F. C., Woo, E. S., & Patierno, S. R. (1994). DNA polymerase arrest by adducted trivalent chromium. *Molecular carcinogenesis*, *9*(3), 122-133.

Bridgewater, L. C., Manning, F. C., Woo, E. S., & Patierno, S. R. (1994). DNA polymerase arrest by adducted trivalent chromium. *Molecular carcinogenesis*, *9*(3), 122-133.

Bright, P., Burge, P. S., O'Hickey, S. P., Gannon, P. F., Robertson, A. S., & Boran, A. (1997). Occupational asthma due to chrome and nickel electroplating. *Thorax*, *52*(1), 28-32.

Browning, C. L., Qin, Q., Kelly, D. F., Prakash, R., Vanoli, F., Jasin, M., & Wise, J. P., Sr (2016). Prolonged Particulate Hexavalent Chromium Exposure Suppresses Homologous Recombination Repair in Human Lung Cells. *Toxicological sciences : an official journal of the Society of Toxicology*, *153*(1), 70–78.

Browning, C. L., Wise, C. F., & Wise Sr, J. P. (2017). Prolonged particulate chromate exposure does not inhibit homologous recombination repair in North Atlantic right whale (Eubalaena glacialis) lung cells. *Toxicology and applied pharmacology*, *331*, 18-23.

Brustmann, H., Hinterholzer, S., & Brunner, A. (2011). Expression of phosphorylated histone H2AX (γ-H2AX) in normal and neoplastic squamous epithelia of the uterine cervix: an immunohistochemical study with epidermal growth factor receptor. *International journal of gynecological pathology : official journal of the International Society of Gynecological Pathologists*, *30*(1), 76–83.

Bryant, H. E., Ying, S., & Helleday, T. (2006). Homologous recombination is involved in repair of chromium-induced DNA damage in mammalian cells. *Mutation research*, *599*(1-2), 116–123.

Budanova, L. F. (1980). Clinical Manifestations and Dynamics of Occupational Bronchial Asthma Induced by Exposure to Hexavalent Chromium in Workers in the Alumina Industry. *Gig. Prof. Zabol.*, 43-46.

Burges DCL, Gannon PFG, Boran A, Burge PS [1994]. Occupational asthma in hard chrome electroplaters. In: Proceedings of the 9th international symposium on
epidemiology in occupational health, September 23–25, 1992, Cincinnati, OH. Cincinnati, OH: US Department of Health and Human Services, Public Health Service, National Institute for Occupational Safety and Health, DHHS (NIOSH) Publication No. 94-112, pp. 476–481.

Burma, S., Chen, B. P., Murphy, M., Kurimasa, A., & Chen, D. J. (2001). ATM phosphorylates histone H2AX in response to DNA double-strand breaks. *Journal of Biological Chemistry*, *276*(45), 42462-42467.

Camyre, E., Wise, S. S., Milligan, P., Gordon, N., Goodale, B., Stackpole, M., Patzlaff, N., Aboueissa, A. M., & Wise, J. P., Sr (2007). Ku80 deficiency does not affect particulate chromate-induced chromosome damage and cytotoxicity in Chinese hamster ovary cells. *Toxicological sciences : an official journal of the Society of Toxicology*, *97*(2), 348–354.

Cannavo, E., & Cejka, P. (2014). Sae2 promotes dsDNA endonuclease activity within Mre11–Rad50–Xrs2 to resect DNA breaks. *Nature*, *514*(7520), 122-125.

Casadevall, M., & Kortenkamp, A. (1995). The formation of both apurinic/apyrimidinic sites and single-strand breaks by chromate and glutathione arises from attack by the same single reactive species and is dependent on molecular oxygen. *Carcinogenesis*, *16*(4), 805-809.

Casadevall, M., da Cruz Fresco, P., & Kortenkamp, A. (1999). Chromium (VI)-mediated DNA damage: oxidative pathways resulting in the formation of DNA breaks and abasic sites. *Chemico-biological interactions*, *123*(2), 117-132.

Case, C. P., Langkamer, V. G., James, C., Palmer, M. R., Kemp, A. J., Heap, P. F., & Solomon, L. (1994). Widespread dissemination of metal debris from implants. *The Journal of bone and joint surgery. British volume*, *76*(5), 701-712.

Catrambone, M., Canepari, S., & Perrino, C. (2013). Determination of Cr (III), Cr (VI) and total chromium in atmospheric aerosol samples. In *E3S Web of conferences* (Vol. 1, p. 07005). EDP Sciences.

Caulin, A. F., & Maley, C. C. (2011). Peto's Paradox: evolution's prescription for cancer prevention. *Trends in ecology & evolution*, *26*(4), 175-182.

Cavalleri, A., & Minoia, C. (1985). Serum and erythrocyte chromium distribution and urinary elimination in persons occupationally exposed to chromium (VI) and chromium (III). *Giornale Italiano di Medicina del Lavoro*, *7*(1), 35-38.

Chen, J., & Stubbe, J. (2005). Bleomycins: towards better therapeutics. *Nature Reviews Cancer*, *5*(2), 102-112.

Chen, Y., Zou, L., Zhang, Y., Chen, Y., Xing, P., Yang, W., Li, F., Ji, X., Liu, F., & Lu, X. (2014). Transforming growth factor-β1 and α-smooth muscle actin in stromal fibroblasts are associated with a poor prognosis in patients with clinical stage I-IIIA nonsmall cell lung cancer after curative resection. *Tumour biology : the journal of the International Society for Oncodevelopmental Biology and Medicine*, *35*(7), 6707–6713.

Chen, Z., Zhang, C., Zhang, M., Li, B., Niu, Y., Chen, L., Yang, J., Lu, S., Gao, J., & Shen, L. (2019). Chromosomal instability of circulating tumor DNA reflect therapeutic responses in advanced gastric cancer. *Cell death & disease*, *10*(10), 697.

Constantinou, A., Davies, A. A., & West, S. C. (2001). Branch migration and Holliday junction resolution catalyzed by activities from mammalian cells. *Cell*, *104*(2), 259–268.

Danadevi, K., Rozati, R., Banu, B. S., & Grover, P. (2004). Genotoxic evaluation of welders occupationally exposed to chromium and nickel using the Comet and micronucleus assays. *Mutagenesis*, *19*(1), 35–41.

Davies, J. M. (1984). Lung cancer mortality among workers making lead chromate and zinc chromate pigments at three English factories. *Occupational and Environmental Medicine*, *41*(2), 158-169.

Davies, J. M., Easton, D. F., & Bidstrup, P. L. (1991). Mortality from respiratory cancer and other causes in United Kingdom chromate production workers. *British journal of industrial medicine*, *48*(5), 299–313.

Dayan, A. D., & Paine, A. J. (2001). Mechanisms of chromium toxicity, carcinogenicity and allergenicity: review of the literature from 1985 to 2000. *Human & experimental toxicology*, *20*(9), 439-451.

de Magalhães J. P. (2015). The big, the bad and the ugly: Extreme animals as inspiration for biomedical research. *EMBO reports*, *16*(7), 771–776.

DeLoughery, Z., Luczak, M. W., Ortega-Atienza, S., & Zhitkovich, A. (2015). DNA double-strand breaks by Cr(VI) are targeted to euchromatin and cause ATR-dependent phosphorylation of histone H2AX and its ubiquitination. *Toxicological sciences : an official journal of the Society of Toxicology*, *143*(1), 54–63.

Department of the Environment (DoE). (1996). Digest of environmental statistics. No. 18. London: HMSO, Department of the Environment.

Elias, Z., Poirot, O., Pezerat, H., Suquet, H., Schneider, O., Daniere, M. C., ... & Cavelier, C. (1989). Cytotoxic and neoplastic transforming effects of industrial hexavalent chromium pigments in Syrian hamster embryo cells. *Carcinogenesis*, *10*(11), 2043-2052.

Environmental Health Department (EHD). (1991a). Report by the Director of Environmental Health on various sites in the South East of Glasgow thought to be contaminated by chromium waste. August. Glasgow: Environmental Health Department, City of Glasgow District Council. epidemiology in occupational health, September 23–25, 1992, Cincinnati, OH. Cincinnati, OH: US Department of Health and Human Services, Public Health Service, National Institute for Occupational Safety and Health, DHHS (NIOSH) Publication No. 94-112, pp. 476–481.

Ewis, A. A., Kondo, K., Dang, F., Nakahori, Y., Shinohara, Y., Ishikawa, M., & Baba, Y. (2006). Surfactant protein B gene variations and susceptibility to lung cancer in chromate workers. *American journal of industrial medicine*, *49*(5), 367-373.

Ewis, A. A., Kondo, K., Dang, F., Nakahori, Y., Shinohara, Y., Ishikawa, M., & Baba, Y. (2006). Surfactant protein B gene variations and susceptibility to lung cancer in chromate workers. *American journal of industrial medicine*, *49*(5), 367-373.

Ewis, A. A., Kondo, K., Lee, J., Tsuyuguchi, M., Hashimoto, M., Yokose, T., ... & Nakahori, Y. (2001). Occupational cancer genetics: infrequent ras oncogenes point mutations in lung cancer samples from chromate workers. *American journal of industrial medicine*, *40*(1), 92-97.

Fernandez-Capetillo, O., Lee, A., Nussenzweig, M., & Nussenzweig, A. (2004). H2AX: the histone guardian of the genome. *DNA repair*, *3*(8-9), 959-967.

Fernández-Nieto, M., Quirce, S., Carnés, J., & Sastre, J. (2006). Occupational asthma due to chromium and nickel salts. *International archives of occupational and environmental health*, *79*(6), 483-486.

Frank, S. A. (2007). *Dynamics of Cancer: Incidence, Inheritance, and Evolution*. Princeton University Press.

Friedberg, E. C., Aguilera, A., Gellert, M., Hanawalt, P. C., Hays, J. B., Lehmann, A. R., ... & Wood, R. D. (2006). DNA repair: from molecular mechanism to human disease. *DNA repair*, *5*(8), 986-996.

Galis, F., & Metz, J. A. (2003). Anti-cancer selection as a source of developmental and evolutionary constraints. *BioEssays*, *25*(11), 1035-1039.

Garcia, V., Phelps, S. E., Gray, S., & Neale, M. J. (2011). Bidirectional resection of DNA double-strand breaks by Mre11 and Exo1. *Nature*, *479*(7372), 241-244.

Gastaldo, J., Viau, M., Bencokova, Z., Joubert, A., Charvet, A. M., Balosso, J., & Foray, N. (2007). Lead contamination results in late and slowly repairable DNA double-strand breaks and impacts upon the ATM-dependent signaling pathways. *Toxicology letters*, *173*(3), 201–214.

George, J. C., Bada, J., Zeh, J., Scott, L., Brown, S. E., O'Hara, T., & Suydam, R. (1999). Age and growth estimates of bowhead whales (Balaena mysticetus) via aspartic acid racemization. *Canadian Journal of Zoology*, *77*(4), 571-580.

Geraci, J. R., Palmer, N. C., & St. Aubin, D. J. (1987). Tumors in cetaceans: analysis and new findings. *Canadian Journal of Fisheries and Aquatic Sciences*, *44*(7), 1289-1300.

Gibb, H. J., Lees, P. S., Pinsky, P. F., & Rooney, B. C. (2000). Lung cancer among workers in chromium chemical production. *American journal of industrial medicine*, *38*(2), 115-126.

Gibb, H. J., Lees, P. S., Pinsky, P. F., & Rooney, B. C. (2000). Lung cancer among workers in chromium chemical production. *American journal of industrial medicine*, *38*(2), 115-126.

Glaser, U., Hochrainer, D., Klöppel, H., & Oldiges, H. (1986). Carcinogenicity of sodium dichromate and chromium (VI/III) oxide aerosols inhaled by male Wistar rats. *Toxicology*, *42*(2-3), 219-232.

Gray, S. J., & Sterling, K. (1950). The tagging of red cells and plasma proteins with radioactive chromium. *The Journal of Clinical Investigation*, *29*(12), 1604-1613.

Griese, M. (1999). Pulmonary surfactant in health and human lung diseases: state of the art. *European Respiratory Journal*, *13*(6), 1455-1476.

Gulanowski, B., Świątek, J., & Kozłowski, H. (1992). Impact of chromium ions on nucleoside triphosphates and nucleic acids. *Journal of inorganic biochemistry*, *48*(4), 289-298.

Gylseth, B., Gundersen, N., & Langård, S. (1977). Evaluation of chromium exposure based on a simplified method for urinary chromium determination. *Scandinavian journal of work, environment & health*, *3*(1), 28–31.

Ha, L., Ceryak, S., & Patierno, S. R. (2004). Generation of S phase-dependent DNA double-strand breaks by Cr (VI) exposure: involvement of ATM in Cr (VI) induction of γ-H2AX. *Carcinogenesis*, *25*(11), 2265-2274.

Halasova, E., Adamkov, M., Matakova, T., Kavcova, E., Poliacek, I., & Singliar, A. (2010). Lung cancer incidence and survival in chromium exposed individuals with respect to expression of anti-apoptotic protein survivin and tumor suppressor P53 protein. *European journal of medical research*, *15 Suppl 2*(Suppl 2), 55–59.

Halasova, E., Matakova, T., Musak, L., Polakova, V., & Vodicka, P. (2008). Chromosomal damage and polymorphisms of DNA repair genes XRCC1 and XRCC3 in workers exposed to chromium. *Neuroendocrinology Letters*, *29*(5), 658.

Halasova, E., Matakova, T., Musak, L., Polakova, V., Letkova, L., Dobrota, D., & Vodicka, P. (2012). Evaluating chromosomal damage in workers exposed to hexavalent chromium and the modulating role of polymorphisms of DNA repair genes. *International archives of occupational and environmental health*, *85*(5), 473-481.

Hannu, T., Piipari, R., Kasurinen, H., Keskinen, H., Tuppurainen, M., & Tuomi, T. (2005). Occupational asthma due to manual metal-arc welding of special stainless steels. *European Respiratory Journal*, *26*(4), 736-739.

Hayes, R. B., Lilienfeld, A. M., & Snell, L. M. (1979). Mortality in chromium chemical production workers: a prospective study. *International Journal of Epidemiology*, *8*(4), 365-374.

Helleday, T., Nilsson, R., & Jenssen, D. (2000). Arsenic[III] and heavy metal ions induce intrachromosomal homologous recombination in the hprt gene of V79 Chinese hamster cells. *Environmental and molecular mutagenesis*, *35*(2), 114–122.

Heyer W. D. (2004). Recombination: Holliday junction resolution and crossover formation. *Current biology : CB*, *14*(2), R56–R58.

Hirose, T., Kondo, K., Takahashi, Y., Ishikura, H., Fujino, H., Tsuyuguchi, M., ... & Monden, Y. (2002). Frequent microsatellite instability in lung cancer from chromate-exposed workers. *Molecular Carcinogenesis: Published in cooperation with the University of Texas MD Anderson Cancer Center*, *33*(3), 172-180.

Holmes, A. L., Wise, S. S., Sandwick, S. J., & Wise Sr, J. P. (2006). The clastogenic effects of chronic exposure to particulate and soluble Cr (VI) in human lung cells. *Mutation Research/Genetic Toxicology and Environmental Mutagenesis*, *610*(1-2), 8-13.

Hu, G., Li, P., Cui, X., Li, Y., Zhang, J., Zhai, X., Yu, S., Tang, S., Zhao, Z., Wang, J., & Jia, G. (2018). Cr(VI)-induced methylation and down-regulation of DNA repair genes and its association with markers of genetic damage in workers and 16HBE cells. *Environmental pollution (Barking, Essex : 1987)*, *238*, 833–843.

Huang, X., & Darzynkiewicz, Z. (2006). Cytometric assessment of histone H2AX phosphorylation: a reporter of DNA damage. *Methods in molecular biology (Clifton, N.J.)*, *314*, 73–80.

Hustedt, N., & Durocher, D. (2017). The control of DNA repair by the cell cycle. *Nature cell biology*, *19*(1), 1-9.

Huvinen, M., Mäkitie, A., Järventaus, H., Wolff, H., Stjernvall, T., Hovi, A., ... & Norppa, H. (2002b). Nasal cell micronuclei, cytology and clinical symptoms in stainless steel production workers exposed to chromium. *Mutagenesis*, *17*(5), 425-429.

Huvinen, M., Uitti, J., Oksa, P., Palmroos, P., & Laippala, P. (2002a). Respiratory health effects of long-term exposure to different chromium species in

stainless steel production. *Occupational medicine (Oxford, England)*, *52*(4), 203–212.

Huvinen, M., Uitti, J., Zitting, A., Roto, P., Virkola, K., Kuikka, P., ... & Aitio, A. (1996). Respiratory health of workers exposed to low levels of chromium in stainless steel production. *Occupational and environmental medicine*, *53*(11), 741-747.

International Agency for Research on Cancer (IARC). (1990). Chromium, nickel and welding. *IARC monographs on the evaluation of carcinogenic risks to humans*, *49*.

Ishikawa, Y., Nakagawa, K., Satoh, Y., Kitagawa, T., Sugano, H., Hirano, T., & Tsuchiya, E. (1994a). Characteristics of chromate workers' cancers, chromium lung deposition and precancerous bronchial lesions: an autopsy study. *British journal of cancer*, *70*(1), 160–166.

Ishikawa, Y., Nakagawa, K., Satoh, Y., Kitagawa, T., Sugano, H., Hirano, T., & Tsuchiya, E. (1994a). Characteristics of chromate workers' cancers, chromium lung deposition and precancerous bronchial lesions: an autopsy study. *British journal of cancer*, *70*(1), 160-166.

Ishikawa, Y., Nakagawa, K., Satoh, Y., Kitagawa, T., Sugano, H., Hirano, T., & Tsuchiya, E. (1994b). “Hot spots” of chromium accumulation at bifurcations of chromate workers' bronchi. *Cancer research*, *54*(9), 2342-2346.

Jackson, J. A., Baker, C. S., Vant, M., Steel, D. J., Medrano-Gonzalez, L., & Palumbi, S. R. (2009). Big and slow: phylogenetic estimates of molecular evolution in baleen whales (Suborder Mysticeti). *Molecular Biology and Evolution*, *26*(11), 2427-2440.

Kalluri, R., & Zeisberg, M. (2006). Fibroblasts in cancer. *Nature reviews. Cancer*, *6*(5), 392–401.

Kano, K., Horikawa, M., Utsunomiya, T., Tati, M., Satoh, K., & Yamaguchi, S. (1993). Lung cancer mortality among a cohort of male chromate pigment workers in Japan. *International journal of epidemiology*, *22*(1), 16–22.

Katabami, M., Dosaka-Akita, H., Mishina, T., Honma, K., Kimura, K., Uchida, Y., ... & Kawakami, Y. (2000). Frequent cyclin D1 expression in chromate-induced lung cancers. *Human pathology*, *31*(8), 973-979.

Kato, S., Han, S. Y., Liu, W., Otsuka, K., Shibata, H., Kanamaru, R., & Ishioka, C. (2003). Understanding the function–structure and function–mutation relationships of p53 tumor suppressor protein by high-resolution missense mutation analysis. *Proceedings of the National Academy of Sciences*, *100*(14), 8424-8429.

Keane, M., Semeiks, J., Webb, A. E., Li, Y. I., Quesada, V., Craig, T., ... & de Magalhães, J. P. (2015). Insights into the evolution of longevity from the bowhead whale genome. *Cell reports*, *10*(1), 112-122.

Keane, M., Semeiks, J., Webb, A. E., Li, Y. I., Quesada, V., Craig, T., Madsen, L. B., van Dam, S., Brawand, D., Marques, P. I., Michalak, P., Kang, L., Bhak, J., Yim, H. S., Grishin, N. V., Nielsen, N. H., Heide-Jørgensen, M. P., Oziolor, E. M., Matson, C. W., Church, G. M., … de Magalhães, J. P. (2015). Insights into the evolution of longevity from the bowhead whale genome. *Cell reports*, *10*(1), 112–122.

Kondo, K., Hino, N., Sasa, M., Kamamura, Y., Sakiyama, S., Tsuyuguchi, M., ... & Monden, Y. (1997). Mutations of the p53 gene in human lung cancer from chromate-exposed workers. *Biochemical and biophysical research communications*, *239*(1), 95-100.

Kondo, K., Takahashi, Y., Hirose, Y., Nagao, T., Tsuyuguchi, M., Hashimoto, M., Ochiai, A., Monden, Y., & Tangoku, A. (2006). The reduced expression and aberrant methylation of p16(INK4a) in chromate workers with lung cancer. *Lung cancer (Amsterdam, Netherlands)*, *53*(3), 295–302.

Kondo, K., Takahashi, Y., Ishikawa, S., Uchihara, H., Hirose, Y., Yoshizawa, K., Tsuyuguchi, M., Takizawa, H., Miyoshi, T., Sakiyama, S., & Monden, Y. (2003). Microscopic analysis of chromium accumulation in the bronchi and lung of chromate workers. *Cancer*, *98*(11), 2420–2429.

Korallus V, Lange H, Ness A. (1982). Relationships between precautionary measures and bronchial carcinoma mortality in the chromate-producing industry. *Arbeitsmedizin Sozialmedizin Präventivmedizin*, 17:159-167.

Kotaś, J., & Stasicka, Z. J. E. P. (2000). Chromium occurrence in the environment and methods of its speciation. *Environmental pollution*, *107*(3), 263-283.

Kyle, R. A., & Shampo, M. A. (1989, June). Nicolas-Louis Vauquelin—discoverer of chromium. In *Mayo Clinic Proceedings*, *64*(6):643.

Langård, S., & Norseth, T. (1975). A cohort study of bronchial carcinomas in workers producing chromate pigments. *Occupational and Environmental Medicine*, *32*(1), 62-65.

Langård, S., & Vigander, T. (1983). Occurrence of lung cancer in workers producing chromium pigments. *Occupational and Environmental Medicine*, *40*(1), 71-74.

Langård, S., Gundersen, N., Tsalev, D. L., & Gylseth, B. (1978). Whole blood chromium level and chromium excretion in the rat after zinc chromate inhalation. *Acta Pharmacologica et Toxicologica*, *42*(2), 142-149.

Langrrd, S. (1990). One hundred years of chromium and cancer: a review of epidemiological evidence and selected case reports. *American journal of industrial medicine*, *17*(2), 189-214.

Lee, C. R., Yoo, C. I., Lee, J. h., & Kang, S. K. (2002). Nasal septum perforation of welders. *Industrial health*, *40*(3), 286–289.

Leonard, S. S., Bower, J. J., & Shi, X. (2004). Metal-induced toxicity, carcinogenesis, mechanisms and cellular responses. *Molecular and cellular biochemistry*, *255*(1), 3-10.

Leroi, A. M., Koufopanou, V., & Burt, A. (2003). Cancer selection. *Nature Reviews Cancer*, *3*(3), 226-231.

Leroyer, C., Dewitte, J. D., Bassanets, A., Boutoux, M., Daniel, C., & Clavier, J. (1998). Occupational asthma due to chromium. *Respiration*, *65*(5), 403-405.

Levy, L. S., & Venitt, S. (1986). Carcinogenicity and mutagenicity of chromium compounds: the association between bronchial metaplasia and neoplasia. *Carcinogenesis*, *7*(5), 831-835.

Levy, L. S., Martin, P. A., & Bidstrup, P. L. (1986). Investigation of the potential carcinogenicity of a range of chromium containing materials on rat lung. *Occupational and Environmental Medicine*, *43*(4), 243-256.

Li Chen, T., LaCerte, C., Wise, S. S., Holmes, A., Martino, J., Wise, J. P., Jr, Thompson, W. D., & Wise, J. P., Sr (2012). Comparative cytotoxicity and genotoxicity of particulate and soluble hexavalent chromium in human and sperm whale (Physeter macrocephalus) skin cells. *Comparative biochemistry and physiology. Toxicology & pharmacology : CBP*, *155*(1), 143–150.

Li Chen, T., Wise, S. S., Holmes, A., Shaffiey, F., Wise, J. P., Jr, Thompson, W. D., Kraus, S., & Wise, J. P., Sr (2009a). Cytotoxicity and genotoxicity of hexavalent chromium in human and North Atlantic right whale (Eubalaena glacialis) lung cells. *Comparative biochemistry and physiology. Toxicology & pharmacology : CBP*, *150*(4), 487–494.

Li Chen, T., Wise, S. S., Kraus, S., Shaffiey, F., Levine, K. M., Thompson, W. D., Romano, T., O'Hara, T., & Wise, J. P., Sr (2009b). Particulate hexavalent chromium is cytotoxic and genotoxic to the North Atlantic right whale

(Eubalaena glacialis) lung and skin fibroblasts. *Environmental and molecular mutagenesis*, *50*(5), 387–393.

Lieber, M. R., Ma, Y., Pannicke, U., & Schwarz, K. (2003). Mechanism and regulation of human non-homologous DNA end-joining. *Nature reviews Molecular cell biology*, *4*(9), 712-720.

Lindberg, E., & Hedenstierna, G. (1983). Chrome plating: symptoms, findings in the upper airways, and effects on lung function. *Archives of Environmental Health: An International Journal*, *38*(6), 367-374.

Lippmann, M. D. B. R. E., Yeates, D. B., & Albert, R. E. (1980). Deposition, retention, and clearance of inhaled particles. *Occupational and Environmental Medicine*, *37*(4), 337-362.

Lisby, M., & Rothstein, R. (2015). Cell biology of mitotic recombination. *Cold Spring Harbor perspectives in biology*, *7*(3), a016535.

Luippold, R. S., Mundt, K. A., Austin, R. P., Liebig, E., Panko, J., Crump, C., ... & Proctor, D. (2003). Lung cancer mortality among chromate production workers. *Occupational and Environmental Medicine*, *60*(6), 451-457.

Luippold, R. S., Mundt, K. A., Austin, R. P., Liebig, E., Panko, J., Crump, C., ... & Proctor, D. (2003). Lung cancer mortality among chromate production workers. *Occupational and Environmental Medicine*, *60*(6), 451-457.

Luippold, R. S., Mundt, K. A., Dell, L. D., & Birk, T. (2005). Low-level hexavalent chromium exposure and rate of mortality among US chromate production employees. *Journal of occupational and environmental medicine*, 381-385.

Ma, S., & Gladyshev, V. N. (2017). Molecular signatures of longevity: Insights from cross-species comparative studies. *Seminars in cell & developmental biology*, *70*, 190–203.

Machle, W., & Gregorius, F. (1948). Cancer of the respiratory system in the United States chromate-producing industry. *Public Health Reports (1896-1970)*, 1114-1127.

MacRae, S. L., Croken, M. M., Calder, R. B., Aliper, A., Milholland, B., White, R. R., ... & Vijg, J. (2015). DNA repair in species with extreme lifespan differences. *Aging (Albany NY)*, *7*(12), 1171.

Maeng, S. H., Chung, H. W., Kim, K. J., Lee, B. M., Shin, Y. C., Kim, S. J., & Yu, I. J. (2004). Chromosome aberration and lipid peroxidation in chromium-exposed workers. *Biomarkers*, *9*(6), 418-434.

Maeng, S. H., Chung, H. W., Kim, K. J., Lee, B. M., Shin, Y. C., Kim, S. J., & Yu, I. J. (2004). Chromosome aberration and lipid peroxidation in chromium-exposed workers. *Biomarkers*, *9*(6), 418-434.

Masuda, A., & Takahashi, T. (2002). Chromosome instability in human lung cancers: possible underlying mechanisms and potential consequences in the pathogenesis. *Oncogene*, *21*(45), 6884-6897.

Matthaios, D., Foukas, P. G., Kefala, M., Hountis, P., Trypsianis, G., Panayiotides, I. G., Chatzaki, E., Pantelidaki, E., Bouros, D., Karakitsos, P., & Kakolyris, S. (2012). γ-H2AX expression detected by immunohistochemistry correlates with prognosis in early operable non-small cell lung cancer. *OncoTargets and therapy*, *5*, 309–314.

Meaza, I., Speer, R. M., Toyoda, J. H., Lu, H., Wise, S. S., Croom-Perez, T. J., Aboueissa, A. E., & Wise, J. P., Sr (2020). Prolonged exposure to particulate Cr(VI) is cytotoxic and genotoxic to fin whale cells. *Journal of trace elements in medicine and biology : organ of the Society for Minerals and Trace Elements (GMS)*, *62*, 126562.

Mei, L., Hu, Q., Peng, J., Ruan, J., Zou, J., Huang, Q., Liu, S., & Wang, H. (2015). Phospho-histone H2AX is a diagnostic and prognostic marker for epithelial ovarian cancer. *International journal of clinical and experimental pathology*, *8*(5), 5597–5602.

Meridian Research. (1994). Selected chapters of an economic impact analysis for a revised OSHA standard for chromium VI: introduction, industry profiles, technological feasibility (for 6 industries) and environmental impacts. Final Report. Contract No. J-0-F-4-0012 Task Order No. 11.

Merritt, K., & Brown, S. A. (1995). Release of hexavalent chromium from corrosion of stainless steel and cobalt—chromium alloys. *Journal of biomedical materials research*, *29*(5), 627-633.

Mikalsen, A., Alexander, J., & Ryberg, D. (1989). Microsomal metabolism of hexavalent chromium. Inhibitory effect of oxygen and involvement of cytochrome P-450. *Chemico-biological interactions*, *69*(2-3), 175-192.

Milligan, J. R., Ng, J. Y., Wu, C. C., Aguilera, J. A., Fahey, R. C., & Ward, J. F. (1995). DNA repair by thiols in air shows two radicals make a double-strand break. *Radiation research*, *143*(3), 273-280.

Minoia, C., & Cavalleri, A. (1988). Chromium in urine, serum and red blood cells in the biological monitoring of workers exposed to different chromium valency states. *Science of the Total Environment*, *71*(3), 323-327.

Mladenov, E., Magin, S., Soni, A., & Iliakis, G. (2016, June). DNA double-strand-break repair in higher eukaryotes and its role in genomic instability and cancer: Cell cycle and proliferation-dependent regulation. In *Seminars in cancer biology* (Vol. 37, pp. 51-64). Academic Press.

Moller, D. R., Brooks, S. M., Bernstein, D. I., Cassedy, K., Enrione, M., & Bernstein, I. L. (1986). Delayed anaphylactoid reaction in a worker exposed to chromium. *Journal of allergy and clinical immunology*, *77*(3), 451-456.

Myler, L. R., Gallardo, I. F., Soniat, M. M., Deshpande, R. A., Gonzalez, X. B., Kim, Y., ... & Finkelstein, I. J. (2017). Single-molecule imaging reveals how Mre11-Rad50-Nbs1 initiates DNA break repair. *Molecular cell*, *67*(5), 891-898.

Nagelkerke, A., van Kuijk, S. J., Sweep, F. C., Nagtegaal, I. D., Hoogerbrugge, N., Martens, J. W., Timmermans, M. A., van Laarhoven, H. W., Bussink, J., & Span, P. N. (2011). Constitutive expression of γ-H2AX has prognostic relevance in triple negative breast cancer. *Radiotherapy and oncology : journal of the European Society for Therapeutic Radiology and Oncology*, *101*(1), 39–45.

Nagy, J. D., Victor, E. M., & Cropper, J. H. (2007). Why don't all whales have cancer? A novel hypothesis resolving Peto's paradox. *Integrative and comparative biology*, *47*(2), 317-328.

Nasser, N. J., Avivi, A., Shafat, I., Edovitsky, E., Zcharia, E., Ilan, N., ... & Nevo, E. (2009). Alternatively spliced Spalax heparanase inhibits extracellular matrix degradation, tumor growth, and metastasis. *Proceedings of the National Academy of Sciences*, *106*(7), 2253-2258.

National Institute for Occupational Safety and Health (NIOSH). (1975a). Criteria for a recommended standard: occupational exposure to chromium (VI). Cincinnati, OH: U.S. Department of Health, Education, and Welfare, Public Health Service, Center for Disease Control, National Institute for Occupational Safety and Health, DHEW Publication No. (NIOSH) 76–129.

Newman, S. J., & Smith, S. A. (2006). Marine mammal neoplasia: a review. *Veterinary Pathology*, *43*(6), 865-880.

Nickens, K. P., Patierno, S. R., & Ceryak, S. (2010). Chromium genotoxicity: a double-edged sword. Chemico-biological interactions, 188(2), 276-288.

Nimonkar, A. V., Genschel, J., Kinoshita, E., Polaczek, P., Campbell, J. L., Wyman, C., ... & Kowalczykowski, S. C. (2011). BLM–DNA2–RPA–MRN and EXO1–BLM–RPA–MRN constitute two DNA end resection machineries for human DNA break repair. *Genes & development*, *25*(4), 350-362.

NIOSH. (2006). The Final Standard on Hexavalent Chromium. Effective and practical protection for workers. Occupational Safety & Health Administration. Washington, DC 20210.

Nowosielska, A., & Marinus, M. G. (2005). Cisplatin induces DNA double-strand break formation in Escherichia coli dam mutants. *DNA repair*, *4*(7), 773-781.

Nunney, L. (2013). The real war on cancer: the evolutionary dynamics of cancer suppression. *Evolutionary applications*, *6*(1), 11-19.

O'Brien, T. J., Ceryak, S., & Patierno, S. R. (2003). Complexities of chromium carcinogenesis: role of cellular response, repair and recovery mechanisms. Mutation Research/Fundamental and Molecular Mechanisms of Mutagenesis, 533(1-2), 3-36.

O'Brien, T. J., Ceryak, S., & Patierno, S. R. (2003). Complexities of chromium carcinogenesis: role of cellular response, repair and recovery mechanisms. *Mutation Research/Fundamental and Molecular Mechanisms of Mutagenesis*, *533*(1-2), 3-36.

O'Brien, T. J., Fornsaglio, J. L., Ceryak, S., & Patierno, S. R. (2002). Effects of hexavalent chromium on the survival and cell cycle distribution of DNA repair-deficient S. cerevisiae. *DNA repair*, *1*(8), 617-627.

Occupational Safety and Health Administration (OSHA), Department of Labor. (2006). Occupational exposure to hexavalent chromium. Final rule. Fed Regist. 71(39):10099-10385.

Occupational Safety and Health Administration (OSHA). (2006). Occupational exposure to hexavalent chromium (Docket No. H054A). Federal Register, 71(39), 10100-10382.

Ochola, D. O., Sharif, R., Bedford, J. S., Keefe, T. J., Kato, T. A., Fallgren, C. M., Demant, P., Costes, S. V., & Weil, M. M. (2019). Persistence of Gamma-H2AX Foci in Bronchial Cells Correlates with Susceptibility to Radiation Associated Lung Cancer in Mice. *Radiation research*, *191*(1), 67–75.

Pannunzio, N. R., Watanabe, G., & Lieber, M. R. (2018). Nonhomologous DNA end-joining for repair of DNA double-strand breaks. *Journal of Biological Chemistry*, *293*(27), 10512-10523.

Papp, J. F. (2015). Mineral Yearbook 2015: Chromium. *United States Geological Survey. Retrieved*, 06-03.

Park, H. S., Yu, H. J., & JUNG, K. S. (1994). Occupational asthma caused by chromium. *Clinical & Experimental Allergy*, *24*(7), 676-681.

Park, S., Li, C., Zhao, H., Darzynkiewicz, Z., & Xu, D. (2016). Gene 33/Mig6 inhibits hexavalent chromium-induced DNA damage and cell transformation in human lung epithelial cells. *Oncotarget*, *7*(8), 8916.

Patierno, S. R., Banh, D., & Landolph, J. R. (1988). Transformation of C3H/10T1/2 mouse embryo cells to focus formation and anchorage independence by insoluble lead chromate but not soluble calcium chromate: relationship to mutagenesis and internalization of lead chromate particles. *Cancer research*, *48*(18), 5280–5288.

Paustenbach, D., Finley, B., Mowat, F., & Kerger, B. (2003). Human health risk and exposure assessment of chromium (VI) in tap water. *Journal of Toxicology and Environmental Health, Part A*, *66*(14), 1295-1339.

Pechova, A., & Pavlata, L. (2007). Chromium as an essential nutrient: a review. *Veterinární medicína*, *52*(1), 1.

Pérez, A., & Pierce Wise, J., Sr (2018). One Environmental Health: an emerging perspective in toxicology. *F1000Research*, *7*, F1000 Faculty Rev-918.

Peterson-Roth, E., Reynolds, M., Quievryn, G., & Zhitkovich, A. (2005). Mismatch repair proteins are activators of toxic responses to chromium-DNA damage. *Molecular and cellular biology*, *25*(9), 3596-3607.

Peterson-Roth, E., Reynolds, M., Quievryn, G., & Zhitkovich, A. (2005). Mismatch repair proteins are activators of toxic responses to chromium-DNA damage. *Molecular and cellular biology*, *25*(9), 3596-3607.

Peto, R., Roe, F. J., Lee, P. N., Levy, L., & Clack, J. (1975). Cancer and ageing in mice and men. *British journal of cancer*, *32*(4), 411-426.

Qin, Q., Xie, H., Wise, S. S., Browning, C. L., Thompson, K. N., Holmes, A. L., & Wise Sr, J. P. (2014). Homologous recombination repair signaling in chemical carcinogenesis: prolonged particulate hexavalent chromium exposure suppresses the Rad51 response in human lung cells. *Toxicological Sciences*, *142*(1), 117-125.

Quievryn, G., Goulart, M., Zhitkovich, J. M., & Zhitkovich, A. (2001). Reduction of Cr (VI) by cysteine: significance in human lymphocytes and formation of DNA damage in reactions with variable reduction rates. In *Molecular Mechanisms of Metal Toxicity and Carcinogenesis* (pp. 107-118). Springer, Boston, MA.

Quievryn, G., Messer, J., & Zhitkovich, A. (2002). Carcinogenic chromium (VI) induces cross-linking of vitamin C to DNA in vitro and in human lung A549 cells. *Biochemistry*, *41*(9), 3156-3167.

Rager, J. E., Suh, M., Chappell, G. A., Thompson, C. M., & Proctor, D. M. (2019). Review of transcriptomic responses to hexavalent chromium exposure in lung cells supports a role of epigenetic mediators in carcinogenesis. *Toxicology letters*, *305*, 40–50.

Randall, J. A., & Gibson, R. S. (1987). Serum and urine chromium as indices of chromium status in tannery workers. *Proceedings of the Society for Experimental Biology and Medicine*, *185*(1), 16-23.

Rao, G. V., Tinkle, S., Weissman, D. N., Antonini, J. M., Kashon, M. L., Salmen, R., Battelli, L. A., Willard, P. A., Hoover, M. D., & Hubbs, A. F. (2003). Efficacy of a technique for exposing the mouse lung to particles aspirated from the pharynx. *Journal of toxicology and environmental health. Part A*, *66*(15), 1441–1452.

Renkawitz, J., Lademann, C. A., & Jentsch, S. (2014). Mechanisms and principles of homology search during recombination. *Nature Reviews Molecular Cell Biology*, *15*(6), 369-383.

Reynolds, M., Stoddard, L., Bespalov, I., & Zhitkovich, A. (2007). Ascorbate acts as a highly potent inducer of chromate mutagenesis and clastogenesis: linkage to DNA breaks in G 2 phase by mismatch repair. *Nucleic acids research*, *35*(2), 465-476.

Richard, F. C., & Bourg, A. C. (1991). Aqueous geochemistry of chromium: a review. *Water research*, *25*(7), 807-816.

Rodrigues, C. F. D., Urbano, A. M., Matoso, E., Carreira, I., Almeida, A., Santos, P., ... & Alpoim, M. C. (2009). Human bronchial epithelial cells malignantly transformed by hexavalent chromium exhibit an aneuploid phenotype but no microsatellite instability. *Mutation Research/Fundamental and Molecular Mechanisms of Mutagenesis*, *670*(1-2), 42-52.

Rogakou, E. P., Boon, C., Redon, C., & Bonner, W. M. (1999). Megabase chromatin domains involved in DNA double-strand breaks in vivo. *The Journal of cell biology*, *146*(5), 905-916.

Ryberg, D., & Alexander, J. (1984). Inhibitory action of hexavalent chromium (Cr (VI)) on the mitochondrial respiration and a possible coupling to the reduction of Cr (VI). *Biochemical pharmacology*, *33*(15), 2461-2466.

Sartori, A. A., Lukas, C., Coates, J., Mistrik, M., Fu, S., Bartek, J., ... & Jackson, S. P. (2007). Human CtIP promotes DNA end resection. *Nature*, *450*(7169), 509-514.

Satoh, K., Fukuda, Y., Torii, K., & Katsuno, N. (1981). Epidemiological study of workers engaged in the manufacture of chromium compounds. *Journal of Occupational Medicine*, 835-838.

Schulte, R.F. (2020) Mineral commodity summaries 2020, in Mineral Commodity Summaries. p 204.

Sebesta, M., Burkovics, P., Juhasz, S., Zhang, S., Szabo, J. E., Lee, M. Y., ... & Krejci, L. (2013). Role of PCNA and TLS polymerases in D-loop extension during homologous recombination in humans. *DNA repair*, *12*(9), 691-698.

Sedelnikova, O. A., & Bonner, W. M. (2006). GammaH2AX in cancer cells: a potential biomarker for cancer diagnostics, prediction and recurrence. *Cell cycle (Georgetown, Tex.)*, *5*(24), 2909–2913.

Sedelnikova, O. A., Rogakou, E. P., Panyutin, I. G., & Bonner, W. M. (2002). Quantitative detection of 125IdU-induced DNA double-strand breaks with γ-H2AX antibody. *Radiation research*, *158*(4), 486-492.

Sehlmeyer, U., Hechtenberg, S., Klyszcz, H., & Beyersmann, D. (1990). Accumulation of chromium in Chinese hamster V79-cells and nuclei. *Archives of toxicology*, *64*(6), 506-508.

Seim, I., Ma, S., Zhou, X., Gerashchenko, M. V., Lee, S. G., Suydam, R., George, J. C., Bickham, J. W., & Gladyshev, V. N. (2014). The transcriptome of the bowhead whale Balaena mysticetus reveals adaptations of the longest-lived mammal. *Aging*, *6*(10), 879–899.

Shaw Environmental. (2006) Industry profile, exposure profile, technological feasibility evaluation, and environmental impact for industries affected by a proposed OSHA standard for hexavalent chromium. Cincinnati, OH: Shaw Environmental, Inc. Contract No. J-9-F-9-0030, Subcontract No. 0178.03.062/1, PN 118851-01 for OSHA, U.S. Department of Labor.

Shi, X., & Dalal, N. S. (1989). Chromium (V) and hydroxyl radical formation during the glutathione reductase-catalyzed reduction of chromium (VI). *Biochemical and biophysical research communications*, *163*(1), 627-634.

Shibata, A., Moiani, D., Arvai, A. S., Perry, J., Harding, S. M., Genois, M. M., ... & Tainer, J. A. (2014). DNA double-strand break repair pathway choice is directed by distinct MRE11 nuclease activities. *Molecular cell*, *53*(1), 7-18.

Shinohara, A., Ogawa, H., & Ogawa, T. (1992). Rad51 protein involved in repair and recombination in S. cerevisiae is a RecA-like protein. *Cell*, *69*(3), 457-470.

Singh, A., Pal, R., Gangwar, C., Gupta, A., & Tripathi, A. (2015). Release of heavy metals from industrial waste and e-waste burning and its effect on human health and environment. *Intern. J. Emerging Res. Manag. Tech*, *4*(12), 51-56.

Singh, R. K., & Krishna, M. (2005). DNA strand breaks signal the induction of DNA double-strand break repair in Saccharomyces cerevisiae. *Radiation research*, *164*(6), 781-790.

Snow, E. T., & Xu, L. S. (1991). Chromium (III) bound to DNA templates promotes increased polymerase processivity and decreased fidelity during replication in vitro. *Biochemistry*, *30*(47), 11238-11245.

Sonoda, E., Sasaki, M. S., Morrison, C., Yamaguchi-Iwai, Y., Takata, M., & Takeda, S. (1999). Sister chromatid exchanges are mediated by homologous recombination in vertebrate cells. *Molecular and cellular biology*, *19*(7), 5166–5169.

Speakman, J. R. (2005). Body size, energy metabolism and lifespan. *Journal of Experimental Biology*, *208*(9), 1717-1730.

Spitz, M. R., Wei, Q., Dong, Q., Amos, C. I., & Wu, X. (2003). Genetic susceptibility to lung cancer: the role of DNA damage and repair. *Cancer epidemiology, biomarkers & prevention : a publication of the American Association for Cancer Research, cosponsored by the American Society of Preventive Oncology*, *12*(8), 689–698.

Stackpole, M. M., Wise, S. S., Goodale, B. C., Duzevik, E. G., Munroe, R. C., Thompson, W. D., Thacker, J., Thompson, L. H., Hinz, J. M., & Wise, J. P., Sr (2007). Homologous recombination repair protects against particulate chromate-induced chromosome instability in Chinese hamster cells. *Mutation research*, *625*(1-2), 145–154.

Standeven, A. M., & Wetterhahn, K. E. (1991). Ascorbate is the principal reductant of chromium (VI) in rat liver and kidney ultrafiltrates. *Carcinogenesis*, *12*(9), 1733-1737.

Standeven, A. M., Wetterhahn, K. E., & Kato, R. (1992). Ascorbate is the principal reductant of chromium (VI) in rat lung ultrafiltrates and cytosols, and mediates chromium–DNA binding in vitro. *Carcinogenesis*, *13*(8), 1319-1324.

Staniek, H., & Wójciak, R. W. (2018). The Combined Effects of Iron Excess in the Diet and Chromium(III) Supplementation on the Iron and Chromium Status in Female Rats. *Biological trace element research*, *184*(2), 398–408.

Stearns, D. M., & Wetterhahn, K. E. (1994). Reaction of chromium (VI) with ascorbate produces chromium (V), chromium (IV), and carbon-based radicals. *Chemical research in toxicology*, *7*(2), 219-230.

Stearns, D. M., Courtney, K. D., Giangrande, P. H., Phieffer, L. S., & Wetterhahn, K. E. (1994). Chromium (VI) reduction by ascorbate: role of reactive intermediates in DNA damage in vitro. *Environmental health perspectives*, *102*(suppl 3), 21-25.

Stearns, D. M., Kennedy, L. J., Courtney, K. D., Giangrande, P. H., Phieffer, L. S., & Wetterhahn, K. E. (1995). Reduction of chromium (VI) by ascorbate leads to chromium-DNA binding and DNA strand breaks in vitro. *Biochemistry*, *34*(3), 910-919.

Steinhoff, D., Gad, S. C., Hatfield, G. K., & Mohr, U. (1986). Carcinogenicity study with sodium dichromate in rats. *Experimental pathology*, *30*(3), 129-141.

Stern, R. M. (1982). *Chromium compounds: production and occupational exposure* (pp. 5-47). Elsevier.

Sugden, K. D., & Stearns, D. M. (2000). The role of chromium (V) in the mechanism of chromate-induced oxidative DNA damage and cancer. *Journal of environmental pathology, toxicology and oncology: official organ of the International Society for Environmental Toxicology and Cancer*, *19*(3), 215-230.

Sun, H., Clancy, H. A., Kluz, T., Zavadil, J., & Costa, M. (2011). Comparison of gene expression profiles in chromate transformed BEAS-2B cells. *PloS one*, *6*(3), e17982.

Sung, H., Ferlay, J., Siegel, R. L., Laversanne, M., Soerjomataram, I., Jemal, A., & Bray, F. (2021). Global Cancer Statistics 2020: GLOBOCAN Estimates of Incidence and Mortality Worldwide for 36 Cancers in 185 Countries. *CA: a cancer journal for clinicians*, *71*(3), 209–249.

Sung, P., & Robberson, D. L. (1995). DNA strand exchange mediated by a RAD51-ssDNA nucleoprotein filament with polarity opposite to that of RecA. *Cell*, *82*(3), 453-461.

Sung, P., Krejci, L., Van Komen, S., & Sehorn, M. G. (2003). Rad51 recombinase and recombination mediators. *Journal of Biological Chemistry*, *278*(44), 42729-42732.

Suzuki, Y., & Fukuda, K. (1990). Reduction of hexavalent chromium by ascorbic acid and glutathione with special reference to the rat lung. *Archives of toxicology*, *64*(3), 169-176.

Takahashi, Y., Kondo, K., Hirose, T., Nakagawa, H., Tsuyuguchi, M., Hashimoto, M., Sano, T., Ochiai, A., & Monden, Y. (2005a). Microsatellite instability and protein expression of the DNA mismatch repair gene, hMLH1, of lung cancer in chromate-exposed workers. *Molecular carcinogenesis*, *42*(3), 150–158.

Takahashi, Y., Kondo, K., Ishikawa, S., Uchihara, H., Fujino, H., Sawada, N., ... & Monden, Y. (2005b). Microscopic analysis of the chromium content in the chromium-induced malignant and premalignant bronchial lesions of the rat. *Environmental research*, *99*(2), 267-272.

Takenaka, T., Yoshino, I., Kouso, H., Ohba, T., Yohena, T., Osoegawa, A., Shoji, F., & Maehara, Y. (2007). Combined evaluation of Rad51 and ERCC1 expressions for sensitivity to platinum agents in non-small cell lung cancer. *International journal of cancer*, *121*(4), 895–900.

Tejada-Martinez, D., De Magalhães, J. P., & Opazo, J. C. (2021). Positive selection and gene duplications in tumour suppressor genes reveal clues about how cetaceans resist cancer. *Proceedings of the Royal Society B*, *288*(1945), 20202592.

Tollis, M., Boddy, A. M., & Maley, C. C. (2017). Peto's Paradox: how has evolution solved the problem of cancer prevention?. *BMC biology*, *15*(1), 1-5.

Tollis, M., Robbins, J., Webb, A. E., Kuderna, L. F., Caulin, A. F., Garcia, J. D., ... & Maley, C. C. (2019). Return to the sea, get huge, beat cancer: an analysis of cetacean genomes including an assembly for the humpback whale (Megaptera novaeangliae). *Molecular biology and evolution*, *36*(8), 1746-1763.

Tsapakos, M. J., & Wetterhahn, K. E. (1983). The interaction of chromium with nucleic acids. *Chemico-biological interactions*, *46*(2), 265-277.

Uziel, T., Lerenthal, Y., Moyal, L., Andegeko, Y., Mittelman, L., & Shiloh, Y. (2003). Requirement of the MRN complex for ATM activation by DNA damage. *The EMBO journal*, *22*(20), 5612-5621.

Voitkun, V., Zhitkovich, A., & Costa, M. (1998). Cr (III)-mediated crosslinks of glutathione or amino acids to the DNA phosphate backbone are mutagenic in human cells. *Nucleic acids research*, *26*(8), 2024-2030.

Wakeman, T. P., Kim, W. J., Callens, S., Chiu, A., Brown, K. D., & Xu, B. (2004). The ATM-SMC1 pathway is essential for activation of the chromium [VI]-induced S-phase checkpoint. *Mutation Research/Fundamental and Molecular Mechanisms of Mutagenesis*, *554*(1-2), 241-251.

Wang, H., Eyert, V., & Schwingenschlögl, U. (2011). Electronic structure and magnetic ordering of the semiconducting chromium trihalides CrCl3, CrBr3, and CrI3. *Journal of Physics: Condensed Matter*, *23*(11), 116003.

Wang, X., Son, Y. O., Chang, Q., Sun, L., Hitron, J. A., Budhraja, A., Zhang, Z., Ke, Z., Chen, F., Luo, J., & Shi, X. (2011). NADPH oxidase activation is required in reactive oxygen species generation and cell transformation induced by hexavalent chromium. *Toxicological sciences : an official journal of the Society of Toxicology*, *123*(2), 399–410.

Wang, Z., Uddin, M. B., Xie, J., Tao, H., Zeidler-Erdely, P. C., Kondo, K., & Yang, C. (2022). Chronic Hexavalent Chromium Exposure Upregulates the RNA Methyltransferase METTL3 Expression to Promote Cell Transformation, Cancer Stem Cell-Like Property, and Tumorigenesis. *Toxicological sciences : an official journal of the Society of Toxicology*, *187*(1), 51–61.

Waqar, S.N., Devarakonda, S.H., Michel, L.S., Maggi, L.B., Watson, M., Guebert, K., Carpenter, D., Sleckman, B.P., Govindan, R., & Morgensztern, D. Morgensztern, D. (2014). BRCAness in non-small cell lung cancer (NSCLC). *Journal of Clinical Oncology*, 32:15_suppl, 11033-11033.

Weber H. (1983). Long-term study of the distribution of soluble chromate-51 in the rat after a single intratracheal administration. *Journal of toxicology and environmental health*, *11*(4-6), 749–764.

Wei, Q., Cheng, L., Amos, C. I., Wang, L. E., Guo, Z., Hong, W. K., & Spitz, M. R. (2000). Repair of tobacco carcinogen-induced DNA adducts and lung cancer risk: a molecular epidemiologic study. *Journal of the National Cancer Institute*, *92*(21), 1764–1772.

Wengner, A. M., Scholz, A., & Haendler, B. (2020). Targeting DNA Damage Response in Prostate and Breast Cancer. *International journal of molecular sciences*, *21*(21), 8273.

Wiegand, H. J., Ottenwälder, H., & Bolt, H. M. (1985). Fast uptake kinetics in vitro of 51Cr (VI) by red blood cells of man and rat. *Archives of toxicology*, *57*(1), 31-34.

Wiegand, H. J., Ottenwälder, H., & Bolt, H. M. (1987). Bioavailability and metabolism of hexavalent chromium compounds. *Toxicological & Environmental Chemistry*, *14*(4), 263-275.

Wilk, A., Waligorska, A., Waligorski, P., Ochoa, A., & Reiss, K. (2012). Inhibition of ERβ induces resistance to cisplatin by enhancing Rad51-mediated DNA repair in human medulloblastoma cell lines. *PloS one*, *7*(3), e33867.

Williams, R. S., Moncalian, G., Williams, J. S., Yamada, Y., Limbo, O., Shin, D. S., Groocock, L. M., Cahill, D., Hitomi, C., Guenther, G., Moiani, D., Carney, J. P., Russell, P., & Tainer, J. A. (2008). Mre11 dimers coordinate DNA end bridging and nuclease processing in double-strand-break repair. *Cell*, *135*(1), 97–109.

Williams, R. S., Williams, J. S., & Tainer, J. A. (2007). Mre11-Rad50-Nbs1 is a keystone complex connecting DNA repair machinery, double-strand break signaling, and the chromatin template. *Biochemistry and cell biology = Biochimie et biologie cellulaire*, *85*(4), 509–520.

Wise Sr, J. P., Wise, S. S., & Little, J. E. (2002). The cytotoxicity and genotoxicity of particulate and soluble hexavalent chromium in human lung cells. *Mutation Research/Genetic Toxicology and Environmental Mutagenesis*, *517*(1-2), 221-229.

Wise, C. F., Wise, S. S., Thompson, W. D., Perkins, C., & Wise, J. P. (2015). Chromium is elevated in fin whale (Balaenoptera physalus) skin tissue and is genotoxic to fin whale skin cells. *Biological trace element research*, *166*(1), 108-117.

Wise, J. P., Jr, Croom-Perez, T. J., Meaza, I., Aboueissa, A. M., López Montalvo, C. A., Martin-Bras, M., Speer, R. M., Bonilla-Garzón, A., Urbán R, J., Perkins, C., & Wise, J. P., Sr (2019b). A whale of a tale: A One Environmental Health approach to study metal pollution in the Sea of Cortez. *Toxicology and applied pharmacology*, *376*, 58–69.

Wise, J. P., Jr, Wise, J., Wise, C. F., Wise, S. S., Zhu, C., Browning, C. L., Zheng, T., Perkins, C., Gianios, C., Jr, Xie, H., & Wise, J. P., Sr (2019a). Metal Levels in Whales from the Gulf of Maine: A One Environmental Health approach. *Chemosphere*, *216*, 653–660.

Wise, J. P., Orenstein, J. M., & Patierno, S. R. (1993). Inhibition of lead chromate clastogenesis by ascorbate: relationship to particle dissolution and uptake. *Carcinogenesis*, *14*(3), 429-434.

Wise, S. S., & Wise Sr, J. P. (2012). Chromium and genomic stability. Mutation Research/Fundamental and Molecular Mechanisms of Mutagenesis, 733(1-2), 78-82.

Wise, S. S., Elmore, L. W., Holt, S. E., Little, J. E., Antonucci, P. G., Bryant, B. H., & Wise, J. P., Sr (2004b). Telomerase-mediated lifespan extension of human bronchial cells does not affect hexavalent chromium-induced cytotoxicity or genotoxicity. *Molecular and cellular biochemistry*, *255*(1-2), 103–111.

Wise, S. S., Holmes, A. L., & Wise Sr, J. P. (2006a). Particulate and soluble hexavalent chromium are cytotoxic and genotoxic to human lung epithelial cells. *Mutation Research/Genetic Toxicology and Environmental Mutagenesis*, *610*(1-2), 2-7.

Wise, S. S., Holmes, A. L., Liou, L., Adam, R. M., & Wise Sr, J. P. (2016). Hexavalent chromium induces chromosome instability in human urothelial cells. *Toxicology and applied pharmacology*, *296*, 54-60.

Wise, S. S., Holmes, A. L., Qin, Q., Xie, H., Katsifis, S. P., Thompson, W. D., & Wise Sr, J. P. (2010). Comparative genotoxicity and cytotoxicity of four hexavalent chromium compounds in human bronchial cells. *Chemical research in toxicology*, *23*(2), 365-372.

Wise, S. S., Holmes, A. L., Xie, H., Thompson, W. D., & Wise, J. P., Sr (2006). Chronic exposure to particulate chromate induces spindle assembly checkpoint bypass in human lung cells. *Chemical research in toxicology*, *19*(11), 1492–1498.

Wise, S. S., Schuler, J. H., Holmes, A. L., Katsifis, S. P., Ketterer, M. E., Hartsock, W. J., Zheng, T., & Wise, J. P., Sr (2004a). Comparison of two particulate hexavalent chromium compounds: Barium chromate is more genotoxic than lead chromate in human lung cells. *Environmental and molecular mutagenesis*, *44*(2), 156–162.

Wise, S. S., Schuler, J. H., Katsifis, S. P., & Wise Sr, J. P. (2003). Barium chromate is cytotoxic and genotoxic to human lung cells. *Environmental and Molecular Mutagenesis*, *42*(4), 274-278.

Wyatt, H. D., & West, S. C. (2014). Holliday junction resolvases. *Cold Spring Harbor perspectives in biology*, *6*(9), a023192.

Wyatt, H. D., Sarbajna, S., Matos, J., & West, S. C. (2013). Coordinated actions of SLX1-SLX4 and MUS81-EME1 for Holliday junction resolution in human cells. *Molecular cell*, *52*(2), 234-247.

Xie, H., Holmes, A. L., Wise, S. S., Gordon, N., & Wise, J. P. (2004). Lead chromate-induced chromosome damage requires extracellular dissolution to liberate chromium ions but does not require particle internalization or intracellular dissolution. *Chemical research in toxicology*, *17*(10), 1362-1367.

Xie, H., Holmes, A. L., Wise, S. S., Huang, S., Peng, C., & Wise Sr, J. P. (2007). Neoplastic transformation of human bronchial cells by lead chromate

particles. *American journal of respiratory cell and molecular biology*, *37*(5), 544-552.

Xie, H., Holmes, A. L., Wise, S. S., Young, J. L., Wise, J. T., & Wise, J. P. (2015). Human skin cells are more sensitive than human lung cells to the cytotoxic and cell cycle arresting impacts of particulate and soluble hexavalent chromium. *Biological trace element research*, *166*(1), 49-56.

Xie, H., Holmes, A. L., Young, J. L., Qin, Q., Joyce, K., Pelsue, S. C., ... & Wise Sr, J. P. (2009). Zinc chromate induces chromosome instability and DNA double strand breaks in human lung cells. *Toxicology and applied pharmacology*, *234*(3), 293-299.

Xie, H., Wise, S. S., & Wise, J. P., Sr (2008). Deficient repair of particulate hexavalent chromium-induced DNA double strand breaks leads to neoplastic transformation. *Mutation research*, *649*(1-2), 230–238.

Xie, H., Wise, S. S., Holmes, A. L., Xu, B., Wakeman, T. P., Pelsue, S. C., ... & Wise Sr, J. P. (2005). Carcinogenic lead chromate induces DNA double-strand breaks in human lung cells. *Mutation Research/Genetic Toxicology and Environmental Mutagenesis*, *586*(2), 160-172.

Xie, H., Wise, S. S., Holmes, A. L., Xu, B., Wakeman, T. P., Pelsue, S. C., ... & Wise Sr, J. P. (2005). Carcinogenic lead chromate induces DNA double-strand breaks in human lung cells. *Mutation Research/Genetic Toxicology and Environmental Mutagenesis*, *586*(2), 160-172.

You, Z., Shi, L. Z., Zhu, Q., Wu, P., Zhang, Y. W., Basilio, A., ... & Hunter, T. (2009). CtIP links DNA double-strand break sensing to resection. *Molecular cell*, *36*(6), 954-969.

Yu, C. H., Huang, L., Shin, J. Y., Artigas, F., & Fan, Z. H. T. (2014). Characterization of concentration, particle size distribution, and contributing factors to ambient hexavalent chromium in an area with multiple emission sources. *Atmospheric Environment*, *94*, 701-708.

Zeidler-Erdely, P. C., Falcone, L. M., Antonini, J. M., Fraser, K., Kashon, M. L., Battelli, L. A., Salmen, R., Trainor, T., Grose, L., Friend, S., Yang, C., & Erdely, A. (2020). Tumorigenic response in lung tumor susceptible A/J mice after subchronic exposure to calcium chromate or iron (III) oxide. *Toxicology letters*, *334*, 60–65.

Zhang, Z., Leonard, S. S., Wang, S., Vallyathan, V., Castranova, V., & Shi, X. (2001). CR (VI) induces cell growth arrest through hydrogen peroxide-mediated reactions. *Molecular and cellular biochemistry*, *222*(1), 77-83.

Zhitkovich, A. (2005). Importance of chromium− DNA adducts in mutagenicity and toxicity of chromium (VI). *Chemical research in toxicology*, *1*(18), 3-11.

Zhitkovich, A., Voitkun, V., & Costa, M. (1995). Glutathione and free amino acids form stable complexes with DNA following exposure of intact mammalian cells to chromate. *Carcinogenesis*, *16*(4), 907-913.

Zhitkovich, A., Voitkun, V., & Costa, M. (1996). Formation of the amino acid− DNA complexes by hexavalent and trivalent chromium in vitro: importance of trivalent chromium and the phosphate group. *Biochemistry*, *35*(22), 7275-7282.

Zhou, B. B., & Elledge, S. J. (2000). The DNA damage response: putting checkpoints in perspective. *Nature*, *408*(6811), 433–439.

LIST OF ABBREVIATIONS

Alt-EJ: Alternative end joining

APC: Adenomatous polyposis coli

ATM: Ataxia telangiectasia mutated

ATSDR: Agency for Toxic Substances and Disease Registry

BLM/Dna2: Bloom helicase/Dna2 helicase

BrdU: 5-bromodeoxyuridine

CIN: Chromosome instability

c-NHEJ: Classical non-homologous end joining

Cr(III): Trivalent chromium

Cr(VI): Hexavalent chromium

Cr: Chromium

CtIP: C-terminal binding protein 1

DAPI: 4′,6-diamidino-2-phenylindole

DNA: Deoxyribonucleic acid

EDTA: Ethylenediaminetetraacetic acid

Exo1: Exonuclease 1

FISH: Fluorescence in situ hybridization

hMLH1: Human MutL homolog 1

hMLH2: Human MutL homolog 2

HR: Homologous recombination

hTERT: Human telomerase

IARC: International Agency for Research on Cancer

ICP-MS: inductively coupled plasma mass spectrometry

IR: Ionizing radiation

MGMT: O^6-methylguanine-DNA methyltransferase

MMR: Mismatch repair

MRN: MRE11, RAD50 and Nbs1 complex

MSI: Microsatellite instability

NIOSH: National Institute for Occupational Safety and Health

OSHA: Occupational Safety and Health Administration

RAD51: RAD51 recombinase

RAD51C: RAD51 paralog C

ROI: Region of interest

RPA: Replication protein A

SCE: Sister chromatid exchange

SSA: Single strand annealing

WTHBF-6: hTERT-immortalized human bronchial fibroblasts

XRCC3: X-Ray Repair Cross Complementing 3

CURRICULUM VITAE

Haiyan Lu

Mailing Address: Wise Laboratory of Environmental and Genetic Toxicology
Department of Pharmacology and Toxicology, School of Medicine
University of Louisville
500 S. Preston St.
HSC-A, room 1403
Louisville, KY 40202

E-Mail: haiyan.lu@louisville.edu

Education

2016-Present Ph.D. student in Pharmacology and Toxicology, University of Louisville, Louisville, KY

2005-2009 M.S. in Pediatrics, Wenzhou Medical College, Wenzhou Zhejiang, China

1998-2003 M.D., Wenzhou Medical College, Wenzhou Zhejiang, China

Professional Experience

2011-2016 Attending, Pediatric Neurologist, The Second Affiliated Hospital of Wenzhou Medical University, Wenzhou Zhejiang, China

2003-2011 Residency, Pediatrician, The Second Affiliated Hospital of Wenzhou Medical University, Wenzhou Zhejiang, China

Professional Appointments

2016-Present Ph.D. student in Pharmacology and Toxicology, University of Louisville, Louisville, KY

2006-2021 Pediatric Neurologist, The Second Affiliated Hospital of Wenzhou Medical University, Wenzhou Zhejiang, China

2003-2005 Pediatrician, The Second Affiliated Hospital of Wenzhou Medical University, Wenzhou Zhejiang, China

Research Experience

2016 – Present

Wise Laboratory of Environmental and Genetic Toxicology, University of Louisville
Ph.D. research in the molecular mechanisms of hexavalent chromium-induced carcinogenesis. Cell culture, in vivo rodent, human tissue, and wildlife studies provide a One Environmental Health perspective of the mechanisms of hexavalent chromium-induced homologous recombination repair suspension and structural chromosome instability.

2005-2009

Guangqian Li Lab, Wenzhou Medical College
M.S. research in the molecular mechanisms of status convulsion. In vivo rodent study explores the mechanism of status convulsion-induced apoptosis.

Publications

1. Lu, H., Deng, X., Li, G., Li, W. The Expression of JNK in the Hippocampus of Status Convulsivus Rat and the Effect of Edaravone. Journal of Wenzhou Medical College, 39(5):p455-459, 2009.

2. Lu, H., Sun, B., Zhao, Q., Chen, W., Yang, Z., Zhou, Z., Lin, Z., Chen, Y. The clinical analysis of 121 cases of intestinal type 71 hand foot mouth disease. Practical Pediatric Journal of China, 26(12) p928-932, 2011.

3. Lu, H., Chen, J., Shi, H. The clinical study of plasma von willebrand factor, D-Dimer in patients with hand foot mouth disease. Practical Medicine Magazine, 27(5) p825-826, 2011.

4. Meaza, I., Speer, R.M., Toyoda, J.H., Lu, H., Wise, S.S., Croom-Perez, T.J., Aboueissa, A., and Wise, Sr., J.P. Prolonged exposure to particulate Cr(VI) is cytotoxic and genotoxic to fin whale cells. Journal of Trace Elements in Medicine and Biology. Dec 62:126562, 2020.

5. Speer, R.M., Meaza, I, Toyoda, J.H., Lu, Y, Xu, Q, Walter, R.B., Kong, M., Lu, H., Kouokam, J.C., Wise, Sr. J.P. Particulate hexavalent chromium alters microRNAs in human lung cells that target key carcinogenic pathways. Toxicol Appl Pharmacol. Jan 28:115890, 2022.

6. Wise, S.S., Lu, H., Toyoda, J.H., and Wise, Sr., J.P. Zinc Chromate is Cytotoxic and Genotoxic to Sperm Whale and Bowhead Whale Cells. Submitted.

7. Lu, H., Browning, C.L, Wise, S.S., Toyoda, J.H. and Wise, Sr., J.P. Bowhead Whale cells Incur Prolonged Particulate Chromate-Induced DNA Double Strand Break Repair but Escape Chromate-Induced Homologous Recombination Repair Inhibition. In Preparation.

8. Lu, H., Croom-Pérez, T. J., Wise, S.S., Speer, R.M., Toyoda, J.H. and Wise, Sr., J.P. Particulate Hexavalent Chromium Induces DNA Double Strand Breaks and Chromosome Instability in Rat Lungs. In Preparation.

Abstracts

Extramural Abstracts

1. Wise, Sr., J.P., Browning, C.L., Wise, S.S., Speer, R., and Lu, H. Homologous Recombination Repair in Chemical Carcinogenesis: Hexavalent Chromium Induces DNA Strand Breaks while Targeting Rad51 to Inhibit Their Repair. Presented at the 19th Annual Midwest DNA Repair Symposium, p. 16, Dayton, Ohio, May 2017.

2. Lu, H., Browning, C.L, Wise, S.S., Toyoda, J.H., Speer, R.M., and Wise, Sr., J.P. Prolonged particulate chromate exposure does not inhibit homologous recombination repair in bowhead whale lung cells. Presented at the Graduate Student Regional Research Conference, Louisville, Kentucky, 2018.

3. Lu, H., Browning, C.L, Wise, S.S., Toyoda, J.H., and Wise, Sr., J.P. Prolonged Particulate Chromate Exposure Does Not Inhibit Homologous Recombination Repair in Bowhead Whale Lung Cells. Presented at the annual meeting of the Ohio Valley Regional Chapter of the Society of Toxicology (OVSOT), Louisville, Kentucky, November 2018.

4. Lu, H., Browning, C.L, Wise, S.S., Toyoda, J.H., Speer, R.M., Raph, S.M., and Wise, Sr., J.P. Homologous Recombination Repair Protects Against Genomic Instability in Bowhead Whale Lung Cells After Prolonged Particulate Chromate Exposure. Presented at the Graduate Student Regional Research Conference, Louisville, Kentucky, February 2019.

5. Lu, H., Browning, C.L, Wise, S.S., Toyoda, J.H., and Wise, Sr., J.P. Homologous Recombination Repair Protects Against Genomic Instability in Bowhead Whale Lung Cells After Prolonged Particulate Chromate Exposure. Presented at the Annual Meeting of the Society of Toxicology (SOT), Toxicological Sciences, 168(1): 2363, 2019.

6. Wise, Sr., J.P. Lu, H., Browning, C.L, Wise, S.S., Toyoda, J.H., and Speer, R.M. Bowhead Whale Lung Cells Maintain Homologous Recombination Repair and Resist Genomic Instability during Prolonged Particulate Chromate Exposure. Environmental and Molecular Mutagenesis Volume 60, Issue S1, p.70.

7. Lu, H., Browning, C.L, and Wise, Sr., J.P. Why Do Whales Have Lower Cancer Rates: Whale Cells Avoid Particulate Chromate Induced Homologous Recombination Repair Inhibition. Presented at the annual meeting of the Ohio Valley Regional Chapter of the Society of Toxicology (OVSOT), Cincinnati. Ohio, October 2019.

8. Wise, Jr., J.P., Lu, H., Meaza, I., Wise, S.S., Croom-Perez, T., Speer, R., Toyoda, J., Ali, A., Cai, L., Liu, K.J., Wise, J.T.F., Young, J.L., and Wise, Sr., J.P. An Environmental Toxicology Assessment of Heavy Metal Accumulation in American Alligators in Florida. Presented at the Ohio Valley Chapter of the Society of Toxicology (OVSOT) annual meeting, October 2019.

9. Croom-Perez, T., Young, J.L., Xu, J., Meaza, I., Lu, H., Wise, S.S., Cai, L., and Wise, Sr., J.P. Characterizing a Mouse Model for the Effects of Whole Life, Low Dose Cadmium Exposure, and High Fat Diet on the Lung. Toxicological Sciences, 168(1): 3430, 2020.

10. Wise, Jr., J.P., Lu, H., Toyoda, J.H., Speer, R.M., Croom-Perez, T., Meaza Isusi, I., Wise, S.S., Young, J.L. Tan, Y., Hoyle, G., Isakov, R., Jaggers, H., Wise, Sr., J.P., and Cai, L. Genotoxicity in the Heart-Brain Axis Following Inhalation of Hexavalent Chromium [Cr(VI)] in a Rat Model. Toxicological Sciences, 174(1): 3130, 2020.

11. Lu, H., Browning C.L. and Wise, Sr., J.P. Why Do Whales Have Lower Cancer Rates: Whale Cells Avoid Particulate Chromate Induced Homologous Recombination Repair Inhibition. Toxicological Sciences, 174(1): 1339, 2020.

12. Lu, H., Browning C.L., Wise, S.S., Speer, R.M, Liu, K.J., and Wise, Sr., J.P. How Chromium Induces Genomic Instability: Lessons from Human and Whale Cells. Presented at the 16th International Symposium on Recent Advances in Environmental Health Research, Jackson, Mississippi, February 2020.

13. Meaza I., Speer M.R., Toyoda, J.H., Lu, H., Wise S.S. Croom-Perez J.T., El-Makarim, A., and Wise, Sr., J. P. Prolonged exposure to particulate Cr(VI) is cytotoxic and genotoxic to fin whale cells. Presented at the summer meeting of the Ohio Valley Society of Toxicology (OVSOT), July 2020.

14. Lu, H., Wise, S.S., Toyoda, J.H., Speer, R.M, Bolt, A., and Wise, Sr., J.P. Whale Cells Are Resistant to Cr(VI)-Induced Loss of Homologous Recombination Repair. Presented at the Ohio Valley Chapter of the Society of Toxicology (OVSOT) annual meeting, November 2020.

15. Lu, H., Wise, S.S., Toyoda, J.H., Speer, R.M., Bolt, A., and Wise, Sr., J.P. Whale Cells Resist Cr(VI)-Induced Loss of Homologous Recombination Repair. Toxicological Sciences, 180:2087, 2021.

16. Lu, H., Wise, S.S., and Wise, Sr., J.P. Can Whales Resist Chromium-Induced Cancer? Presented at the Annual Meeting of the Society of Toxicology (SOT), March 2021.

17. Lu, H., Wise, S.S., Toyoda, J.H., Speer, R.M, Bolt, A., and Wise, Sr., J.P. Whale cells are resistant to Cr(VI)-induced chromosome instability. Presented at the annual meeting of the Genetic Toxicology Association, May 2021.

18. Lu, H., Wise, S.S., Toyoda, J.H., Speer, R.M, Bolt, A., and Wise, Sr., J.P. A Whale of a Tale: Whale Lung Cells Resist Particulate Cr(VI)-Induced Chromosome Instability. Environmental and Molecular Mutagenesis Volume 62, Issue S1, p.63-64, 2021.

19. Meaza, I., Toyoda, J.H., Lu, H., Williams, A.R., Wise, S.S., and Wise Sr. J.P. Particulate Hexavalent Chromium Induces Loss of RAD51 Leading to Increased Genomic Instability, A Driver of Carcinogenesis. Environmental and Molecular Mutagenesis Volume 62, Issue S1, p57, 2021.

20. Kouokam, J.C., Speer R. M., Meaza I., Toyoda J. H., Lu, H., Kong M. and Wise, Sr, J.P. Particulate hexavalent chromium-induced toxicity involves the inflammatory response in human lung fibroblasts. Presented at the Annual Meeting of the Environmental Mutagenesis and Genomics Society (EMGS), 2021.

21. Lu, H., Wise, S.S., Hoyle, G., Toyoda, J.H., Speer, R.M, Croom-Perez, T.J., Meaza, I., Wise, Jr., J.P., Kouokam, J.C., Young J.L., Cai, L., Kondo, K., Wise, Sr., J.P. Particulate Hexavalent Chromium Inhibits Homologous Recombination Repair in Rat Lung. Presented at the annual meeting of the Ohio Valley Chapter of the Society of Toxicology (OVSOT), November 2021.

22. Toyoda, J.H., Cahill, C.R., Wise, S.S., Speer, R.M., Lu, H., Kouokam, J.C., and Wise, Sr., J.P. Securin Disruption and Chromosome Instability Persist After Chronic Hexavalent Chromium Exposure. Presented at the annual meeting of the Ohio Valley Chapter of the Society of Toxicology (OVSOT), November 2021.

23. Meaza I., Toyoda, J.H., Lu, H., Williams, A.R., and Wise Sr. J.P. Particulate Hexavalent Chromium Causes DNA Repair Inhibition Leading to Increased Chromosome Instability in Human Bronchial Epithelial Cells. Presented at the annual meeting of the Ohio Valley Chapter of the Society of Toxicology (OVSOT), November 2021.

24. Wise, Jr., J.P., Young, J.L., Lu, H., Meaza, I.I., Toyoda, J., Wise, S.S., Speer, R., Croom-Perez, T., Cai, L., Wise, Sr., J.P. A Toxic Aging Coin: Cr(VI) Neurotoxicity and Gerontogenicity. Presented at the annual meeting of the Ohio Valley Chapter of the Society of Toxicology (OVSOT). November 2021.

25. Lu, H., Wise, S.S., Hoyle, G., Toyoda, J.H., Speer, R.M, Croom-Perez, T.J., Meaza, I., Wise, Jr., J.P., Kouokam, J.C., Young J.L., Cai, L., Kondo, K., Wise, Sr., J.P. Particulate Hexavalent Chromium Inhibits Homologous Recombination Repair in Rat Lung. To be presented at the annual meeting of the Society of Toxicology (SOT), March 2022.

26. Toyoda, J.H., Speer, R.M., Meaza, I., Lu, H., Kouokam, J.C., Williams, A.R., and Wise, Sr., J.P. Hexavalent Chromium Induces Numerical Chromosome Instability Via Securin Disruption in Human Cells but Not in Whale Cells. To be presented at the annual meeting of the Society of Toxicology (SOT), March 2022.

27. Meaza I., Toyoda, J.H., Lu, H., Williams, A.R., and Wise Sr. J.P. Chromate-Induced Loss of RAD51 and Increased Chromosome Instability in Human Bronchial Epithelial Cells. To be presented at the annual meeting of the Society of Toxicology (SOT), March 2022.

28. Wise, Jr., J.P., Young, J.L., Lu, H., Meaza, I.I., Toyoda, J., Wise, S.S., Speer, R., Croom-Perez, T., Cai, L., Wise, Sr., J.P. A Toxic Aging Coin: Cr(VI) Neurotoxicity and Gerontogenicity. To be presented at the annual meeting of the Society of Toxicology (SOT), March 2022.

29. Kouokam, J.C., Speer, R.M., Meaza, I., Toyoda, J.H., Lu, H., Kong, M. and Wise, Sr., J.P. Analysis of the effects of particulate hexavalent chromium on global gene expression in human fibroblasts reveal the involvement of inflammation. To be presented at the annual meeting of the Society of Toxicology (SOT), March 2022.

30. Lu, H., Wise, S.S., Toyoda, J.H., Wise Jr. J.P., Speer, R.M, Bolt, A.M., Meaza, I., Wise, C.F., Wise, J.T.F., Young, J.L., and Wise Sr. J.P. Of Whales and Men, How Great Whales Evade Metal Induced Cancer. To be presented at the annual meeting of the Society of Toxicology (SOT), March 2022.

31. Wise, S.S., Toyoda, J.H., Lu, H., Meazza, I., Wise, Sr., J.P. Chromosome Instability and Cellular Transformation of Human Lung Cells Chronically Treated with Particulate Hexavalent Chromium. To be presented at the Annual Meeting of the Society of Toxicology (SOT), March 2022.

32. Meaza, I., Toyoda, J.H., Lu. H., Williams, A.R., Kouokam, J.C., and Wise, Sr., J.P. Missing Protein! Have You Seen it? Reward: to Cure Cancer. To be presented at the Annual Meeting of the Society of Toxicology (SOT), March 2022.

33. Lu, H., Wise, S.S., Hoyle, G., Toyoda, J.H., Speer, R.M, Croom-Perez, T.J., Meaza, I., Wise, Jr., J.P., Kouokam, J.C., Young J.L., Cai, L., Kondo, K., Wise, Sr., J.P. Subchronic Particulate Hexavalent Chromium Exposure Inhibits Homologous Recombination Repair in Rat Lung. To be presented at the Graduate Student Regional Research Conference, Louisville, Kentucky, March 2022.

Intramural Abstracts

1. Lu, H., Browning, C.L, and Wise, Sr., J.P. Autophagy does not play a main role in Rad51 dysfunction after prolonged Cr(VI) exposure in human lung cells. Presented at Research!Louisville, Louisville, Kentucky, 2017.

2. Lu, H., Wise, Sr., J.P. Homologous Recombination Repair Protects against Genomic Instability in Bowhead Whale Lung Cells after Prolonged Particulate Chromate Exposure. Presented at Research!Louisville, Louisville, Kentucky, 2018.

3. Lu, H., Browning, C.L. and Wise, Sr., J.P. Why Do Whales Have Lower Cancer Rates: Whale Cells Avoid Particulate Chromate Induced Homologous Recombination Repair Inhibition. Presented at Research!Louisville, Louisville, Kentucky, 2019.

4. Wise, S.S., Miller, E., Daniel, S., Meaza, I., Toyoda, J.H., Lu, H., Speer, R. M., Young, J. L., Isakov, R., Jaggers, H., Wise, Jr., J. P., Croom-Perez, T. J., Cai, L., Hoyle, G. and Wise, Sr., J. P. Effects of Chronic Exposure to Particulate Chromate in Rat Lungs. Presented at Research!Louisville, Louisville, Kentucky, 2019

5. Lu, H., Wise, S.S., Hoyle, G., Toyoda, J.H., Speer, R.M, Croom-Perez, T.J., Meaza, I., Wise, Jr., J.P., Kouokam, J.C., Cai, L., Wise, Sr., J.P. Particulate Hexavalent Chromium Induces DNA Double Strand Breaks in Rat Lung. Presented Research!Louisville, Kentucky, October 2021.

6. Meaza, I., Toyoda, J.H., Lu, H., Williams, A.R., Wise, S.S., and Wise Sr. J.P. Particulate Hexavalent Chromium Targets RAD51, the Key Protein in Homologous Recombination Repair, Leading to Increased Genomic Instability, A Driver of Carcinogenesis. Presented at Research!Louisville, Louisville, Kentucky, October 2021.

7. Kouokam, J.C., Speer, R.M., Meaza, I., Toyoda, J.H., Lu, H., Kong, M., and Wise, Sr., J.P. The involvement of the inflammatory response in particulate hexavalent chromium-induced toxicity. Presented at Research!Louisville, Kentucky, October 2021.

<u>Seminars and Oral Presentations</u>

1. Homologous Recombination Repair Protects Against Genomic Instability in Bowhead Whale Lung Cells after Prolonged Particulate Chromate Exposure. Presented at Department of Pharmacology &Toxicology Seminar, Louisville, February 2019.

2. Whale Cells are Resistant to Cr(VI)-induced Loss of Homologous Recombination Repair. Presented at the annual meeting of the Ohio Valley Chapter of the Society of Toxicology (OVSOT), November 2020.

3. Can Whales Resist Chromium-Induced Cancer? Presented at the annual meeting of the Ohio Valley Chapter of the Society of Toxicology (OVSOT), November 2020.

4. Whale Cells Resist Cr(VI) Carcinogenesis. Presented at 3MT University of Louisville, March 2021

5. Can Whales Resist Chromium-Induced Cancer? Presented at the annual meeting of the Society of Toxicology (SOT), March 2021.

6. Whale Cells Are Resistant to Cr(VI)-induced Chromosome Instability. Three Minute Poster Talk with the Genetic Toxicology Association Annual Meeting, May 2021.

7. Translating Particulate Hexavalent Chromium-Induced Chromosome Instability from Human Lung Cells to Experimental Animals, Human Lung Tumors and Whale Cells. Presented at the Department of Pharmacology &Toxicology Seminar, Louisville, May 2021.

8. Hexavalent Chromium Inhibits Homologous Recombination Repair in Rat Lung. Presented at the annual meeting of the Ohio Valley Chapter of the Society of Toxicology (OVSOT), November 2021.

Meetings Attended (current year and previous 5 years)

2017 Research!Louisville

2018 Annual Meeting, Ohio Valley Chapter of the Society of Toxicology (OVSOT)
Research!Louisville
Graduate Student Regional Research Conference

2019 Annual Meeting of the Society of Toxicology (SOT)
Annual Meeting, Ohio Valley Chapter of the Society of Toxicology (OVSOT)
Research!Louisville
Graduate Student Regional Research Conference

2020 Annual Meeting of the Society of Toxicology (SOT)
Annual Meeting, Ohio Valley Chapter of the Society of Toxicology (OVSOT)
American Society for Cell Biology
Graduate Student Regional Research Conference

2021 Annual Meeting of the Society of Toxicology (SOT)
Annual Meeting, Ohio Valley Chapter of the Society of Toxicology (OVSOT)
Summer Meeting, Ohio Valley Chapter of the Society of Toxicology (OVSOT)
Annual Meeting of Genetic Toxicology Association (GTA)
Research!Louisville
Annual Meeting of the Environmental Mutagenesis and Genomics Society (EMGS)

2022 Annual Meeting of the Society of Toxicology (SOT)

Honors, Awards and Professional Activities

2022 Dharm V. Singh Carcinogenesis Graduate Student Endowment Award, Carcinogenesis Specialty Section, Society of Toxicology

2022 Travel Award, University of Louisville

2021 Second place, short oral presentation award, Ohio Valley Chapter of the Society of Toxicology

2021 Graduate Student Council Fall Research Grant, University of Louisville

2021 Abstract Award, Genetic Toxicology Association 2021 Annual Meeting

2021 First place, short oral presentation award, Society of Toxicology

2021 Graduate Student Council Spring Research Grant, University of Louisville

2020 Second place, short oral presentation award, Ohio Valley Chapter of the Society of Toxicology

2019 Student Travel Award, Society of Toxicology

2017 Graduate Student Council Research Grant, University of Louisville

Professional and Academic Memberships

2016 – Present Graduate Student Member – Society of Toxicology
Ohio Valley Regional Chapter, Metals Specialty Section, Carcinogenesis Specialty Section, Women in Toxicology Special Interest Group

Field Work

2018-2021 Whale biopsy collection in the Gulf of Maine

Techniques and Skills

Cell culture
Western blot analysis
Immunofluorescence
Confocal microscopy
Chromosome analysis
Single cell gel electrophoresis
Flow cytometry
PCR
RT-qPCR
DNA transformation

Plasmid transfection
Rat chemical inhalation exposures
Rat and mouse lung inflation, anesthesia, euthanasia, handling
Tissue staining (hematoxylin and eosin, picrosirius red, immunofluorescence)
Fluorescence in situ hybridization (FISH)
Wildlife primary cell line establishment
Whale ID and biopsy processing